DIRECTED ENERGY WEAPONS (DEW)
HIGH POWER MICROWAVE (HPM)
6.1 PROGRAMS
FY20 ANNUAL REPORT

Mr. Ryan Hoffman, Program Manager

NAVAL SCIENCE & TECHNOLOGY

**Directed Energy Weapons (DEW) High Power
Microwave (HPM) Program
Annual Report for FY20**

Table of Contents

Directed Energy Weapons (DEW) High Power Microwave (HPM) Fundamental Research Program Annual Report for FY20

Introduction

Program Officer
Ryan Hoffman, Office of Naval Research

The Directed Energy Weapons (DEW) Program of ONR was initiated in response to the rapid development and growing threat of directed energy technologies by adversaries. Directed energy weapons are defined as electromagnetic systems capable of converting chemical or electrical energy to radiated energy and focusing it on a target, resulting in physical damage that degrades, neutralizes, defeats, or destroys an adversarial capability. The U.S. Navy uses HPM to gain and sustain tactical, operational, and strategic advantage in the arena of EM Maneuver Warfare and Integrated Defense for U.S. forces across the full range of military operations, including power projection and integrated defense missions. The ability to focus radiated energy reliably and repeatedly at range, with precision and controllable effects, while producing measured physical damage, is the measure of DEW system effectiveness. In anticipation of DEW advancements, the ONR HPM Program comprises a portfolio of initiatives and research projects which seek to provide the science and engineering basis for means and methodologies to provide the Navy advanced HPM technologies, systems, and techniques enabling a new class of weapons that will be highly effective in the battlespace. The goal is to be the most effective steward of DEW systems.

Asymmetric threats are proliferating worldwide and likely will continue to do so until such time as effective countermeasures are deployed. Often enough, Rules of Engagement will restrict kinetic engagement with asymmetric threats contingent on the particulars of the scenario. DEW systems – or more specifically for this report, HPM weapons – are expected to allow Naval commanders significantly more flexible responses to a number of asymmetric threats, including various small surface craft and unmanned aerial vehicle (UAV) threats. This flexibility is possible since the restrictions on engaging targets might be removed or reduced based on recognition of 1) the low collateral damage and 2) the non-lethal and reversible effects associated with HPM weapons.

HPM weapons create pulses of electromagnetic energy over a broad spectrum of known radio and microwave frequencies, causing either temporary or permanent results on electronics within targeted systems at scalable effects. HPM weapon systems can be used to disrupt, disable, or potentially destroy critical electronic circuitry in target systems, even in restricted scenarios, while also having the advantage of low cost per shot. HPM weapons deliver electromagnetic energy through coupling of the electromagnetic wave to target circuits through aperture or cable points of entry, thereby inducing currents in the circuitry capable of causing a variety of effects. Potential effects include erroneous signals, system lock-up, shutdown, loss of communications between systems, and physical damage.

As DEW falls within the Fundamental Research part of the broad ONR Science & Technology Investment Portfolio, projects funded are long-term initiatives, covering basic research or applied science. These investigations can have a five to twenty year horizon. Across the HPM technology thrust areas, research projects within the program include performers from academia, industry, government laboratories, and small businesses. Moreover, the program includes performers whose research is financed through Navy SBIR/STTR funding. In addition, science and technology solutions from an international technical community are afforded through ONR Global, which funds projects that foster cooperation in areas of mutual interest with global partners. The program encourages the cross-pollination of ideas and

collaboration among performers worldwide, and offers an annual review where performers provide updates on the status of their research and present results to their DEW peers. Furthermore, data and facilities sharing are encouraged within the program. This approach contributes to increased success for the program and for the Navy.

Focus areas cover HPM sub-systems that optimize power and/or energy density at the electronic target for a variety of platform sizes and capabilities while minimizing size, weight, power and cost. Examples of related areas for S&T investment and research include supporting technologies such as power electronics, pulsed power drivers, power modulators, as well as frequency agile RF sources and antennas.

Additional research focus areas include research into electronic system coupling, interaction, and effects with the first goal of enabling development of predictive effects tools for current systems. A second goal of this work includes an exploration of in band and out of band coupling and interaction mechanisms. This exploration will exploit developing advances in frequency and bandwidth agility both to identify new potential weapon system possibilities as well as to achieve significant improvements in size, weight, power, and cost in new variants of existing systems.

Research Challenges and Opportunities

- RF coupling and modeling tools to capture complex EM wave interactions with electronics and associated enclosures, RF component disruption, along with novel techniques for experimental validation. Prediction of effects on electronics with improved techniques for HPM lethality testing and analysis. Analysis of HPM coupling mechanisms, electronic device interaction physics, and component level effects validated through experiment. Development of tools and techniques for more efficient identification and utilization of novel RF waveforms.

- Pulsed power/power electronics; including high energy density capacitors, power conditioning, high voltage switches, dielectric insulators, 3D printed/novel materials and power modulator pulse forming networks that enable higher duty cycle operation

- Solid state and vacuum electronic based HPM sources that provide frequency and waveform parameter tunability and are reconfigurable to adapt to changing requirements; computer codes for modelling HPM physics to enable the next generation of devices

- Wide bandwidth high power amplifiers that provide the ability of very rapid waveform adjustment.

- High power, low profile, or conformal antenna designs and capable radome materials, novel array concepts, high power beam steering techniques and distributed beam forming approaches.

- Novel HPM sensors, instrumentation and algorithms are of interest for measurement of waveforms and diagnosing system performance as well as applied to Electronic battle damage indication (eBDI).

Efficient Insulators for High Power Radio Frequency Devices

Grant No. N00014 -17-1-2848

Annual Report for Fiscal year 2020

Period of Performance: September 1, 2017 to August 31, 2020

Prepared by:

Professor Jane Lehr, Principal Investigator
University of New Mexico
Department of Electrical and Computer Engineering
MSC 01 1100
Albuquerque NM 87131-0001
Tel: (505) 277-1749
Fax: (505)277-1439
Email: jmlehr@unm.edu

Section I: Project Summary

1.   Overview of Project

Abstract: Electrical failure by an electrical breakdown along the surface – known as surface flashover or snapover – is overwhelmingly the nemesis of any high-power system. Generally, high voltage design attempts to mitigate this failure mechanism by increasing the insulator length,which results in increased size and weight, as well as inductance. For vacuum electronic devices (VED), such as those used in Directed Energy applications, the insulator is particularly problematic and reduces the power handling capability.

University of New Mexico has developed a high gradient insulator structure using a high quality, vacuum compatible ceramic from Sienna Technologies. The high gradient insulator (HGI) technique increases the flashover electric field by exploiting the scaling of the physics. For the first time, a radial high gradient insulator has been designed so that the radial electric field is uniform. The high-performance ceramic enables the HPM source to be manufactured using "hard tube" techniques that have been demonstrated for very long-lived vacuum tubes to realize a reduced size and weight with higher reliability and longer lifetimes and will drastically reduce the size, weight and power of the VED. The insulator will replace the traditional axial stack which degrades the condition of the high voltage pulse. System level benefits result from eliminating the ancillary vacuum equipment currently required for HPM devices as well as allowing for an integrated, system level design. The technology is transferable to other industries such as accelerators, power electronics, renewable energy resources and aviation.

Objective: The overall concept of a radial high gradient insulator for the suppression of vacuum flashover uses four key innovations (*high performance ceramic material*, *a radial geometry*, *high gradient insulator configuration and electric field control by interface shaping)* which has resulted in unprecedented surface flashover levels over three times that of other ceramic insulators. In transitioning the concept to realization, the following objectives were derived:

1.   *Validate Tangential Electric Field Design Criterion:* Our initial hypothesis is that the discharge is driven by the tangential electric fields (as opposed to the total electric field). This allows for the shaping of the insulator surface as a parameter to control the electric fields. A key objective then was to validate the tangential electric field component as the key design parameter using the axial flashover field levels obtained from testing. Conceptually, this appears straight forward, but the existing literature focuses entirely on an angle without regard to the spatial variation of the immersing electric field. This is critically important because the radial high gradient insulator geometry considers each thin layer an angled insulator.

Most insulators are configured in an axial geometry so that the electric field gradient is linear. In a radial configuration such as for the high power radio frequency (HPRF) source application, the electric fields are radial and vary as 1/r from anode to cathode. This places severe constraints on the design. To increase the operating voltage in the axial, Smith demonstrated that conical frustums had significantly higher flashover than cylinders and 45 degree angles were optimal. The conical shape increases the discharge path length. This is also the origin of the common practice of putting grooves in surfaces. This widely used practice has the underlying presumption of a uniform axial field distribution.

2.   *Determine Key Parameter (|I| or I/M?)* Increasing the surface flashover potential of insulators in vacuum with a high gradient geometry was first proposed by Eion Gray and (somewhat) demonstrated by

Tetra Corporation. The key concept was to exploit the high flashover electric fields at small gaps by decomposing a large length of insulator into smaller lengths by inserting floating conductive layers. Caporosa and colleagues at Lawrence Livermore National Laboratory (LLNL) further developed HGI using other polymers than mylar as well as the ceramic alumina and used many layers of thin (~ 1mm) insulator. In the early 21st century, Leopold and colleagues took a radically different approach and studied electron trajectories to show that the metal layers served to deflect electrons away from the surface. Their simulations and companion experiments show that an insulator to metal length ratio (I/M) of three was the critical parameter. It may be noted that both approaches seem to be validated with data.

3. *Identify Key Success Metric* It was identified earlier in the program that it was difficult to compare between samples. This is partly because of the destructive nature of surface flashover where each data point requires one test sample. So statistically significant data is time consuming. It was also because some comparative polymer samples were found to have a high flashover potential. Since the samples were often of different lengths, direct comparisons were difficult. This made it very difficult to prove that either the use of vacuum compatible materials or the high gradient insulator geometry was leading to performance improvements. A methodology or metric was identified as a key aspect to show improvement.

Introduction:

Surface flashover has long plagued high voltage and HPRF system design and is widely acknowledged as the predominant failure point. Coaxial geometries – where the cathode (K) is the inner conductor – are advantageous because of symmetry and closed geometry confines the electric fields. However, the coaxial geometry also presents a significant challenge because the logarithmic variation of the electric field results in the application of a large factor-of-safety. This is easily achieved in system sections where the coaxial power flow is insulated with vacuum or high withhold-strength transformer oil. The weak point for failure by surface flashover occurs at the insulating barrier between these two at the vacuum/ dielectric interface. This is typically obviated by using an insulating shroud around the HPRF device with much larger sections to seal the vacuum section. However, the resultant structure increases the overall size of the HPRF system with increases in size, weight and power. Moreover, it also introduces a large reactive inductance into the power flow, which reduces the overall efficiency and eliminates the advantages of fast turn on cathode technologies.

Figure 1 An AlN HGI fabricated by Sienna Technologies and tested at UNM. HGIs have alternating layers of insulator and metal. Our ceramic HGIs may be baked for use in vacuum electronics.

A radial insulator and a short length of dielectric to seal the vacuum section, increases overall system efficiency and performance and reduces the size and weight by eliminating the vacuum insulator shroud. However, the voltage and dimensions often result in an electric field that exceeds the vacuum surface flashover threshold and results in an electrical breakdown along the vacuum - dielectric interface. In a radial geometry, the challenge is even greater because the logarithmic electric field is parallel to the applied field, energizing the discharge, and the peak electric field far exceeds the average electric field.

We have conceived a technical approach towards a radial insulator with superior voltage handling even along the vulnerable vacuum- insulator surface. Moreover, the radial insulator is ceramic and thus highly suitable for use with a high-power vacuum electronic device. The ceramic is a polycrystalline formulation of aluminum nitride with low secondary electron emission coefficient, low outgassing, high temperature capability and moderate relative dielectric constant. The ability to heat the VED "tube" is highly desirable as it is well known to increase their voltage handling capability and reliability.

In this effort, to minimize the dimensions, three innovations are proposed: (1) configuring a radial HGI architecture, (2) contouring the surface and, (3) using a high-quality, high temperature ceramic to enable "bake out" of HPRF vacuum electronics. This HGI is conceptualized in a first-of-its-kind radial configuration enabled by the ceramic manufacturer, Sienna Technologies. The ceramic is an aluminum nitride (AlN) in polycrystalline form, which uses novel processing to produce a high breakdown strength

material with a very low secondary electron emission property and wide temperature capability. To date, HGI has only been fabricated in cylindrical samples because of the need to hot press.

Background:

A HGI segments an insulator in the electric field direction by interspersing layers of metal to exploit the increased flashover electric field at reduced insulator lengths, as shown in Figure 1. All other researchers fabricated HGI in cylindrical geometries – linear HGI – for posts using polymers (Kapton, PMMA, Lexan) and alumina as insulators. For testing purposes, the samples are characterized by the electric field parallel (tangential) to the surface and the average field $E = \frac{V_0}{d}$.

For a radial insulator, the electric field is not uniform. For a coaxial VED, such as the relativistic magnetron shown in Figure 2 (a), with inner conductor radius a, outer radius b, and a voltage V_0, the electric field is radial and has a magnitude given by

$$E(r) = \frac{V_0}{r \, ln\left(\frac{b}{a}\right)} \, \hat{r}$$

The electric field varies with radius and has the highest value at the inner conductor radius a. From a design perspective, this is problematic since the system must be reliable to the highest electric field in the system. Thus, the optimum electric field distribution is constant. To achieve this goal, we combine two approaches: a HGI architecture and contouring the interface to control the tangential electric field.

In this radial HGI concept, the metal layers are positioned at various radii in the insulator as shown in the Figure 2 (b). For a small number of metal layers, the radial electric field will have a significantly smaller peak value but will dip between layers. This improvement in insulation efficiency has a complex profile and indicates that a large number of thin layers of insulator and metal can approximate uniformity. A uniform radial electric field is achieved if the voltage varies linearly with radius,

$$V(r) = \text{K} \cdot r$$

This is a general result. For the development of a radial insulator, the challenge is to force this voltage profile along the insulator interface. For the radial insulator, this may be achieved by contouring surface and imposing this voltage profile on the component of electric field that is tangential to the surface. The rationale for this is that the tangential electric field is the force driving the initiating electron avalanche that results in surface flashover. We show by rigorous derivation that the interface contour that partitions the voltage is one where the surface varies as *1/r* between the inner and outer conductors. The electrostatic modeling and tangential electric field is shown in **Figure 2** for a 10 cm diameter vacuum tube charged to 750 kV, which yields tangential surface fields of 70 kV/cm.
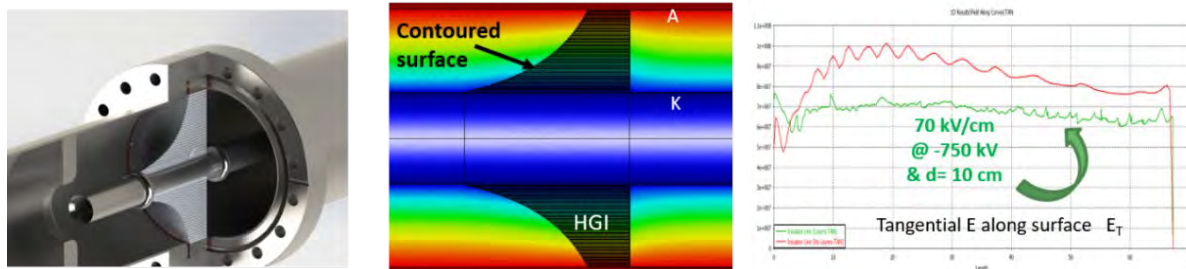
Figure 2 The ceramic high gradient insulator shown (a) inserted into a relativistic magnetron, (b) in cross section in a coaxial structure and (c) the uniform electric field distribution from a conceptual design for a 10 cm outer diameter insulator for vacuum tube charged to 750 kV with a very reasonable surface tangential electric field of 70 kV/cm.

High Gradient Insulator Background & Prior Art: The high gradient insulator concept, originally called a microstack for its similarity to a vacuum stack, was initially proposed by Eion Gray and then demonstrated by Elizondo from Tetra Corporation with SBIR funding (Elizondo, 1992). The HGI segments a cylindrical insulator by interspersing layers of metal to exploit the increased flashover electric field at reduced insulator lengths, as shown in Figure 3. This dependence had first been reported by Hawley (1968) and then shown by Milton (1972). The Tetra effort showed modest improvements and reasonably cited manufacturing issues for the lack of larger gains. Researchers at LLNL used the HGI concept as a key technology underpinning the dielectric wall accelerator and did extensive testing with many layers using several insulators and reported 4X increase in flashover using HGI. In 2005, Leopold and colleagues used a radically different approach in the design of HGI by using an analysis based on electron trajectories and the ratio of the length insulator (I) to that of the metal (M) as a key metric. Leopold's samples, in sharp contrast to the earlier efforts, used thick bands metal to interrupt the electron trajectory along the insulator

Figure 3 The cylindrical HGI structure intersperses the insulator length (I) with a length of metal (M).

surface. Leopold's electron trajectory-based hypothesis was supported by his experiments and showed that an I/M ratio < 3 showed improvement in the flashover strength. The research approach and results were compelling and introduced the quantity I/M as a parameter-of-interest. Leopold's approach using the I/M ratio was so beguiling that it was also used by the LLNL researchers to evaluate their designs. The LLNL group kept their approach of many thin layers but incorporated the I/M parameter in their studies. In a targeted I/M study, LLNL hypothesized that flashover potential would increase as they used ratios as high as 100 (Harris 2008). These investigations showed clear improvements in the flashover voltage but the path towards further improvements proved murky without a theory of operation. It may be noted that these endeavors were all conducted in samples where the planar layers were formed into cylinders.

2.   Activities and Accomplishments

AlN High Gradient Insulator Testing: Fabricated samples were tested in a dedicated, compact vacuum surface flashover test stand. Vacuum levels may be varied up to 10^{-7} Torr. The voltage is applied by a compact, low energy Marx generator capable of voltages over 400 kV with a risetime of 20 ns and a pulsewidth of 250 ns. Initial test samples were designed in the manner suggested by Leopold's compelling modeling efforts with low I/M ratios and other samples were generated with higher I/M ratios for comparison. A variety of configurations with different I and M and I/M were fabricated and tested with sufficient events (50 shots per sample or loss of surface resistivity) for meaningful results. The testing results seemed promising and compared favorably with the accepted value for surface flashover of alumina of 50 kV/cm, but also below a polymer test sample in our system.

The surface flashover testing was conducted on samples of different designs and materials with a range of the design variables I/M in order to identify the critical factors. Our initial attempts to identify trends to inform the next iteration of designs was confusing because of the large variety of design parameters and materials. First, the samples were labeled with letters which could be correlated with the Sienna designations. This is shown in the temporal order of testing in Figure 4 where the ordinate is the average flashover electric field and the abscissa is the sample length. The sample identifier designation is located at the top of each bar and described in the table.

In looking at the summarized data, no trends were identified. This is a common issue with surface flashover research in general where parameters include vacuum level, voltage parameters (peak, pulse width, etc.), material (outgassing propensity, secondary electron emission yield (SEEY) curves, conditioning, processing, surface finish), as well as triple points and their shielding. The variability in test conditions makes comparison between samples questionable at best. For the HGI insulators this is further compounded by the large number of design parameters. Moreover, since the physics mechanism of operation of the HGI

is insufficiently known, the possible testing space is large. Perhaps the most critical missing aspect is a clear understanding of a success metric – an unbiased method to identify progress. This resulted in two endeavors: a computational investigation of HGI operation to narrow the parameter space and the search for a metric to identify success.

Modeling and Simulation of HGI Structures: HGI development has long been hampered by the lack of a detailed working theory of operation. This notion, powerfully articulated by John Harrison (AFRL/DEH) during a site visit, was gained during his LLNL tenure developing HGI for the Dielectric Wall Accelerator. The LLNL effort adopted the nomenclature of Leopold but used thin layers of dielectric with a wide range of I/M ratios up to 100, with frustratingly mixed results. Both high (LLNL) and low (Leopold) I/M ratios appear to show improvement in surface flashover initiation levels. Recent results from CAEP show modest improvements and frustration, but also showed surprising evidence of an anode-initiated flashover for a large fraction of their testing. Of course, with the reported efforts being primarily experimental, questions regarding differences in materials as well as fabrication techniques are always present.

Although plasma simulations are extensively used in single insulator vacuum surface efforts, only vague references are made to modeling HGIs - with Leopold's particle trajectory studies the notable exception. Recognizing the enormous parameter space, UNM initiated a modeling effort using the Particle-in-Cell Direct Simulation Monte Carlo Code ALEPH to tease out the relationships between the parameters and performance. The simulations proved complex but we were ultimately rewarded with unexpected insights.
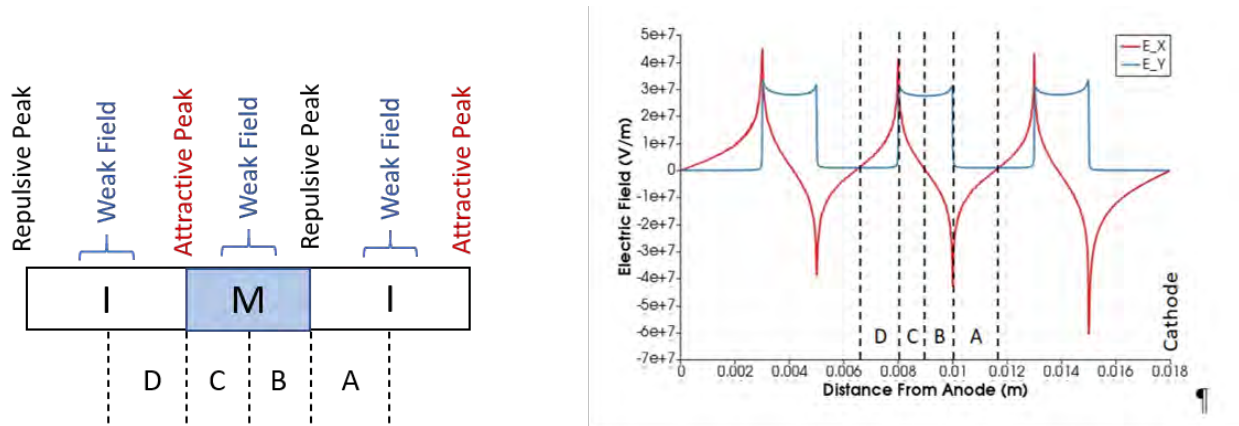
Figure 4 Cartoon of HGI layer with qualitative descriptions for the perpendicular electric field (right) and cross section of a typical HGI electric field. Ex is perpendicular and Ey is parallel to the surface. Zones A-D are labeled for the middle cell.

A test-particle model, called the Simplified Avalanche Parameterization (SAP), was conceived and developed which requires only the HGIs theoretical electric field structure as input. This permits the comparison of various HGI designs based on the potential growth of a secondary electron emission avalanche (SEEA) given an arbitrary electron source, such as the cathode triple junction (CTJ) or emission from randomly located surface defects. We developed the following results:

- Our simulations found that a metal layer adjacent to the cathode will deflect electron emission from the CTJ away from the surface and improve holdoff voltage. Additionally, the computational results indicate that an insulating layer adjacent to the anode will be beneficial. This may be related to the observation of Zhu [2] that metal-edged HGIs appear to flashover starting from the anode side.

- The HGI concept has an implicit requirement for the design layers (cells) to be independent. The likelihood of coupling between HGI cells was examined analytically and through multiple computational approaches. Larger cells are more likely to behave independently and an equation

has been approximated for when coupling may begin to occur. An insulator with a secondary electron yield that remains large at higher energies will also be more sensitive to coupling. However, even without cell coupling, an HGI can exhibit surface flashover though other failure mechanisms and thus minimizing cell coupling will not guarantee a higher holdoff voltage.

- Established that Zone C, the downstream side of an insulating layer where the field is electron attractive, may be an essential location for triggering a SEEA along an HGI surface. Our experimental holdoff voltages agree with the theoretical ranking of HGI performance based on the avalanche growth that can be initially sustained in this region. Surface defects around the middle of an insulating layer are the most likely to trigger a SEEA as they can grow along the portion of the attractive downstream side most capable of sustaining the avalanche. The length of this avalanching region will depend on the secondary electron yield (SEY) curve and the HGI geometry.

- Careful conditioning was shown in the literature [1] [3] [4] to be essential to achieve maximal HGI performance. Our results agree with this conclusion because a SEEA's maximum size is very sensitive to surface defect location, and thus if an emission site can be destroyed the holdoff voltage could be significantly improved.

- Extensive Aleph and SAP modeling of HGIs were conducted using geometries with metal layer widths from 20 micrometers to 2.5 mm and insulating layers from 40 micrometers to 5 mm. Our results indicate that thin layers will result in better holdoff voltages. This disagrees with the Leopold's hypothesis that the layer width ratio I/M is the determining factor for optimal performance.

- At some point, the benefit of decreasing layers will stop due to alternative failure mechanisms, such as the noise in the electric field due to surface roughness overwhelming the HGI field, triple point initiated vacuum arcing between adjacent metal layers, or cell coupling. When these alternative failure mechanisms dominate will depend on the fabrication details.

- While HGIs at atmospheric pressure were not our primary concern in this study, initial testing indicated two factors that may hinder HGI performance in these conditions. First, there will potentially be a larger number of electron strikes along the surface because the periodic field structure will both attract and repel electrons. The repelled electrons will be less likely to actually escape the surface region compared to the vacuum case because of the mean free path and thus these electrons may still be near to the surface when the electron reaches an attractive region. Whether the higher number of electron strikes will lead to a SEEA will depend on the mean free path, which limits the electron energy. Second, the parallel electric field is enhanced over the insulating segments, which facilitates easier breakdown, but is reduced over the metal layers, which hinders breakdown. Thus, the use of thicker metal layers may be able interrupt the streamer breakdown mechanisms but would require further analysis.

The modeling effort has thus provided key guidance for HGI design. It shows the advantage of an asymmetric HGI with a metal layer at the cathode end and an insulating layer at the anode end. We have explained the significance of the I/M ratio and explored cell coupling.

Flashover Electric Field Scaling with Insulator Length: The other, more mundane, observation is that since it is known that both the vacuum surface flashover field and electric field vary with gap distance or discharge length, comparing samples with different lengths was misleading. Recognizing that one way to compare the different samples is to normalize the threshold electric field values with their length dependence, a survey of the literature was performed to find the dependence. Arnold (1982) cites Hawley as noting some dependence with length. Gray's original hypothesis centered on the observation that thin layers of insulator have higher flashover fields, but the specific dependence is not given. Miller (1993) acknowledges the length dependence that $E \propto d^{-\alpha}$ and that "appears to be ~ 0.5". It is somewhat

surprising that the observed decrease in flashover electric field with increasing length is neither more widely used in practice nor explored. Furthermore, the "path length" argument is often evoked for using undulating corrugations in insulator surfaces. This is often justified by a rule of thumb and citing that the effective discharge path length is longer. A more precise argument may be that corrugated surfaces improve flashover thresholds by disrupting the path of avalanching currents until the pathway through a gas is reached. While thresholds for electrical breakdown initiation are typically cited as a constant value, it has long been noted (though largely in obscure references) that electrical breakdown generally varies with length. This is true for bulk breakdown in vacuum, solids and gases and also for surface flashover in vacuum. One reason for its obscurity is the large number of other variables also known to affect breakdown – notably the applied pulse width and pressure. A validation exercise was devised to test the scaling of vacuum surface flashover with discharge length using 3D printed cylinders in order to normalize between samples. In addition to providing insight, this allowed for a metric for determining the success of the HGI samples. It was recognized that samples with different lengths could not be compared One issue in comparing samples of varying length is comparing samples of different lengths with a normalization procedure. While the scaling with length has been discussed in the literature, it is seldom used in practice despite being significant. It may be noted that for a length of ~4 cm, the value drops to 50% of its value at 1 and at 2.5 cm, it is twice the value.

In order to compare the vacuum surface flashover field for the samples, as well as other configurations found in the literature, we verified the scaling with length using samples made with a Formlabs™ 3D SLA printer. We concluded that the length scaling is 0.35 and verified with the Milton data. We note that the differences between two coefficients are minor at long gaps. The experiments with polymer resins validated the scaling of electric field with insulator length to be of the form $E_L = E_{1cm} \cdot L^{-0.35}$. This is the vacuum surface flashover electric field normalized to the value at 1 cm. This is plotted in **Figure 5** to the value for monolithic AlN at 1 cm. The peak holdoff electric fields for the tested HGIs are shown with their letter designations. This plot then provides a clear metric for comparison and shows that the HGI has potential to yield a higher surface flashover electric field than can be expected with an insulator.

Sample Identifier	Sienna Designation	Material
A	HS-728 Refurbished	4Mo/3AlN
B	HS 729 Refurbished	4Mo/3AlN
C	HS-730 Refurbished	4Mo/3AlN
D	HS 755	4Mo/3AlN
E	HS 767	4Mo/3AlN
F	HS 762	22AlN/21Cu
G	HS 768-1	22AlN/21Cu
H	4 Kovar - 3AlN	4Ko/3AlN
I	KER 22 sample 1 AlN	22KER/21Cu
J	KER 22 sample 2 AlN	22KER/21Cu
K	HS-728 AlN	4Mo/3AlN
L	HS-729 AlN	4Mo/3AlN
M	HS-730 AlN	4Mo/3AlN
N	7 layer AlN	7Cu/6AlN
O	HS 772-2	4Mo/3AlN
P	HS 772-1	4Mo/3AlN
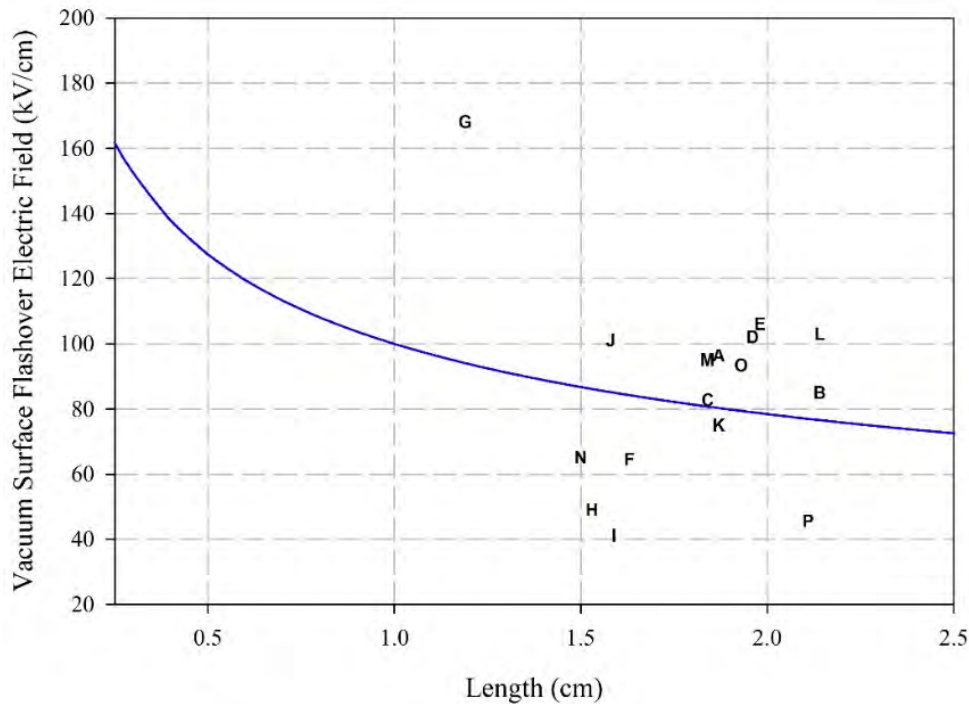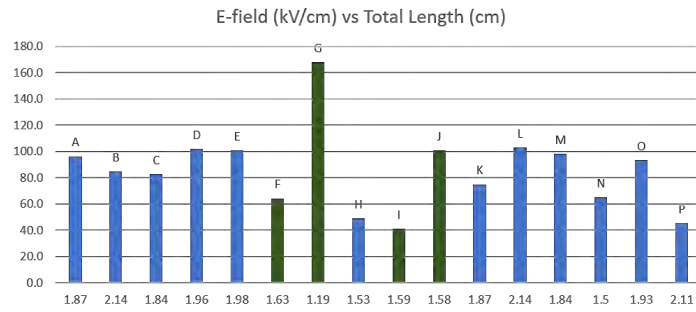
Figure 5 (a)The samples are designated by a letter corresponding to the internal Sienna one for ease of categorizing. In (b), the experimental results showing the peak electric field for vacuum surface flashover by their letter designation showing no clear trend. The total sample length is also given and shows the differences of approximately a factor of two. The green bars are those with small insulator lengths I and the blue with longer ones. (c) The AlN HGI compared to the scaling law for insulator flashover with length provides a clear metric for evaluation. The letters denote the specific HGI parameters listed in Figure 4. The HGI shows potential for significant improvements for surface flashover electric fields.

3.   Findings and Conclusions

Simulations using the ALEPH code were initiated in the middle of the program to provide a working theory of operation for improvement. The modeling proved to be significantly more difficult than anticipated but ultimately was successful and provided guidelines. Most significant was identifying that the first layer at the cathode should be conducting and the layer next to the anode, insulating. To date, all HGIs have been made symmetrical. Simulations also showed the competing processes which explained the seemingly contradictory experimental results which are intricately linked to "cell coupling" of the periodic nature of the HGI structure. It shows that thin layers of insulator limit cell coupling but the layers should not be too thin or defects will dominate. An upper limit on performance is indicated. The computational model also shows that defect in the insulator is critically important for initiation. This is notable since it is not part of the dominant theory, the secondary saturated electron emission avalanche theory of vacuum flashover. The demonstration incorporating the simulation results has not yet been fabricated.

After some significant testing of HGI structures, and repeated review of existing literature, it became apparent that substantial comparisons could only be made if the samples were normalized to length. In the widely cited Pillai-Hackam model, the scaling with insulator length in the direction of the electric field, is given as $1/\sqrt{\ell}$, and this dependence has been cited as evidence for the accuracy of the model. In a detailed search of early surface flashover literature, only vague references regarding the power of the scaling could be found. However, it is known in both laboratory experiments and design practice that the surface flashover threshold decreases as the length increases. Using 3D printed SLA polymer materials, the surface flashover potential was found to scale as

$$E_{SF} = E_1 \ell^{-0.35}$$

Where E_1 is the vacuum surface flashover at an insulator length of 1cm in a uniform field. This allowed a comparison between samples of different lengths. More importantly, however, it provides an unbiased methodology to evaluate the success of high gradient insulators and a meaningful figure-of-merit. Configurations with flashover initiation above the scaling law show improvements. For example, Sample G shows a significant improvement of over 70%.

4.   Plans and Upcoming Events

The final testing, using the results gleaned from the simulation work, needs to be fabricated and tested. Even without that final verification, this work is garnering some excitement in the technical community, particularly now that the figure-of-merit has been developed. The Energy Manipulation Group at Lawrence Livermore National Laboratory has requested a seminar, as has the Albuquerque Chapter when it resumes meeting – and we have not published these results yet.

Future work should look at triple point junctions. This testing was done without any triple point shielding to insure that comparisons were on the bulk. Most flashovers seemed to initiate from the cathode but we now know that the first layer is critical – and has not been tested. Triple point junctions alone are interesting because electron emission in excess of what can be explained by field enhancement has been observed and may indict that an additional mechanism is operative.

Since this may be fabricated radially, a full demonstration should be done. However, some early work on insulators in radial geometry by Benwell and Kovaleski showed that shielding both the anode and cathode resulted in reduced holdoff potential. Also, there is an increased interested in lower tech radial insulators from polymers and some relatively easy fabrication could easily be incorporated. There is a tendency to use the 45 degree insulator in radial geometries. The 45 degree insulator is interesting because it triggers anode-initiated breakdown which is poorly understood. In fact, angled insulators may be used to preferentially study anode-initiated breakdown which seems to occur at a higher threshold than that from the cathode.

The simulation work pointed to a mechanism which depends on surface defects. Chinese researchers have been studying surface flashover intensely for over a decade and have recently shown that fluorination can double the flashover strength of polymers. Fluorination, a surface plasma treatment, was originally developed to make the paint to stick to inert plastics such as those in the PE family. It cleans and modifies the surface simultaneously. The Chinese are talking about charge trapping. It may be possible fluorine plasma treatment may expose positively charged dangling bonds on the LDPE or any treated plastic surfaces. The published results are notable and worthy of investigation – and perhaps combined with a high gradient insulator geometry.

5. Transitions and Impacts

Student J. Cameron Pouncey is a Smart Scholar slated for NSWC Dahlgren and spends summers in Virginia working on HPRF systems for Jacob Walker. He will aid in transitioning the results of this research into their devices.

Student Leonardo Rossetti has joined the Naval Research Laboratory's Electromagnetic Effects Section with PI Zachary Drikas (202-767-6629 / zachary.drikas@nrl.navy.mil).

Student Cameron Harjes will become a student intern at the Air Force Research Laboratory's Directed Energy Directorate after spending the summer as a Scholar.

The Air Force Research Laboratory' Directed Energy Directorate (POC Brad Hoff) has indicated strong interest in the technology. The Program Manager for THOR has cited the surface flashover of the insulator as the single biggest threat to system reliability and it interested in transitioning this technology to fieldable systems.

Veras is interested in incorporating some form of this technology into an anti-drone system.

6. Collaborations

- The Naval Surface Warfare Center- Dahlgren Division keeps in close contact regarding this effort.
- Prof. David Wetz and I are in discussion regarding future collaborations.
- Dr. Allen Gardner has been to visit UNM.
- Dr. Patrick Kelly, Lockheed Martin has expressed interest in incorporating this technology into vacuum tubes and directed energy technology.
- The Air Force Research Laboratory' Directed Energy Directorate and their contractor Leidos has expressed interest in transitioning this work into deployable systems.

7.   Personnel

Principal investigator   Prof. Jane Lehr/ 0.5 person month/ National Academy: N
Co-investigator   N/A
Business Contact   N/A
Team Members   Dr. Lisa Fisher/ 3 person months/ National Academy: N
Subs   Dr. Ender Savrun/ / 0.25 person months/ National Academy: N

8.   Students

Graduate Students: (2)   J. Cameron Pouncey, Cameron Harjes
Undergraduate students: (3)   Ken Van Le, Nikita Dougan, Grant Guttromson

9.   Technology Transfer

The Air Force Research Laboratory' Directed Energy Directorate (POC Brad Hoff) has indicated strong interest in the technology. The Program Manager for THOR has cited the surface flashover of the insulator as the single biggest threat to system reliability and it interested in transitioning this technology to fieldable systems.

Verus is interested in incorporating some form of this technology into an anti-drone system.

Lockheed Martin has asked to collaborate on efforts using this technology.

This technology has applications in aircraft electrification.

10.   Products, Publications, Patents, License Agreements, etc.
Publications resulting from this project:

L.E. Fisher, C.D. Harjes and J.M. Lehr, "Initiation and Growth of the Secondary Electron Avalanche along High Gradient Insulators in Vacuum, accepted for publication to IEEE Trans. On Dielectrics and Electrical Insulation, October 2020.

Pouncey, J. Cameron, and Jane M. Lehr. "A parametric SPICE model for the simulation of spark gap switches." *Review of Scientific Instruments* 91.3 (2020): 034704.

Pouncey, Jon Cameron, and Jane M. Lehr. "Triggering of Pressurized Gas Switches with a Class I Laser." *IEEE Transactions on Plasma Science* 48.7 (2020): 2531-2537.

Pouncey, Jon Cameron, and Jane M. Lehr. "Absorption of 1535-nm Laser Pulses in Insulating Oils." *IEEE Transactions on Plasma Science* 48.6 (2020): 2175-2179.

Pouncey, Jon Cameron, Jane M. Lehr, and D. V. Giri. "Erection of compact Marx generators." *IEEE Transactions on Plasma Science* 47.6 (2019): 2902-2909.

<u>Books</u>   None

<u>Book Chapter</u>   None

<u>Theses & Dissertations</u>

     a.   Title: ***Inhibiting Surface Flashover in Vacuum with High Gradient Insulators***
     b.   Institution: University of New Mexico
     c.   Author: Cameron D. Harjes
     d.   Completion Date: May 2020
     e.   Acknowledgement of Federal Support? Yes

     a   Title: ***Advancing Compact Pulsed Power***
     b.   Institution: University of New Mexico
     c.   Author: Cameron Pouncey
     d.   Completion Date: May 2020
     e.   Acknowledgement of Federal Support? Yes

<u>Websites</u>   None

<u>Patents:</u>   None

<u>Other Products</u> None

11.   Point of Contact in Navy
Yeong-Jer (Jack) Chen
NSWCDD, E13
yeongjer.chen@navy.mil
Date of last contact: August 12, 2020

Jordan Chaparro
NSWCDD, E12
jordan.chaparro@navy.mil
Date of last contact: April 24,2020

12. Acknowledgement/Disclaimer:

RF Coupling Revisited

Grant No. N00014 -17-1-2932

Annual Summary Report for Fiscal year 2020

Period of Performance: October, 1, 2019 to September 30, 2020

Prepared by:

Professor Anthony Caruso, Principal Investigator
University of Missouri, Kansas City, MO
Department of Physics and Astronomy
5110 Rockhill Rd.
Flarsheim Hall, Room 257
Kansas City, MO 64110
Tel: (816) 235-2505
Fax: (816) 235-5221
Email: carusoan@umkc.edu

Principle Investigator: Anthony N. Caruso, 816-235-2505, carusoan@umkc.edu
Department of Physics and Astronomy
University of Missouri-Kansas City (UMKC), MO.

Section I: Project Summary

12. Overview of Project

Abstract:
The problem of undesirable RF coupling to wires and electronics has been receiving high interest for several decades. Coupling can be unintentional, originating from nearby radiators, especially in the rising congestion in the wireless spectrum, or due to the rising threat of High Power Microwave (HPM) weapons. In this work, we develop a combined experimental and modeling approach to quantify coupling to realistic wire systems and we also develop general guidelines to protect wires and electronic circuity from unintentional and intentional interference.

Objective:
The objective of the proposed work is to develop rules-of-thumb to predict HPM source dependent effect coupling parameters, for any arbitrary collection/geometry of wires/traces/wire-bonds, in a dielectric or metallic enclosure. Such studies are directly applicable to unmanned aerial vehicles (UAVs) or circuits composed of PCB's/wire-bundles. The work is a combined experimental, simulation and theory effort.

The underlying physics is based on the fundamental modes or eigen-currents induced in sections of wire(s) from impinging RF, and their nearest neighbor interactions. This may be viewed as charge flowing through a scatterer, which can be decomposed into a weighted summation of fundamental modes. It is the support and strength of these modes that form the basis for their frequency-dependent coupling and primary/secondary induction.

The current-state-of-research in RF effects/coupling work focuses on the prediction of the statistical coupling properties, which can be set up within arbitrary enclosures. Such efforts do not address the actual coupling to the electronics within these enclosures, although that is the future-art in development.

Introduction:

Electromagnetic weapons in the radio frequency range (700-MHz to 95-GHz) at on-target power densities that induce tenths- to ones-of-volts onto a printed circuit board trace, free wire, or other integrated circuit input (hereafter high-power microwaves or HPM) represent a single event effect (SEE) threat to microelectronics and their downstream applications. Developing a deeper understanding of how HPM couple to wires, traces, chasses, integrated circuits, and/or their enclosures, as a function of the source properties, is the objective of this proposed effort. A stretch objective is to understand further the secondary and tertiary coupling effects, including direct and inductive coupling. At the conclusion of this work, the vision is a balance of empirical- and simulation-derived results that will drive a generally applicable and pragmatic model (i.e., rules-of-thumb) that may be used to inform both the offensive and defensive side of HPM design and electronics and their enclosures.

Since at least the mid-1960s through today, electronic warfare – and to a lesser extent HPM – testing has been a staple for what is now MIL STD 464C. Empirical testing has been, and will likely continue to be, used as there is no current ability to generate sufficient (i.e., simple, but mostly accurate) models. This effects testing has been employed against assets ranging from motor vehicles to desktop computers to unmanned aerial vehicles to smartphones to instrument landing systems. While with enough detail and empirical feedback data, some models have been developed, but the models are not generalizable. Of those models that seek to be generalizable, they are too complicated to set up, inaccurate and/or ill-pragmatic. A new approach, which stands on the shoulders of this previous work, but harnesses the utility/power of new capabilities, is needed.

These new capabilities, whose confluence will take the above work to a new level, include the ability to: (a) map or predict the three-dimensional layout of complex electrical structures (e.g., wiring harness but not necessarily multilayer printed circuit boards); (b) automatically transfer the physical maps into simulation; (c) automatically approximate the complex permittivity/permeability of the materials; (d) run multi-source-parameter permutations on supercomputers inexpensively (through the ability to parallelize and run on an order-of-magnitude more cores/memory than two years earlier); (e) validate simulations through automated empirical measurements; and, (f) most of all, use machine learning methods to extract trends that the humans cannot.

In this work, we will design, build and test, an empirical measurement and simulation system capable of demonstrating the new capabilities described above to develop a predictive capability that is both simple and accurate enough to be useful for HPM effects and design needs.

Background:

One of the main techniques for predicting interference in metallic enclosures is the Random Coupling Model (RCM). The RCM addresses enclosures or cavities that are much larger than the wavelength of concern. Under this condition, the wave propagation inside the cavity is chaotic, meaning that any small change in the cavity or its components will lead to profoundly different outcomes. Based on the properties of the enclosure or cavity, such as its quality factor, statistical information about the voltages generated at the ports can be induced. In RCM, the ports can represent apertures in the enclosures or the input ports of devices and electronic circuitry inside the enclosure. Therefore, RCM aims to quantify the statistics of the interactions between the enclosures and its constituents. There are a number of other models (e.g., Dynamical Energy Analysis) and their predecessors that are important and form the basis for the work proposed here. We refer the reader to an exhaustive compilation of these works if greater background is desired (http://anlage.umd.edu/RCM/) as it is important that we shift gears to describe the background of the new effort proposed here.

Recently, we encountered a promising approach that uses an equivalent circuit approach to simulate RF coupling to systems loaded with nonlinear components [1]. This modeling approach is based on the fact that any antenna in the receiving mode, or in our wiring system through which back-RF coupling can occur, can be replaced by the classical Thevenin circuit shown in Fig. 1 [1]. The Thévenin equivalent circuit involves two main components defined at the receiving port of the antenna or the wire case a door by the

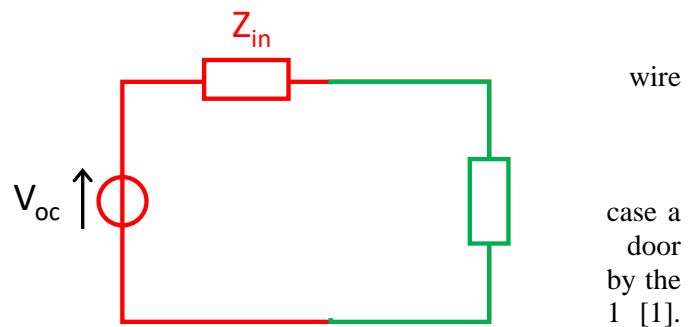Fig. 1: Thévenin equivalent circuit of coupling to a wire system [1].

wiring system: (i) the open-circuit voltage, Voc, and (ii) the input impedance Zin [2]. The input impedance Zin is typically replaced by an equivalent circuit as shown in Fig. 2. For typical antennas, the equivalent circuit consists of a series of parallel RLC circuits. Typically, one RLC circuit is needed for each resonance in the frequency band of interest. The Voc can be calculated by simulating the receiving antenna or the wiring system terminated with a very large load, ideally infinite. If a frequency-domain solver is used, the time domain Voc can be easily achieved via an inverse Fourier Transform.

The advantages of the equivalent circuit approach in Fig. 1 and Fig. 2 are:

1. It provides physical insight into the response of the wiring system. For example, if the equivalent circuit of a wiring system contains larger capacitance values, then it will quickly discharge the currents and voltages generated by a short pulse high power electronic microwave (HPEM) excitation preventing the buildup of energy in the nonlinear devices.

2. The above approach involves performing one full-wave simulation to calculate the Voc and Zin of the wiring system. After that, we can use much faster circuits simulations to simulate RF coupling to hundreds of possible nonlinear loads that can be connected to the wiring system. These simulations will be much faster when performed using a circuits solver such as LTSPICE than if they were performed using a full-wave solver. Also, this will allow us to simulate, in a feasible computational time, practical electronics and microcontrollers which tens of components.
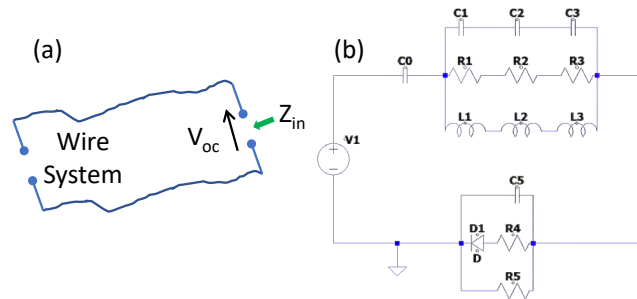

Fig. 2: (a) Dipole Antenna and (b) the circuit that emulates its input impedance [1].

In this work, we will use this approach to study RF coupling to wiring systems with nonlinear loads in realistic environments. More importantly, we also propose a combined approach where computational electromagnetics modeling will go hand-in-hand with experimental measurements.

13. Activities and Accomplishments

RF Coupling to Practical Wire Configurations with Multiple Nonlinear Loads

In many practical Devices Under Test (DUTs), the lengths of the wires connecting the different electronic components is comparable to the incident wavelengths. Therefore, the wires act as receiving antennas that convey the incident electromagnetic radiation to the electronic components and boards. The electronic components and boards act as loads to the wires. Therefore, to accurately quantify coupling to the DUT, the entire system of wires and electronic components needs to be accounted for. Direct RF coupling to the electronic components and boards starts to increase as the frequency of the incident radiation increases. In this report, we will quantify coupling to the wire systems that feed common electronic components and in future reports we will focus more on direct coupling to the electronic components and boards.

Wire Configuration with Multiple Nonlinear Loads

We successfully developed an accurate and computationally efficient full-wave model of the voltages and currents coupled to a wire system with multiple nonlinear loads. The model is based on the interaction between the full-wave and the schematics circuit simulator of CST-Microwave Studio (CST-MWS) [3]. Specifically, the wire system is simulated using full-wave analysis, and an equivalent circuit or S-parameters block is then developed. The loads are attached to the ports of this equivalent circuit or S-parameter block, and the entire system is then solved using the circuit/SPICE solver of CST MWS. This approach has the accuracy of the full-wave model plus the computational efficiency of the circuit/SPICE approach. Moreover, if the loads are varied and the wire system and excitation do not change, the full-wave analysis does not need to be repeated. The loads can be varied in the circuit/SPICE part of the solution at a considerable saving in computational cost. To illustrate the accuracy of this approach, the following example is introduced.

Consider the square loop shown in Fig. 3a with an overall contour length of 40 cm, $\ell = 10$ cm, and a 0.25 mm wire radius and excited by the Gaussian pulse shown in Fig. 4. Two different ports at two opposite locations on the loop are defined; the ports can be at any location, and the number of loads/ports can be more than two. The schematic view is shown in Fig. 3b. Any linear/nonlinear loads can be connected to the ports of the block that represents the wire loop's full-wave response.

Two linear loads have been chosen to compare this approach's accuracy with the Method of Moments (MOM)-based solver FEKO, a frequency-domain solver that cannot handle nonlinear load analysis [4]. Two configurations have been tested: (1) assigning 50 Ω for Load 1 and 1 MΩ for Load 2, and (2) assigning 100 Ω for Load 1 and 1 MΩ for Load 2. Any load variations do not require the re-simulation of the wire's full-wave response and therefore only requires a few seconds using the circuit/SPICE solver. Fig. 5 shows the coupled voltage to Load 1 calculated using both CST and FEKO. The model shows excellent agreement between the CST results and the independent full-wave FEKO, validity the CST approach.

In summary, the CST full-wave–Circuit/SPICE interface can be used as an accurate computationally efficient way to simulate a multi-load system. However, it doesn't provide physical insight into the coupling mechanism. In the next Section, we develop an equivalent circuit for the wire system which provides physical insight into the coupling mechanism and helps predict the effects on the attached electronic components.
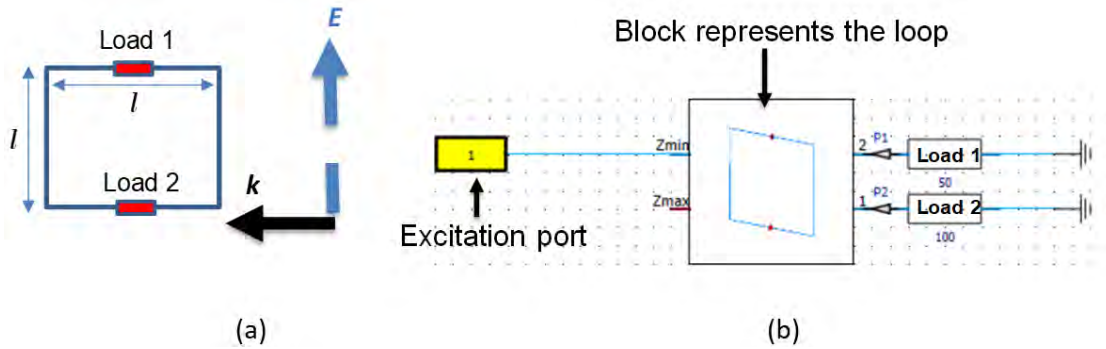

Fig. 3: (a) Sketch showing the loop configuration under investigation and the excitation direction, (b) Equivalent schematic view of the system.
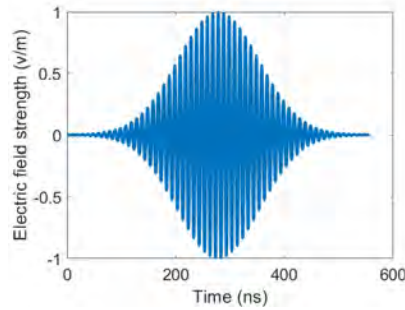

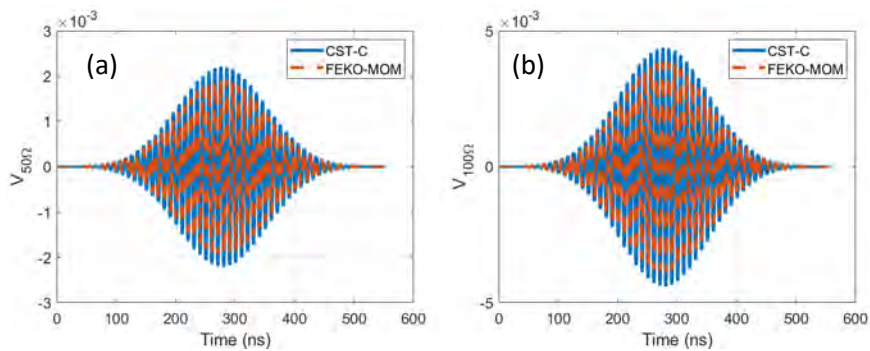Fig. 4: Electric field of the incident Gaussian Sinusoidal incident pulse.

Fig. 5: TD voltage across Load 1 when it is assigned an impedance value of (a) 50 Ω, (b) 100 Ω.

Voltage buildup in nonlinear loads: An Equivalent Circuit Approach

Diodes play a wide range of roles in electronic circuitry. Moreover, several electronic components have integrated diodes, especially for protection against Electrostatic Discharge (ESD). In this section, we study RF coupling to diodes. The dimensions of most discrete diodes are in the millimeter range requiring incident radiation in the millimeter range before any significant direct coupling can occur to these components. Therefore, the majority of RF coupling to diodes in the microwave range will occur via the wires connecting the diodes to the other components. We will develop guidelines on how the wires' properties affect coupling to common electronic components such as diodes.

Diodes typically have maximum ratings such as maximum reverse voltage and maximum forward rectified current. For example, the RB886CST2R Schottky diode has a maximum reverse voltage of 15 V and maximum forward rectified current of 10 mA [5]. The BAT54 Schottky diode has a maximum reverse voltage of 30 V and maximum forward rectified current of 200 mA [6]. We will also show how our tools can predict the incident excitation that will cause the voltage and current through the diode to exceed its maximum operating conditions.

For example, consider the square loop shown in Fig. 6a with a contour length of 40 cm and a 0.25 mm wire radius. We will use the Equivalent Circuit Approach (ECA) to model the wire loop with the linear/nonlinear loads. The equivalent circuit consists of two parts: the open-circuit voltage and an input impedance of the wires in addition to the loads' characteristics. The wire system was loaded by a nonlinear Schottky diode whose nonlinear response can be accurately modeled using the circuit in Fig. 6b. The diode D_{id} in Fig. 6b is an ideal diode, R_F is the forward resistance set to 190 Ω, R_R is the reverse resistance set to 40 MΩ, and C_j is the diode capacitance that will be varied to show its effect on the voltage buildup across the diode. Two Gaussian sinusoidal pulses are used to excite the loop: (*i*) A pulse whose amplitude is 10 V/m and (*ii*) A pulse whose amplitude is 100 V/m. Both pulses are designed to have the same characteristics i.e. a center frequency of 0.355 GHz, a 10 % bandwidth, and a 4 MHz PRF. The 10 V/m Gaussian pulse is shown in Fig. 7.
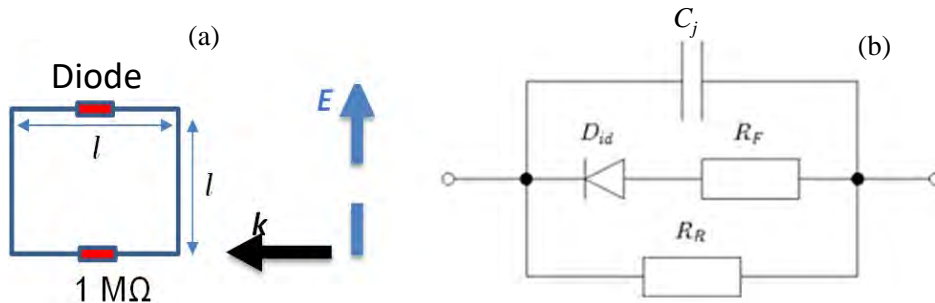

Fig. 6: (a) Sketch showing the loop configuration under investigation and the excitation direction, (b) Equivalent circuit of the nonlinear Schottky diode.
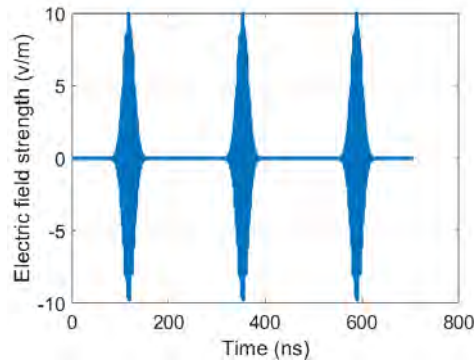
Fig. 7: Electric field of the incident pulse with 10 V/m amplitude.

The junction capacitance of the diode, C_j, is varied from 1 pF to 500 pF. For these capacitance values, Fig. 8a and Fig. 8b show the coupled voltage for the 100 V/m and 10 V/m Gaussian sinusoidal pulses, respectively. The electric field of the pulse in Fig. 8a is ten times larger than the pulse in Fig. 8b, yet the coupled voltage in Fig. 8a is more than ten times larger than the coupled voltage in Fig. 8b due to the nonlinear nature of the load. For example, when $C_j = 1$ pF, the negative peak of the coupled voltage in Fig. 8a is -15 V, which is more than ten times larger than the negative peak of the coupled voltage in Fig. 8b, -1 V. Hence, increasing the amplitude of the incident electric field might lead to a larger increase in voltage coupled to nonlinear loads which should be taken into consideration when studying effects. The DC voltage buildup vanishes for most C_j values in Fig. 8b due to the lower incident electric field used in this case. For example, for $C_j = 25$ pF and after 1200 ns, Fig. 8a shows that the buildup voltage is -2.5 V, whereas Fig. 8b shows that the buildup voltage is almost zero.

Both Fig. 8a and Fig. 8b show that the coupled voltage decreases as the junction capacitance C_j increases. For example, Fig. 8a shows that increasing C_j from 1 pF to 25 pF decreases the buildup voltage at 1200 ns from -5 V to -2.5 V. The physical explanation of this trend is that the coupled charge to the wire configuration, Q, depends only on the wire and the excitation and not the load [7]. The voltage across the diode, V, is inversely proportional to its capacitance following the classical formula $V = Q/C_j$ as hypothesized in [7]. Therefore, increasing C_j will decrease the coupled voltage. Thus, the results in Fig. 8 indicate that significant DC voltage buildup in a nonlinear component, which leads to energy storage, only appears when the incident electric field exceeds a certain threshold and for certain C_j values of the nonlinear diode.
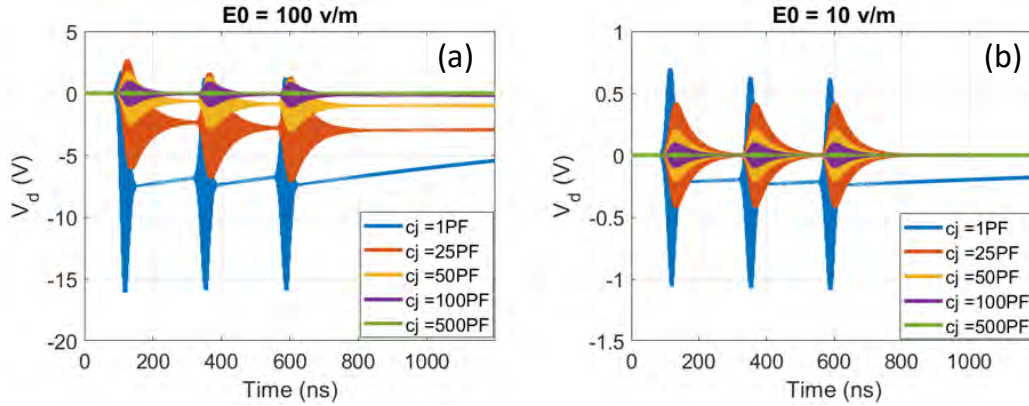
Fig. 8: Induced voltage across the nonlinear diode calculated using the Thévenin Equivalent circuit approach (SPICE) for different capacitance values when the loop is excited by (a) 100 V/m pulse, (b) 10 V/m.

The C_j values in Fig. 6 are fictitious, but they clearly show the coupling trends. However, it is important to test the above conclusions for practical diodes. Therefore, 5 different practical diodes are used as the load for the loop shown in Fig. 6a. Fig. 9 shows that the voltage across the studied diodes follows the conclusions reported above. That is, the diodes with the smallest capacitance will have the highest coupled voltage and vice versa.
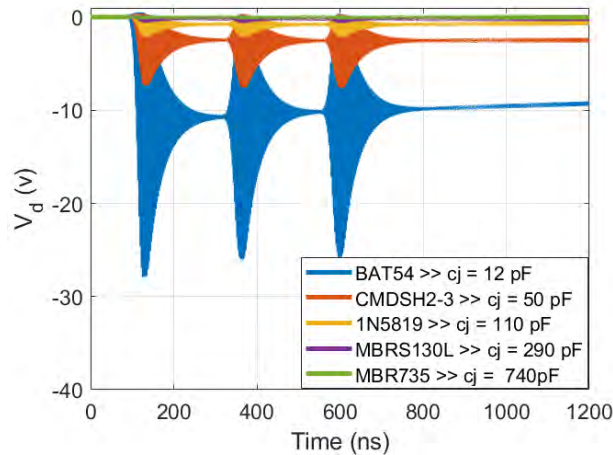

Fig. 9: Induced voltage across the nonlinear diode calculated using the Thévenin equivalent circuit approach (SPICE).

Experimental Validation of the Voltage Build-up Across a Nonlinear Component

The following experimental setup was developed to test the existence of the voltage build-up across a RB886CST2R Schottky diode as shown in Fig. 10. The diode was soldered to a square wire loop at one end and the other end of the wire loop was attached via a coaxial cable to an oscilloscope. The input impedance of the oscilloscope was varied to create different effective impedances, through the coaxial cable, to the wire loop. The GTEM was excited by a waveform generator followed by an amplifier to boast the incident field to the desired level. In the experiments below, the waveform generator was programmed

26

to generate a Gaussian Sinusoidal pulse centered around 777 MHz with a 10% bandwidth. The electric field amplitude was boosted to around 150 V/m. In the current experimental setup, we can only access the oscilloscope measurements which measure the voltage across the load opposite to the diode shown in Fig. 6a. However, we can use this voltage to infer the voltage and the current through the diode.

Fig. 11 shows the voltage across the load for different Pulse Repetition Frequencies (PRFs). For PRF below 10 kHz, there was no voltage build up. The higher the PRF the higher the build-up voltage. For example, at a PRF of 2.5 MHz, the voltage buildup reached a steady state value of -15 V. The experimental measurements in Fig. 11 prove the existence of the voltage buildup shown in the simulations in Fig. 8 and Fig. 9. This voltage buildup across the diode can potentially exceed the maximum allowable reverse voltage of the diode, affecting its functionality. Further experiments and simulations will be performed to quantify the voltage buildup and its effect on the operation status of the diode.
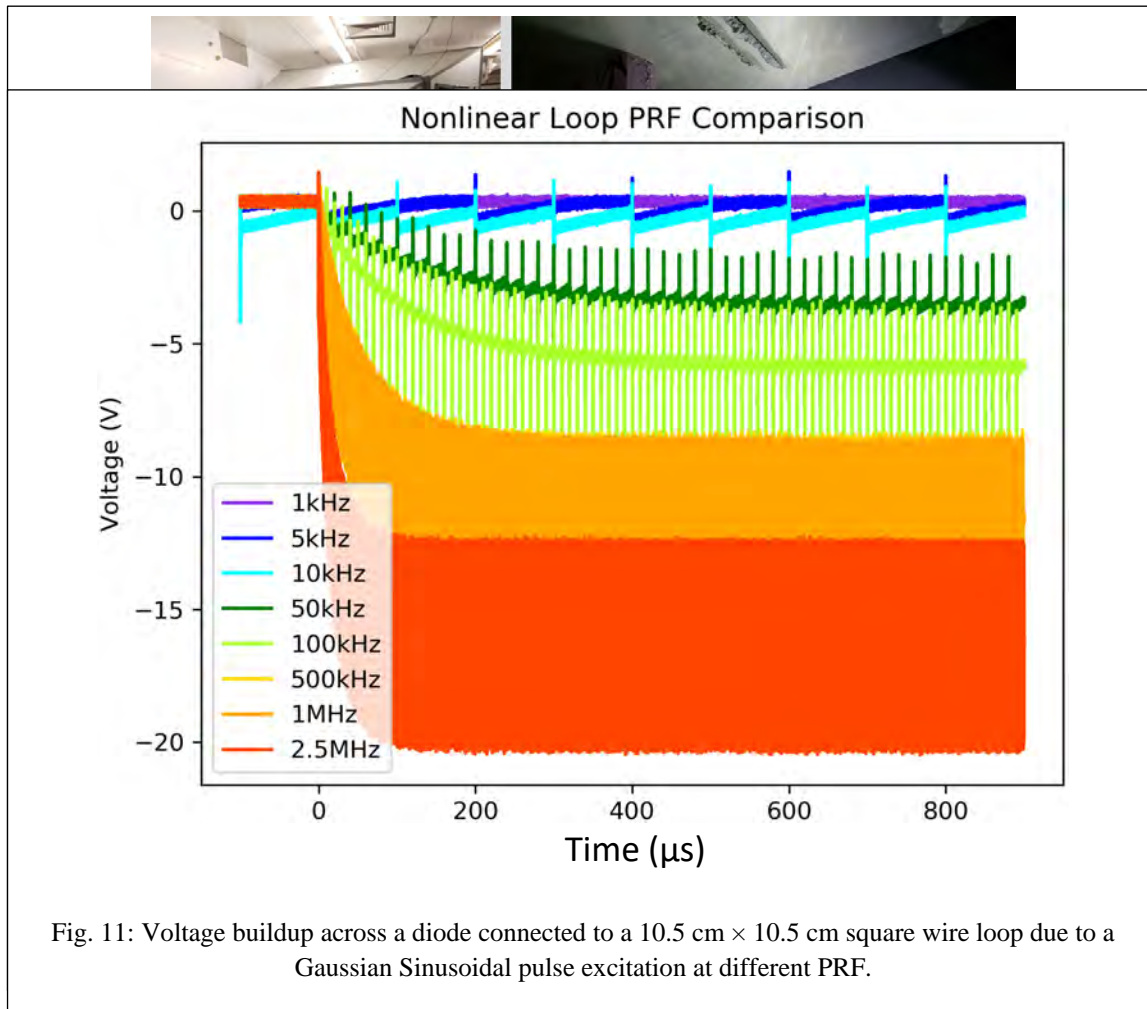

Fig. 11: Voltage buildup across a diode connected to a 10.5 cm × 10.5 cm square wire loop due to a Gaussian Sinusoidal pulse excitation at different PRF.

14.   Findings and Conclusions

Most of the previously reported studies do not fully quantify the reason behind the voltage buildup across nonlinear devices and when this voltage buildup occurs. Fig. 12a shows the square wire loop where the diode is attached. The wire system in Fig. 12a was excited by a Gaussian Sinusoidal pulse centered around
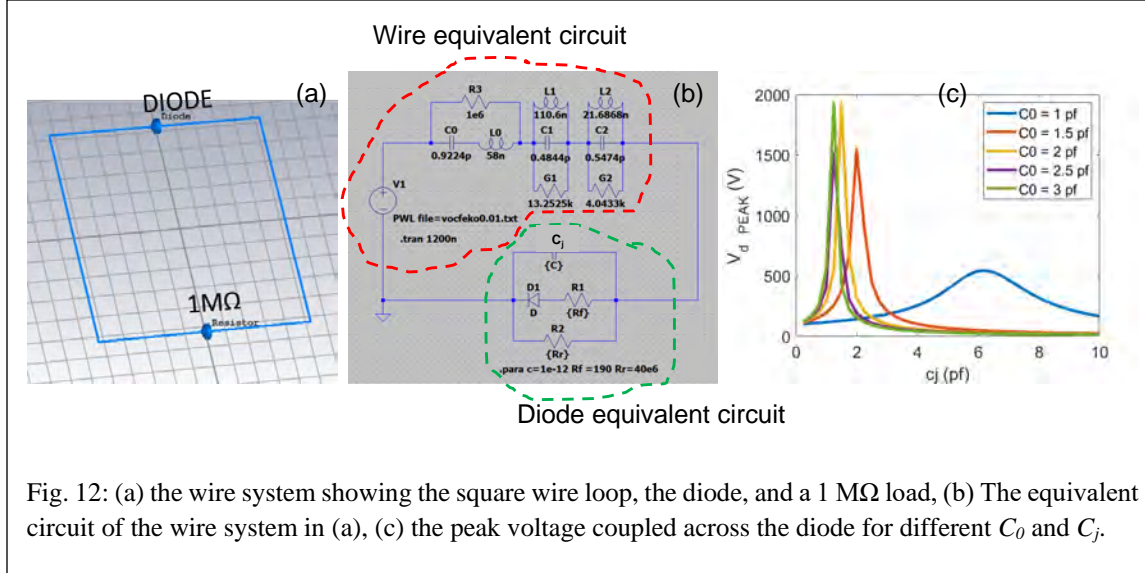

Fig. 12: (a) the wire system showing the square wire loop, the diode, and a 1 MΩ load, (b) The equivalent circuit of the wire system in (a), (c) the peak voltage coupled across the diode for different C_0 and C_j.

0.33 GHz. Fig. 12b shows the equivalent circuit of the system in Fig. 12a divided into an equivalent circuit for the wires connected to the equivalent circuit of the diode. We varied both the junction capacitance of the diode, C_j, as well as varying one of the capacitances in the equivalent circuit of the wires, C_0. Variations in C_0 can be created by varying the wire properties, whereas variations in C_j can be achieved when different diodes are used. For each case, we calculated the peak voltage across the diode and plotted the results in Fig. 12c. Fig. 12c clearly shows that decreasing the diode's junction capacitance C_j increases the peak voltage across the diode up to a certain value similar to the trend discussed in the previous section. A significant finding is that once the junction capacitance becomes significantly smaller than the wire capacitance, C_0, the trend reverses. That is, for C_j values much smaller than C_0, decreasing C_j will cause the peak voltage across the diode to decrease. For example, at $C_0 = 1$ pF, decreasing C_j from 10 pF to 6 pF increases the peak voltage across the diode from 200 V to a maximum value of 500 V. But decreasing C_j further causes the peak voltage across the diode to drop. This more accurately defines the dependency of the buildup voltage across the diode and helps in predicting the effects of different excitations on the wire system in Fig. 12a.

28

References:

[1] R. Michels, M. Willenbockel, and F. Gronwald, "A Parametric Study of an Energy Storage Effect due to Nonlinear Components and HPEM-Excitation," in 2019 International Symposium on Electromagnetic Compatibility - EMC EUROPE, Barcelona, Spain, 2019, pp. 59–64, doi: 10.1109/EMCEurope.2019.8871855.

[2] M. Kotzev, X. Bi, M. Kreitlow, and F. Gronwald, "Equivalent circuit simulation of HPEM-induced transient responses at nonlinear loads," Adv. Radio Sci., vol. 15, pp. 175–180, Sep. 2017, doi: 10.5194/ars-15-175-2017.

[3] https://www.3ds.com/products-services/simulia/products/cst-studio-suite/

[4] https://altairhyperworks.com/product/FEKO

[5] https://www.mouser.com/datasheet/2/348/rohm%20semiconductor_rb886cs-1201530.pdf

[6] https://media.digikey.com/pdf/Data%20Sheets/ON%20Semiconductor%20PDFs/BAT54(A,C,S).pdf

[7] R. Michels, M. Schaarschmidt, and F. Gronwald, "Experimental Investigation of a Nonlinear Energy Storage Effect due to High Power Electromagnetic Excitation," Advances in Radio Science, vol. 18, no. E, pp. 75-82, 2020.

15.   Plans and Upcoming Events

Throughout this project, we developed several computational tools such as the Characteristic Mode Analysis (CMA) and the Equivalent Circuit Approach (ECA) to predict RF coupling to a wide range of wire systems with linear/nonlinear loads. We also performed unique experimental measurements to validate the predictions of our computational tools. Our immediate plan of action is to show how the unique tools we have developed so far can be beneficial for practical configurations and not just for simple wire systems. Therefore, we plan to study RF coupling to various consumer electronic components connected to multiple realistic cables, harnesses, and twisted wire pairs. An example, of a practical system is shown in Fig. 13. In Fig. 13, we will replace each electronic component with its equivalent circuit to quantify the coupled voltages and currents at different points in the system.

Fig. 13: (a) Example of a practical wiring system and (b) proposed models for common electronic components.
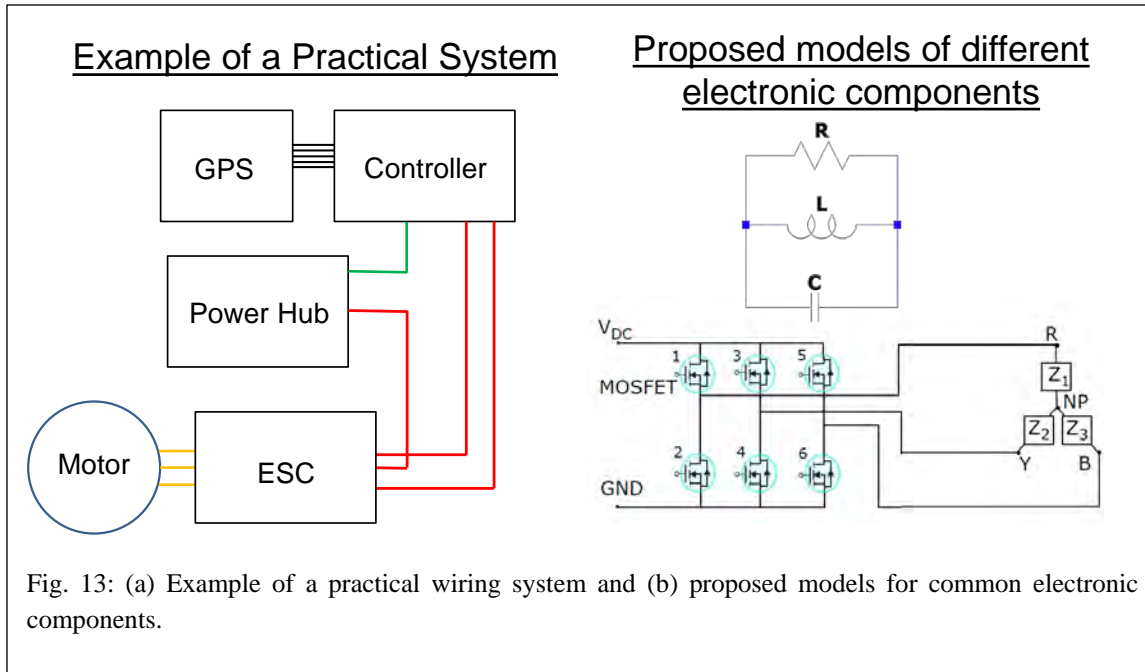
We also plan to focus more on the direct coupling to common electronic components with no wires attached. Direct coupling to electronic components might dominate at higher frequencies and we propose to identify the frequencies where direct coupling to electronic components is significant. A comparison between coupling to common electronics with and without wires attached will also be performed.

The ultimate goal of this work is to develop a computational physics-based RF-coupling prediction tool. The key to this tool is that it will be physics-based and not statistical, and therefore it should be capable of predicting RF coupling to new DUTs not used in its development.

Milestones:

Year 1

   1- CMA of Single Wire
   2- CMA of few Wires

Year 2

   1- CMA of practical Wire Systems
   2- Big Data acceleration of CMA
   3- CMA of wires in a realistic environment (e.g. PCB, perforated metallic cavities, in the vicinity of a UAV frame)

Year 3

   1- Statistical analysis of multiple wire configurations
   2- Develop general RF coupling guidelines to practical wire systems
   3- RF coupling analysis of nonlinear DUT.

Year 4
   1- Continue the analysis of practical wire systems to develop general RF coupling guidelines and trends
   2- Quantify direct RF coupling to common consumer electronics over a wide range of frequencies.

5. Transitions and Impacts

The highly efficient computational tools and trends, validated using experimental measurements and accelerated using Big Data techniques, will be augmented with adequate Graphical User Interfaces (GUI) and documentations and presented for the general use of ONR and its defense contractors, e.g. Verus Research (http://www.verusresearch.net/). Moreover, the CMA conclusions and the statistical analysis will be used in FY2021 to prepare several journal papers and monographs to act as accurate guidelines for RF coupling and interference mitigation and protection.

6. Collaborations

➤ Professor Daryl Beetner, Missouri University of Science and Technology, Electromagnetic Compatibility Lab
➤ Associate Professor, Victor Khilkevich, Missouri University of Science and Technology, Electromagnetic Compatibility Lab
➤ Associate Professor, Zhen Peng, University of Illinois, Electrical and Computer Engineering Department.
➤ Assistant Professor, Sayan Roy, South Dakota School of Mines & Technology, Electrical Engineering Department

7. Personnel

Principal investigator
   Anthony N. Caruso, National Academy Member (Y/**N**)

Co-investigator or Co-PI
   Ahmed Hassan, National Academy Member (Y/**N**)

Business Contact
   Linda Daugherty, Leta Moler

Team Members:
   Deb Chatterjee, Praveen Rao, John Lancaster, Mohamed Hamdalla, Kalyan Durbhakula, Waleed Al-Shaikhli, Khulud Alsultan, Khadimul Islam, Clayton Kettlewell, Benjamin Bissen, Mustafa Yildirim, National Academy Member (Y/**N**)

8. Students

Undergraduate Students: Clayton Kettlewell, Mustafa Yildirim.

Graduate Students: Benjamin Bissen, John Lancaster, Mohamed Hamdalla, Kalyan Durbhakula, Waleed Al-Shaikhli, Khulud Alsultan, Khadimul Islam

9. Technology Transfer

None

10. Products, Publications, Patents, License Agreements, etc.
Publications resulting from this project:

<u>Archival Publications</u> (publication reference information (article title, authors, journal, date, volume, issue) can be automatically entered using a DOI)

    a.   *Article Title:* Predicting Electromagnetic Interference to a Terminated Wire Using Characteristic Mode Analysis
    b.   *Journal*: ACES JOURNAL
    c.   *Authors*: M. Hamdalla, A. N. Caruso, A. M. Hassan
    d.   *Keywords*: Field-to-wire coupling, Characteristic Mode Analysis, Shapes, Full-wave analysis
    e.   *Distribution Statement*: Distribution A.
    f.   *Publication Status*: Published
    g.   *Publication Identifier Type*: DOI
    h.   *Publication Identifier*: https://doi.org/10.47037/2020.ACES.J.351128
    i.   *Publication Date*: 2020
    j.   *Volume*: 35
    k.   *Issue*: 11
    l.   *First Page Number*: 1318-1319
    m.   *Publication Location*: New Jersey, USA
    n.   *Acknowledgement of Federal Support?* Yes
    o.   *Peer Reviewed*? Yes

    a.   *Article Title:* Prediction of Experimental Electromagnetic Coupling to a UAV Model Using Characteristic Mode Analysis
    b.   *Journal*: IEEE Transactions on Electromagnetic Compatibility
    c.   *Authors*: M. Hamdalla, Benjamin Bissen, V. Khilkevich, D. G. Beetner, A. N. Caruso, A. M. Hassan
    d.   *Keywords*: Field-to-wire coupling, Characteristic Mode Analysis, Shapes, Full-wave analysis
    e.   *Distribution Statement*: Paper is still under preparation and has not been submitted. Authors will submit the paper for review and approval. However, authors believe paper can be Distribution A.
    f.   *Publication Status*: Under Preparation
    g.   *Publication Identifier Type*:
    h.   *Publication Identifier*:
    i.   *Publication Date*: 2021
    j.   *Volume*:
    k.   *Issue*:
    l.   *First Page Number*:
    m.   *Publication Location*: New Jersey, USA
    n.   *Acknowledgement of Federal Support?* Yes
    o.   *Peer Reviewed*? Yes

a. *Article Title:* Characteristic Mode Analysis Justification of the Stochastic Electromagnetic Field Coupling to Randomly Shaped Wires.
b. *Journal*: IEEE Transactions on Electromagnetic Compatibility
c. *Authors*: M. Hamdalla, V. Khilkevich, D. G. Beetner, A. N. Caruso, A. M. Hassan
d. *Keywords*: Field-to-wire coupling, Characteristic Mode Analysis, Shapes, Full-wave analysis
e. *Distribution Statement*: Paper is still under preparation and has not been submitted. Authors will submit the paper for review and approval. However, authors believe paper can be Distribution A.
f. *Publication Status*: Under Preparation
g. *Publication Identifier Type*:
h. *Publication Identifier*:
i. *Publication Date*: 2021
j. *Volume*:
k. *Issue*:
l. *First Page Number*:
m. *Publication Location*: New Jersey, USA
n. *Acknowledgement of Federal Support?* Yes
o. *Peer Reviewed*? Yes

a. *Article Title:* Scalable and Fast Characteristic Mode Analysis Implementation Using a Hybrid CPU/GPU Platform
b. *Journal*: IEEE Open Journal of Antennas and Propagation
c. *Authors*: Khulud Alsultan, Mohamed Hamdalla, Sumitra Dey, Anthony N. Caruso, Praveen Rao, and Ahmed Hassan
d. *Keywords*: Big Data, Characteristic Mode Analysis
e. *Distribution Statement*: Paper is still under preparation and has not been submitted. Authors will submit the paper for review and approval. However, authors believe paper can be Distribution A.
f. *Publication Status*: Under Preparation
g. *Publication Identifier Type*:
h. *Publication Identifier*:
i. *Publication Date*: 2021
j. *Volume*:
k. *Issue*:
l. *First Page Number*:
m. *Publication Location*: New Jersey, USA
n. *Acknowledgement of Federal Support?* Yes
o. *Peer Reviewed*? Yes

Conference Papers

1. J. Hunter, S. Xia, A. Harmon, A. M. Hassan, V. Khilkevich, D. Beetner, "Modeling and Statistical Characterization of Electromagnetic Coupling to Electronic Devices," *URSI National Radio Science Meeting*, Boulder, CO, January 4-9, 2021.
2. M. Hamdalla, B. Bissen, A. N. Caruso, and A. M. Hassan, "Experimental Validations of Characteristic Mode Analysis Predictions Using GTEM Measurements," *IEEE International Symposium on Antennas and Propagation and USNC-URSI Radio Science Meeting at Montréal, Québec, Canada, July 5-10, 2020.*

3. M. Hamdalla, A. N. Caruso, and A. M. Hassan, "Predicting Electromagnetic Interference to a Terminated Wire Using Characteristic Mode Analysis," *Proceedings of the Annual Review of Progress in Applied Computational Electromagnetics (ACES)*, Monterey, CA, March 22-26, 2020.
4. M. Hamdalla, A. N. Caruso, Ahmed M. Hassan, "Characteristic Mode Analysis of the Effect of the UAV Frame Material on Coupling and Interference," *IEEE International Symposium on Antennas and Propagation and USNC-URSI Radio Science Meeting at Atlanta (2 pages)*, Georgia, USA, 7-12 July 2019.
5. M. Hamdalla, J. Hunter, Y. Liu, V. Khilkevich, D. Beetner, A. Caruso, Ahmed M. Hassan, "Electromagnetic Interference of Unmanned Aerial Vehicles: A Characteristic Mode Analysis Approach," *IEEE International Symposium on Antennas and Propagation and USNC-URSI Radio Science Meeting at Atlanta (2 pages)*, Georgia, USA, 7-12 July 2019.
6. K. Durbhakula, J. Lancaster, J. Hunter, Y. Liu, D. Beetner, V. Khilkevich, D. Chatterjee, A. Caruso, Ahmed M. Hassan, "Electromagnetic Coupling Analysis of Printed Circuit Board Traces using Characteristic Mode Analysis," *IEEE International Symposium on Antennas and Propagation and USNC-URSI Radio Science Meeting at Atlanta (2 pages)*, Georgia, USA, 7-12 July 2019.
7. K. Alsultan, P. Rao, A. N. Caruso, and Ahmed M. Hassan, "Scalable characteristic mode analysis using big data techniques," *International Symposium on Electromagnetic Theory (EMTS 2019)*, San Diego, CA, USA, May 27-31, 2019.
8. M. Z. M. Hamdalla, W. Al-Shaikhli, J. Lancaster, J. D. Hunter, L. Yuanzhuo, V. Khilkevich, D. G. Beetner, A. N. Caruso, and Ahmed M. Hassan, "Characteristic Mode Analysis of Electromagnetic Coupling to Wires with Realistic Shapes," *International Symposium on Electromagnetic Theory (EMTS 2019)*, San Diego, CA, USA, May 27-31, 2019.
9. C. Hartshorn, K. Durbhakula, D. Welty, D. Chatterjee, J. Lancaster, Ahmed M. Hassan, A. N. Caruso, "Crosstalk and Coupling to Printed Circuit Board Metallic Traces with Arbitrary Shapes," *Proceedings of the AMEREM 2018 Conference*, Aug 27-31, Santa Barbra, CA, 2018.
10. M. Hamdalla, J. Roacho-Valles, J. Hunter, D. Beetner, Ahmed M. Hassan, A. N. Caruso, "Electromagnetic Analysis of Unmanned Aerial Vehicles Using Characteristic Mode Analysis," *Proceedings of the AMEREM 2018 Conference*, Aug 27-31, Santa Barbra, CA, 2018.
11. C. Hartshorn, M. Hamdalla, J. Lancaster, Ahmed M. Hassan, A. N. Caruso, "Electromagnetic Vulnerability of Wires with Arbitrary Shape," *Proceedings of the AMEREM 2018 Conference*, Aug 27-31, Santa Barbra, CA, 2018.
12. M. Hamdalla, Ahmed M. Hassan, A. N. Caruso "Characteristic Mode Analysis of Unmanned Aerial Vehicles with Realistic Shapes and Material Composition," *IEEE International Symposium on Antennas and Propagation and USNC-URSI Radio Science Meeting at Boston*, MA, 2018.

11. Point of Contact in Navy

➤ Ryan Hoffman, ONR, ryan.hoffman@navy.mil, Date of Last Research Progress Meeting: 09/11/2018
➤ Matthew McQuage, Naval Surface Warfare Center Dahlgren, matthew.mcquage@navy.mil, Date of Last Research Progress Meeting: 09/11/2018

12. Acknowledgement/Disclaimer

Fundamental Studies for Nanoscale Vacuum Electronic Emission Devices

Prepared by:

Professor Ravi P Joshi, Principal Investigator
Texas Tech University
Department of Electrical and Computer Engineering
2500 Broadway MS 3102/Campus
Lubbock TX 79424
Tel: 806-834-7979
Email: ravi.joshi@ttu.edu
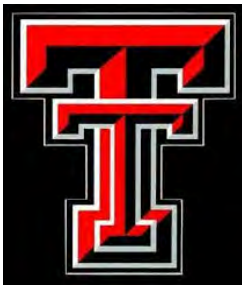
Grant Number: N00014-18-1-2382
Date Prepared: January 30, 2021
Project Title: Fundamental Studies for Nanoscale Vacuum Electronic Emission Devices
Annual Summary Report: FY2020
Principle Investigator: Ravi P Joshi, 806-834-7979, Email: ravi.joshi@ttu.edu
Texas Tech University, Lubbock, TX 79409.

Section I: Project Summary

1. Overview of Project

Abstract: The goals of this research focus on simulations and basic research for electron emission in vacuum electronics and high power applications. Study of outgassing is important as it can alter the space-charge and efficiency of high power microwave (HPM) systems. Optimization of emission currents is another objective for robust electron beam generation for HPM devices. Hence, study of electron emission in arrays taking account of screening, field enhancement at emitters, and dynamic space-charge effects becomes important and merits analysis. The presence of oxide layers at emitter surfaces or the impact of defects or surface treatments also influence performance and enhanced lifetime of the high power systems. All of the above aspects have been studied as part of this research and are discussed in this report.

Objectives: Cathode emitters are important components of high power microwave devices. For example, in the magnetically insulated transmission line oscillators (MILOs), quality of cathode arrays have been shown to affect the beam quality, uniformity, stability, and performance. Our project focusses on physics-based modeling and complements the MILO development at Texas Tech University (TTU) for the Navy. This effort helps the MILO work with regard to: (a) understanding and optimizing electron emission as the source of microwave power, (b) optimal spacing and design of emitter arrays, and (c) in evaluating the role of outgassing and schemes for its mitigation in HPM systems.

Introduction: Project activities so far have included electron emission, outgassing, current-voltage characteristics for emitter arrays taking account of screening and proximity effects, and the role of surface defects in modifying electron emission with some useful material physics dimensions. Collaboration with Dr. J. Mankowski and Dr. Sanati (TTU) have brought synergies.

Background: Study of emission from cathodes is being studied at multiple levels: (a) electron emission from surface emitters based on self-consistent calculations of quantum tunneling with wavefunction modifications by electric fields and an oxide layer, (b) temperature-dependent outgassing with supporting Molecular Dynamics (MD) analysis in copper and carbon fibers, and (c) current from emitter arrays including electric field modifications due to proximity, screening, and space-charge effects with many-body Coulomb interactions.

2. Activities and Accomplishments

(A) Modeling Electric Fields for Emitter Arrays

The proximity effect of emitters in an array is well known and leads to screening which lowers field emission and total current. Since field screening increases with reductions in emitter separation, high density close-packed arrays would not necessarily produce maximal total current output. At the edges and rim of an array, the screening influence is reduced since the number of neighbors falls. While current enhancements from array edges might seem a favorable outcome, there is an increased risk of heating and emitter degradation in the peripheral locations.

Carbon fiber cathodes offer many advantages over traditional metallic cathodes, such as low outgassing, which leads to lower plasma expansion and longer high-power microwave (HPM) pulse generation. Carbon fiber cathodes outperform both their metallic and velvet counterparts in terms of long-life operation and long-pulsed microwave generation. In experiments, bimodal carbon fibers were seen to radiate more microwave power than CsI-coated cathodes, or bare unimodal cathodes. Hence, bimodal emitter arrays are examined here.

Electron transport in such arrays was modelled based on a kinetic particle-in-cell scheme. The treatment comprehensively included: (i) many-body interactions, (ii) mutual coupling between emitters based on the Linear Charge Model (LCM), and (iii) evolution of the internal electric fields associated with the space-charge via a particle-particle-particle-mesh (P^3M) scheme. An overall honeycomb structural arrangement of bimodal emitters was chosen as it is reported to produce higher currents than a rectangular pattern.

Figure 1(a) shows the honeycomb arrangement with nineteen emitters all with 1.0 μm heights. The steady state current shown in Figure 1(b) was obtained. The curve (Fig. 1b) flattens out for distances beyond ~2.5 μm in keeping with reports that found shielding to be negligible for separations larger than 2.5 times the emitter height. Figure 1(c) shows electric field scaling factors at different tips of a nineteen-emitter array as a function of emitter separation. The largest reduction is for the central emitter, with milder effects going outwards from the center.
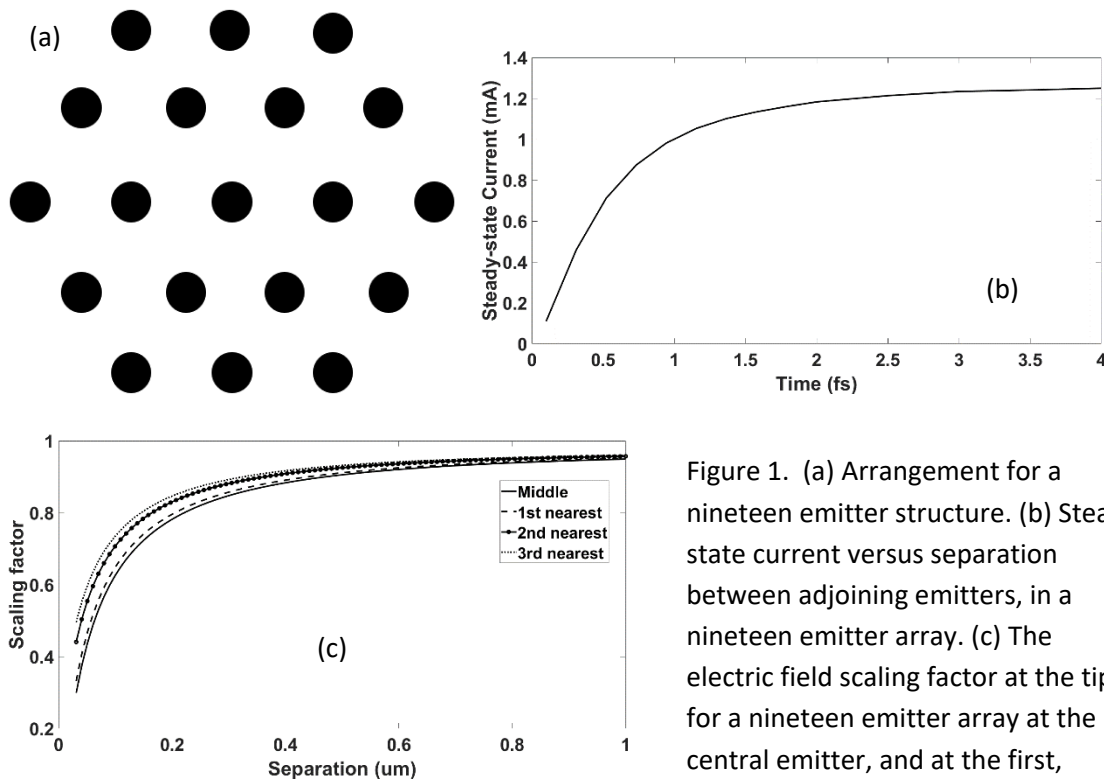
Figure 1. (a) Arrangement for a nineteen emitter structure. (b) Steady state current versus separation between adjoining emitters, in a nineteen emitter array. (c) The electric field scaling factor at the tip for a nineteen emitter array at the central emitter, and at the first, second and third nearest emitters from the center.

Figure 2 shows steady state currents obtained versus number of (1 μm) emitters with emitter spacing as the second variable. Best results are for separations beyond 2.5 μm, though the onset of diminishing gains is obvious. Also, current is actually predicted to reduce for emitter spacings below 0.2 μm due to strong screening regardless of the number of emitters used.
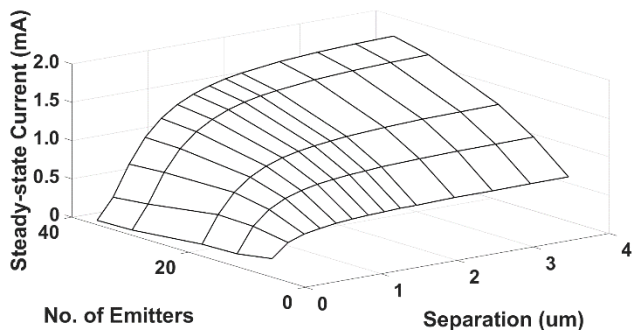

Figure 2. Results showing the total current versus number of emitters in an array, with the nearest neighbor separation as a second variable.

Results of steady state currents for a nineteen-emitter array with a bimodal distribution are shown in Fig. 3, with one set of emitters of height 1.0 μm and a shorter group with 0.9 μm height. Three different configurations are given in Figures 3(a)-3(c). Results for the total current from the seven-emitter array shown in Figure 4 for a nearest neighbor distance of 0.1 μm reveal the alternating arrangement of Fig. 3(b) yields the highest current.
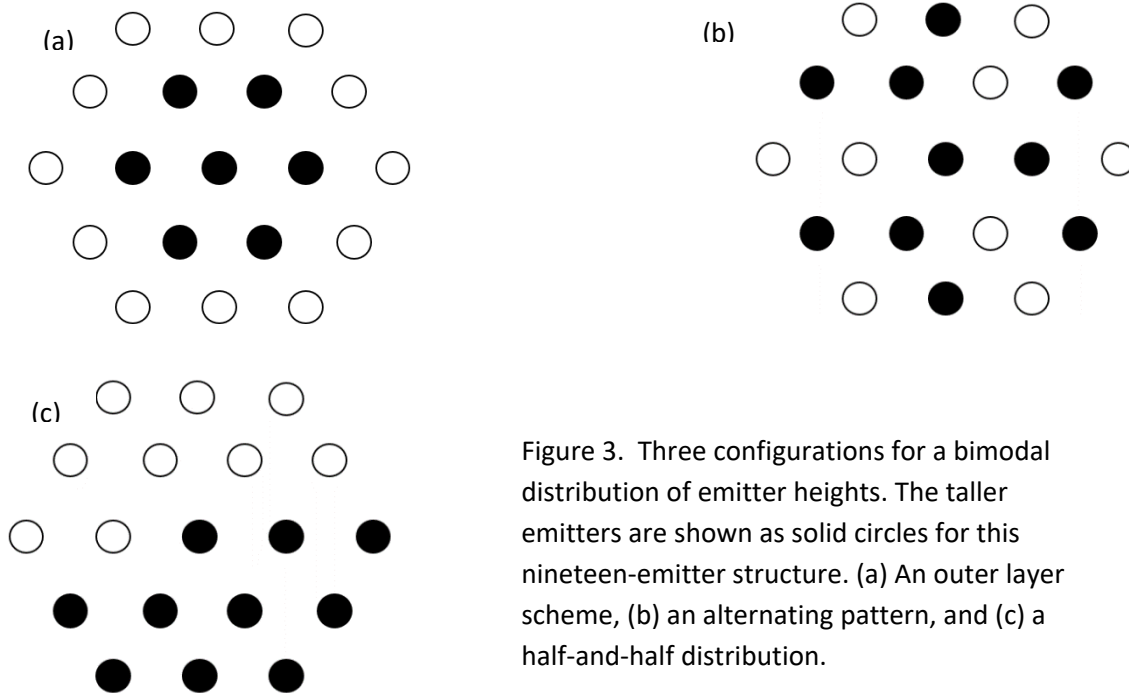
(a)

(b)

(c)

Figure 3. Three configurations for a bimodal distribution of emitter heights. The taller emitters are shown as solid circles for this nineteen-emitter structure. (a) An outer layer scheme, (b) an alternating pattern, and (c) a half-and-half distribution.

Numerous simulations were carried out which seemed to indicate the following maximum output current strategy for arranging emitters in the hexagonal array: (i) Placement of a tall emitter at the center of the hexagonal structure. (ii) Next, begin placing short-and-long emitters in an alternating manner. (iii) Having completely finished placing emitters at all sites along the outermost periphery, move to the next largest closed path. (iv) Repeat the procedure of assigning either long or short emitters in an alternating manner, with progressive movement to ever smaller rings. (v) However, if in the process of completing the entire placement, the final structure were to have three successive emitters of the same length along any of the three primitive axes, then reject the arrangement. In such a situation, a new choice of emitter placement would have to be restarted from the previously completed ring to avoid the occurrence of three successive emitter placements along any of the basis directions.
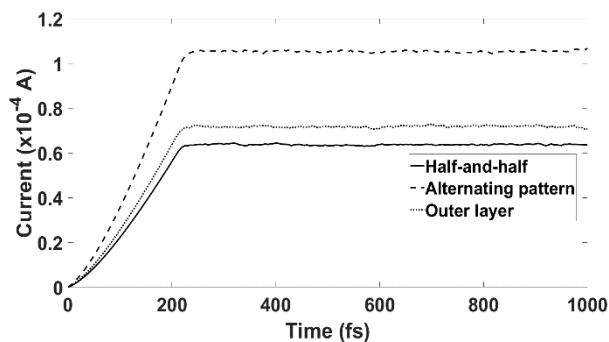

Figure 4. Time dependent total current predicted for the three bimodal nineteen-emitter array configurations described in Figure 3. The largest current magnitude results from the alternating scheme.

As an example, four possible arrangements for a thirty-seven emitter array are shown in Figures 5(a)-5(d). Only the last configuration (alternate-strategy) meets all conditions of the outlined scheme. The resulting currents for the four cases are shown in Fig. 6, with the highest current of ~5.5x10^{-5} A seen to result from the structure based on the alternate-strategy.
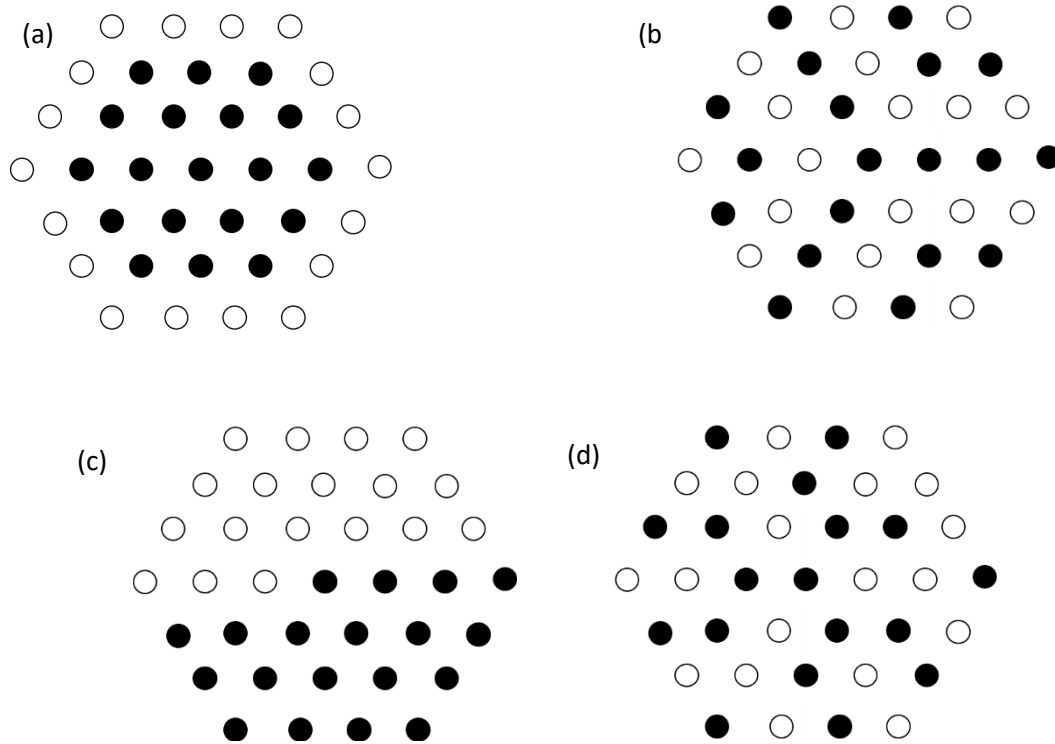

Figure 5. Four bimodal configurations of thirty-seven emitters. Taller emitters are shown as solid circles. (a) An outer layer scheme, (b) alternating pattern, (c) half-and-half scheme, and (d) an alternate-strategy.

(B) Simulations of Outgassing and Sticking in Copper Electrodes

Gas desorption from materials can be an important factor in plasma formation in high power microwave systems. This can then lead to breakdown, surface flashover, anode-cathode gap closure and pulse shortening. Outgassing though, which has received some attention, represents
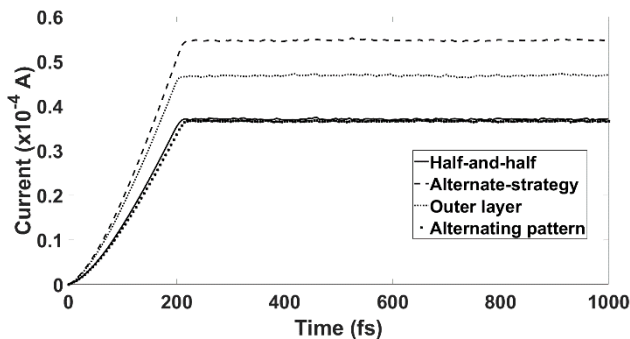

Figure 6. Time dependent total current predicted for the four bimodal thirty-seven emitter array configurations described in Figure 10. The largest current magnitude results from the alternate-strategy.

only part of the overall picture. For a complete analysis, it is also important to assess the possible attachment or deposition which can either lead to gaseous entry back into the metal from the near-vacuum region of an HPM device, or physiosorption at the surface. For simulations of the sticking coefficient, simulations were

carried out to gauge the reflection or absorption of hydrogen atoms from the surface of a copper slab. The reflection coefficient was simply obtained from the fraction of incident particles that re-emerged back after interacting with the copper. Results for temperature-dependent diffusion coefficients for hydrogen in pure copper and in the presence of a discrete set of vacancies, are shown in Figure 7. For comparison, data reported previous by various groups are also shown in Figure 7 for ideal copper. A fairly good agreement between data and the calculations is evident. *Due to trapping of H atoms at a vacancy the values in Figure 7 with vacancy sites leads to lower diffusion.*
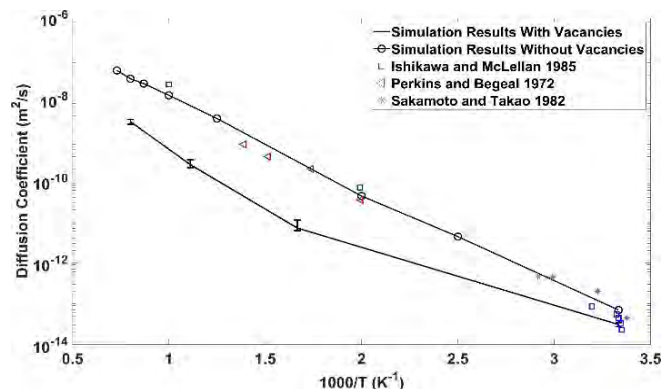

Figure 7. Comparison between the temperature dependent diffusion coefficients for hydrogen obtained from the simulations, and various data points reported in the literature.

Simulations for the reflection and absorption of hydrogen incident from the vacuum onto the copper surface were also performed at different energies and angles. Results for normal incidence are shown in Figure 8 at 800K. The main feature is that at low incident energy, ability to bounce back easily is low, and leads to low reflection coefficients. At high energies, the atoms are mainly transmitted through, again leading to a lower reflection. Hence, a local maxima in the reflection curve is predicted. The simulations also yielded adsorption and absorption data which is presented in Figure 9 for normal incidence. As evident from the figure, adsorption is predicted to occur for incident energies below 10 eV, while absorption would dominate above 10 eV.

(C) Modeling Results for Carbon Fibers

Outgassing from carbon fibers was studied based on an atomic-level approach using the LAMMPS software tool that included atomic bonding. The carbon fiber structure was generated using an approach based on interconnection of an array of graphene sheets resembling ladder like structures that can structurally self-organize. Graphene sheets of 5 different lengths were formed using VMD software. Eventually, a stable carbon fiber system (51,000 atoms) was obtained. Two alternate views of the structure are given in Figure 10. The molecular dynamics simulations for hydrogen out-gassing from carbon fibers are continuing, and results are expected soon.
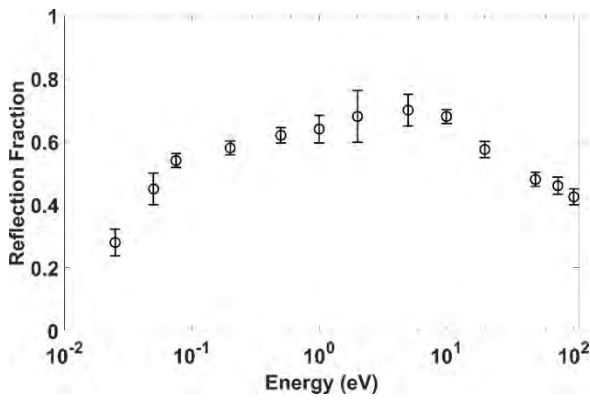
41

Figure 8. Energy-dependent reflection coefficient at normal incidence of hydrogen impinging on the surface of a copper electrode, calculated from Molecular Dynamics simulations.
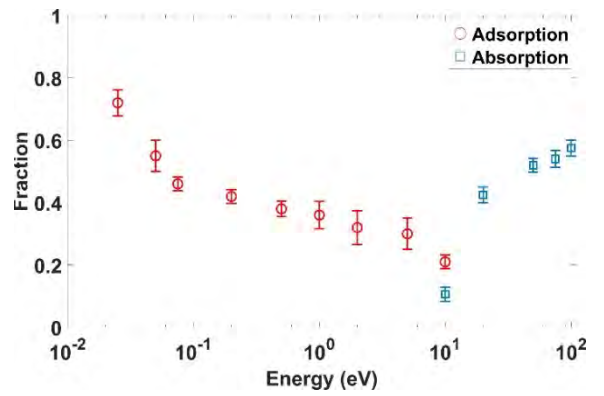

Figure 9. Molecular Dynamics calculations of energy-dependent adsorption and absorption of hydrogen at normal incidence on the surface of a copper electrode.
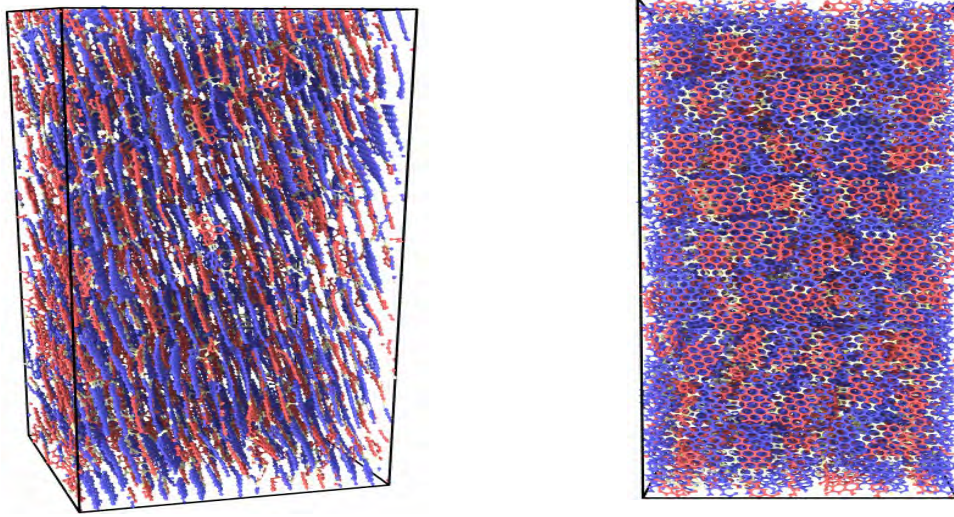
Figure 10. Structure for carbon fibers build from atomic bonding. Two different views are shown.

(D) Role of Surface Defect on Electron Wavefunctions and Emission

Calculations of wavefunctions [$\psi(z)$] are important for obtaining the tunneling probability that helps yield the emission current. In addition to $\psi(z)$, the electrode work function (Φ_B) is another parameter that dictates emission. In order to probe the above details, Density Functional Theory was applied for predictions of both the electronic wavefunctions [$\psi(z)$] and the electrode workfunction (Φ_B). Results both for homogenous and pure copper, as well as an oxygen layer at the surface, are shown in Figure 11. The black curve is for the copper-vacuum system, while the red curve denotes the system consisting of bulk copper, monolayer of oxygen on the surface, followed by vacuum. The interface with the vacuum is shown by the dashed vertical lines. The work functions are predicted to be ~4.5 eV and 3.6 eV for the two systems, with a monoatomic oxygen layer lowering Φ_B.
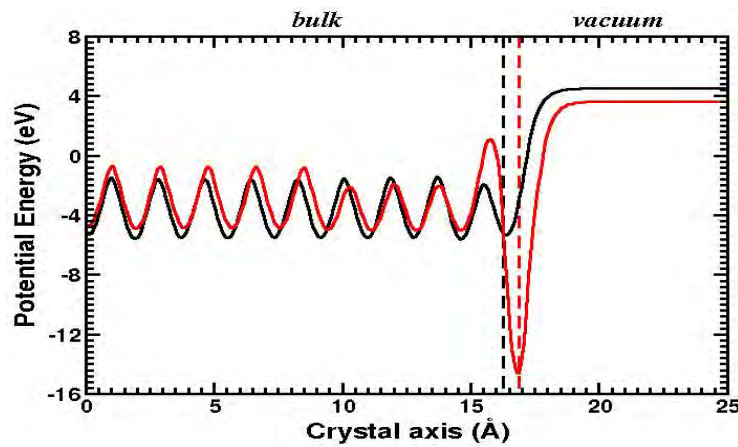

Figure 11. Energy versus position in copper-vacuum and copper-oxygen (monolayer)-vacuum systems. The work functions are predicted to be ~4.5 eV and 3.6 eV, respectively, for the two systems along 100.

43

3. Findings and Conclusions

(i) Molecular Dynamics (MD) simulations of outgassing from electrodes were carried out successfully. Also, sticking coefficients of hydrogen gas atoms as a function of incident energy and angle were also obtained. Vacancies would reduce out-gassing.
(ii) Electron transport for emitter arrays simulated. Optimized strategy possible.
(iii) Finally, analysis of both the electronic wavefunctions [$\psi(z)$] and the Work Function [Φ_B] performed for copper with oxide overlayer. Decreases in emission likely with use.

In conclusion, numerous tasks were performed over the past 12-months all of which were aimed at improving the modeling capability and understanding of high-power microwave devices.

4. Plans and Upcoming Events
(a) Plans to complete calculations of outgassing from carbon fibers. Compare with available data.
(b) Probe the finite-size effects on thermal conductivity of copper and carbon-fiber emitters.

5. Transitions and Impacts
None.

6. Collaborations
Dr. Mahdi Sanati, Physics Department, Texas Tech University

7. Personnel
Principal investigator	Ravindra P. Joshi
Co-investigator or Co-PI	Andreas Neuber, John Mankowski, James Dickens
Business Contact	Amy Cook, TTU Associate Vice-President for Research
Team Members	None others
Subs	None

8. Students
Dong Guo – PhD student // S. Sami – PhD student // Joy Acharjee – MS student (graduated).

9. Technology Transfer
None.

10. Products, Publications, Patents, License Agreements, etc.
Archival Publications #1

a. Article Title: Simulations of Field Emission from Copper Electrodes with Inclusion of Oxygen Surface Layer and Work Function Changes Based on First-Principles Calculations
b. Journal: Journal of Applied Physics
c. Authors: S. N. Sami, L. Diaz, M. Sanati, and R. P. Joshi
d. Keywords: Electron emission, Workfunction, Oxide overlayer
e. Distribution Statement: Unrestricted distribution
f. Publication Status: Published
g. Publication Identifier Type: Digital Object Identifier (DoI)
h. Publication Identifier: https://doi.org/10.1063/5.0028918

There are currently two other journal articles under review as given below.

S. N. Sami, M. Sanati, and R. P. Joshi, "Simulations of Hydrogen Outgassing and Sticking Coefficients at a Copper Electrode Surface: Dependencies on Temperature, Incident Angle and Energy," submitted for publication, October 2020.

D. Guo, W. Milestone, and R. P. Joshi, "Molecular Dynamics Based Evaluations for Maximum Current Output from Bimodal Electron Emitter Arrays," submitted for publication, December 2020.

In addition, the following four presentations were made at the Pulsed Power and Plasma Science (ICOPS-2020) conference in Orlando. The specific details are:

L. Silvestre, R. P. Joshi, J. Stephens, J. Dickens, J. Mankowski, A. Neuber, ″Development of a Vlasov Equation Based Numerical Model of Multipactor Discharge,″ IEEE Int'l Conference on Plasma Science, Institute of Electrical and Electronics Engineers, Singapore (Virtual/Remote), December 2020.

X. Qiu, M. Saed, J. Mankowski, J. Dickens, A. Neuber, and R. P. Joshi, ″Investigations of Geometric Modifications and Static Magnetic Fields on Multipactor Mitigation in Rectangular Waveguides,″ IEEE Int'l Conference on Plasma Science, Institute of Electrical and Electronics Engineers, Singapore (Virtual/Remote), December 2020.

T. Buntin, M. Abide, J. Dickens, A. Neuber, R. P. Joshi, J. Mankowski, ″Explosive Emission Cathode Evaluation for a Magnetically Insulated Line Oscillator,″ IEEE Int'l Conference on Plasma Science, Institute of Electrical and Electronics Engineers, Singapore (Virtual/Remote), December 2020.

M. Abide, T. Buntin, J. Dickens, A. Neuber, R. P. Joshi, J. Mankowski, ″S-Band Magnetically Insulatd Line Oscillator (MILO) with Adjustable Cathode/Beam Dump Overlap,″ IEEE Int'l Conference on Plasma Science, Institute of Electrical and Electronics Engineers, Singapore (Virtual/Remote), December 2020.

11.   Point of Contact in the Navy

Dr. Ryan Hoffman, Program Officer, Office of Naval Research

12. Acknowledgement/Disclaimer

Electrochemical Prime Power Supply for a Repetitively Operated High-Power Marx Generator

Grant No. N00014-17-1-2847

Annual Report for Fiscal Year 2020

Period of Performance: October 1, 2019 to September 30, 2020

Prepared by:

Professor David Wetz, Principal Investigator
Associate Professor Electrical Engineering Department
University of Texas at Arlington
Department of Electrical and Computer Engineering
416 Yates Street, Rm. 537
Arlington, TX 76019
Tel: (512) 788-0848
Email: wetz@uta.edu

Grant or Contract Number: N00014-17-1-2847
Date Prepared: December 12, 2020
Project Title: Electrochemical Prime Power Supply for a Repetitively Operated High Power Marx Generator
Annual Summary Report: October 1, 2019 to September 30, 2020
Principle Investigator: PI David Wetz, 5127880848, wetz@uta.edu, University of Texas at Arlington (UTA), Arlington, Texas, 76019

Section I: Project Summary

1.   Overview of Project

Abstract:
The US Navy has active research projects aimed at bringing electrically powered weaponry to the fleet, referred to as directed energy weapon (DEW) systems. Though many technical advances are being made, most are still in the research phase with many unanswered questions still to be answered before they will be deployed. These loads can only be as effective as the power supply that drive them. Though every DEW power supply is different, two common elements that many share are the prime power supply and the intermediate energy storage, respectively. Regardless of whether the DEW is deployed on a ship or on a smaller platform, it must have a reliable and resilient power source from which to draw its prime power. The prime power supply may directly drive the DEW load, or it may feed energy to an intermediate energy storage device that supplies high power to the load. A power supply that operates on its own or in some sort of hybrid fashion with the platform's existing power source is required. Energy storage in the form of ultracapacitors (UCs) and lithium-ion batteries (LIBs) hold a great deal of promise for use as a prime power source for DEWs. These supplies must source high power in as compact a form factor as possible so there is still a great deal of research to be performed to understand how these devices will operate, age, and fail when operated at high power so that they can be properly considered and sized. A small amount of time this year was focused on developing empirically derived sizing tools that can be used when considering LIBs and UCs, respectively. Through additional support from the U.S. Army's Combat Capabilities Development Command C5ISR Center, significant progress was made toward development of a battery sizing tool that utilizes empirical data. This year, the most effort was put toward designing, constructing, and commissioning a high voltage testbed, as high as 80 kV, on which to study high voltage capacitors at rates of charge and discharge. Though high voltage intermediate energy storage capacitors are technologically more mature and documented, there are still research challenges to overcome. Discharging and recharging them at high current in a repetitive manner has been found to be hard on them, and the testbed developed here provides a means to study them and determine what could cause failure in this mode of operation.

Objective:
The research supported by this grant has objectives to study primary and intermediate energy storage devices used in pulsed power supplies. The first year and a half of the three-year effort was focused on studying primary energy storage devices and establishing a framework for an empirically based sizing tool. The second year and a half focused on developing a pulsed power test stand on which to study high voltage intermediate energy storage capacitors. The progress made on both objectives will be discussed here.

Introduction:
Abbreviation List: DEW: Directed Energy Weapon, UC: Ultracapacitor, LIB: Lithium-ion Battery, COTS: Commercial-Off-the-Shelf, DE: Directed Energy, EDLC: Electric Double Layer Capacitor, UTA: University of Texas at Arlington, PPEL: Pulsed Power and Energy Laboratory, HVPPC:

High Voltage Pulsed Power Capacitor, CC: Constant Current, CLC: Capacitive-Inductive-Capacitive, VI: Virtual Instrument, cDAQ: Compact Data Acquisition, and EMI: Electromagnetic Interference

Task 1: Electrochemical Energy Storage Sizing Tool Development
Electrochemical energy storage is being studied across the US Navy to fulfill the electrical power requirements that have arisen in their effort to become a more electric fleet. Many different chemistries are available commercially off the shelf (COTS), and each has unique properties with respect to its voltage, power, energy, impedance, and size characteristics, among many others. This makes choosing the correct energy storage for any application difficult and unfortunately there is no one-size-fits-all approach that can be taken. Energy storage manufacturers often design cells specifically for an application when approached by a customer. Even though they are designed for a specific application, the manufacturers often make them available commercially to other customers once fabricated, meaning that cells of countless geometries are available with very few industry standards available. This only increases the challenges faced when sizing energy storage for an application using COTS devices. When choosing a chemistry, there are many factors that should be considered. The high-power density of lithium-ion batteries and ultracapacitors makes them attractive for use in DE applications since they demand a compact power supply that can supply high power transiently. UCs are also referred to as electric double layer capacitors (EDLCs) for reference. UCs make sense in applications that require a power supply with high power, long life, and high safety but not high energy store. When higher energy stored is required, a LIB is likely a better choice, but they come with many tradeoffs that must be considered. Within the LIB category, there are many different chemistries to choose from, most of which have not been studied significantly under high power operation. These vast choices make the design of a prime power supply for DE applications a non-trivial task. During the first year of this effort, UCs and LIBs were studied to assess their operation and usable capacity at high power. Because these technologies are rarely used at the power levels required by DE applications, little is understood about how they perform, age, fail, and how to properly size them for high-power applications. In the second year of this three-year effort, a framework was developed to advance the development of a MATLAB/SIMULINK® based sizing tool that can be used to assist pulsed power engineers with the design of compact prime power supplies; however, towards the end of the second year, the focus of the research changed towards studying high voltage intermediate storage capacitors and development of the sizing tool was stopped. This year we were asked by US Army's Combat Capabilities Development Command C5ISR Center to expand the development of the sizing tool, and with their additional funding, we were able to do so. That progress will be reported here.

Task 2: Study of High Voltage Pulsed Power Capacitors (HVPPCs) at High Charge and Discharge Rates
In many DE power supplies, the prime power supply referenced in Task 1 is used to transfer energy into an intermediate energy storage element that is used to supply high peak power to the load. In many cases, HVPPCs are used as the intermediate energy storage. Electrostatic dielectric film capacitors with self-healing electrodes have proven to be the most reliable for pulsed power applications where short pulse discharges are required. Problems have been observed in high voltage capacitors when attempting to recharge them quickly between repetitive discharges. The capacitors are proprietary and not a great deal is known about their construction or any special design features. It is assumed that the capacitor being studied is a polypropylene metallized film capacitor. The capacitor has a rated capacitance of just under 30 nF and voltage rating of 100 kV. The capacitor is being used as storage within a multi-staged Marx generator driving a DE load. In

order to study its performance and lifetime in an emulated operational scenario that involves a high rate discharge, high rate recharge, and a second high rate discharge, a testbed has been designed and assembled. The stand's design and construction was started in the second fiscal year of the grant. This year was spent continuing that development and many challenges were faced this year but it is now working reliably and is being used to study high voltage capacitors.

Background:
Since 2010, the University of Texas at Arlington's (UTA's) Pulsed Power and Energy Laboratory (PPEL) has been supporting the Office of Naval Research (ONR) in its study of electrochemical energy storage devices, power systems, and pulsed power systems. LIBs and UCs have been considered as technologies with potential for use in compact pulsed power systems. A Microsoft Excel based sizing tool was started in 2014 and was incrementally improved upon for future use in studying how different LIB and UC technologies compare with respect to power supply size and weight. That tool has been considerably expanded over the years, including with support of this grant and support from the US Army's Combat Capabilities Development Command C5ISR Center. In the middle of the second fiscal year, the effort of this grant was redirected towards designing and setting up a testbed on which HVPPCs could be studied at high rates of discharge and recharge, respectively. The testbed is needed to study the performance and eventual failure mechanisms of the types of metalized film capacitors used in repetitive rate Marx generators. During this third year, the testbed was worked on with considerable difficulty but as of this writing, it is working reliably.

2. Activities and Accomplishments

Task 1: Sizing Tool Progress

As described in the objectives section, the first year and a half of this effort was focused on studying ultracapacitors for use as a prime power supply for a pulsed power system and on studying new methods for properly sizing high rate prime power supplies. This effort has been previously documented in previous FY reports; however, it is worth noting that this year we were asked by US Army's Combat Capabilities Development Command C5ISR Center to expand the development of the sizing tool. Since the focus of this effort had shifted to studying intermediate energy storage capacitors, the Army funded an additional student to continue this work. Only a quick summary will be given here of the status of the tool.

The tool was developed using the framework that was started last year but with significant changes. Over the years, the PPEL has tested many different lithium-ion batteries and ultracapacitors for many different customers, developing a substantial database across a host of different C-rates at different temperatures. Using a reference written by Traub [1], the constant current data is converted into constant power curves, and an empirical data curve fitting tool that is built into MATLAB, is used to fill in data between the C-rates tested. The user enters the constant power that the supply must provide, the time it must supply it for, a minimum voltage, a maximum voltage, a size limit, and a weight limit. The tool then produces an output table that tells the user the minimum number of series/parallel cells that are needed to match their requirements for each cell type within the database. If certain cells are not able to meet the requirements, the cell is not presented as an option. A plot is shown that estimates the battery's conduction voltage and current. The tool only considers lithium-ion batteries at this time and recharge capability has not been built into it, but that functionality is coming soon. Figure 1 shows a screen capture of the tool as well as some sample curve fits that are within the cell database used by the tool for sizing.
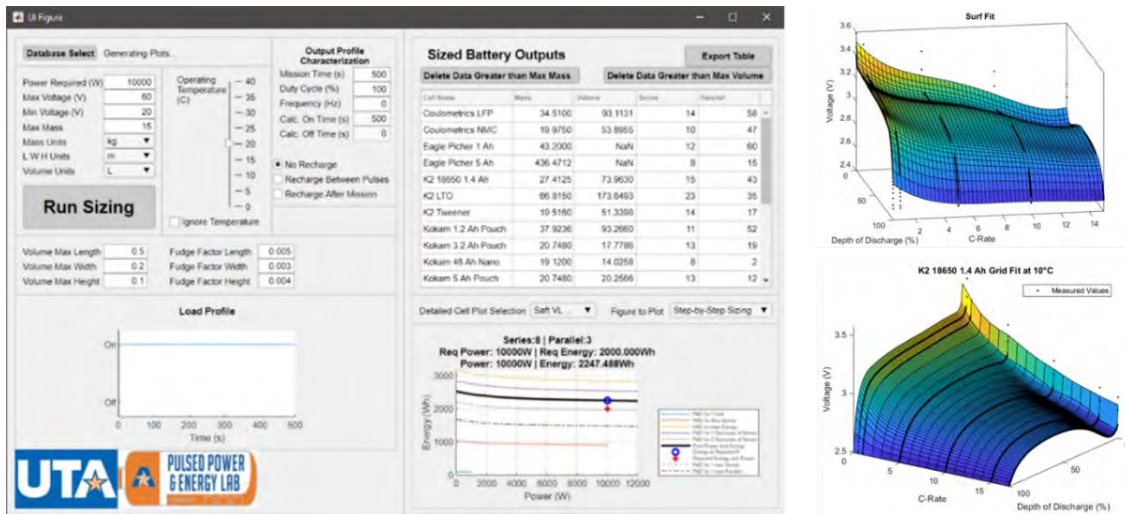
Figure 1. Screen capture of the UTA energy storage sizing tool (left) and sample curve fits (right). The black lines in the curve fits represent empirically collected data that it is fitted to.

Task 2: High Voltage Pulsed Power Capacitor Testing Progress

The second task executed this FY was to complete the design, construction, and commissioning of a CLC testbed that is used to subject HVPPCs to high current pulsed charge and discharge currents. As previously written, a HVPPC manufacturer has observed problems when attempting to repetitively charge and discharge capacitors at high pulsed currents. To assist in better understanding what is causing the failure, a capacitive-inductive-capacitive (CLC) testbed was designed, constructed, commissioned, and used. A schematic diagram of the testbed is shown in Figure 2.
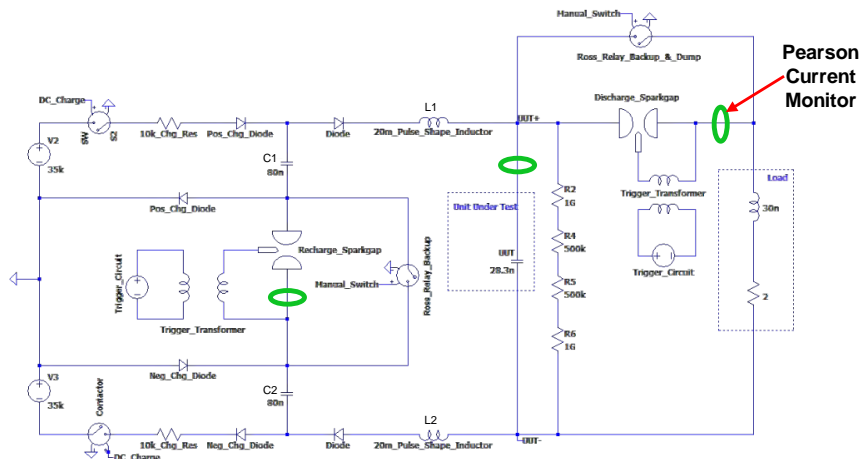

Figure 2. CLC circuit schematic describing the testbed constructed to study HVPPC operation.

Simply described, two 40 kV DC power supplies, of opposing polarity, are used to charge two 80 nF HVPPCs, C1 and C2, that act as an intermediate energy storage. The unit under test is 30 nF capacitor labeled UUT. Initially the two 80 nF capacitors are charged using the power supplies. The UUT is charged up differentially to 80 kV. Once charged, 'Discharge_Sparkgap' is triggered causing the UUT to discharge its current into the load. A 2 Ω load is needed to simulate the load impedance of the DE application. Initially the 2 Ω load was constructed using several large water resistors connected in parallel however, there was too much inductance in the load path and this

51

caused ringing during the discharge. To eliminate that easily, only one 18 Ω resistor has been used to date to critically damp the system. In the future, the load inductance will be reduced so that the intended 2 Ω load can be studied. Once the discharge is completed, capacitors C1 and C2, respectively, are connected in series. As shown in the schematic, there are two ways of connecting those capacitors in series. The first is the 'Recharge_Sparkgap;' however, because there is no real voltage difference between the two points in the circuit, it does not conduct even when it is triggered. Because of this, it was removed from the circuit and instead the connection is manually made using a 70 kV Ross Relay and this seems to work well to recharge the capacitor. Now that UUT is recharged, the intent is to trigger 'Discharge_Sparkgap' again to discharge it; however, this too this has been problematic. A second trigger circuit was connected in parallel with the first to trigger the spark gap and while it should work, it doesn't seem to. This is an issue that is still being worked through but for the time being, a second manual Ross Relay is used to manually discharge the circuit and this again is working well for the time being. Figure 3 contains three simulation results, one of each of the discharge, recharge, discharge events, respectively, into a 2 Ω load.
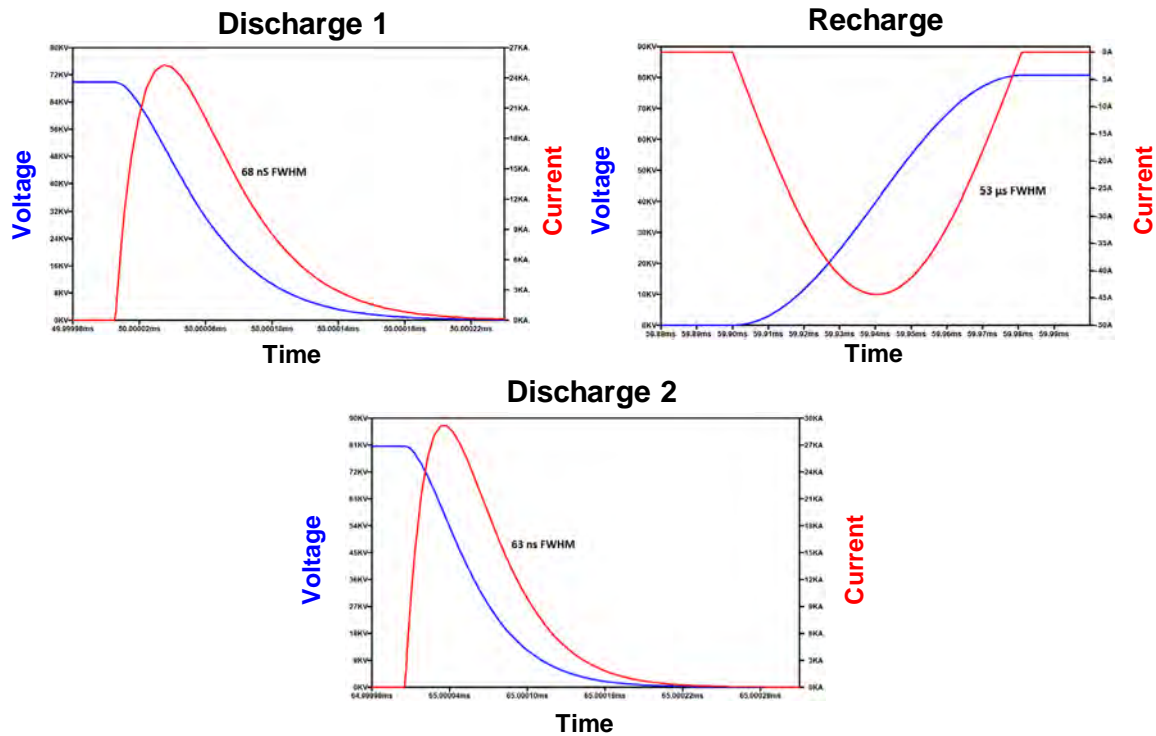

Figure 3. Simulated results of the CLC circuit during the first capacitor discharge (above), high rate recharge (middle), and second discharge (below), respectively.

Photographs of the testbed are shown in Figure 4. The testbed was assembled last year; however, it went through several revisions this year as problems were encountered during testing. The high voltage components are all contained within an aluminum enclosure that is lined with a pan liner and then filled with transformer oil for dielectric insulation. The 80 nF capacitors, the capacitor under test, and the spark gaps were all provided by the sponsors. The charging inductors were contracted out for assembly. The spark gaps are triggered using the circuit shown in Figure 5, which also went through several revisions this year. Simply described, a 300 μF capacitor is charged to 600 V and then discharged through a step-up transformer using a high-side SCR. A major problem encountered this year concerns the trigger transformers used to step up the trigger voltage to breakdown the sparkgap(s). Initially an automotive sparkplug trigger transformer was used but it

did not work since the primary and secondary coils shared a ground. A homemade design was tried but it was not stepped up enough. Multiple commercial vendors were sought but the cost was more than the funding available. Finally, Zeonics, an Indian company, was found. Two reasonable cost transformers were procured, one that steps up 800 V to 50 kV, with 50 kV DC isolation, and another that steps up 1 kV to 140 kV, with 100 kV DC isolation. Photographs of the isolation transformers are shown in Figure 6.
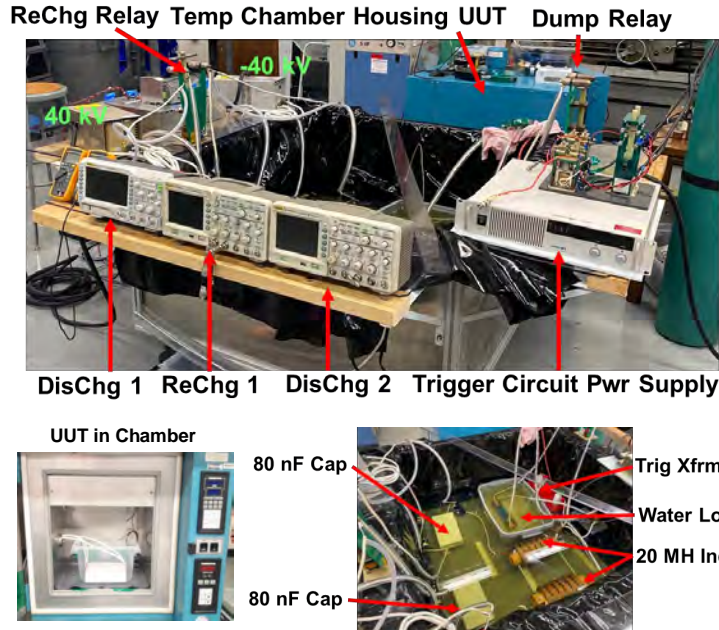

Figure 4. Photographs of the assembled CLC testbed. An overall photograph of the full testbed is shown above. A zoomed in view of the components held within the enclosure are shown in the bottom right and the UUT is stored in an oil bath in the temperature chamber shown in the bottom left.
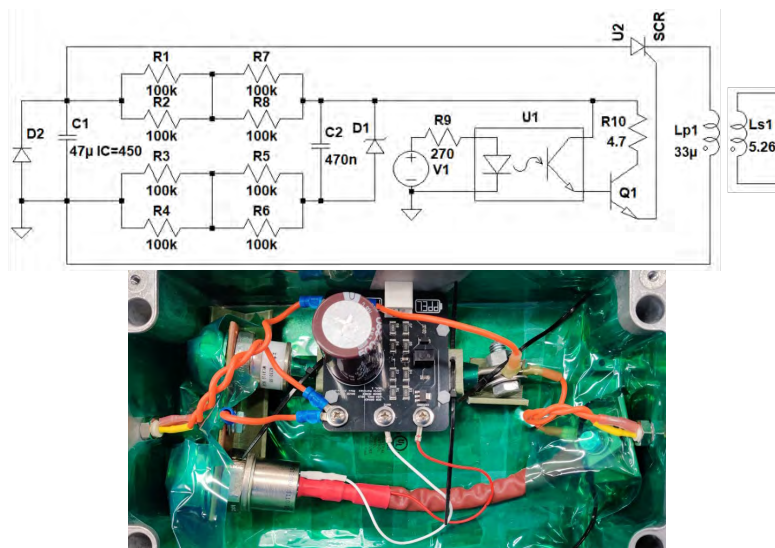

Figure 5. Schematic diagram (above) and assembled (below) spark gap trigger circuit.

50 kV Isolation Transformer

140 kV Isolation Transformer

Figure 6. Photograph of the step-up isolation transformers used to trigger the spark gaps.

A National Instruments (NI) cDAQ chassis is used to control the system as well as sample and digitize some of the data. A custom Virtual Instrument (VI) panel, seen in the lower part of Figure 7, was created to interact with the power supplies and control the whole process. To isolate the NI controller from the high voltage system, fiber optic circuit boards, seen in Figure 8, were designed and fabricated to interface the digital signals of the two systems. To interface the analog signals, analog/fiber converters, also seen in Figure 8, were procured by a company called AA Labs. A signal diagram describing the control and data acquisition setup is shown in Figure 9.
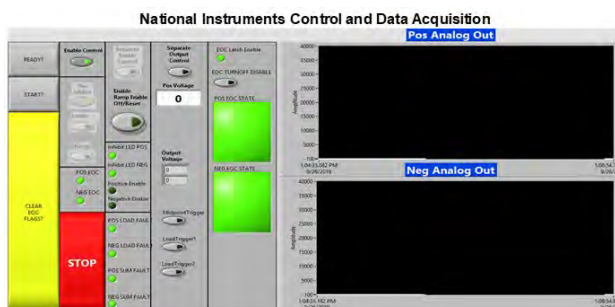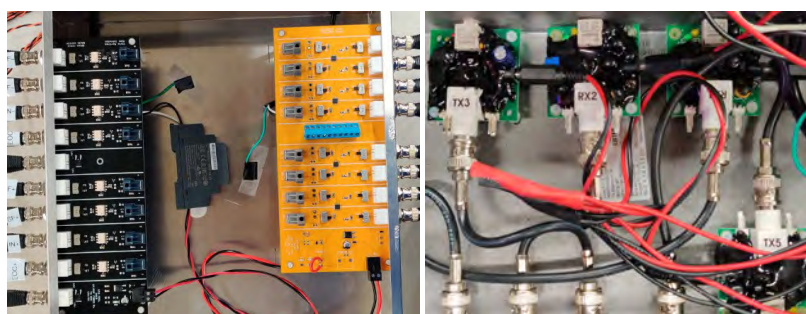

Figure 7. Custom LabView VI (below).

Figure 8. Digital/fiber converter boards (top) and analog/fiber converter boards (bottom)

Throughout the year, there were many problems encountered that had to be overcome. There were unexpected breakdown events, trigger transformer problems, spark gap trigger problems, EMI problems, etc., that all had to be overcome. As of this writing, the CLC testbed is working reliably at charge voltages as high as 35 kV. The inductance needs to be lowered to be able to install the 2 Ω load without ringing and that will be done soon so that a full test series on a new capacitor can be started.
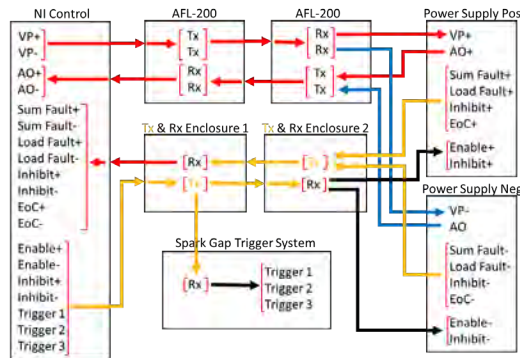
Figure 9. CLC testbed communication diagram.

3. Findings and Conclusions

The sizing tool was shown earlier and since that was primarily executed using Army funding this year, it will not be discussed further here. By the time the CLC testbed was reliably operational, there were no spare capacitors available to test from the manufacturer who observed problems. A similar capacitor from another manufacturer has been used in all the commissioning experiments and to date there have not been any problems observed with it. A controlled experimental test plan has not been executed but some results obtained into an 18 Ω load at 15 kV, 20 kV, and 30 kV charge voltages are shown in Figure 10. Roughly 100 total tests have been performed on the UUT stored in a 70°C chamber without any evidence of failure. *It is unclear if this is because of the lower discharge current cause of the higher load or if this brand of capacitor doesn't have the same problems.* Now that the system is working reliably, a controlled test series into a lower impedance is planned soon.
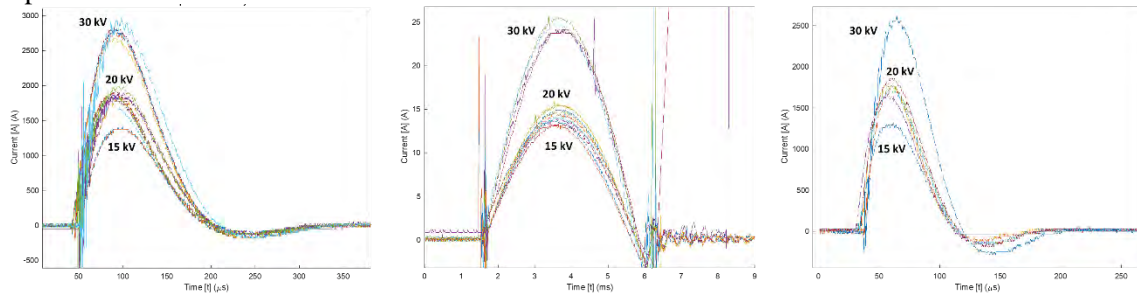

Figure 10. Data collected at 15 kV (30 kV diff), 20 kV (40 kV diff.), and 30 kV (60 kV diff) charge voltages, respectively during the 30 nF capacitor discharge 1 (left), 30 nF capacitor recharge (middle), and 30 nf capacitor discharge 2 (right).

4. Plans and Upcoming Events

The grant is ending soon; however, Covid-19 has slowed progress and a no cost extension has been obtained so the work will continue into the next FY. The plan is to begin a controlled test series into a lower impedance, as close to 2 Ω as can be obtained without ringing. Hopefully a capacitor from the manufacturer who has observed problems will become available and at least one will be studied before the effort comes to an end.

5. Transitions and Impacts

To date, the knowledge gained has been transitioned to many organizations working in the directed energy (DE) area. As the work continues, presentations and reports will be written to transition the knowledge gained to any organization interested in learning more about it.

6. Collaborations

We have collaborated with:

Jordan Chapparo – NSWC-DD, Yeong-Jer Chen – NSWC-DD, Frank Hegeler – Naval Research Laboratories (NRL), Dale Coleman – Sandia National Laboratories, Emily Schrock – Sandia National Laboratories, Josh Gilbrech – Air Force Research Laboratories – Kirtland, and Mark Schneider – General Atomics

7. Personnel

Principal investigator: Dr. David Wetz – 3 months (approx. 400 hours), National Academy Member (N)

Business Contact: Jeremy Forsberg, ogcs@uta.edu

Team Members: Listed as students below

Subs: None

8. Students

Chris Martinez: MSEE student (grad. Dec. 2019), Alex Johnston: PhD EE Student, Zach Bailey: PhD EE student Cameron Johnston: EE Undergraduate (UG) Student, Hayden Atchison: EE UG Student, and Cole Tschritter: EE UG Student

9. Technology Transfer

None

10. Products, Publications, Patents, License Agreements, etc.

Conference Papers

C.F. Martinez, J.L. Sanchez, **D.A. Wetz**, and D.A. Dodson, 'Fast Recharge of High Voltage Capacitors,' Proceedings of the 2019 IEEE Pulsed Power and Plasma Sciences Conference, June 23 – 28, 2019, Orlando, Florida.

Reporting

Monthly reports compiled and delivered to ONR. A status brief was submitted for the 2020 DE Program Review.

11. Point of Contact in Navy

Ryan Hoffman – ONR PM (contacted on multiple occasions)

Matthew McQuage – NSWC-DD (contacted on multiple occasions)

Frank Hegeler – NRL (contacted on multiple occasions)

Yeong-Jer Chen - (contacted on multiple occasions)

Jordan Chaparro - (contacted on multiple occasions)

12. Acknowledgement/Disclaimer

Novel High Power Microwave System Designs Using Nonlinear Transmission Lines

Prepared by:

Dr. Allen L. Garner, Principal Investigator
Associate Professor and Undergraduate Program Chair, School of Nuclear Engineering
Purdue University
516 Northwestern Ave.
West Lafayette, IN 47906
Tel: (765) 494-0618
Email: algarner@purdue.edu

Grant or Contract Number: N00014-18-1-2341
Date Prepared: 28JAN2021
Project Title: Novel High Power Microwave System Designs Using Nonlinear Transmission Lines
Annual Summary Report: FY2020
Principal Investigator: Allen L. Garner, (office): 765-494-0618, algarner@purdue.edu, Purdue University

Section I: Project Summary

1.   Overview of Project

Abstract: Nonlinear transmission lines (NLTLs) are of great interest to the Navy for solid state high repetition rate directed energy systems. This project investigates the suitability of novel composite materials for NLTLs in a high power microwave (HPM) source. Since understanding the current state of NLTL research will guide potential areas of improvement, we have performed an extensive review of current NLTL technology and topologies and published this effort in *IEEE Access*. We have constructed composites with various volume loadings of barium strontium titanate (BST) and/or nickel zinc ferrite (NZF), which exhibit nonlinear permittivity and permeability, respectively. We report the linear permittivity of BST, NZF, and BST/NZF composites as a function of volume loading and the linear permeability as a function of frequency and volume loading. We observe notable increases in permeability as we exceed 15% NZF for the NZF composites and 10% NZF for the NZF/BST composites. We observe reasonable agreement between effective medium theories (EMTs), finite element simulation using CST Microwave Studios, and experiment from 1 to 4 GHz for the various composites. The main outstanding challenge is measuring bulk BST permittivity for entering in the model. Ongoing work for measuring nonlinear permittivity and permeability and assessing the dielectric breakdown strength of the materials is discussed.

Objective: The goal of this project is to evaluate the feasibility of creating novel nonlinear dielectric materials by mixing nonlinear inclusions into a polymer base dielectric. The resulting composite dielectric properties will be measured using a vector network analyzer (VNA) to determine the complex permittivity and permeability of the composite. This will provide a baseline for determining the relationship between the volume loading of the nonlinear electric and nonlinear magnetic inclusions in a material to the dielectric properties of the composite. These measurements will be used to develop a model based on common effective medium theories, such as the Maxwell Garnett model, to guide material design. This model can be coupled with electromagnetic simulations to optimize an NLTL system as a radio frequency (RF) source.

Introduction: Increased global volatility motivates the development of devices for nonlethal deterrence. Directed energy devices can provide forceful persuasion at a distance for both civilian and military peacekeepers. Additionally, increasing occurrences of vehicular terrorism further drive the development of technology to stop vehicles from a distance before they can injure civilians or destroy property. Militarily, disabling motorized attacks before contact with troops is critical for reducing casualties while keeping the attackers alive for future interrogation. Directed energy technology can provide these capabilities, although system size often limits application in the field.

Thus, developing compact HPM devices could facilitate fielding devices for nonlethal defense with increased standoff range or for radar or weapons systems for aircraft or ships. This effort assesses the design of novel NLTLs by examining the impact of composites comprised of various

combinations of dielectric and magnetic inclusions and leveraging various geometries, such as tapering, used in conventional transmission lines for matching. This may increase efficiency and energy in the RF output as it relates to pulse width while also providing additional flexibility in design.

Background:
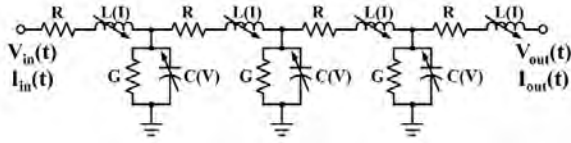
Fig. 1 Lumped element representation of a nonlinear transmission line (NLTL) comprised of both nonlinear capacitance $C(V)$ a function of voltage and inductance $L(I)$ a function of current that translates an input voltage $V_{in}(t)$ and current $I_{in}(t)$ into an output voltage $V_{out}(t)$ and output current $I_{out}(t)$. An NLTL may be constructed with nonlinear capacitance and/or inductance. In general, loss may be included through a resistance R in series with the inductor or a conductance G in parallel with the capacitance.

Materials are a challenge for NLTL design. Figure 1 shows a simple example of a NLTL. One may represent a conventional transmission line with lumped elements as an inductor in series with a resistor on the top line and a capacitor in parallel with a shunt conductor in the vertical lines, where the resistor and conductor represent losses. An NLTL has a similar setup, as shown in Figure 1, except that either the inductor or capacitor (or both) vary with current or voltage, respectively. This modulates the delivered pulse to generate an RF signal with tunability of the NLTL important for controlling the frequency of the resulting RF.

While NLTLs are growing in importance for generating RF, challenges remain in constructing them with high voltage and power capabilities, as required in many HPM applications, and in tunability for wideband applications or capability to be used at multiple frequencies. Based on the definitions above and the circuit diagram in Figure 1, one method to generate an NLTL involves using a varactor, whose capacitance varies with applied voltage, generally sigmoidally (rapidly increasing over a narrow voltage range). Understanding the importance of this dependence is critical for understanding the potential flexibility in design. Early NLTLs often used nonlinear capacitance to induce this phenomena, resulting in soliton formation.

Varactors are generally low voltage devices, which presents a challenge for high power applications. Additionally, the frequency cannot be tuned for a given varactor. A recent alternative growing in popularity involves using ferrites to provide nonlinear inductance in meandering NLTLs. Texas Tech University (TTU), the Air Force Research Laboratory (AFRL), and others have also developed and applied such approaches for gyromagnetic NLTLs for HPM and high power radio frequency applications. The initial TTU NLTLs provided peak voltages of approximately 50 kV with 15% power efficiency and frequencies of a few GHz. TTU next considered the impact of material, such as nickel-zinc, yttrium iron garnet, magnesium-zinc, and lithium ferrites, on performance. They demonstrated that varying the material's bias magnetic field provided active delay control and that the material's ferromagnetic resonance line width played a significant role in microwave generation. TTU next showed that one could effectively tune the output by controlling the bias voltage, which subsequently impacted the electrical properties of the NLTL due to its nonlinear nature, enabling the construction of a single, frequency-agile device

capable of operating from 1.8 to 2.6 GHz with powers from 1 MW to 3 MW; however, higher voltages (on the order of 40 kV) resulted in corona discharge, limiting application at higher voltages. Thus, attaining higher powers required combining multiple NLTLs, which TTU demonstrated for arrays of either two or four NLTLs. The NLTL could then be incorporated into a solid-state HPM source to generate microwave pulses with a microwave frequency of 2.1 GHz with a pulse repetition frequency of 65 MHz. AFRL designed a spatially dispersive ferrite NLTL with axial bias that was frequency tunable from 0.95 to 1.45 GHz with instantaneous power levels of tens of MW, and durations from 4 to 17 ns.

A Russian group from the Institute of High Current Electronics has also studied gyromagnetic RF sources using NLTLs. Their early work used saturated NiZn ferrites as an active nonlinear medium and found an optimum length of approximately 1 m for producing a 1000 pulse burst at 200 Hz repetition rate for a peak RF power of 260 MW with a central frequency of 1.2 GHz and of 0.25 GHz at -3 dB level and 0.4 GHz at -10 dB level. They have also demonstrated electronically controlled beam steering by connecting two NLTLs to one high voltage driver with each NLTL capable of producing RF pulses from 50-700 MW at frequencies from 0.5 to 1.7 GHz with 100 Hz repetition rate. Gyromagnetic NLTLs have also generated high power ns RF pulses with field strengths up to 40 kV/cm, durations from 4 to 25 ns, and frequency from 0.6 to 1.0 GHz to provide flexible output at laboratory scale for biological experiments. They have also subsequently extended their frequency output to 4 GHz with a peak voltage of 175 kV for 100 Hz repetition rates during one second. Their ferrite line in the NLTLs implements a continuous unit of NiZn rings of M200VNP type of a total length of 700 mm. At lower frequencies (~300 MHz), they have also used a gyromagnetic NLTL as a peak power amplifier of an input pulse. They applied a 500 kV pulse with a full-width-half-max duration of 7 ns to the NLTL to increase the pulse amplitude to 740 kV while reducing the pulse duration to ~2 ns. This increased the power from ~ 6 GW on the input to ~13 GW on the output at a 1 kHz pulse repetition rate in burst mode.

Alternatively, the University of New Mexico developed a hybrid line consisting of both nonlinear capacitors and inductors. While this is a promising approach that could provide some ability for tunability, one must attain appropriate inductance and capacitance behavior to achieve a constant transmission line impedance.

2.   Activities and Accomplishments
ELECTROMAGNETIC PROPERTY MEASUREMENTS

Our first major accomplishment involved publishing a review article on NLTL system design and development in *IEEE Access*. This review summarized the various NLTL topologies designed to achieve these design objectives. Specifically, we summarized modeling and experimental studies for three primary topologies: the lumped element NLTL, the split ring resonator, and the traditional transmission line geometry using nonlinear materials. The lumped element NLTL and the traditional transmission line constructed with nonlinear materials lend themselves to higher power applications, while the split ring resonator is better suited for applications involving antennas. We provided a detailed summary of past studies for these topologies and conclude by exploring ongoing work and future opportunities for technological development. Table 1 summarizes lumped element NLTL designs and parameters.

We have also almost completed two manuscripts concerning the measurement of linear permittivity and permeability for composites comprised of either (1) NZF or BST or (2) both NZF and BST, and one manuscript summarizing the nonlinear permeability of composites containing NZF or NZF and BST.

Table 1. Summary of lumped element NLTLS.

Input Pulse Amplitude (V)	Input Pulse Duration (ns)	RF Generation Frequency (GHz)	RF Generation Output Peak Power	Nonlinear Component	Modeling Method
1.85	0.05	-	-	C	SONNET
6,000	600	0.05-0.08	5 kW	C&L	Korteweg-de Vries
5	400	0.025-0.055	0.31 W	C	Korteweg-de Vries
5	400	0.015-0.07	0.27 W	C&L	Korteweg-de Vries
10	150	0.04	-	C	SPICE
30,000-50,000	60	1	20 MW	L	-
4,000-43,000	50	-	-	C	LT Spice
400	3270	0.004	8 kW	C	LT Spice
500	600	-	-	C	-
500	34	0.2	-	C	LT Spice
5	50	0.8	0.125 W	C&L	LT Spice
1,000	-	0.033	-	C&L	-

* tunable output frequency; C = Capacitor; L = Inductor.

We mixed composites containing volume fractions between 5 and 25% of barium strontium titanate (BST) or nickel zinc ferrite (NZF) spherical inclusions in a silicone matrix. The dielectric and magnetic parameters were measured from 1-4 GHz using a coaxial airline. The relative permittivity increased from 2.74±0.01 for the polydimethylsiloxane (PDMS) host material to 7.45±0.33 after combining PDMS with a 25% volume fraction of BST inclusions. The relative permittivity of BST and NZF composites was relatively constant across all measured frequencies. The relative permeability of the composites increased from 1.001±0.001 for PDMS to 1.43±0.04 for a 25% NZF composite at 1 GHz. The relative permeability of the 25% NZF composite decreased from 1.43±0.05 at 1 GHz to 1.17±0.01 at 4 GHz. The NZF samples also exhibited low dielectric and magnetic loss tangents from 0.005±0.01 to 0.091±0.015 and 0.037±0.001 to 0.20±0.038, respectively, for all volume fractions, although the dielectric loss tangent did increase with volume fraction. For BST composites, all volume fraction changes of at least 5% yielded statistically significant changes in permittivity; no changes in BST volume fraction yielded statistically significant changes in permeability. For NZF composites, the change in permittivity was statistically significant when the volume fraction varied by more than 5% and the change in permeability was statistically significant for variations in volume fraction greater than 10%. The DC electrical breakdown strength of NZF composites decreased exponentially with increasing volume fraction of NZF, while BST composites exhibited no statistically significant variation with

volume fraction. Of particular note since the FY-2020, we completed breakdown experiments, as summarized in Fig. 2.
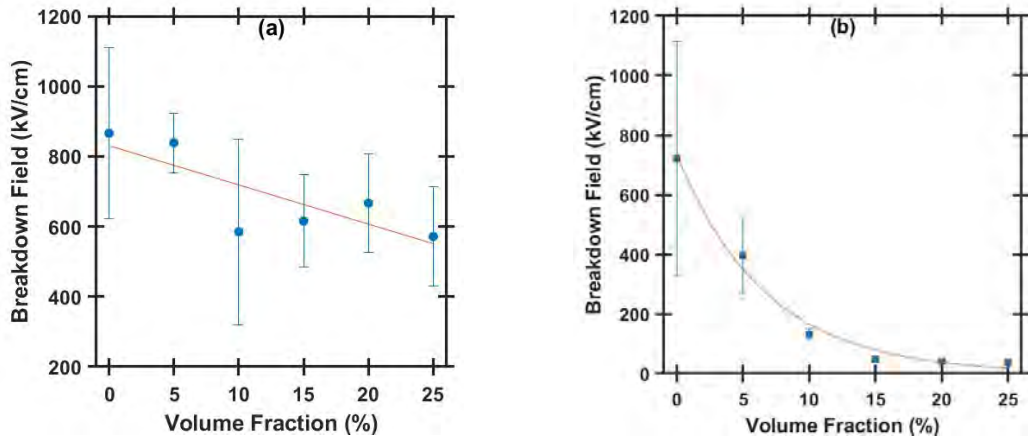

Fig 2 The breakdown electric field for composites with (a) barium strontium titanate (BST) or (b) nickel zinc ferrite inclusions in a silicone (PDMS) matrix. The results are the average of four measurements and the error bars represent the standard deviation of the breakdown electric field values. The fit line has $R^2 = 0.65$, which is expected since an analysis of variance (ANOVA) indicates that changes in breakdown electric field with BST volume loading are not statistically significant. The error bars represent the standard deviation of the electric field values with $R^2 = 0.988$.

Table 2. DC dielectric breakdown threshold in kV/cm for composites with various volume loadings of BST and NZF in a PDMS matrix. Values are reported as the average of four measurements with error determined by standard deviation. Samples labeled N/A were not tested.

		NZF Volume Fraction (%)			
		0	5	10	15
BST Volume Fraction (%)	0	710.42±279.07 kV/cm	395.68±111.041	133.51±14.58	49.90±8.64
	5	838.86±73.72	567.59±247.00	392.24±155.37	N/A
	10	585.15±229.28	597.53±68.15	428.50±13.58	401.20±150.73
	15	644.29±111.25	N/A	423.75±103.53	N/A

We investigated composites manufactured with various volume loadings of both nonlinear magnetic (nickel zinc ferrite) and nonlinear dielectric (barium strontium titanate) inclusions in a silicone matrix. Increasing the volume fraction of barium strontium titanate (BST) and nickel zinc ferrite (NZF) increased the permittivity with a stronger dependence on BST volume fraction. Increasing NZF volume fraction increased the magnetic permeability, while changing BST volume fraction had no effect. The DC dielectric breakdown voltage decreased exponentially with increased NZF volume fraction. Adding as little as 5% BST to an NZF composite more than doubled the breakdown threshold compared to a composite containing NZF alone. For example, adding 10% BST to a 15% NZF composite increased the breakdown strength by over 800%. The combination of tunability of permittivity and permeability by managing BST and NZF volume fractions with the increased dielectric breakdown strength by introducing BST make this a

promising approach for designing high power nonlinear transmission lines with input pulses of hundreds of kilovolts.
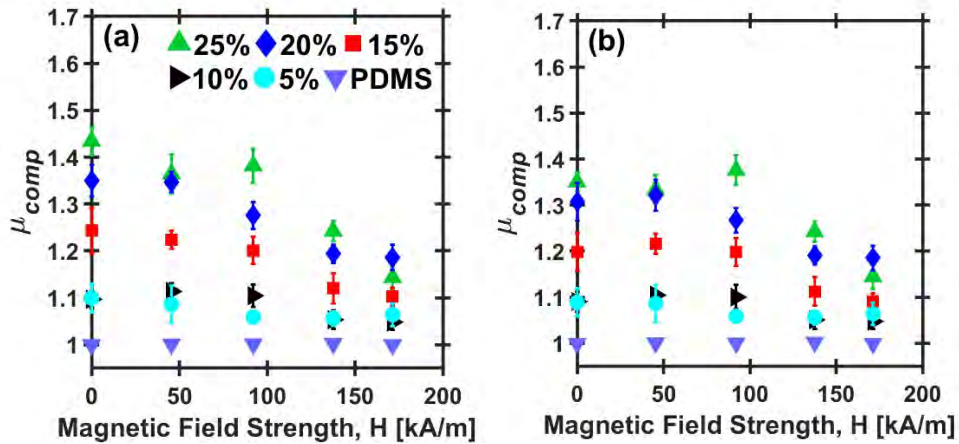
Fig 3 Variation in the real component of the relative permeability μ_{comp} of a composite with 0% (just PDMS), 5%, 10%, 15%, 20%, and 25% volume loadings of NZF inclusions in PDMS as a function of bias magnetic field strength at (a) 1 GHz and (b) 2 GHz. The values reported are the mean of four measurements with error bars determined using standard deviation.
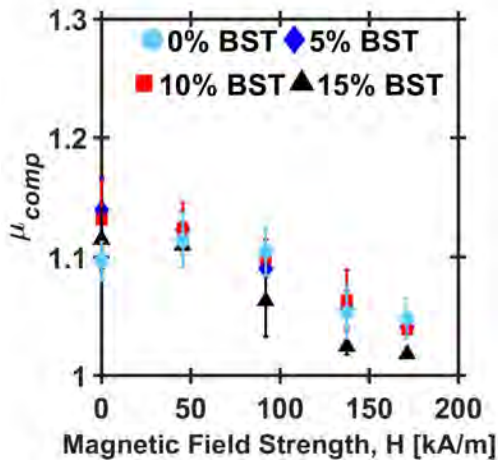
Fig 4 Relative permeability μ_r of a composite containing 10% NZF and 0%, 5% , 10%, and 15% BST in PDMS as a function of bias magnetic field strength at 1 GHz. The permeability is not affected by the addition of BST. The values reported are the mean of four measurements with error bars determined using standard deviation.

We next measured the nonlinear permeability and magnetic loss tangent of composites comprised of various volume loadings of NZF or NZF and BST inclusions encapsulated in a silicon matrix. We measured the relative permeability from 1- 4 GHz using a coaxial airline while biasing the samples in an external DC magnetic field from 0 – 171 kA/m. The permeability decreased from 1 to 4 GHz for each volume fraction but increased with increasing magnetic field strength at low magnetic field strengths with sufficient NZF volume loading. The magnetic loss tangent of the composites increased with increasing frequency and/or NZF volume fraction but were suppressed by increasing the external magnetic field strength. Adding BST to an NZF composites did not cause a significant change in permeability compared to NZF alone, based on an analysis of variance (ANOVA) and multiple comparison test.

Figure 3 shows μ_{comp} as a function of H for various volume fractions of NZF at 1 and 2 GHz. In general, μ_{comp} increases with increasing volume

fraction, but this effect is significantly dampened at higher frequencies. Of similar interest is the nonlinearity of the permeability for each volume fraction. Significant changes in the permeability with respect to the magnetic field only occur when the NZF volume loadings $\geq$ 15%. Figure 4 also demonstrates the feasibility of using NZF volume loading to tune μ_{comp}, which could suggest the potential to tune NLTL impedance for matching to either a pulsed power driver or output. At all frequencies, the data for 10% NZF compared to the 5% NZF was never statistically significant. The difference between 25% NZF and 20% NZF was only significant at $H = 92.09 \pm 4.06$ kA/m. Changing volume fraction by more than 10% caused statistically significant differences in μ_{comp} for most field strengths and volume loading changes. The reduced statistical significance at higher field strengths is expected as we approach the saturation permeability. These results suggest that inclusion loading should be modified by at least 10% to induce noticeable changes in μ_{comp}.

Dual inclusion composites containing various volume fractions of BST and NZF were manufactured and subjected to the same test methods as the single inclusion. Fig. 4 shows that adding BST inclusions to a composite containing 10% NZF in PDMS will not influence μ_{comp}. This is advantageous because, while not measured here, adding BST inclusions increase the composite's permittivity, which should theoretically reduce the risk of breakdown between the center and outer conductors, while still permitting the use of H for biasing the NZF. Moreover, since BST exhibits nonlinear permittivity with electric field, combining BST and NZF may permit simultaneously achieving nonlinearity in both permittivity and permeability to form an electromagnetic shockwave.

COMPOSITE CALCULATIONS
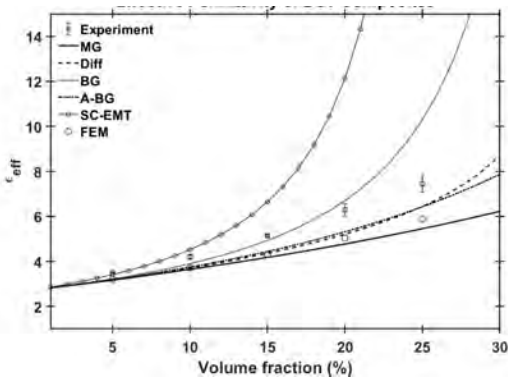
Fig 5 BST composite modeling results for effective permittivity for spherical inclusions compared with measurements.
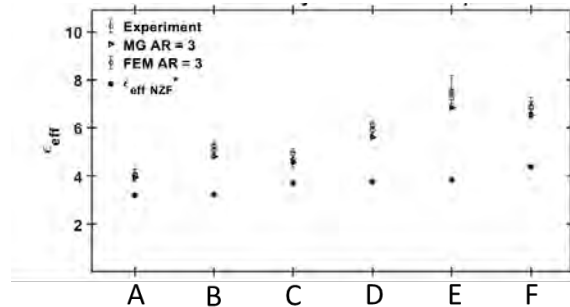
Fig 6 Effective permittivity of BST and NZF dual inclusion composites at 1 GHz with AR = 3 for the BST inclusions. A – 5% NZF and 5% NZF; B – 5% NZF and 10% BST; C- 10% NZF and 5% BST; D - 10% NZF and 10% BST; E – 10% NZF and 15% BST, and F – 15% NZF and 10% BST.

We applied the finite element method (FEM) and various effective medium theories (EMTs) for determining the effective permittivity and permeability of composites containing BST and NZF inclusions in a silicon-based host as a function of volume loadings of the inclusions up to 25% at 1-4 GHz. The modelling results suggest limited agglomerates of powders with high aspect ratios may enhance the effective dielectric properties of BST composites with strong dielectric contrast. The three-phase composites containing both BST and NZF were treated as two-phases composites by using two approaches sequentially for predicting effective real permittivity.

For composites containing only BST, we first assumed spherical shape for the inclusions (AR = 1) in FEM and various EMTs. Figure 5 compares experimental data with FEM and EMT for AR = 1. FEM models agree reasonably well with the Maxwell Garnett (MG), the differential (diff) mixing rule, and Asymmetric-Bruggemann (A-BG) equations, but they overall underestimate effective permittivity (ϵ_{eff}) even at low volume fraction. The Bruggemann (BG) rule agrees with the other approaches at low volume fractions but greatly over-predicts ϵ_{eff} as the volume fraction increases, because the symmetric BG rule only holds for low volume fractions if the composite system is nonsymmetric. Figure 6 shows the modelling results for the effective permittivity of the dual inclusion composites ϵ_{eff} compared with the measurements. Generally, the Maxwell-Garnett mixing rule and simulations using CST assuming aspect ratios of 3 agree well with experimental measurements.

3.   Findings and Conclusions

The results to date have demonstrated the feasibility of tuning the dielectric and magnetic properties of composites comprised of BST and/or NZF in a ceramic material. Additionally, both simulation and effective medium theories (EMTs) can predict these values for potential use in future high power microwave device modeling.

4.   Plans and Upcoming Events

Key tasks and accomplishments for FY2020 follow:
1) Submit composite experimental and simulation manuscripts.
2) Send sample NLTLs to the University of Michigan to test using their high voltage pulsed power supplies (inductive adder and/or Marx bank).
3) Test sample NLTLs using our 10-ns Blumlein pulse generator.
4) Receive and test inductive adder purchased using a DURIP; apply to NLTLs.
5) Continue to develop a model of a full high power microwave system model that may be used in future system design and development.
6) Develop and test tapered NLTLs.

Recommendations for Future Work: Explore tunability of RF output using multiple NLTLs with various volume loadings.

5.   Transitions and Impacts

Not applicable.

6.   Collaborations

Jack Chen, Naval Surface Warfare Center Dahlgren Division
Eagle Harbor Technologies
Ryan McBride, University of Michigan
Walter Sessions, GTRI
Somnath Sengupta, Powerhouse Consulting

7. Personnel

Principal Investigator: Allen L. Garner, 0.95 person-months, National Academy Member (N).
Teams Members:
Xiaojun Zhu, graduate student, 6 person-months, National Academy Member (N).
Travis Crawford, graduate student, 3.8 person-months, National Academy Member (N).
Andrew J. Fairbanks, graduate student, 2.6 person-months, National Academy Member (N).
Business Contact: Lisa Meyers
Subs: GTRI < 1 month

8. Students

3 graduate students /5 undergraduate students (research for credit)

9. Technology Transfer

We are continuing to work with Jack Chen from NSWCDD concerning the incorporation of NLTLs into high power microwave systems and Brad Hoff from AFRL concerning NLTL physics and characterization of the electromagnetic properties. We will continue to work with them as we finalize the review and begin measuring nonlinear electromagnetic properties.

10. Products, Publications, Patents, License Agreements, etc.

Publications resulting from this project:

1. A. J. Fairbanks, A. M. Darr, and A. L. Garner, "A Review of Nonlinear Transmission Line System Design," *IEEE Access* **8**, 148606 – 148621 (2020).

2. T. D. Crawford, A. J. Fairbanks, J. A. Hernandez, T. N. Tallman, and A. L. Garner, "Nonlinear Permeability Measurements for Nickel Zinc Ferrite and Nickel Zinc Ferrite/Barium Strontium Titanate Composites from 1-4 GHz," *IEEE Transactions on Magnetics*, Under Preparation.

3. A. J. Fairbanks, T. D. Crawford, J. A. Hernandez, J. D. Mateja, X. Zhu, T. N. Tallman, and A. L. Garner, "Electromagnetic Properties of Multiphase Composites Containing Barium Strontium Titanate and Nickel Zinc Ferrite Inclusions from 1-4 GHz," *Composites Science and Technology*, Under Preparation.

4. A. J. Fairbanks, T. D. Crawford, J. A. Hernandez, J. D. Mateja, X. Zhu, T. N. Tallman, and A. L. Garner, "Electromagnetic measurements of composites containing barium strontium titanate or nickel zinc ferrite inclusions from 1-4 GHz," *Composites Science and Technology*, Under Preparation.

5. X. Zhu, A. J. Fairbanks, T. D. Crawford, and A. L. Garner, "Modelling Effective Dielectric Properties of Composites Containing Barium Strontium Titanate and/or Nickel Zinc Ferrite Inclusions in the Microwave Range," *Composites Science and Technology*, Under Preparation.

Conference Oral Presentation Abstracts

1. A. J. Fairbanks, X. Zhu, J. A. Hernandez, T. D. Crawford, J. D. Mateja, T. N. Tallman, A. L. Garner, "Experimental and Simulation Evaluation of Composite Materials for NLTL System Design," 22nd Annual Directed Energy Science & Technology Symposium, Student Workshop, 11 March 2020, West Point, NY, USA.

Conference Poster Presentation Abstracts

None

Theses

X. Zhu, "Assessing Effective Medium Theories for Designing Composites for Nonlinear Transmission Lines," MS Thesis, Nuclear Engineering, Fall 2019.

11.   Point of Contact in Navy

Jack Chen, NSWCDD, yeongjer@navy.mil, 02MAR2020
Katie Sheets, AFRL, katherine.sheets@us.af.mil, 02MAR2020.
Jon Cameron Pouncy, NSWCDD, 25SEP2020.

12. Acknowledgement/Disclaimer

Nanoscale Effects on Gas Breakdown and Electron Emission

Grant No. N000014-17-1-2702

Annual Report for Fiscal Year 2020

Period of Performance: October 1, 2019 to September 30, 2020

Prepared by:

Dr. Allen L. Garner, Principal Investigator
Associate Professor and Undergraduate Program Chair, School of Nuclear Engineering
Purdue University
516 Northwestern Ave.
West Lafayette, IN 47906
Tel: (765) 494-0618
Email: algarner@purdue.edu

Grant or Contract Number: N000014-17-1-2702
Date Prepared: 28 January 2021
Project Title: Nanoscale Effects on Gas Breakdown and Electron Emission
Annual Summary Report: FY2020
Principal Investigator: Allen L. Garner, 765-494-0618, algarner@purdue.edu
Purdue University

Section I: Project Summary

1.   Overview of Project

Abstract: Accurately predicting gas breakdown voltage is becoming increasingly important as the trend toward electronics miniaturization increases. Microelectromechanical systems (MEMS), such as microactuators, pressure sensors, and high-frequency circuits, require microscale gaps and high operating voltages. Accurate breakdown voltage predictions for these systems will prevent discharges that could damage or destroy the device. Conversely, microplasmas use microdischarges for various applications, such as electric micropropulsion and environmental mitigation. Present research trends focus on developing micro- and nano-vacuum electronics for providing increased power densities and frequency for directed energy applications, including radar platforms for shipboard and aircraft systems. In particular, the Air Force and Navy have ongoing efforts exploring the field emission (FE) characteristics of arrays of carbon nanotubes, particularly exploring the implications of distance between emitters and variation of work function on electric field characteristics.

Objective: This effort will elucidate the impact of nanoscale effects on gas breakdown for microscale and smaller gaps by combining experiment, numerical analysis, and theoretical analysis. Specifically, it will assess the impact of surface irregularities, which alter the work function and field enhancement factors that drive field emission. This research fills a gap in understanding the influence on surface structure for electron emission and breakdown, which have significant implications for efficiency and equipment durability.

Introduction: Accurately predicting gas breakdown voltage is becoming increasingly important as the trend toward electronics miniaturization increases. From a directed energy perspective, which is critical for Navy and Air Force applications, present research trends focus on developing micro- and nano-vacuum electronics to provide increased power densities and frequency for shipboard and aircraft radar platforms. In particular, the Air Force and Navy have ongoing efforts exploring the field emission characteristics of arrays of carbon nanotubes, particularly exploring the implications of distance between emitters and variation of work function on electric field characteristics. Directed energy systems using laser or intense electromagnetic systems, including pulsed power and high power microwave technologies, are constantly striving to achieve very high power densities using high frequency and more compact systems. As one goes to these smaller systems, higher electric fields arise and issues concerning breakdown, field emission, and space-charge limited flows increase significantly.

Background: Elucidating the impact of nanoscale effects on gas breakdown for microscale and smaller gaps requires combining experiment, numerical analysis, and theoretical analysis. Initial efforts involve the following:

- Assessing and applying analytic models relating field emission and space-charge limited flow, both at vacuum and general pressure, will elucidate the potential impact of space charge on field enhancement to determine the point at which pressure no longer contributes.
- Performing experiments and developing analytic models will determine the impact of surface roughness and various flaws on surface on the work function and field enhancement, which measures the energy necessary to remove an electron from the cathode and plays a crucial role in the determining the field emission current.
- Performing molecular dynamics simulations to determine the implications of electrode geometry on electron emission and space charge effects to provide data for continuum breakdown theories.

These results will then be applied to understand experimental and theoretical analyses of gas breakdown for microscale gaps and smaller. Specific next steps will include:
- Further coupling the existing electron emission and breakdown models to the one-dimensional Schrödinger equation to develop a universal breakdown model from the classical Paschen law to quantum scale for multiple gases.
- Analytic and numerical models developed by the Principal Investigator's group will be modified to incorporate the effects of surface roughness and space charge on field enhancement and work function and compared to the parametric experiments.
- Experimental measurements will be performed for gaps from microscale to approximately 100 nm at vacuum and atmospheric pressure to provide a basic parametric study of the mechanisms responsible for breakdown across a wide range of parameters.

This effort will ultimately pave the way for future work unifying all relevant modes of breakdown and electron emission across gap pressure and distance for numerous applications relevant to the Department of Defense, including directed energy, field emission, and micropropulsion.

2.   Activities and Accomplishments

FY 2020 continued to focus on extending our previous theories to pressures between vacuum and atmospheric, and length scales from micro- to nanoscale, and performing experiments on breakdown and electron emission down to nanoscale at atmospheric pressure. We additionally completed incorporation of surface roughness into determining work function, and submitted an invited Perspective manuscript on nexus theory to the *Journal of Applied Physics.* We began particle-in-cell simulations to characterize changes in the ionization coefficient at nano- and microscale gaps where the ratio of the electric field to gas pressure invalidated standard semi-empirical representations of the values. Two students defended their Ph.D. dissertations: Amanda Loveless (Nuclear Engineering) and Russell Brayfield (Agricultural and Biological Engineering).

We will next summarize our efforts over the past year, focusing on the following accomplishments: (1) Finalization of unification of quantum breakdown effects with gas breakdown and electron emission, (2) Derivation of gas breakdown condition for pin-to-plate geometry, (3) work function determination as a function of surface roughness, and (4) nanoscale breakdown experiments.

UNIFIED EMISSION AND BREAKDOWN THEORY FROM QUANTUM SCALE TO PASCHEN'S LAW

In FY-2019, we outlined the unification of gas breakdown to electron emission down to quantum scales. In FY-2020, we completed this work and submitted the manuscript to *Physical Review Research* for consideration. The wide range of operating conditions for applications such as micro- and nano-electromechanical systems, microplasmas, and directed energy that go down to

microscale and range from vacuum to atmospheric pressure. complicates the derivation of a single scaling law for electron emission, and gas breakdown complicates theoretical assessments. Theoretical studies resort to unifying two to three mechanisms piecemeal. This study defines a common set of scaling parameters across the range of dominant mechanisms to derive a single, unified theory that yields asymptotic solutions for quantum space-charge limited emission (QSCL), classical space-charge limited emission (CSCL), space-charge limited emission with collisions (MG), Fowler-Nordheim field emission (FN), field emission driven gas breakdown, and classical gas breakdown defined by Paschen's law (PL). These equations are universal (true for any gas) across all regimes except for PL, which contains a single, material-dependent parameter. This approach reproduced various nexuses corresponding to the transitions across multiple mechanisms, such as QSCL to CSCL, CSCL to FN, CSCL to MG to FN, and field emission-driven breakdown as described by FN to PL, using a single common framework to facilitate experimental designs concerned with crossing these regimes. Furthermore, we demonstrated the conditions for more complicated nexuses, such as matching QSCL, CSCL, MG, and FN.
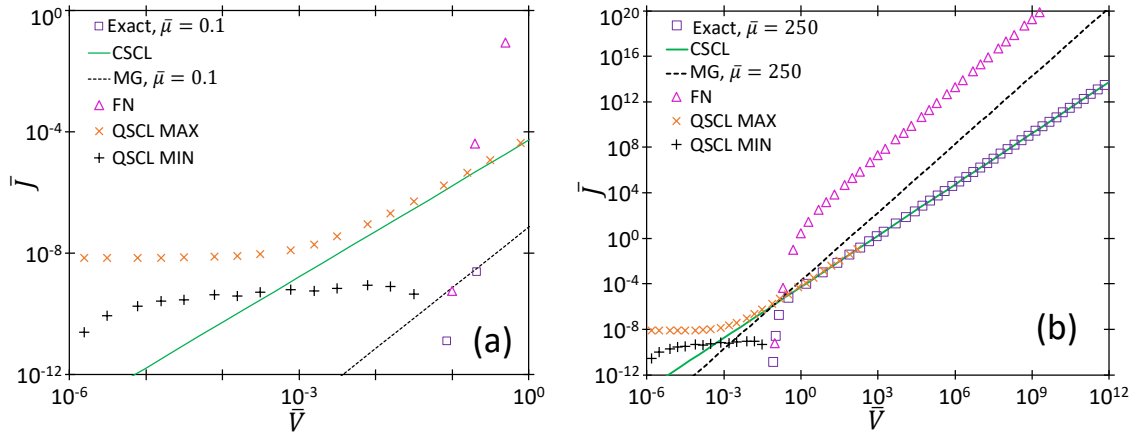

FIG. 1. Dimensionless current density $\bar{J}$ as a function of dimensionless breakdown voltage $\bar{V}$ for a 10 nm gap demonstrating the transitions of the exact solution between QSCL, CSCL, FN, and MG focusing on (a) the transition from QSCL to CSCL and (b) the full spectrum of transitions.

Reducing gap distances below ~100 nm requires additionally considering the implications of QSCL on emission. The dimensionless quantum equations give a minimum and maximum solution for QSCL, as shown in Fig. 1. Figure 1(a) shows the intersection of each solution of the QSCL solution with CSCL. In particular, the solution ultimately follows the CSCL once $\bar{V}$ is sufficiently large to overcome quantum effects. Figure 1(b) shows the nexus between QSCL, CSCL, MG, and FN at a fixed $\bar{\mu} = 250$. This point represents a state of high sensitivity where small perturbations in experimental conditions may shift the system into any of these emission regimes.

Figure 2 shows state diagrams demonstrating the transitions between the asymptotic solutions of the various emission mechanisms at $\bar{\mu} = 500$ and 5000 to examine the relative importance of each mechanism. First, there are two curves representing the transition between CSCL and FN. The blue dashed line indicates the direct transition from CSCL to FN. The magenta "x" denote the enhancement of space-charge-limited emission due to QSCL, indicating that QSCL occurs at a lower voltage than CSCL, shifting the nexus between space-charge-limited emission down from the prior CSCL/FN intersection. As such, the region between the magenta "x" and the blue dashed line indicates where quantum enhancement occurs. These curves are independent of $\bar{\mu}$. At the

highest $\bar{\mu}$ (closest to vacuum), the quantum enhancement from QSCL occurs to the left of the nexus between CSCL, MG, and FN (cf. Fig. 2(c)). Reducing the mobility to $\bar{\mu} = 500$ causes the transition from CSCL and MG to shift sufficiently to the left such that all four solutions match at $\bar{d} \approx 10^3$ (cf. Fig. 2(a)), giving a fourth order nexus between QSCL, CSCL, MG, and FN. It is also possible at sufficiently high $\bar{V}$ to transition from FN to MG to CSCL without experiencing the quantum enhancement at even small $\bar{d}$.
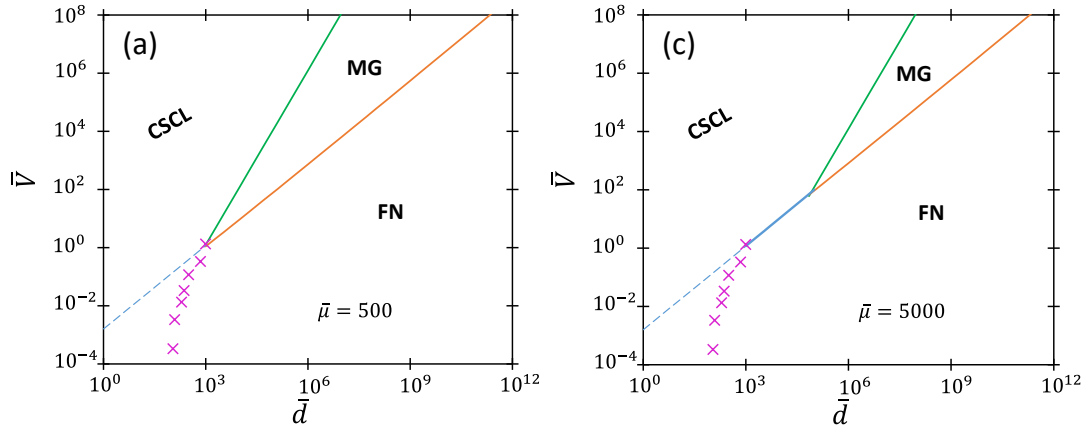
FIG. 2. Dimensionless breakdown voltage, $\bar{V}$, as a function of dimensionless gap distance, $\bar{d}$, demonstrating the respective regions where each emission mechanism should dominate for dimensionless mobilities of (a) $\bar{\mu} = 500$ and (c) $\bar{\mu} = 5000$. The dashed line denotes the continuation of the nexus between the classical Child-Langmuir law (CSCL) and the Fowler-Nordheim (FN) law. The "x" denote the contribution due to quantum effects (QSCL), which shifts the transition from FN to space-charge limited emission to lower $\bar{V}$. In this case, (a) denotes a fourth order nexus between QSCL, CSCL, and FN.
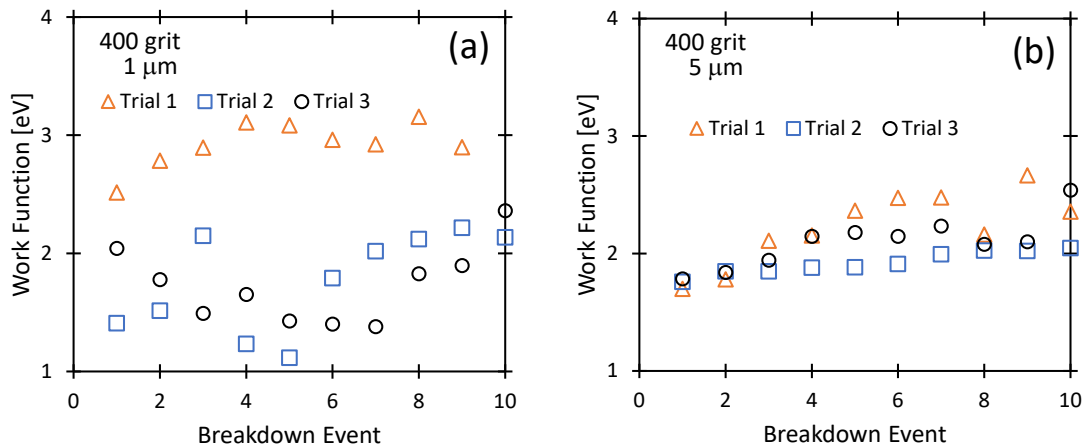

FIG. 3. Work function as a function of breakdown event for 400 grit polishing at initial interelectrode gap distances (neglecting potential changes due to crater formation) of (a) 1 μm, (b) 5 μm, and (c) 10 μm. Each point represents data from each individual breakdown event from Brayfield *et al*. (2019).

PIN-TO-PLATE GAS BREAKDOWN THEORY

We modified a previous theory coupling PL and field emission to account for pin-to-plate geometries by replacing the field enhancement, which has been used primarily as a fitting parameter, with the appropriate vacuum electric field. This requires explicitly accounting for the spatial dependence of ionization and non-uniform space charge in Poisson's equation. We derive a breakdown equation of the form previously obtained for planar geometry that agrees well with experimental data with the work function as the fitting parameter. The work function was consistently lower (~2 eV) than anticipated (~4.5 eV), but was generally fairly consistent (~± 7 %). We then derived closed form solutions in the limit of low ionization, corresponding to the field emission regime, and recovered an analytic solution for a parallel plate geometry in the limit of small gap distance that differed from prior analytic results because of the explicit consideration of spatial dependence in charge density. This theory may ultimately be applied to other nonplanar geometries by applying the appropriate equation for vacuum electric field.

We first applied the breakdown theory to experimental data from Brayfield *et al*. (2019) using a pin with a 0.5 μm tip radius and gap distances of 1, 5, and 10 μm. Figure 3 shows the fitted ϕ from a numerical solution of our theory using data we published previously. Because we incorporated the work function into the scaling parameters, changing the work function changes all of the scaling terms, which changes every subsequent variable (all of the dimensionless terms). Thus, care must be taken when comparing nondimensional values for different work functions. We numerically determined ϕ that equated $\bar{E}_b$ with the experimentally determined, nondimensionalized breakdown voltage.

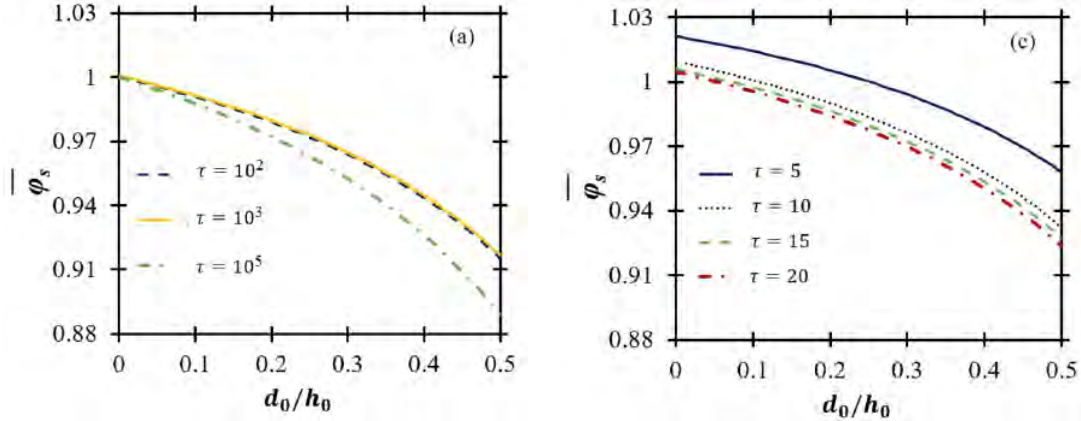# THEORETICAL ANALYSIS OF WORK FUNCTION OF A WAVY SURFACE

FIG. 4. Effective surface work function $\bar{\phi}_s$ as a function of d_0/h_0 for large (a) and small (b) τ, where d_0 is the peak height of the waviness, h_0 is the distance from the scanning Kelvin probe (SKP) tip to the center of the wavy surface, and $\tau = T/x_0$, where T is the period of the wavy surface and x_0 is the step distance of the SKP along the surface.

The work function may affect the physical, electrical, and chemical behavior of surfaces, making it important for numerous applications and phenomena, including field emission, gas breakdown, and nanotechnology. We have previously reported our application of error propagation to quantify the sensitivity of breakdown predictions to various parameters and showed that microscale breakdown is very sensitive to work function when field emission dominates breakdown. Despite

this importance, studies examining the impact of surface roughness on work function have only examined the amplitude and not the period of the waviness, which becomes increasingly important with reduced device size. We extended these previous scanning Kelvin probe (SKP)-based mathematical models for predicting the work function of a metallic surface with surface waviness by explicitly including the period. For a given ratio of surface roughness amplitude to the distance from the SKP to the center of the waviness, increasing the period or reducing the SKP step distance reduced the surface's effective work function. In the limit of infinite period (or low SKP step size) and low surface roughness amplitude, the work function approached that expected with a concomitant reduction in the gap distance with no surface roughness. The effective surface work function approaches zero and may become negative as the SKP tip approaches the surface, suggesting the importance in these corrections for nanoscale measurements. As the SKP step size approaches the surface roughness period, the effective work function becomes infinitely large. Figure 4 demonstrates this behavior.

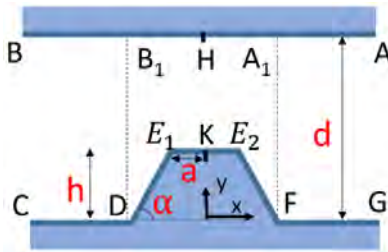## NANOSCALE GAS BREAKDOWN AND ELECTRON EMISSION EXPERIMENTS

FIG. 5: Electrode system for assessing field enhancement effect on microscale breakdown.

As addressed in previous reports, we have constructed multiple nanoscale emitters based on the geometry in Fig. 5 [19] at Birck Nanotechnology Center at Purdue and with the University of Chicago. The nanoscale data from the first batch of chips constructed at Birck has been analyzed and incorporated into a manuscript in preparation for publication. Child-Langmuir (CL) current scales linearly with $V^{3/2}$. For FN, $\ln(I/V^2)$ scales linearly with $1/V$, where I is the current. Finally, MG emission current scales with V^2, giving linear fits when the emitted current is dominated by MG [2].
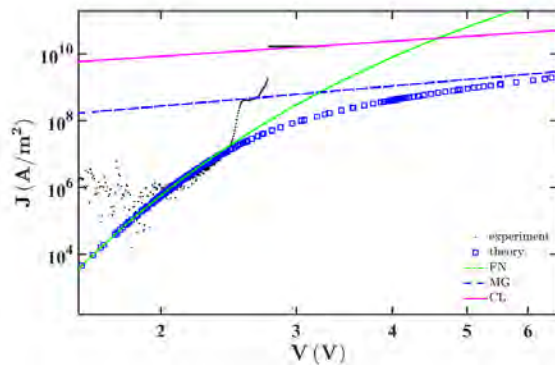

FIG. 6: Experimental data for a 28 nm ± 10 nm gap and a fitted emission area of 64 nm^2 based on our previously derived full theory showing FN dominated emission transitioning to breakdown as the device fails.

The only observable linear trends were with certain portions of the FN curve. The parameter space of the devices was selected such that the protrusion width $2a$ and the gap distance d-h are independently evaluated. Figure 6 shows that emission current is clearly FN dominated until breakdown for a 28 nm ± 10 nm gap with a fitted emission area of 64 nm^2, regardless of the mobility used.

The plateau regions that initially appeared to correlate to MG and CL emission on their individual plots actually arise due to device failure. Microscope observations showed that the devices heated and ultimately melted, which contributed to the devices transitioning directly to breakdown and accounts for the constant current at the higher applied voltages (the devices have essentially shorted). Figure 7

shows the behavior for a 125 nm ± 10 nm gap with a fitted emission area of 64 nm^2 with mobilities of (a) 0.0003 m^{2}V^{-1}s^{-1} and (b) 0.001m^{2}V^{-1}s^{-1}. The higher mobility condition estimate in Fig. 7(b) confirms behavior we predicted theoretically previously. The emission current is a combination of FN and space charge effects, but does not reach the MG or CL asymptotes.

Figure 8 repeats this process for a gap of 450 nm ± 10 nm and a fitted emission area of 64 nm^2 with mobilities of (a) 0.003 m^{2}V^{-1}s^{-1} and (b) 0.01 m^{2}V^{-1}s^{-1}. The transition does not occur in this case with behavior transitioning directly from FN to breakdown, as observed for microscale breakdown.
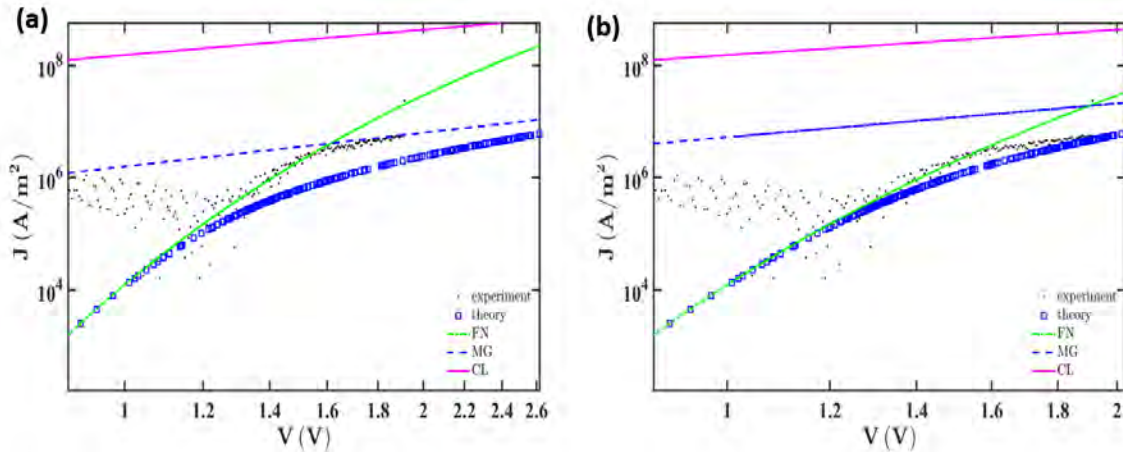
FIG. 7: Transition behavior for mobilities of (a) 0.0003 m^{2}V^{-1}s^{-1} and (b) 0.001 m^{2}V^{-1}s^{-1} showing predicted transition behavior at the higher mobility limit for a 125 nm gap.
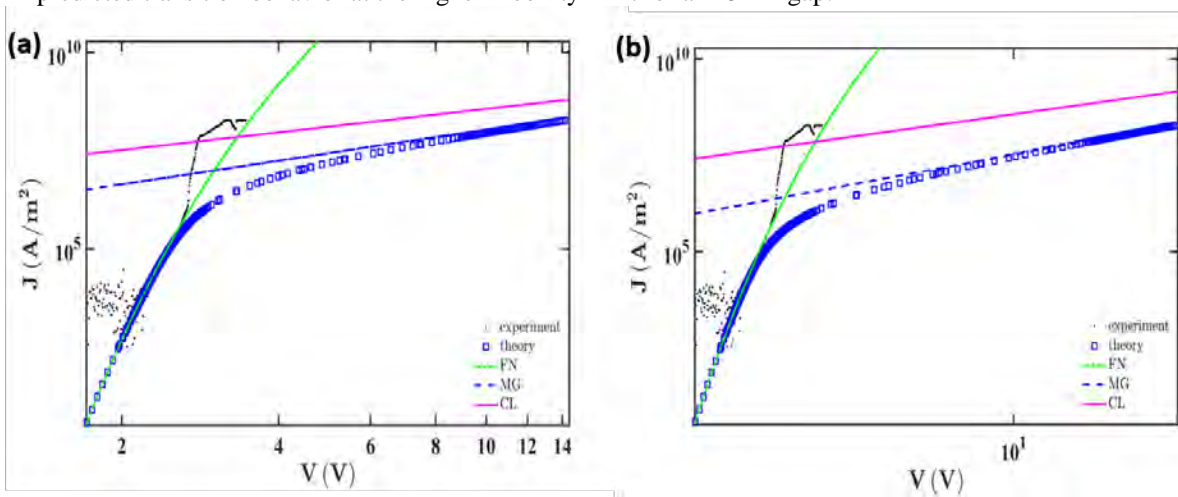

FIG. 8: JV plot for a device with gap of 450 nm ± 10 nm and a fitted emission area of 64 nm^2 with mobilities of (a) 0.003 m^{2}V^{-1}s^{-1} and (b) 0.01 m^{2}V^{-1}s^{-1} showing no transition behavior, moving directly from FN dominant emission to breakdown.

3. Findings and Conclusions

These efforts have further elucidated gas breakdown and electron emission at nanoscale. Our published work in FY-2020 showed the impact of surface roughness on work function and summarized our theoretical and experimental efforts at unifying electron emission mechanisms and breakdown. Our ongoing theoretical work has extended this analysis and our experiments, which have been delayed due to COVID-19-related delays at the University of Chicago, have provided some insight into field emission and space-charge limited emission at atmospheric pressure. Since many directed energy devices are exploring nanoscale devices and vacuum may not be perfect, our results provide insight into how electron emission, including space-charge limited emission, may drive breakdown at nanoscale. Molecular dynamics simulations, particle-in-cell simulations, and experiments at intermediate pressures in FY-2021 will begin characterizing this regime and elucidate device design limitations.

4. Plans and Upcoming Events

Upcoming significant events:
1) Submit Invited Perspective paper on emission mechanism transition to the *Journal of Applied Physics*.
2) Submit Invited Perspective paper on space-charge limited emission transition to the *Journal of Applied Physics*.
3) Assess electron emission at nanoscale experimentally and using simulations.
4) Complete theoretical assessment of surface roughness on work function.
5) Complete nanoscale experiments, particle-in-cell and molecular dynamics simulations.

Future transitions:
1) Continue discussions with AFRL – particularly concerning sub-microscale breakdown experiments as this expands to sub-atmospheric pressure.
2) Work with NRL to transition breakdown theory (Kevin Jensen) and surface roughness effects (Ray Allen) for larger devices.
3) Continue discussions with NSWCDD (Matt McQuage and Jack Chen) concerning relevant 6.2 applications of the studied phenomena.
4) Discussions with Sandia National Laboratories about electron emission and breakdown.

5. Transitions and Impacts

None at present, although future goals for Year 3 are outlined in Section 4.

6. Collaborations

Guodong Meng, international collaborator, N/A, National Academy Member (N), China
Ágúst Valfells, international collaborator N/A, National Academy Member (N), Iceland
Yangyang Fu, N/A, Academy Member (N), Michigan State University
Peng Zhang, N/A, Academy Member (N), Michigan State University
L. K. Ang, N/A, Academy Member (N), Singapore
John Luginsland, N/A, Academy Member (N), Confluent Sciences
Yee-Sin Ang, N/A, Academy Member (N), Singapore

7.   Personnel
Principal Investigator: Allen L. Garner, .98 person-months, National Academy Member (N).
Teams Members:
Amanda M. Loveless, Post-Doctorate, 1.5 person-months, National Academy Member (N).
Amanda M. Loveless, graduate student, .9 person-months, National Academy Member (N).
Russell S. Brayfield, graduate student, 5.7 person-months, National Academy Member (N).
Andrew J. Fairbanks, graduate student, 1 person-months, National Academy Member (N).
Haoxuan Wang, graduate student, 0.5 person-months, National Academy Member (N).
Business Contact: Lisa Meyers
Subs: None

8.   Students
5 graduate students/1 undergraduate student assisting (research for credit) during reporting period

9.   Technology Transfer
None.

10.   Products, Publications, Patents, License Agreements, etc.
Publications resulting from this project:

<u>Archival Publications</u>

1. **[MINI-COURSE]** A. L. Garner, A. M. Loveless, J. N. Dahal, and A. Venkattraman, "A Tutorial on Theoretical and Computational Techniques for Gas Breakdown in Microscale Gaps," *IEEE Transactions on Plasma Science* **48***,* 808-824 (2020).

2. J. R. Malayter and A. L. Garner, "Theoretical Assessment of Surface Waviness on Work Function," *AIP Advances* **10**, 095110 (2020).

3. **[INVITED PERSPECTIVE]** A. L. Garner, G. Meng, Y. Fu, A. M. Loveless, R. S. Brayfield II, and A. M. Darr, "Transitions between electron emission and gas breakdown mechanisms across length and pressure scales," *Journal of Applied Physics*, Under Review.

4. A. M. Loveless, A. M. Darr, and A. L. Garner, "Unification of Electron Emission and Breakdown Mechanism Theories from Quantum Scales to Paschen's Law," *Physical Review Research*, Under Review.

5. **[INVITED PERSPECTIVE]** P. Zhang, Y. S. Ang, A. L. Garner, Á. Valfells, J. W. Luginsland, and L. K. Ang, "Space-charge limited current in nanodiodes: Ballistic, Collisional and Dynamical Effects," *Journal of Applied Physics*, Under Preparation.

6. A. M. Loveless, L. I. Breen, and A. L. Garner, "Analytic theory for field emission driven microscale gas breakdown for a pin-to-plate geometry," *Journal of Applied Physics*, Under Preparation.

<u>Conference Papers</u>

1. A. M. Loveless, A. M. Darr, R. S. Brayfield II, J. R. Malayter S. A. Lang, and A. L. Garner, "Nanoscale Feature Implications on Electron Emission and Gas Breakdown," Trans. Am. Nucl. Soc. **121**, 399-401 (2019).

Conference Oral Presentations

1. R. S. Brayfield II, A. M. Darr, W. Li, A. J. Fairbanks, H. Wang, *A. M. Loveless*, and A. L. Garner, "Nano/Micro-Meter electrode topology Effects on Electron Emission," 22nd Annual Directed Energy Science & Technology Symposium, Student Workshop, 11 March 2020, West Point, NY, USA.

2. *A. M. Loveless*, A. M. Darr, and A. L. Garner, "Implications of Electrode Geometry on Electron Emission and Microscale Gas Breakdown," 22nd Annual Directed Energy Science & Technology Symposium, Student Workshop, 11 March 2020, West Point, NY, USA.

3. *A. M. Loveless*, A. M. Darr, R. S. Brayfield II, J. R. Malayter, S. A. Lang, and A. L. Garner, "Nanoscale Feature Implications on Electron Emission and Gas Breakdown," Trans. Am. Nucl. Soc. **121**, 399-401 (2019).

4. *J. Malayter* and A. L. Garner, "Theoretical Assessment of Surface Waviness on Work Function," 2019 Fall Undergraduate Research Expo, West Lafayette, IN, 18 November 2019.

Conference Poster Presentations

None this period

Invited Colloquia and Seminars

1. *A. L. Garner*, "Electron Emission and Gas Breakdown from Quantum to Classical Lengths," Plasma Seminar Series, University of Washington, Seattle, WA, 02 December 2019.

2. *A. L. Garner*, "Theoretical and Experimental Unification of Electron Emission Mechanisms," Department of Electrical and Computer Engineering, Boise State University, Boise, ID, 04 December 2019.

3. *A. L. Garner*, "Unified Electron Emission Theory and Experimental Validation," Department of Electrical and Computer Engineering, University of New Mexico, Albuquerque, NM, 06 December 2019.

4. *A. L. Garner*, "Unified Electron Emission Theory and Experimental Validation," Oak Ridge National Laboratory, Oak Ridge, TN, 03 March 2020.

5. *A. L. Garner*, "Re-envisioning Electron Emission Physics," Sandia National Laboratories, Albuquerque, NM, 17 August 2020. (Delivered remotely due to COVID-19).

11.   Point of Contact in Navy

Kevin Jensen, NRL, 20SEP2020; Joe Schumer, NRL, 19NOV2019; Jack Chen, NSWCDD, 28JUN2019; Wilkin Tang, AFRL, 04JUN2020; Don Schiffler, AFRL, 18SEP2020; Katie Sheets, AFRL, 02MAR2020.

12.   Acknowledgement/Disclaimer

Theory and Experiments on Magnetically Insulated Line Oscillator (MILO)

Grant No. N00014-19-1-2262

Annual Report for Fiscal Year 2020

Period of Performance: October, 1, 2019 to September 30, 2020

Prepared by:

Professor Ronald Gilgenbach, Principal Investigator
University of Michigan
Department of Nuclear Engineering and Radiological Sciences
2355 Bonisteel Blvd
1905 Cooley Building
Ann Arbor, MI 48109-2104
Tel: (734) 763-1261
Email: **rongilg@umich.edu**

Grant or Contract Number: N00014-19-1-2262
Date Prepared: 1/6/2021
Project Title: Theory and Experiments on Magnetically Insulated Line Oscillator (MILO)
Annual Summary Report: FY2020
Principle Investigator:
Ronald M. Gilgenbach
(734) 763-1261
rongilg@umich.edu
University of Michigan, Ann Arbor, MI, US

Section I: Project Summary

1. Overview of Project

Abstract: The University of Michigan has made progress on the development of novel moderate current (~10 kA) MILO concepts, which may address the previous low efficiency and narrow bandwidth of MILOs. We have performed simulations using Microwave Studio CST (Computer Simulation Technology AG), to investigate the feasibility of MILO operation with reduced pulsed power driver requirements. These simulations indicate a viable 5-cavity MILO design at 300 kV and 10 kA. We have constructed the complete solution of the Brillouin flow in planar MILO or planar Relativistic Magnetron (RM), or some combination of the two, in cylindrical geometry with axial electron flow (as in cylindrical MILO), in cylindrical geometry with azimuthal electron flow (as in cylindrical magnetron and cylindrical RM), and in the radially converging flow in Magnetically Insulated Transmission Line (MITL), as in a linear transformer driver (LTD)).

Objective: This project aims to improve understanding of the fundamentals of Magnetically Insulated Line Oscillators through improvements in computational modeling and analytic theory backed by experimental results. This improved understanding will be applied to the development of efficient, multi-tone MILOs, and (with the aid of the University of New Mexico (UNM)) transitioned to Naval Surface Warfare Center Dahlgren Division (NSWCDD) for testing on high value targets of interest.

Introduction: The MILO is a crossed-field device, basically, a linear magnetron, in which the magnetic field is self-generated by the electron current, thereby eliminating the need for external magnets or magnetic field coils. This means that the MILO is more compact, and lighter, than other high power microwave (HPM) sources, including the relativistic magnetron.

Background: The goal of this research program is to generate multi-spectral, high power microwaves from the Magnetically-Insulated-Line Oscillator. The topic of MILO was investigated extensively throughout the 1990s with excellent results, particularly at the Air Force Research Laboratory (AFRL). However, since that time there have been major developments in: 1) low impedance, high current pulsed power (Linear Transformer Driver); 2) 3-D electromagnetic (EM) particle in cell (PIC) codes; and 3) innovative manufacturing techniques (e.g., additive manufacturing/3D printing) that justify a new examination of MILO in the USA. It should be mentioned that Chinese laboratories have extensively investigated MILO and LTD in recent years, so it is crucial that the US refresh and rejuvenate MILO research to avoid technological surprises.

Previous ONR research at the University of Michigan (UM) demonstrated that the Multi-frequency Recirculating Planar Magnetron (MFRPM) concept could generate 10s of MW, high power microwaves in two different frequency bands, simultaneously. It is expected that the MILO could generate even higher power levels at single or multiple frequencies. This research will consist of analytic theory, 3-D EM PIC simulations and experiments.

The primary thrusts of this research include: a theoretical analysis of the Buneman-Hartree condition for MILO; analysis of MILO efficiency, gain, and startup; the viability of multi-frequency MILO; the effects of a modest external magnetic field; the compatibility of new low impedance drivers (such as LTD) for MILO; opportunities for additive manufacturing of MILO; and technology transfer for NSWC Dahlgren.

The first year of this research program concentrated on fundamental research to develop the scaling laws (e.g., Buneman-Hartree condition), computational modeling and single frequency experiments on the MILO. The second and third year will become more applied MILO research with technology transfer to the Naval Surface Warfare Center Dahlgren. UM will collaborate closely with University of New Mexico as well as NSWC Dahlgren.

MILOs were largely developed in the USA (1980's-2000), but recently have seen intensive research and development by potential competitor countries. Our goal is to address, via focused and transitional HPM research, some of the critical problems facing Navy operations due to asymmetric electronic threats, such as those faced by Marine warfighters in forward operating bases, to those in littoral waters, and protection of high value targets, such as U.S. embassies in potential hot spots around the globe. These asymmetric electronic threats can come in the form of small airborne electronic drones, perhaps even commercial-off-the-shelf (COTS)-type devices employed in boat or automobile-size machines.

2. Activities and Accomplishments

In the first full year of this research project, we continued to make great strides in analytic theory and simulation, while also conducting several experimental campaigns. Experimental research during the reporting period was impacted by COVID restrictions at the university, but the schedule has recovered in the last few months of 2020.

Analytic Theory of MILO

MILO and relativistic magnetron are both crossed-field devices capable of generating high-power microwaves. The RM is topologically the kilowatt-class microwave source that powers the microwave ovens, but upgraded in power exceeding a million times. The MILO is similar to RM but does not require an external magnetic field. These two are thus very different, yet similar, devices. RM possesses a moderately high efficiency (approaching that of the microwave oven). The MILO has a much lower efficiency, but has a tremendous system advantage because of its substantial reduction in size and weight (no external magnet) compared with RM.

The theoretical foundation for MILO was amazingly weak, though this device has been in existence for more than 30 years. One can find numerous erroneous statements, and grossly in-adequate scaling formulas, in the MILO literature. This poor understanding of the MILO, in comparison with the RM, greatly hindered an effort to find an optimal crossed-field configuration, if one exists, that would combine the advantages of MILO and RM.

This forced us to provide a foundational study of Brillouin flow that is applicable to both MILO and RM. This is important because the Brillouin flow is now generally regarded as the prevalent equilibrium state in crossed-field devices, from which the Hull-cutoff condition (HC) and the Buneman-Hartree condition (BH) can be derived. The urgency of this problem may be understood if one notes that BH has never appeared in the open literature for a cylindrical MILO with an axial electron flow (which is the most common MILO configuration). Our intensive study of the Brillouin flow led to the following novel results.

It is found that the most appropriate description of HC and BH, for both MILO and RM, is in terms of the AK (Anode-Cathode) voltage drop (V_a) and the total magnetic flux (A_a) within the crossed-field gap. The traditional use of the magnetic field (B) is inconvenient because the self-magnetic field could be strong and difficult to account for. The use of the current (I) is also inconvenient because there are three (3) components of currents in the Brillouin flow: the current on the anode, the current on the cathode, and the current carried by the electrons in the Brillouin hub.

In terms of V_a and A_a, we have found an analytic, closed form solution of the Brillouin flow and the associated HC and BH. This is applicable to both MILO and RM, or some combination of the two, as in the case where the total magnetic flux (A_a) is partially provided by an externally imposed magnetic field, and partially provided by the wall currents on the MILO. Note that we have obtained the BH for the MILO for the first time.

Once we assume that the Brillouin flow is the prevalent flow for both MILO and RM, and the associated HC and BH are established (at a given combination of V_a and A_a), the mechanism for spoke formation and for conversion of the potential energy to RF then become identical in MILO and in RM, or some combination of the two, as pointed out in Item 2.

Scaling laws have been constructed for all parameters, whether the diode voltage V_a is relativistic or not. This analysis is important to explore the possibility of a low voltage MILO.

Our general analysis has been successfully extended to the radially converging Brillouin flow that would exist, for example, in the linear transformer driver, which has become the basic building block for the architecture in modern pulsed-power technology. Our complete characterization in the Brillouin flow (once V_a and A_a, and the geometry are given) allows a ready evaluation of the severity of the diocotron instability, which has long been suspected to cause the leakage current observed in the deeply insulated (or not so deeply insulated) region of MITL.

In summary, our group has now constructed the complete solution of the Brillouin flow in planar MILO or planar RM, or some combination of the two, in cylindrical geometry with axial electron flow (as in cylindrical MILO), in cylindrical geometry with azimuthal electron flow (as in cylindrical magnetron and cylindrical RM), and in the radially converging flow in MITL (as in a LTD). A comprehensive treatise on this subject is being drafted, covering this wide range of devices.

MILO Design and Experiment
Initial experiments focused on establishing the magnetic insulation achievable with the MELBA pulsed power driver in its present configuration (-300 kV, 10 kA, 500 ns pulsewidth). To that end, a **smooth-bore planar** MILO was constructed and tested (Figure 1). This MILO's self-generated magnetic field could be supplemented with an external magnetic field, either through embedded

permanent magnets or a pulsed electromagnet. Undergraduate researcher Emma Guerin created a test stand for permanent magnets and mapped the expected magnetic field in the AK gap region for a range of potential AK gaps. No viable configuration of permanents was identified, and a pair of electromagnet coils were used to supply the supplemental magnetic field.
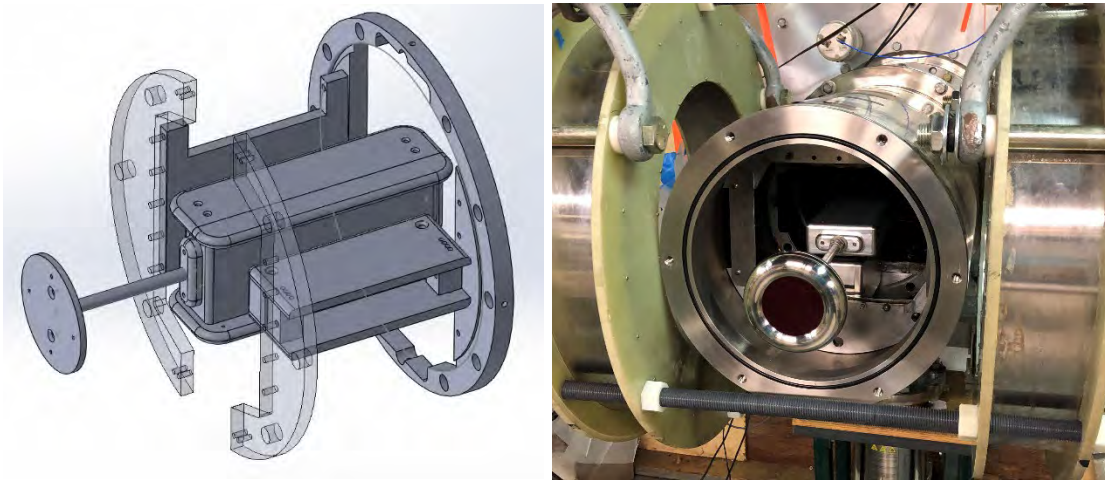

Figure 2: (left) CAD model of smooth-bore planar MILO. (right) Assembled smooth-bore planar MILO mounted in the chamber with magnetic field coils rotated to provide a transverse magnetic field. The red velvet cathode is the primary source of axial electron emission, but a strip of velvet is also present on the smooth-bore cathode surface to provide radial electron emission.

Initial tests of the planar smooth-bore MILO indicated a 10 kA electron beam at nominally 300 kV could be obtained from the MELBA pulsed power driver, and would successfully insulate the diode at the 1-2 cm AK gaps tested. Subsequently, a planar MILO was simulated in Microwave Studio CST, with and without an external magnetic field.

Subsequent communications with the ONR program manager and other collaborators within the DoD indicated that a planar MILO was not of DoD interest, so our efforts were refocused on the development of a viable cylindrical MILO for use with the MELBA driver. This corresponded with the beginning of laboratory restrictions related to COVID-19, so there was a strong focus on simulation. Using the theoretical framework developed by our group (Figure 2), we projected a MILO could be driven by a -300 kV source supplying as little as 7 kA and still maintain magnetic insulation through its self-generated magnetic field.

From this baseline we designed a **smooth-bore cylindrical** MILO experiment with no slow-wave structure (SWS) (Figure 3) and fielded it on the MELBA pulsed power driver (Figure 4). This series of shots produced voltages of ~-250 kV and 10-15 kA of current at peak voltage. To control the peak current, the axial gap in the downstream diode was varied from 2 to 4 cm, with the smaller gap producing higher peak current and improved magnetic insulation. This experiment established that magnetic insulation was achievable for relevant MILO geometries.
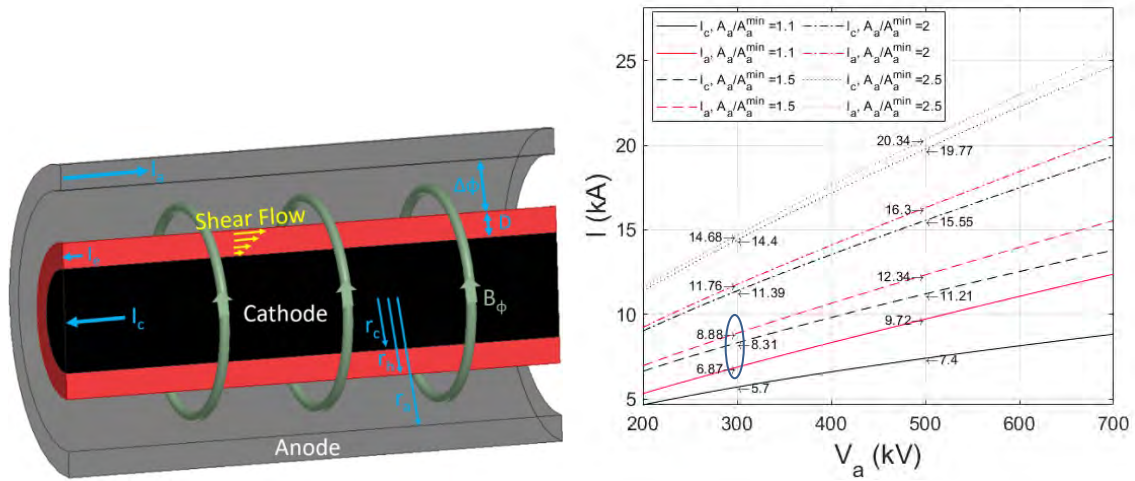
Figure 3: (left) Cylindrical MILO geometry labeled with various important parameters (right) Predictions of the necessary anode (I_a) and cathode (I_c) current to insulate a cylindrical diode to varying degrees. Hull cutoff is achieved with A_a/A_a^{min} set to 1; at higher ratios, the diode becomes more strongly insulated.
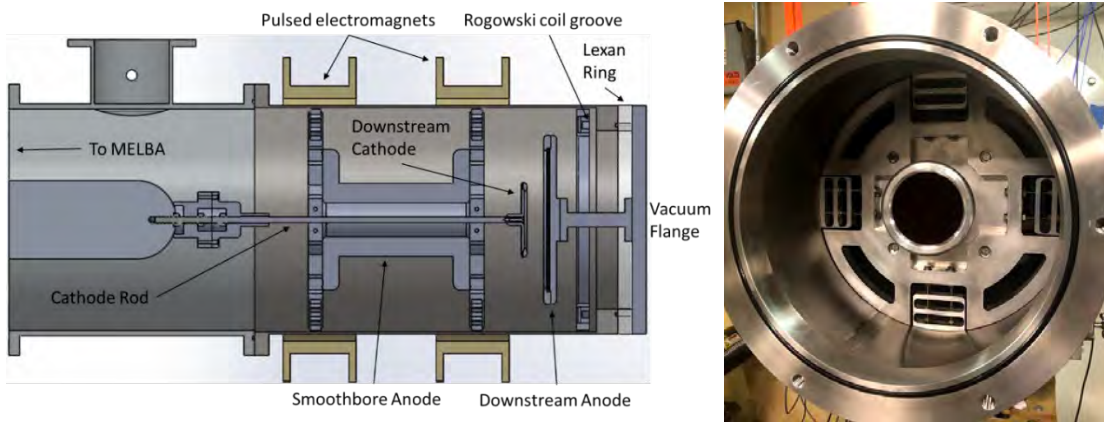

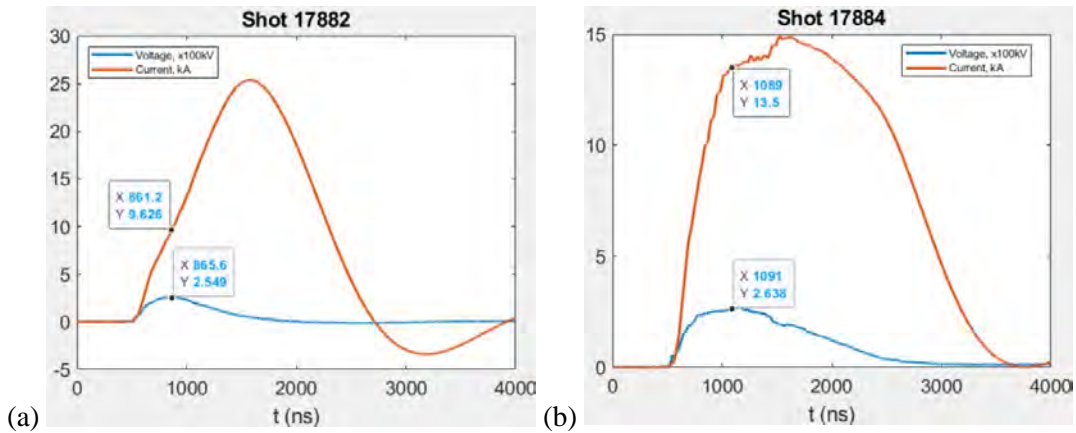Figure 4: Experimental configuration of the smooth-bore cylindrical MILO. (left) CAD model. (right) As installed.

Figure 5: MELBA experimental demonstration of the smoothbore MILO diode where the downstream diode gap is (a) 2 cm and (b) 4 cm.

Subsequently, a **6-cavity cylindrical** MILO was designed and simulated in CST Microwave Studio. In simulation, π-mode operation was observed at 1 GHz (Figure 5), with 12 kA total current (required from the pulsed power generator), 2 kA SWS current (available to produce microwave power), and negligible chamber current (indicating magnetic insulation) as shown in Figure 6. This prototype was then fabricated for testing (Figure 7).
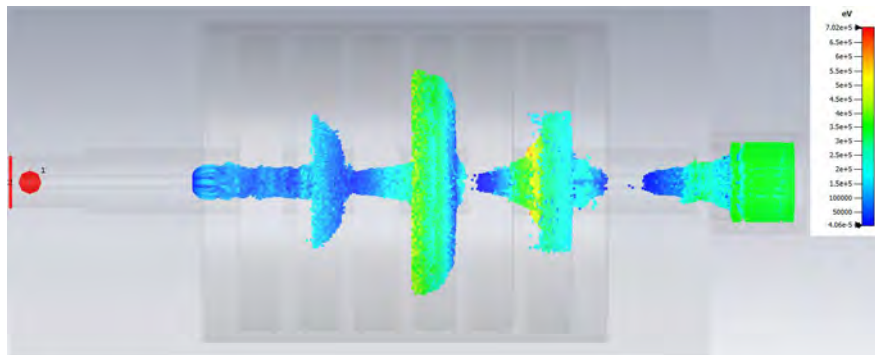
Figure 6: Simulation of electrons interacting with the π-mode RF fields of the MILO slow-wave-structure.
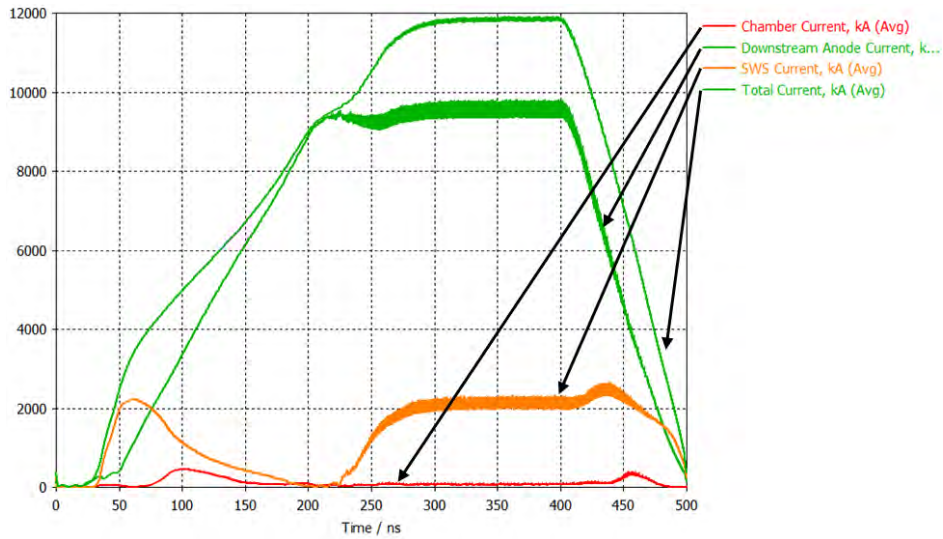
Figure 7: Simulated, time-averaged electron current collected on each component of the cylindrical MILO. During oscillation, the MILO draws ~2 kA to the SWS and 9.5 kA to the downstream diode, for a total injected current of 12 kA. The low chamber current indicates the beam is well-confined by the time it reaches the downstream collector diode.

While awaiting fabrication of the 6-cavity MILO, a **5-cavity MILO with extraction** was designed and simulated. In simulation, π-mode operation was observed at 1 GHz, with 8 kA total current, 1 kA SWS current, negligible chamber current, and 80 MW microwave power generated, as shown in Figure 8.

(a)   (b)
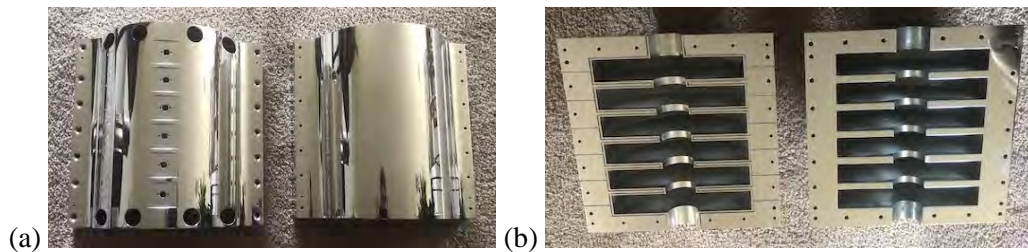
Figure 8: Prototype slow wave structure RF hardware, designed for a preliminary experiment without microwave extraction. The goal of this experiment was to demonstrate the efficacy of oscillator startup on MELBA.

86
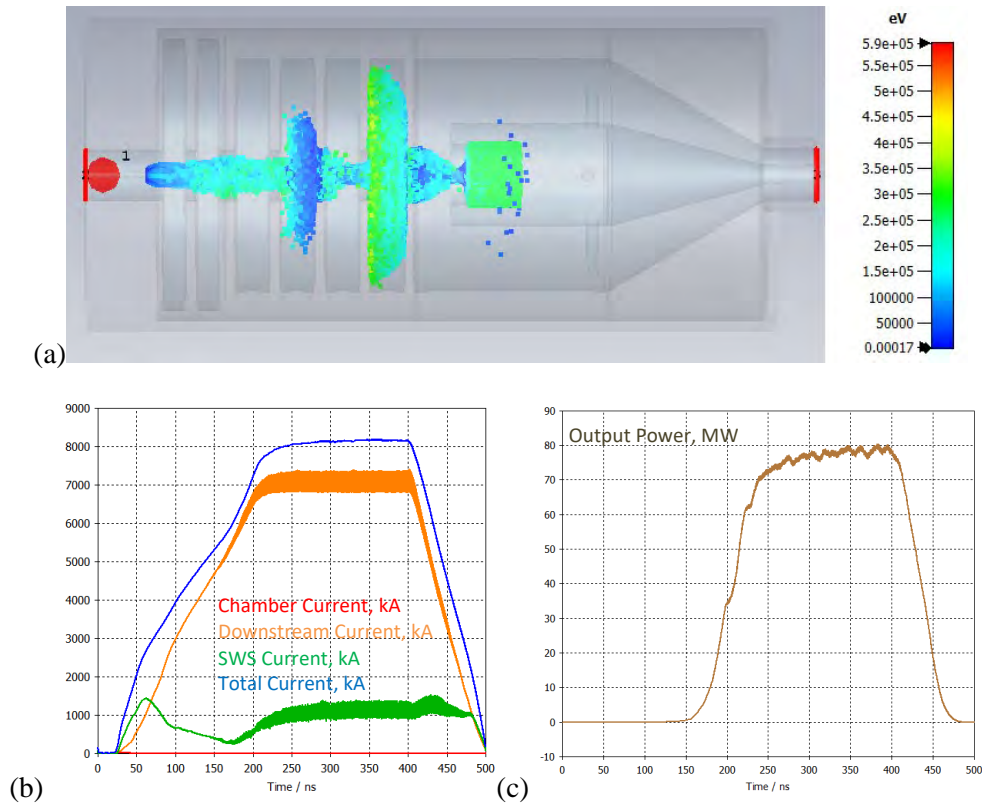
Figure 9: Simulations of a candidate MILO design with microwave extraction. (a) Spoke formation in the SWS buncher RF cavities. (b) Electron current draw in various parts of the device. At the voltage flat top, just over 8 kA in total is delivered, with 7 kA deposited on the downstream anode and 1 kA in the smoothbore coaxial diode. (c) Window-averaged output power in MW, demonstrating that approximately 80 MW are extracted at the voltage flat top.

3.   Findings and Conclusions

Our group has now constructed the complete solution of the Brillouin flow in planar MILO or planar RM, or some combination of the two, in cylindrical geometry with axial electron flow (as in cylindrical MILO), in cylindrical geometry with azimuthal electron flow (as in cylindrical magnetron and cylindrical RM), and in the radially converging flow in MITL (as in a LTD). This will improve our understanding of the MILO, and assist the effort to find an optimal crossed-field configuration, if one exists, that would combine the advantages of MILO and RM.

A moderate-current (~10 kA) MILO has been designed and initial demonstrations of feasibility have been conducted.

4.   Plans and Upcoming Events

In December 2020, YY Lau gave an invited plenary lecture at the International Conference on Plasma Science. A comprehensive analysis of magnetically insulated diodes is currently being finalized, and will be submitted for publication in early 2021. In the last few months of 2020, we tested the 6-cavity MILO, then fabricated (and conducted initial experiments using) the 5-cavity

MILO with extraction. Subsequent experiments will diagnose current flows in the device and explore alternate cathode geometries to improve power and efficiency.

5. Transitions and Impacts

One PhD student was directly supported by this grant, but discussion of MILO theory and experiments in group settings expanded education on this topic to 6 graduate and 3 undergraduate students.

6.   Collaborations
We have several active HPM projects within the DoD which are closely related to this effort:

- "High-Power Microwave Generation by Compact Linear Transformer Driver Technology", Ryan McBride ONR Young Investigator, 6/2018 – 5/2021
- "Multipactor and Breakdown Susceptibility and Mitigation in Space-based RF Systems", Multi-University Research Initiative (MURI), AFOSR #FA9550-18-1-0062, 8/2017 – 7/2022
- "High Power Recirculating Planar Amplifiers", AFOSR #FA9550-15-1-0097, 3/2015 – 8/2020
- Y.Y. Lau, "Integrated model for design optimization and manufacturing tolerance analysis for vacuum electron devices", DARPA # HR0011-16-C-0080, 4/21/16 - 12/31/20
- "Exploration of Fundamental Limits to High Power Electromagnetic Amplification" Multi-University Research Initiative (MURI), AFOSR, 7/15/20- 7/14/25
- Y.Y. Lau, "Study of Electrical Contact under AC and Nonlinear Conditions," AFOSR# FA9550-18-1-0153, 02/15/18 - 02/14/22

7.   Personnel

Principal investigator Ronald M. Gilgenbach, 0.27 person months, National Academy Member (N)
Co-PI YY Lau, 0.27 person months, National Academy Member (N)
Co-PI Nicholas M. Jordan, 2 person months, National Academy Member (N)

8.   Students
3 graduate (1 funded from this ONR grant) and 1 undergraduate students assisted work on this project

9.   Technology Transfer
We have attempted to plan laboratory visits for Yeong-Jer "Jack" Chen, John Kreger and Matt McQuage from NSWC Dahlgren as well as Walter Sessions at Georgia Tech Research Institute (GTRI), but COVID travel restrictions have prevented those visits to date. We will work to accommodate a visit when possible.

10.   Products, Publications, Patents, License Agreements, etc.
Peer-reviewed journals:
Y.Y. Lau, D. Packard, C. J. Swenson, J. W. Luginsland, N. M. Jordan, and R. M. Gilgenbach, "Explicit Brillouin flow solutions in magnetron, magnetically insulated line oscillator, and radial magnetically insulated transmission line," under preparation.

D. Chernin, A. Jassem, and Y. Y. Lau, "Thermal Electron Flow in a Planar Crossed-Field Diode," *IEEE Transactions on Plasma Science*, vol. 48, no. 9, pp. 3109–3114, Sep. 2020.

Packard, Cooleybeck, Jordan, Sporer, Mazarakis, Lau, Gilgenbach, McBride, "HFSS and CST Simulations of a GW-Class MILO", IEEE Transactions on Plasma Science Special Issue on HPM Generation, vol. 48, no. 6, pp. 1894-1901, June 2020.

Conference Presentations:
Y. Y. Lau, "The Child-Langmuir Law and the Physics of Diodes," ICOPS 2020, Dec 2020.
[Invited Plenary] [virtual]

D.A. Packard, N.M. Jordan, A. Cooleybeck, C.J. Swenson, R.D. McBride, Y.Y. Lau, R.M. Gilgenbach, "External Magnetic Field Effects in Magnetically Insulated Line Oscillators", ICOPS 2020, Dec 2020. [virtual] [accepted]

D. Packard, YY Lau, C. Swenson, N. Jordan, B. Sporer, R. Shaparov, R. McBride, R. Gilgenbach, "Theory, Simulations, and Experiments on Magnetically Insulated Line Oscillator (MILO) at the University of Michigan", APS-DPP, Virtual, Nov 2020. [accepted]

N.M. Jordan, D.A. Packard, S.C. Exelby, P.C. Campbell, B.J. Sporer, A.P. Shah, G.V. Dowhan, T.J. Smith, C.J. Swenson, Y.Y. Lau, R.D. McBride, R.M. Gilgenbach, "High Power Microwave and Pulsed Power Development at the University of Michigan", IPMHVC 2020, Knoxville, TN, May 2020. **[Invited]** [conference cancelled]

Drew A. Packard, Christopher J. Swenson, Anna Cooleybeck, Brendan J. Sporer, Alexander E. Mazarakis, Nicholas M. Jordan, Y. Y. Lau, Ryan D. McBride, and Ronald M. Gilgenbach, "Simulations and Experiments on Magnetically Insulated Line Oscillators at the University of Michigan", International Vacuum Electronics Conference 2020, Monterey, CA, Oct 2020. [Accepted] [Virtual]

D.A. Packard, N.M. Jordan, Y.Y. Lau, R.M. Gilgenbach, B.W. Hoff, "Experimental Investigations of High Power Microwave Sources at the University of Michigan", DEPS Directed Energy Student Workshop, West Point, MD, Mar 2020.

N.M. Jordan, D.A. Packard, C.J. Swenson, Y.Y. Lau, R.M. Gilgenbach, "Axial Magnetic Field Effects on Magnetically Insulated Line Oscillators (MILO)", 61st APS-DPP, Ft. Lauderdale, FL, Oct 2019.

11.   Point of Contact in Navy
Kreger, John D CIV NSWCDD, E13 <john.kreger1@navy.mil>

Date of last contact: January 8, 2020.

12. Acknowledgement/Disclaimer

A High Repetition Rate, Long Lifetime Magnetically Insulated Line Oscillator (MILO)

Prepared by:

Dr. John Mankowski, Principal Investigator
Center for Pulsed Power and Power Electronics (P3E)
Texas Tech University
Department of Electrical and Computer Engineering
2500 Broadway, MS3102
Lubbock, TX 79409-3102
Tel: (806) 834-3168
Email: john.mankowski@ttu.edu
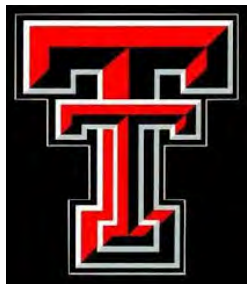
Grant or Contract Number: N00014-18-1-2384
Date Prepared: 1/25/2021
Project Title: A High Repetition Rate, Long Lifetime Magnetically Insulated Line Oscillator (MILO)
Annual Summary Report: FY2020
Principle Investigator:

Texas Tech University (TTU)
Center for Pulsed Power and Power Electronics (P3E)
Dr. John Mankowski
john.mankowski@ttu.edu

Co- Principle Investigators:

Texas Tech University (TTU)

Dr. James Dickens
james.dickens@ttu.edu

Dr. Andreas Neuber
andreas.neuber@ttu.edu

Dr. Ravi Joshi
ravi.joshi@ttu.edu

Financial POC:

Texas Tech University (TTU)
Office of Research Service
Ms. Amy Cook
amy.cook@ttu.edu

Section I: Project Summary

1.   Overview of Project

The overall goals of this project are to design, fabricate and test a 1 GW class magnetically insulated line oscillator (MILO) capable of high repetition rates. The MILO source will be a hardtube design with advanced materials for high rep-rate operation. To that end, we are using particle in cell (PIC) simulation code to model the MILO source structure and materials for a prediction of output RF power and efficiency. In conjunction with the MILO development, we are constructing a low impedance (~10 Ω) Marx generator to drive the MILO and test in single shot mode. Since the project is 9 months into a 3-year program, the bulk of this report discusses the MILO PIC simulations and Marx generator development.

The fundamental objective of this applied research is to develop an enabling technology for future pre-detonation Counter Improvised Explosive Device (CIED) systems. HPRF system power requirements are primarily driven by range (stand-off), and the pulse repetition frequency correlates to the desired speed of the USMC tactical vehicle. Current conventional microwave tube technology used for such systems is limited by output power to single digit MW and total system weight can exceed 20,000 lbs. By comparison, relativistic High Power Microwave (HPM) sources such as Relativistic Magnetrons (RelMags) and Magnetically Insulated Line Oscillators can be driven by short pulse Marx generator pulsed power devices and produced with total weights on the order of 2,000 lbs or less in compact form factors. This reduction in weight by an order of magnitude has potential to enable integration into a wide variety of Marine Corps tactical vehicles to include MRAP and HMMWV. If the size and weight can be further reduced, there is even potential to employ this counter IED technology on small unmanned ground vehicles with on board power. Additionally, there is potential to utilize this emerging technology for countering emerging Unmanned Aerial System threats. RelMags and MILO tube designs offer potential for achieving substantial increases in peak output RF power compared to existing commercial-off-the-shelf (COTS) magnetron and klystron tubes, but at the expense of efficiency. The inherent shortcoming of these relativistic tubes is pulse shortening which is an important factor when operating in the relativistic regime. Additionally, the lifetime of these novel tube design geometries has not been characterized.

Abstract:

This report details the development of a hardtube Magnetically Insulated Line Oscillator for testing in the high repetition rate regime. A brief background of the project is first discussed. The narrative portion of activities and accomplishments are divided into three segments. The first part details the completed MILO system components and initial MILO testing. The second part reports on the cathode material testing. The third part reports on a pulse generator for triggering of the Marx. Finally, findings and plans are presented for the upcoming year.

Objective: The objective of this research is to develop a 1 GW class, hardtube MILO that will be capable of high repetition rate operation.

List of Figures

Background:
The program objective is to design and construct a high-power microwave source capable of high RF power (> 1 GW) and high repetition rate. To this end we are proposing the development of a hard tube magnetically insulated line oscillator. This type of performance can be achieved by fabrication using advanced materials and sealed tube technology as well as design optimization through PIC code simulation. The high diode peak power will induce extreme temperatures within tube components. Advanced materials such as pyrolitic graphite can withstand these conditions which will result in shot lifetimes many orders of magnitude greater than traditionally used materials. These operating conditions will also create plasma within the AK gap which can result in pulse shortening. Sealed tube technology has been shown to reduce plasma generation as well as decrease plasma lifetime. Finally, PIC code simulation will be used to optimize MILO performance resulting in higher power efficiency and lower losses.

2. Activities and Accomplishments
MILO Source – Assembly and Initial Testing

The MILO center cavity design was based upon a desired S-band frequency of approximately 3 GHz. Equations by Fan were used for numerous parameters including vane width, cathode radius and anode-cathode gap. These are illustrated in Figure 1. The selected parameter values are shown in Table 1.
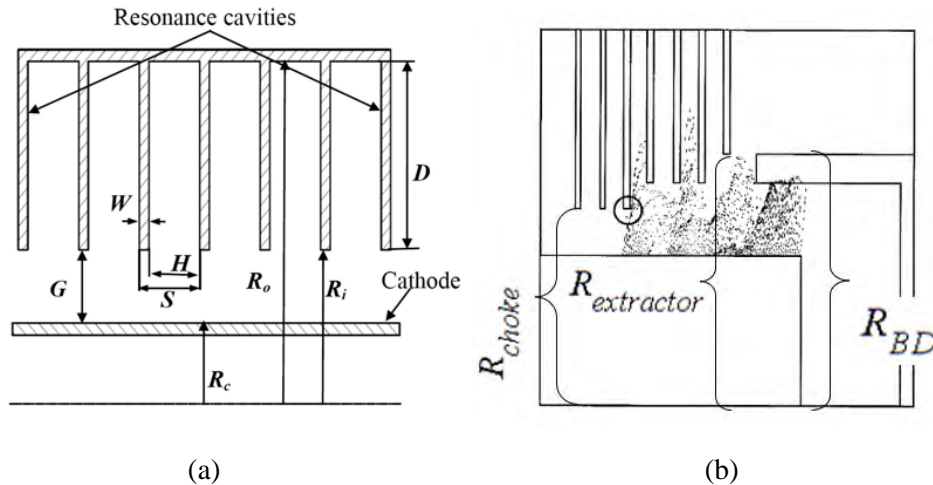

(a)   (b)

Figure 10. Baseline MILO cavity parameters.

Table 1. Selected parameter values of the MILO cavity.

Cathode Radius (R_C)	25.00 mm
SWS Vane Length (D)	24.98 mm
Exterior Radius (R_o)	63.23 mm
Interior Radius (R_i)	38.25 mm
Cathode-Anode Gap (G)	13.25 mm
Choke Vane Radius (R_{choke})	35.00 mm
Extractor Vane Radius (R_{vane})	41.22 mm
Beam Dump Radius (R_{BD})	39.40 mm
Periodicity of Vanes (S)	21.93 mm
Gap Distance (H)	14.93 mm
Vane Thickness (W)	7 mm

The baseline model was then modeled in CST Particle-in-Cell simulation software, as shown in Figure 2. A major goal was to optimize the MILO output power by varying some parameters which could be mechanically alterable via an external bellows structure. Some of these varied parameters are shown in Figure 3. These include stub distance, overlap and extractor gap, with key components labelled.
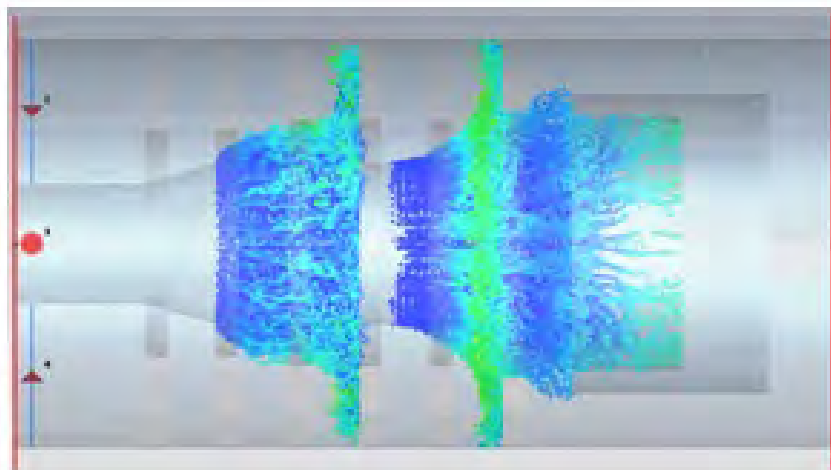

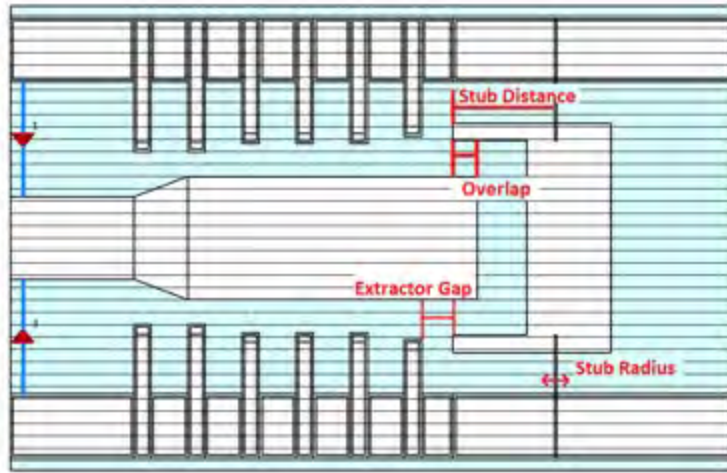Figure 11. PIC simulation of the TTU MILO.

Figure 12. MILO model in the PIC simulation code indicating variable parameters.

The results of the maximum output RF power variation for various parameter sweep ranges is shown in Table 2. Note that the parameter with the resultant maximum output power and largest power range is the overlap parameters.

*Table 2. Maximum output power range for various parameter sweeps.*

Sweep	Values	Max Output Power
Stub Distance	**37.6 – 45.6 mm** (2 mm Steps)	**3.75 – 4.25 GW** (Max @ 45.6 mm)
Stub Radius	**0.5 – 2.0 mm** (0.5 mm Steps)	**3.76 – 4.05 GW** (0.5 mm)
Overlap	**3 mm – 9 mm** (2 mm Steps)	**3.74 – 4.48 GW** (9 mm)
Extractor Gap	**11 – 15 mm** (2 mm Steps)	**3.87 – 4.05 GW** (13 mm)

The simulation model from Figure 2 was then mechanically designed using AutoCad Inventor with the result shown in Figure 4. Some of the key components include the cathode assembly (magenta), cavity vanes and beam dump (gray), and output waveguide (orange). As previously mentioned, a unique aspect of this MILO is the capability of externally varying several parameters which are the beam dump overlap and extractor gap. This has been done by mounting the beam dump and posts to the output waveguide which is mounted to the output window (cyan). The output window is attached to the chamber through a linear translator bellows. By varying the bellows length we can vary the beam dump overlap width between 10 mm and 25 mm.
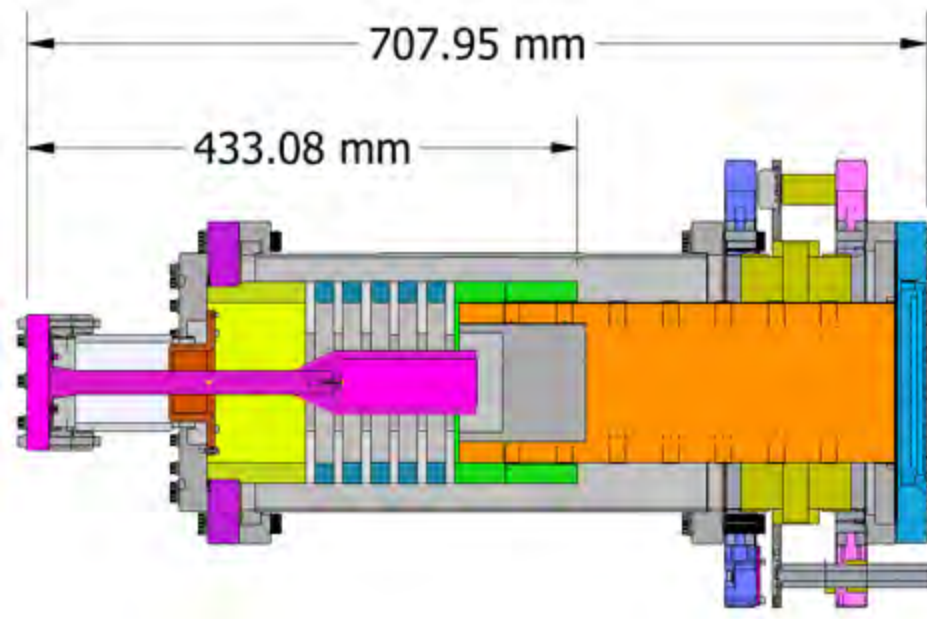
Figure 13. Inventor solid model of the TTU MILO

All components of the MILO have been fabricated and assembled. Additionally, these are all bakeable parts except for the cathode emitter which is fashioned from silk velvet and is shown in Figure 5. The completed assembly mounted to the pulsed power Marx generator driver is shown in Figure 6.
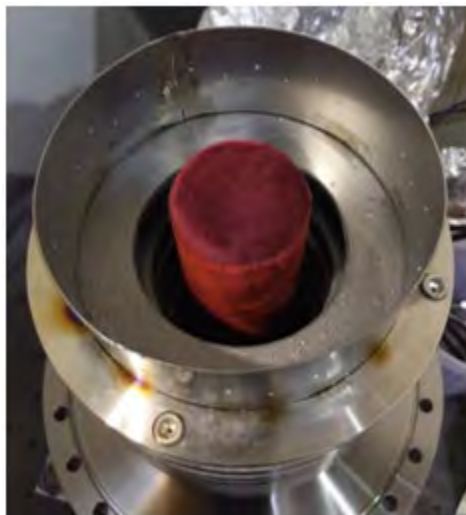
Figure 14. Silk velvet cathode emitter material affixed to the MILO cathode.
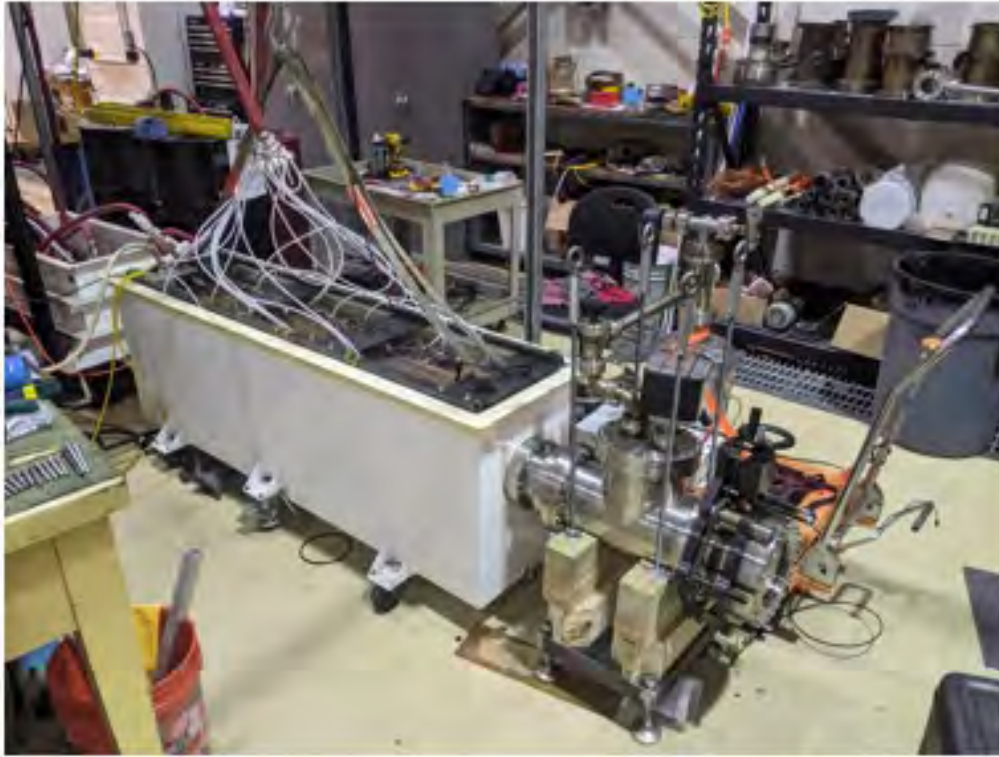
Figure 15. MILO system including the Marx generator and MILO assembly.

The Marx generator is a low impedance pulsed power driver capable of delivering > 50 kA to the MILO. It features two 220 nF, 50 kV Maxwell capacitors at each of the 18 stages. Thus the open circuit output voltage can be as high as 900 kV. The typical output voltage and current into the low impedance MILO is 325 kV and 55 kA.

The output current and voltage at a charge voltage of 30 kV is shown in Figure 7. In this case the voltage peaks at 150 kV and the current peaks at 22 kA. The resultant MILO impedance, in Figure 7b, declines during the pulse from 15 ohm to 5 ohm for an average of 10 ohm. This variation during the pulse is typical.

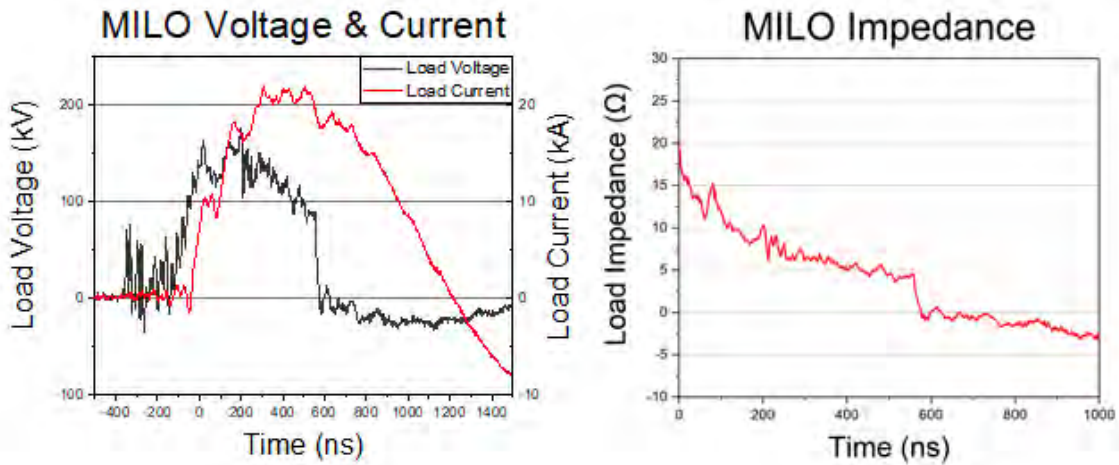*Figure 16. Marx generator output into the MILO charged to 30 kV.*

The pulsed power input from Figure 7a resulted in the RF output shown in Figure 8 below. The RF output power is very low, < MW, but it does show MILO beginning to turn on. Frequency analysis shows that this RF output is in the S-band as expected.
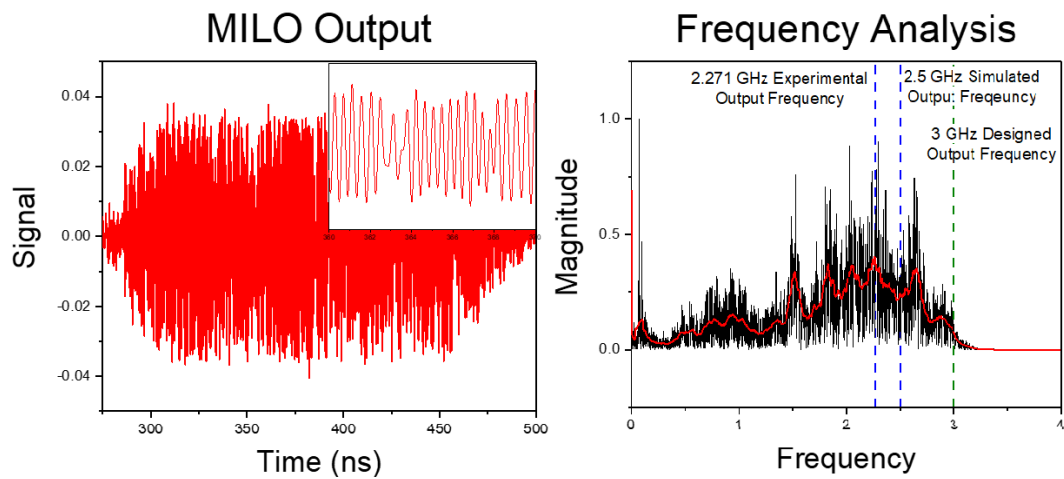

Figure 17. Output voltage and current from the 18-stage Marx at 25 kV charge.

Two in-house cathode materials and one commercially available cathode material have been tested and compared. Critical criteria include high current density (>100 A/cm^2), turn-on times less than 100 ns, bakeability, and long lifetime. The end use is for MILO cathode development, as pictured in Figure 5. The primary cathode materials under test were commercially available bi-modal Carbon Fiber Velvet (ESLI) and TTU woven Carbon Fiber Velvet.

In order to manufacture our own carbon fiber velvet, a loom was purchased for weaving. The primary carbon fiber thread of choice was a 3000 strand, 7 μm diameter type. This thread was wrapped around the warping board and cut to length. The thread count determines the weave width which for testing was 22 count for a width of 10 cm. The cut thread is then sleighed through heddles in the loom in a predefined pattern. Groups of heddles are then attached to different foot pedals that are raised and lowered individually. After tying the threads to the front and back apron rods, a shuttle is wound with cloth to weave through the threads. After a group of heddles is raised the shuttle is run through perpendicular to the threads, setting the pattern into the weave. An image of the threads on the loom is shown in Figure 9.

Figure 18. Carbon fiber thread mounted on the loom.

Once the cloth has been woven and is cut from the loom, the process of weaving the velvet pattern is begun. Needles are threaded through the loops created in the plain weave cloth, shown in Figure 10. Once all the needles are threaded, a high vacuum rated carbon-based epoxy is applied to the back of the weave. After the epoxy dries, the needles are removed and a surgical blade is used to cut the loops in to upright tufts.
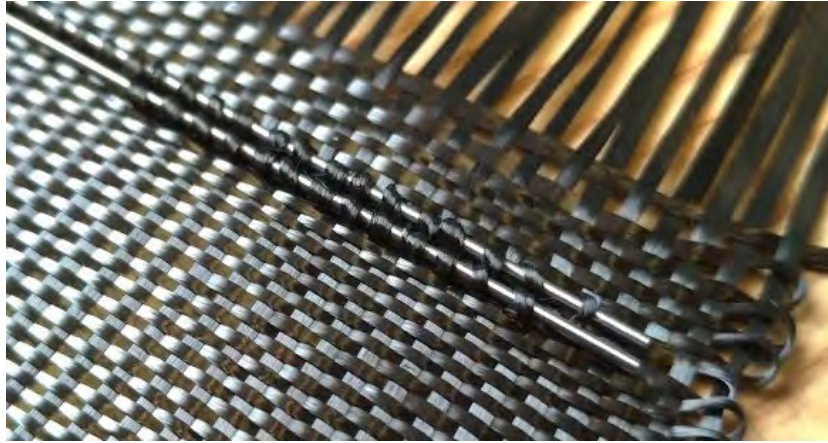
Figure 19. Needles looped through the plain weave.

The velvet cloth is then epoxied to a stainless steel base for testing in the vacuum chamber. Each upright tuft contains approximately 3000 fibers resulting in a total number of fibers of 3.3 million on a small, 5 cm diameter cathode, shown in Figure 11.

Figure 20. TTU carbon fiber velvet small cathode

The ESLI and TTU carbon fiber cathodes were tested in a vacuum chamber shown in Figure 12. The cathode position is variable using a linear translator which appears on the left side of the image. The anode is a honeycomb transparent design fashioned from pyrolitic graphite. The tube is driven with a 1kJ Marx generator.

Figure 21. Cathode testing chamber.

Numerous shots were taken with each cathode type varying the AK gap distance and applied voltage. A typical shot recording the voltage and current on the ESLI cathode and TTU cathode is shown in Figure 13. The resultant impedance at these conditions is shown in Figure 14.
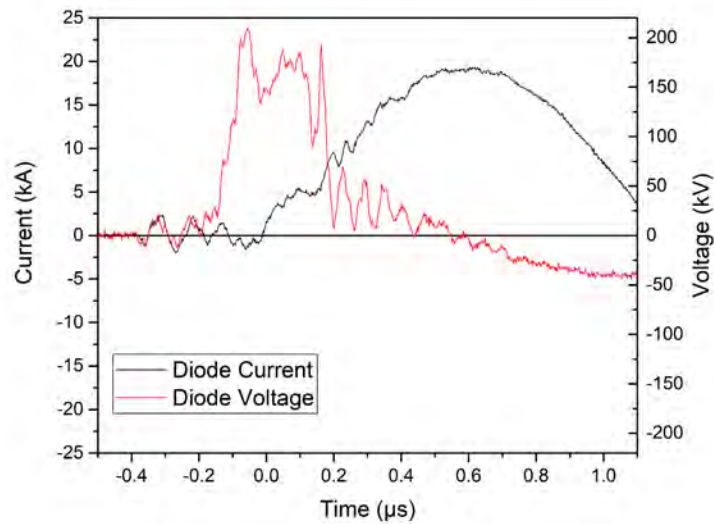
(a)
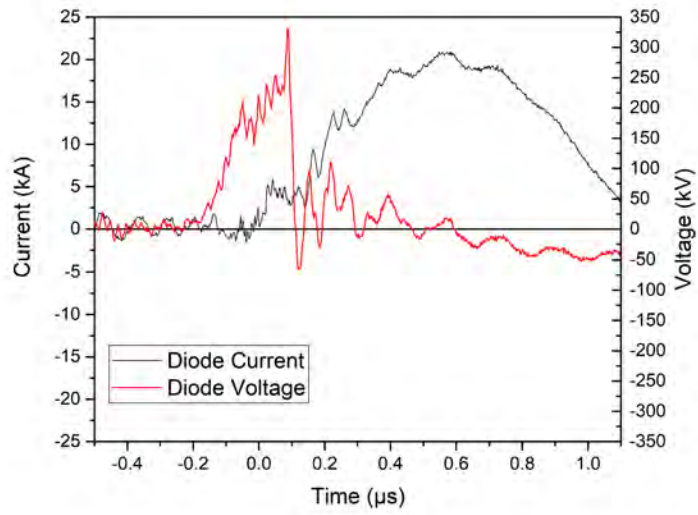
(b)

Figure 22. Voltage and current waveforms with the ESLI cathode (a) and TTU cathode (b) tested at a Marx charge voltage of 20 kV and an AK gap distance of 15 mm.
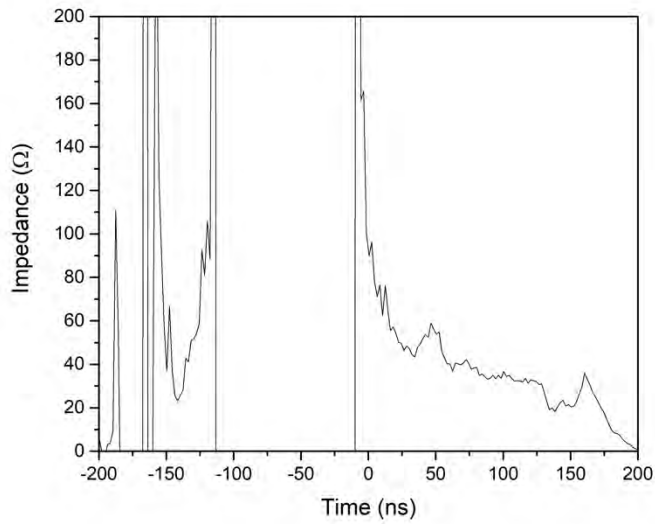
(a)
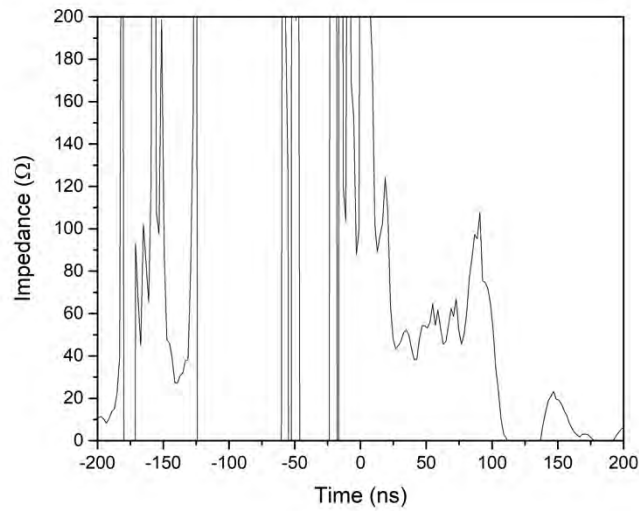
(b)

Figure 23. Load impedance with the ESLI cathode (a) and TTU cathode (b) tested at a Marx charge voltage of 20 kV and an AK gap distance of 15 mm.

The significant impedance values occur between 0 and 100 nsec. For the ESLI cathode, the impedance starts at 60 ohm and gradually falls to 30 ohm during this time period. The TTU cathode takes slightly longer to turn on (at 20 nsec), stays relatively flat at 50 ohm between 25 and 75 nsec, then rises quickly to 100 ohm between 75 and 100 nsec indicating that the cathode emission begins turning off. It appears that the TTU cathode does not perform quite as well at these particular parameter settings. In general, the TTU cathode performed similarly to the ESLI cathode yet had more variability. This is indicative of poorer emission uniformity of the TTU cathode which is to be expected since the carbon fiber tufts are much less uniform than the ESLI carbon fiber.

Trigger Pulse Generator

A high voltage pulse generator is required for reliable triggering of the Marx generator. This specific design is unique in its quick rise times and ability to re-trigger reliably at high repetition rates (~100Hz). This pulser is composed of two parts, control and high voltage. While both parts are crucial in the success of the end product, the high voltage board is what actually generates the high voltage pulse. The control board, however, interfaces with a remote PC to determine when and the high voltage board should be triggered, as well as important aspects of the output pulse such as repetition rate and amplitude. An image of the pulser hardware is shown in Figure 15.

105

Figure 24. Trigger generator hardware.

The control board is vital to the success of the overall project. The main purpose of the control board is to minimize the number of connections needed between a remote PC and the high voltage board. In doing so, the control board is able to receive information from the PC and send one single-pulse input to the high voltage board. This means the control board determines repetition rate, pulse amplitude, and any operational information the user should see on the PC. This specific microcontroller (model PIC16F18857) was chosen because it has more than enough GPIO pins for this application (up to 36), allows for communication via UART and SPI, and has an internal clock speed of up to 32 MHz. The PIC16 program flow control is shown in Figure 16.
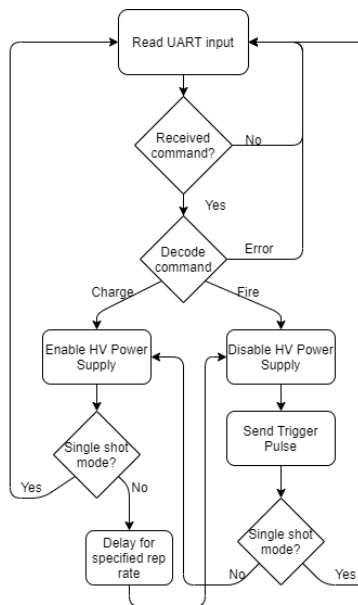
Figure 25. PIC16 program flow control.

The PC side Graphical User Interface (GUI), written using the Python *tkinter* library, is shown Figure 17. Input settings are repetition rate, number of pulses, and pulse amplitude. The input control include Fire and Stop buttons, spark gap tube output valve, and Marx capacitor charge.
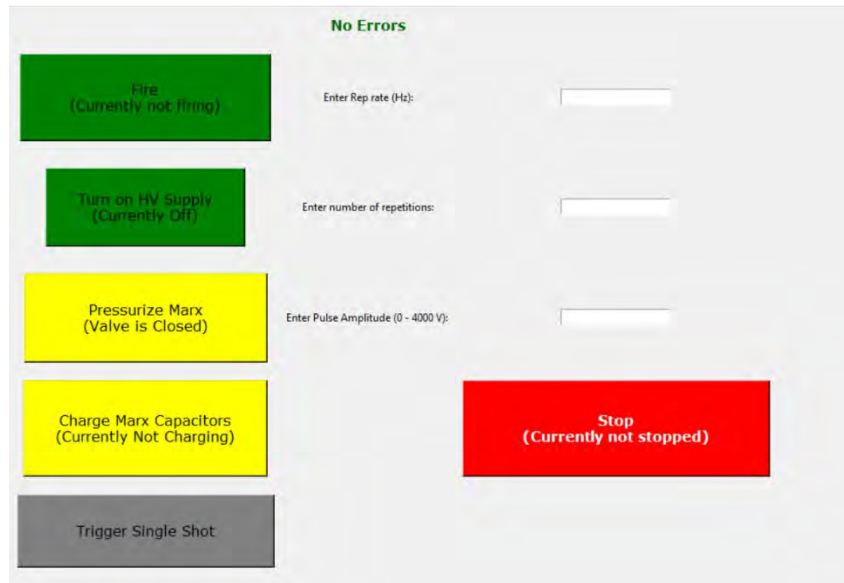
Figure 26. PC-side GUI of the trigger generator.

The typical output voltage waveform is shown in Figure 18. Here the pulser is fired into an open load using a 1:4 step up transformer. The input charge voltage is 2.5 kV.
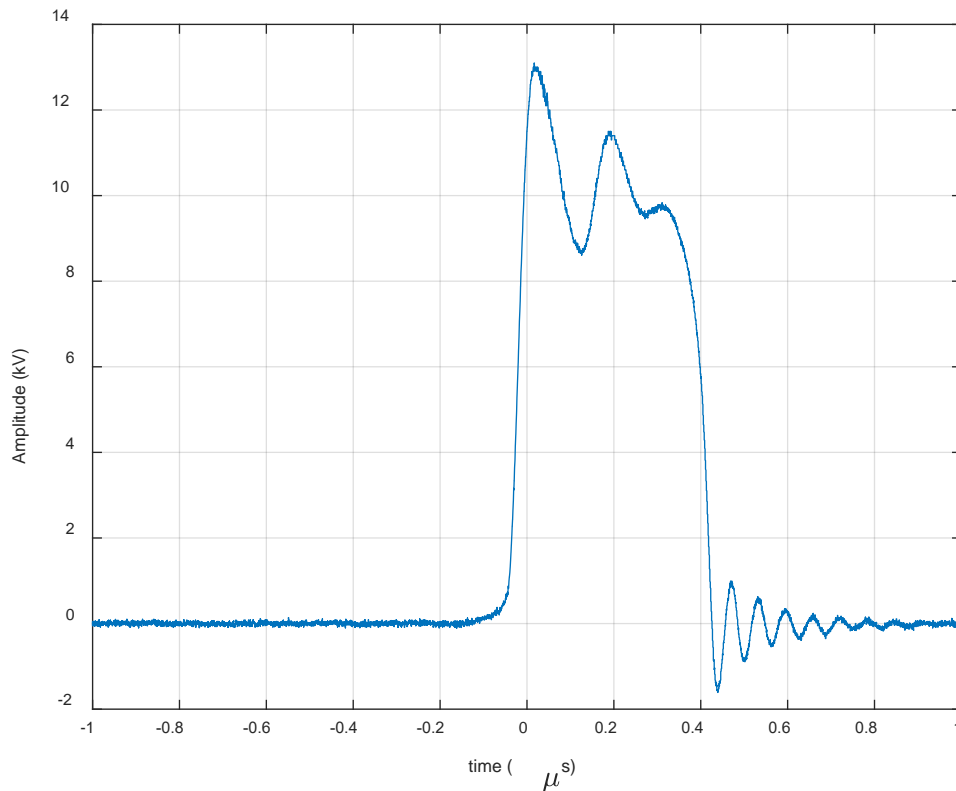
Figure 27. Output waveform with a 1:4 turns ratio transformer into an open load.

3. Findings and Conclusions

There are several findings and conclusions during CY 2020 of this program. First, the fabrication of the MILO source was completed and testing began. Second, testing of the Marx generator was completed. Initial tests confirmed RF output from the MILO source. Testing of the in-house fabricated carbon fiber velvet and commercially available velvet was performed. Finally, the solid state trigger generator was tested and completed.

4. Plans and Upcoming Events

Plans are to continue to test the MILO source at increasing input current levels. Highest level so far has been 35 kA and plans are to test above 50 kA. Additionally, optimization of the beam dump overlap distance will be performed at select input charge voltages. Testing of the TTU cathode will be completed. Finally, the silk velvet cathode currently used in the MILO will be replaced with a custom carbon fiber cathode.

5.   Transitions and Impacts

None

6.   Collaborations

None

7.   Personnel

Principal investigator: John Mankowski, 1 month effort

Team Members: Machinist, Lee Waldrep, 3 month effort
                         Technician, Joel Perez, 2 month effort
                         Technician, Dino Castro 2 month effort

8.   Students
2 PhD students, 1 Master's student, 1 undergraduate assistant

9.   Technology Transfer
None at this time.

10.   Products, Publications, Patents, License Agreements, etc.

Publications resulting from this project:

Abide, M., Dickens, J., R. Joshi, Neuber, A., and Mankowski, J., "Simulation of an S-band MILO with Adjustable Beam Dump," *Plasma*, 2 (2), 2019.

Buntin, T., Collier, L., James, C., Dickens, J., Mankowski, J., and Neuber, A., "Magnetic Shielding Effectiveness of Layered Medium-Walled Structures," *2019 IEEE Pulsed Power and Plasma Science Conference*, 2019.

Abide, M., Buntin, T., Dickens, J., Neuber, A., Joshi, R., and Mankowski, J., "Low-Impedance S-Band MILO," *2019 IEEE Pulsed Power and Plasma Science Conference*, 2019.

T. Buntin, M. Abide, K. Nagao, J. Dickens, R. Joshi, A. Neuber, and J. Mankowski, "Explosive Emission Cathode Evaluation for a Magnetically Insulated Line Oscillator (MILO)," *2020 IEEE International Conference on Plasma Science*, 2020.

J. Williams, J. Dickens, A. Neuber and J. Mankowski, "A Solid-State, High-Voltage Pulse Generator with Microcontroller Control," *2020 IEEE International Conference on Plasma Science*, 2020.

M. Abide, T. Buntin, J. Dickens, A. Neuber and J. Mankowski, "S-Band Magnetically Insulated Line Oscillator (MILO) with Adjustable Cathode/Beam Dump Overlap," *2020 IEEE International Conference on Plasma Science*, 2020.

11.   Point of Contact in Navy

Contact: Matt Mcquage, NSWCDD, E05
Contact information: matthew.mcquage@navy.mil
Date of last contact: Kickoff meeting on 7/31/2018

12. Acknowledgement/Disclaimer

Ultra-High-Efficiency Relativistic Magnetron and Improved MILO Capabilities

Grant No. N00014 -19-1-2155

Annual Report for Fiscal year 2020

Period of Performance: October, 1, 2019 to September 30, 2020

Prepared by:

Professor Edl Schamiloglu, Principal Investigator
University of New Mexico
Department of Electrical and Computer Engineering
Albuquerque NM 87131-0001
Tel: (505) 277-6095
Email: edls@unm.edu

Principle Investigator: Edl Schamiloglu, 505-277-6095, edls@unm.edu, University of New Mexico, Department of Electrical and Computer Engineering; Salvador Portillo, 505-277-1311, sportil@unm.edu, University of New Mexico, Department of Electrical and Computer Engineering

Section I: Project Summary

1.   Overview of Project

The relativistic magnetron is the most compact and efficient high power microwave source. The University of New Mexico (UNM) has been studying relativistic magnetrons for over 16 years. Our recent work proposed a relativistic magnetron with diffraction output (MDO) without a physical cathode, where a virtual cathode (VC) forms in the interaction region to power the MDO with efficiency comparable to that of an MDO with a transparent cathode. We then proposed a magnetic mirror field for an MDO that can completely eliminate axial loss current. This half-cusp-like magnetic field configuration replaces the downstream VC that was described in our earlier work and demonstrates >90% efficiency in simulations. We believe that this MDO with VC and magnetic mirror will not suffer from pulse shortening since there is no physical cathode electrode in the interaction space for impedance collapse to take place. Hence, we believe this configuration can operate at exceptionally long pulse lengths. Most recently, in a collaboration with the Technion group in Israel we introduced the split cathode which also eliminates axial leakage current but in a much simpler implementation than the magnetic mirror.

UNM has also been developing a magnetically insulated line oscillator (MILO) over the past few years to study plasma formation and evolution in the device and mitigating such plasmas to achieve higher efficiency operation. We plan to study simulation and experimental strategies for achieving higher efficiency MILO operation and multi-tone capabilities. UNM will also be advancing pulsed power drivers for MDOs and MILOs using a fast, high energy Marx generator and a linear transformer driver (LTD).

In terms of the Navy relevance of the project, this project will extend the UNM/University of Michigan (UM) successful HPRF partnership to MILOs, that were largely developed in the USA (1980's-2000), but recently have seen intensive research and development by potential competitor countries. Our goal is to address, via focused and transitional HPRF research, some of the critical problems facing Navy operations due to asymmetric electronic threats, such as those faced by Marine warfighters in forward operating bases to those in littoral waters, and protection of high value targets, such as U.S. embassies in potential hot spots around the globe. These asymmetric electronic threats can come in the form of small airborne electronic drones, perhaps even COTS-type devices employed in boat or automobile-sized machines.

Abstract: This annual report summarizes activity on the recently awarded ONR grant "Ultra-High-Efficiency Relativistic Magnetron and Improved MILO Capabilities" covering the period October 01, 2019 – September 30, 2020.

Objective: The objectives of this research are to increase the HPRF power/electron beam power efficiency of relativistic magnetrons and explore the MILO to further improve its performance. The MILO portion of this research is in collaboration with UM.

Introduction: The University of New Mexico group excels in designing novel HPRF source concepts of relevance to the Navy, and then validating the source designs in experiments. UNM is proposing an ultra-high-efficiency relativistic magnetron that has demonstrated an outstanding 92% efficiency (beam-to-RF) in particle-in-cell (PIC) simulations. This is a record for any HPRF source! In addition, UNM is seeking to further the magnetically insulated line oscillator through basic studies of surfaces plasmas within the device. This project seeks to continue this basic research program that has been in collaboration with our colleagues at the University of Michigan. Investigating frequency agile MDOs and MILOs will be an important consideration of our work.

Ultra-High-Efficiency Relativistic Magnetron

Our most recent focus has been on the MDO with a magnetic mirror to suppress axial leakage current. However, this focus has changed since FY20 Q4. The PI met with Yakov Krasik and John Leopold (Technion, Haifa, Israel) at the PPPS-2019 conference in Orlando and discussed the matter of electron beams in a squeezed state and applying them to magnetrons. Those discussions led to a collaboration and joint publication (listed in this report). It also led to funding for Technion from ONR Global. The gist of the idea is presented in Fig. 1.

The use of a "split cathode" allows for trapping of the electrons in a squeezed state but without requiring the formation of a virtual cathode. This suppresses all leakage current and is a much simpler implementation than a magnetic mirror field.

The split cathode might also be the silver bullet to enable testing UNM's MDO at Naval Surface Warfare Center Dahlgren Division (NSWCDD). The cryomagnet that NSWC acquired has a very long magnetic field and there is concern that electrons might follow the magnetic field lines and destroy the output window. Use of the split cathode might mitigate this and enable progress with experiments there.

Finally, on the experimental front, labs were closed to all students between March 18 and July 05, 2020 due to COVID. Once the labs reopened with safety measures instituted, the students were able to proceed with upgrading the PI-110A accelerator with solid state resistors, as shown in Fig. 2.
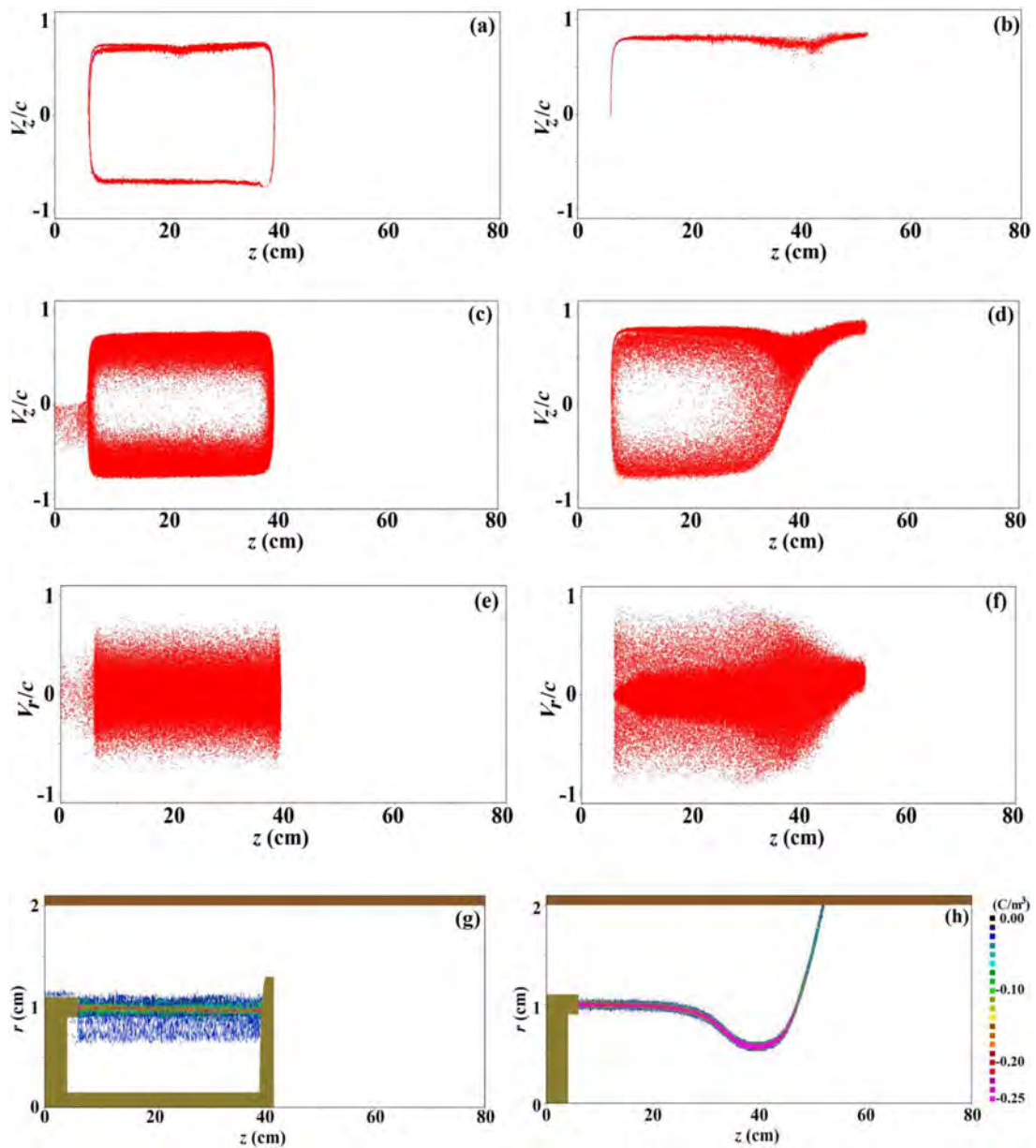
Figure 1. [z, V$_z$] phase space for the reflector [(a) at 6 ns and (c) at 45 ns] and for the magnetic mirror [(b) at 6 ns and (d) at 45 ns] cases. [z,V$_r$] phase space for the reflector (e) and the magnetic mirror (f) cases at 45 ns. Electron charge density distribution at 45 ns for the reflector (g) and the magnetic mirror (h) cases [the color bar is the same for (g) and (h)].

Figure 2. Photograph of the PI-110A accelerator used for MDO experiments showing solid state resistors replacing liquid resistors (photographed July 13, 2020).

The Magnetically Insulated Line Oscillator

The MILO is a crossed field high power microwave (HPM) generator comprised of two structures, an inner conductor that serves as an electron field emitter, and an outer conductor that contains the slow wave structure and ultimately where the electromagnetic energy is generated. Figure 3 (repeated from last year's report for convenience) shows a schematic of the Air Force Research Laboratory (AFRL) hard tube (HT) MILO.

Our MILO overall goals are to develop solutions to allow the MILO to deliver the highest possible energy and peak powers. To this end, we are approaching the problem in a multipronged manner. First, we are collaborating with AFRL/RX colleagues and with a small business (DexMat) to develop high current density cathodes based on carbon nanotubes that can meet the current required by HPM sources with fast turn on at low fields and with little outgassing. Second, we are heavily invested in numerical simulations to solve the essential problem of frequency agility/variability and gap closure. Our models have successfully showed that we have solved the former and have applied for a patent on this solution. Third, we are conducting fundamental research on plasma evolution from desorbed neutrals. These neutrals, mostly hydrocarbons, are adsorbed into the first few monolayers of all materials, and when heated, are liberated and then become ionized, which in turn leads to gap closure and end the production of radiation (analogous to poisoning of the beam and turning the device off).

These problems are key to fundamentally changing the path to providing the naval warfighter an asymmetric capability to engage multiple disparate targets and thus dominate the battlefield. This will be done via an HPM source that is compact, long pulse, high peak power and frequency agile.
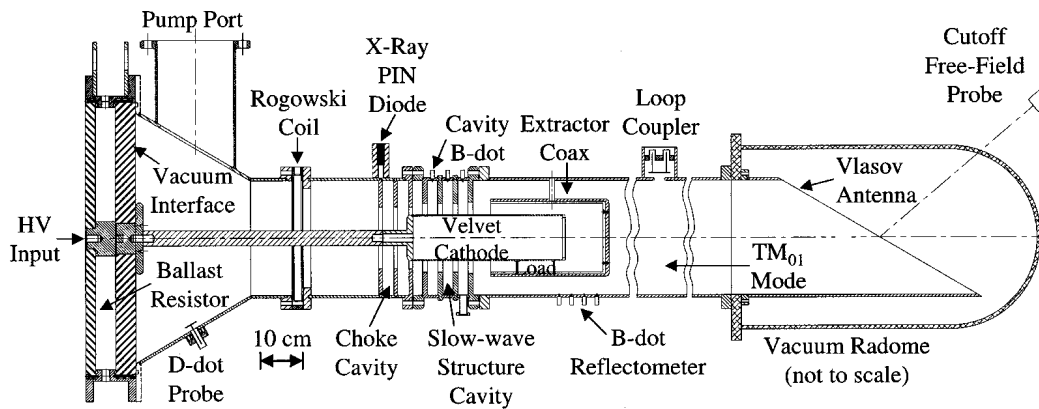
Figure 3. Schematic of the AFRL HT MILO.

List of Abbreviations

A-K – anode-cathode gap
CsI – cesium iodide
ECE – Electrical and Computer Engineering
HPRF – high power RF
HT MILO – hard tube MILO
LTD – linear transformer driver
MDO – magnetron with diffraction output
MILO – magnetically insulated line oscillator
NSWCDD – Naval Surface Warfare Center
Dahlgren Division
PIC – particle-in-cell
TC – transparent cathode
TFA – time-frequency analysis
TLD – thermoluminescent dosimeter
UM – University of Michigan
UNM – University of New Mexico
VC – virtual cathode

Administrative Point of Contact
Melissa Dee Sanchez – Sponsored Projects Specialist
(505) 277-7647, osp@unm.edu

Background: The approach that is being followed in the research under this grant is to i) utilize comprehensive PIC simulations using UNM's various virtual prototyping tools (ICEPIC, MAGIC, CST Particle Studio, and LSP, which can handle surface plasmas in the MILO) and then validate the simulations using experiments. A modified PI-110A accelerator is used for the MDO experiments and a Marx/PFL will be used to drive the MILO. The MILO will be fitted with spectroscopic diagnostics to compare experimental results with LSP simulations.

2. Activities and Accomplishments
The current reporting period is October 01, 2019 – September 30, 2020.

As we entered this fiscal year our plans were to develop an experimental capability to demonstrate the MDO with magnetic mirror field (requiring an additional coil and power supply) or a half-cusp magnetic field (by using a flux-excluding aluminum flange if feasible). A team of EE senior design students came up with the design of the power supply and coil.

However, in the summer of 2020, as we were exchanging emails with our colleagues at the Technion in Haifa, Israel, an alternate idea emerged which required no additional coils or power supply. This is the idea of the split cathode that we described earlier. This is a better approach and we have pivoted to focus on this.

In July we tested the MDO with transparent cathode and endcap on the PI-110 with the new solid state resistors. We were observing very strange waveforms, including reflections. We then decided to step back and remove the MDO and install the A6 relativistic magnetron with radial extraction and we observed normal behavior (Fig. 4). The load voltage was around 350 kV with a 0.6 T magnetic field. We fixed the calibration for the PFL voltage; the amplitude and waveform looked normal with no oscillations. The current pulse was 30 ns, 6 kA without the initial spike. We think that MDO caused weird reflections and spikes, but not sure why yet. We observed the 2π mode using the directional coupler at 4.74 GHz.
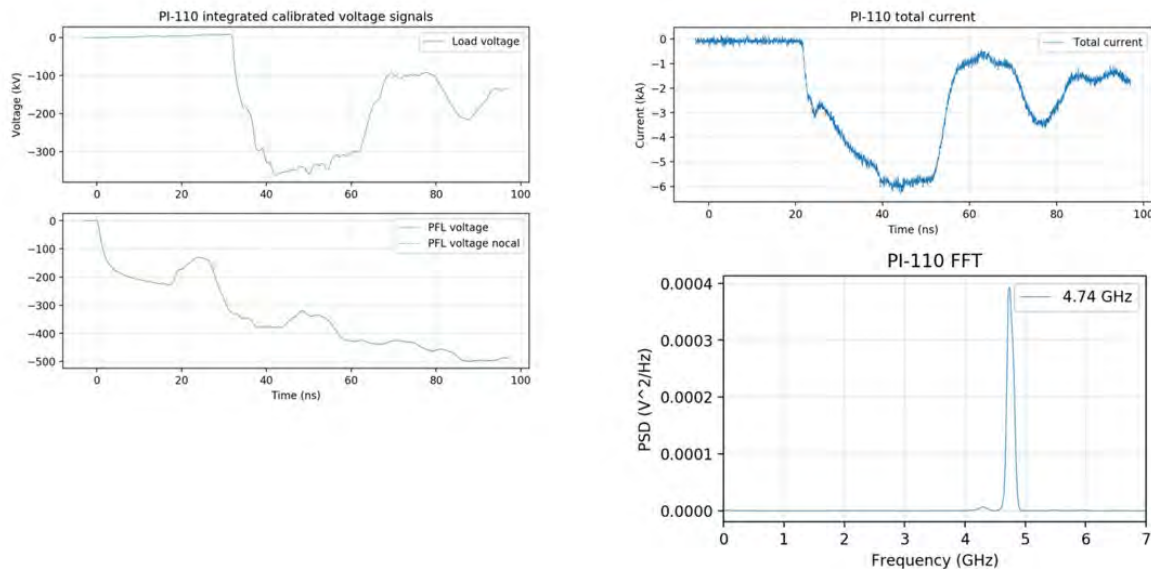

Figure 4. Left: Load voltage (top) and PFL voltage (bottom). Right: Total current (top) and FFT (bottom).

Our cathode test bed, based on a Linear Transformer Driver (LTD) of NRL design, is functioning completely. We are testing cathodes from the standard 'felt' material to very advanced carbon nanotube devices. The advanced carbon cathode material is from AFRL/RX, and we are part of a Small Business Technology Transfer (STTR) group awarded a grant to work on development of large area cathodes based on carbon nanotube materials 'sewn' into large area structures. Drexel University will be responsible for assembling the larger area cathodes, and DexMat corporation will be providing the base material. UNM will perform the cathode characterization. This work is ongoing and we are awaiting additional materials from Drexel University and DexMat.

The key to developing effective sources lies in developing HPM devices with long pulses, high repetition rate, frequency selectability, and multiple spectrum energy deposition. UNM has long said that internal geometric changes can provide a path forward on these problems, especially as they are intrinsically tied together in some sense. The MILO's slow wave structure (SWS) in our canonical model is comprised of several cavities that act as blockers for any wave going back, but also three cavities above the cathode that act as the SWS. These cavities disrupt the symmetry leading to breaking of insulated flow and spoke to generation of electrons 'feeding' the standing waves generated by explosive emission of electrons from the cathode. That is to say, the drift electron velocity is in synchronism with the phase velocity of these waves. These standing waves are fixed in the shape and size of the cavity. These cavities can be represented as LCR circuits. Changing the capacitance changes the resonant frequency. Researchers have tried to achieve this by adding inductive blocks into the cavities all the while losing energy. Our method of changing capacitance by reducing the entrance aperture actually enhances the spectral content and the energy produced.

Figure 5 shows our canonical MILO. Recall that we chose this unsophisticated geometry to reduce computation time. This geometry has cavities that are symmetrical; that is the aperture size is the same as the width of the cavity. This geometry produces the designed 2.4 GHz fundamental and a standard pulselength, as shown in Fig. 6.
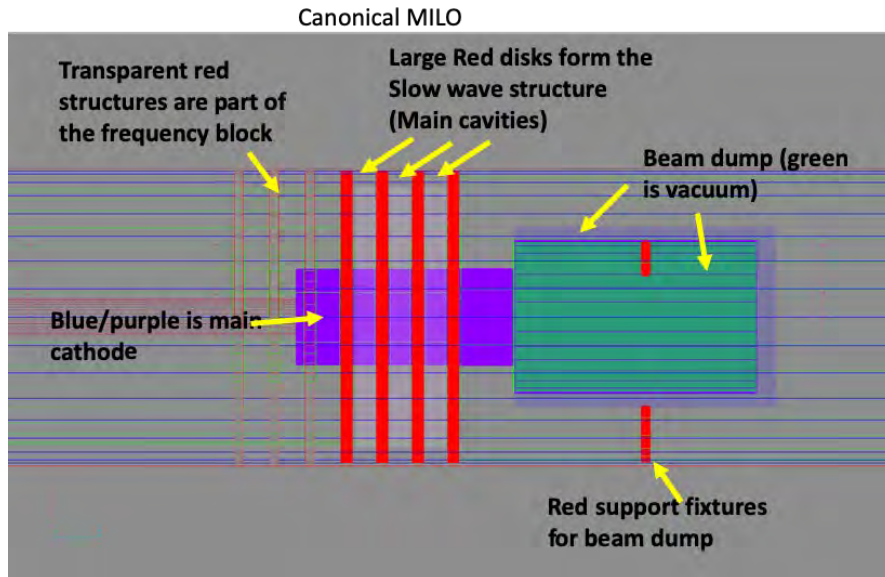
Figure 5. Canonical MILO geometry with symmetrical cavities.
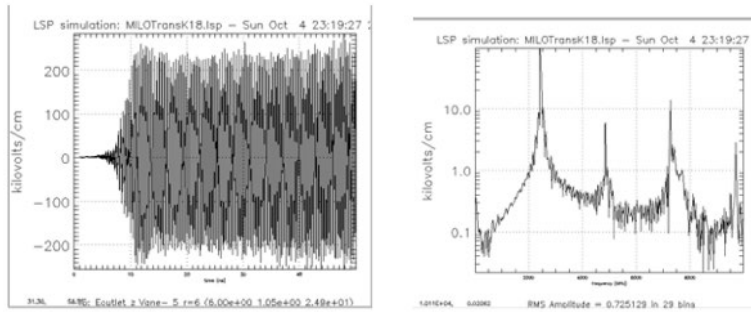
Figure 6. Pulse and spectral content produced by canonical MILO.

As mentioned earlier, the resonant condition of the cavities means that this is essentially an LCR circuit. The resonance is controlled by the capacitance and inductance; that is by the aperture. To this end, we have implemented a scheme whereby the aperture of the MILO is reduced. We have tried several variations including depth of block and aperture reduction as well as aperture increase. Figure 7 shows the new geometry.
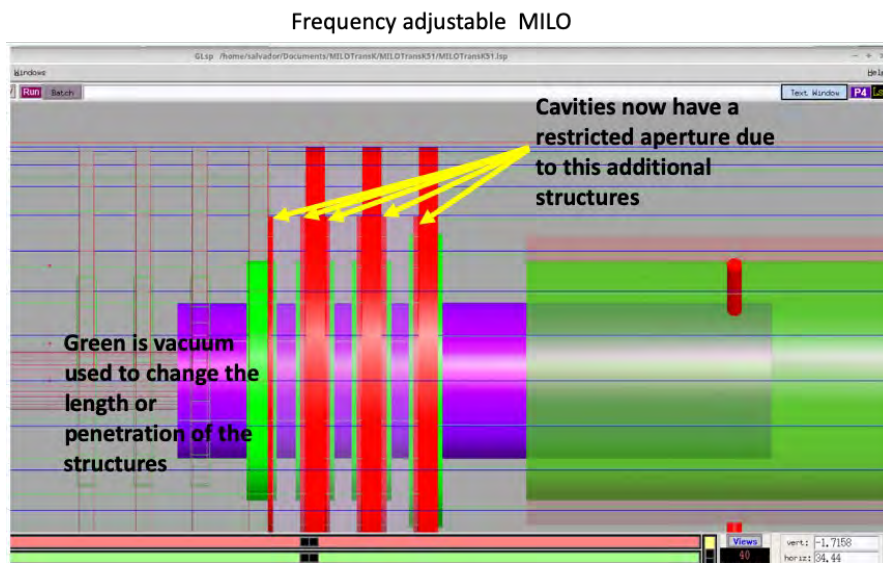
Figure 7. Frequency tunable geometry. Notice the aperture reduction as the thickness of these blocks increases.

We have decreased the aperture (entrance) size as well as increased it. Figure 8 shows a particle trajectory plot, in 2D, as well as the time domain plot of the pulse. This particular geometry increased the aperture entrance.
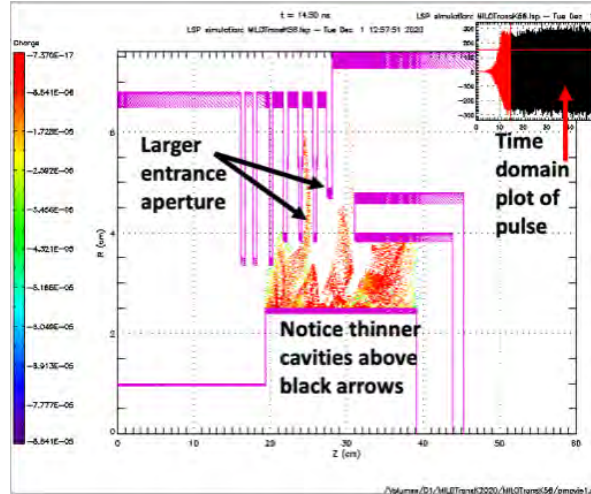
Figure 8. Particle trajectory plot of a frequency adjustable MILO geometry. Plot also shows the time domain pulse. Notice the cavities in the SWS are not symmetric.

This frequency adjustability/variability is command controlled. By this we mean that a change of the internal geometry, as we have been saying for some time, via mechanical means, can alter the spectral output of a MILO. This method yields narrowband frequencies just like the canonical device. Figure 9 shows the FFT of four shots, canonical, two with smaller cavity apertures, and one with a larger aperture. The narrowband spectral content has a controllable spread of approximately 375 kHz, which is about 15% of center frequency. This is controlled by the size of the aperture. In a larger MILO, such as a 1.3 or 1.6 GHz device, we would expect about 500 kHz variation. Also notice that this modification 'cleans' up the narrowband peak. The 2.4 GHz signal contains a small side lobe which is reduced with our method.
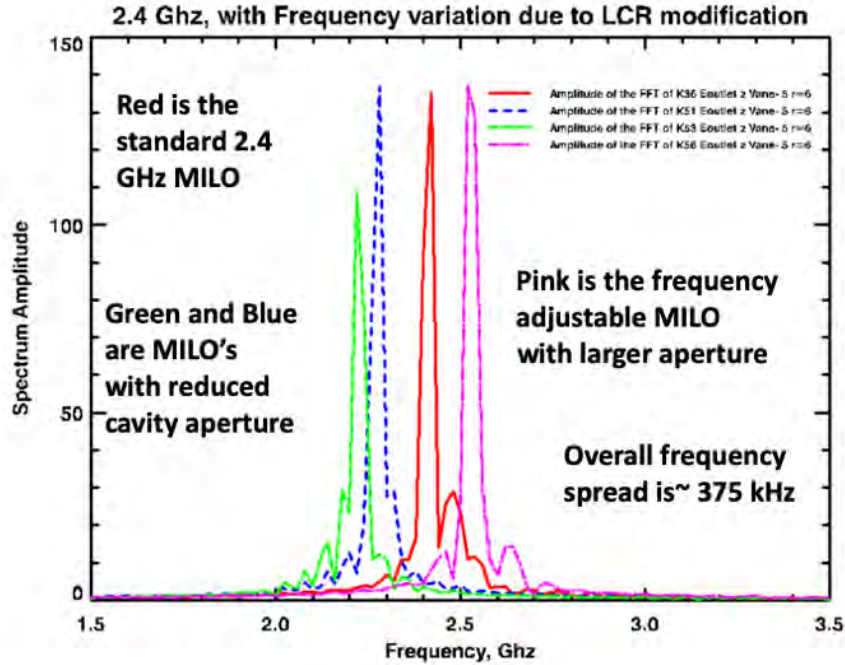
Figure 9. Spectral output of four different MILO's of same size using our NOVEL frequency variable control method. The spread is on the order of 10%.

The temporal pulse is also affected somewhat because there is a small delay in the onset of oscillations if we are very aggressive while closing the aperture. This is expected as the disturbance that alters the magnetic insulation is smaller. Nonetheless the oscillations do start, and this delay can be considered minimal with a long pulse. If our method of reducing neutrals extends the pulse to a microsecond, then losing 5 ns in the beginning does not alter the energy content of the pulse. Figure 10 shows a composite image of two different shots, one with a slightly shorter pulse and one with a longer pulse than the canonical. In other words, we can also control the pulse start-up, albeit slightly. Additionally, it appears that we can also increase the peak fields as shown in Fig. 10 (bottom).
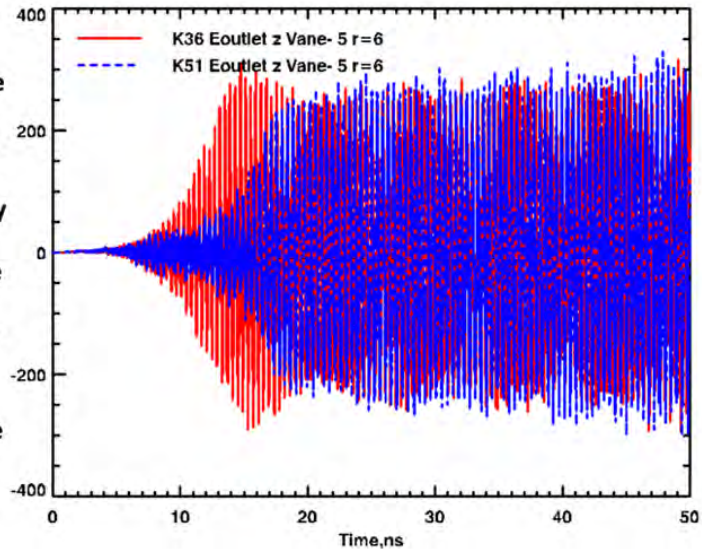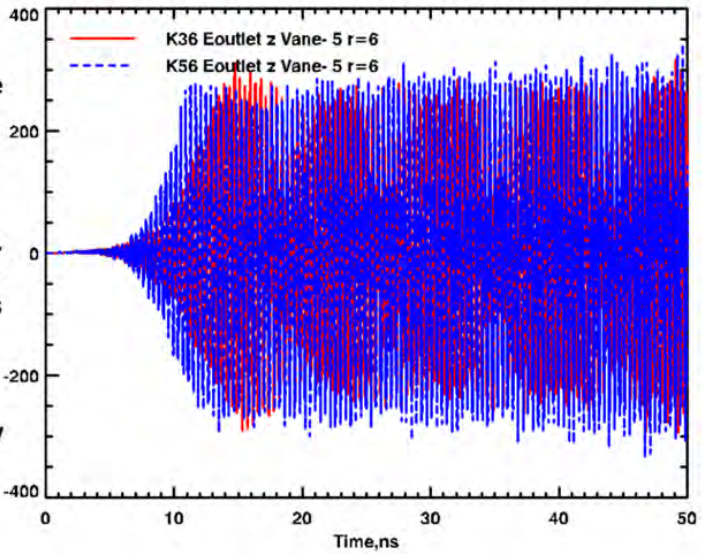
Figure 10. A composite image showing the time domain pulse of a standard 2.4 GHz MILO. One image has a smaller aperture (top) and the other has a larger aperture (bottom).

All of these simulations have been performed with a very fast rise time voltage pulse, 500 kV, and there is much to be gained by trying combinations of rise time along with a full physics simulation to include neutrals and beam neutralization.

Our plasma measurements on HPM sources, which are needed to solve the issue of gap closure, are ongoing and we fielded a preliminary spectroscopic set-up on UNM's MDO magnetron driven by a nearly 20 ns FWHM voltage pulse of 350 kV. However, at present there is no direct method for measuring the time-dependent voltage in the magnetron interaction region so this voltage represents the voltage output of the

Marx into a transmission line. This electrical signal is available if needed. Additionally, we fielded a Bremsstrahlung time-resolved PIN diode and it might be possible at a later time to determine the load voltage from this using a radiation law unfold. The main diagnostic was a 6 chord spectrometer array which we detail below. The tapering of the anode in the MDO is meant to match impedance and allow for greater power transmission. The A6 magnetron, in this case, is utilizing a transparent cathode which replaces the solid circular cathode with 6 cathode emitters placed at optimum azimuthal locations with respect to each cavity to enhance start-up of oscillations. Images of the MDO are given in Figs. 11 and 12.

A 6-chord linear fiber array (IF112D-6-0) of 1 mm core and NA = 0.5 or F/1, spaced 15 mm apart from each other, is fielded radially at the output of the MDO, as shown in Figs. 11 and 12. The MDO interaction region is 300 mm from the output vacuum window comprised of a 25 mm thick clear acrylate piece. A plastic panel with equally spaced apertures is used to space and hold in place the collimating assembly. The assembly is comprised of 6 chords each with one 5mm diameter collimating fused silica lens of focal length 8.3mm, f/1.66 directly coupled via SMA connectors to the fiber. The array spans 6 m to the spectrometer, which is located in a Faraday cage behind the accelerator. The spectrometer is a 0.5m F/6.5 Andor Shamrock 500i with three gratings (600/1200/2400) lp/mm coupled onto an iStar 334T 1024x1024 array ICCD. All chords are looking at different parts of the interaction going from the center to the edge of the MDO radially outward.

The array is a bespoke design terminating into a coherent linear array embedded in an additively manufactured photopolymer resin structure that holds the fibers in place. The array is directly coupled to the spectrometer slit via common optomechanical components. The timing of radiation production to image capture using a DG535 coupled to a Marx trigger was established in prior shots such that any future shots were sure to be captured by the spectrometer system. Multiple shots were taken with different gratings and on different spectral regions. There was some variability within the shots and this was taken into account.

What follows in Figs. 13-16 shows some of our data as captured by this system, initial analysis, and thoughts for additional data analysis and experiment.
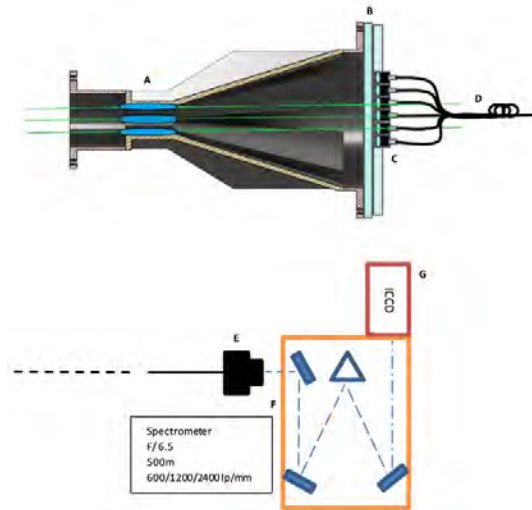
Figure 11. (A) MDO interaction region and main plasma region; (B) Acrylate window; (C) panel with 6 SMA fiber collimators positioned 15 mm apart; (D) 6 m fiber bundle; (E) linear fiber array to slit adapter; (F) 500 mm Andor spectrometer; (G) iStar 334T ICCD.
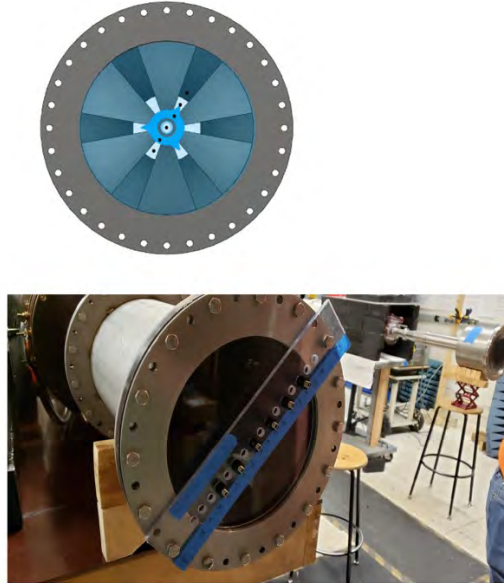
Figure 12. (Top) Front view of the fiber bundle – small dots are fiber aiming points. (Bottom) Image of apparatus in place.
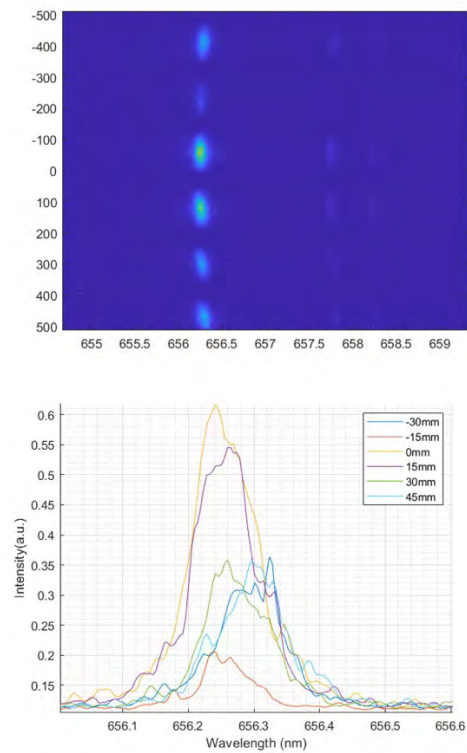
Figure 13. (Top) Spectra taken from 654.7 to 659.7 nm with slit width of 400 μm, exposure time of 1μs, and 2400 lp/mm. The spectral resolution is ~0.14 nm. (Bottom) 3-point moving averaged lineout of the 6 fibers.
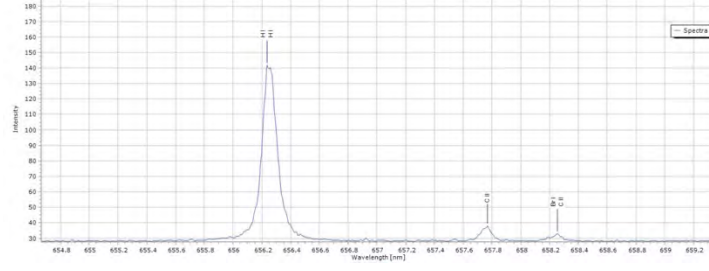
Figure 14. H-alpha line with two CII line.
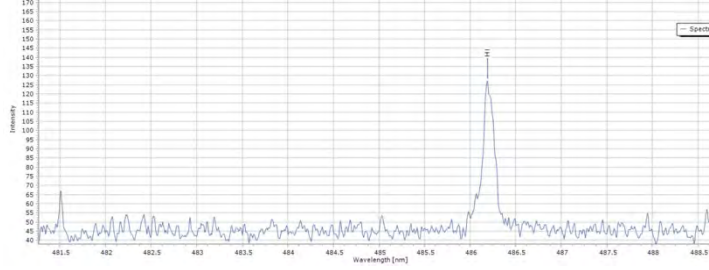
Figure 15. H-beta line.
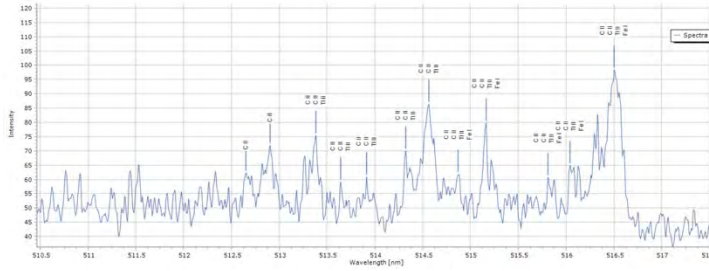
Figure 16. Sample spectra from one MDO shot.

We test for local thermodynamic equilibrium (LTE) using the McWhirter criterion on the H-line. For an assumed electron temperature of 1eV and cold ions,

$$N_w = 1.6e12 * T_e^{0.5} * E_H^3 \tag{1}$$

$$N_w = 4.336 * 10^{17} \; \frac{1}{cm^3}. \tag{2}$$

We require the density to be $4.336 * 10^{17} \; \frac{1}{cm^3}$ to be in LTE. To determine density, we require the use of the quasi-static stark half-width equation

$$L_D = \sqrt{\frac{\varepsilon_0 * kT_e}{N_e * e^2}}, \tag{3}$$

$$N_d = \left(\frac{4}{3}\right) \pi * N_e * \lambda_{center}^3, \text{ and} \tag{4}$$

$$\lambda_{1/2} = (8.16 * 10^{-19}) * \left(1 - 0.7 * N_d^{\frac{1}{3}}\right) * \lambda_{center}^2 * (n_1^2 - n_2^2) * \left(\frac{z_p^{\frac{1}{3}}}{z_e}\right) * N_e^{2/3} \tag{5}$$

125

(We are planning on taking additional data with a standard lamp to determine baseline for broadening.)
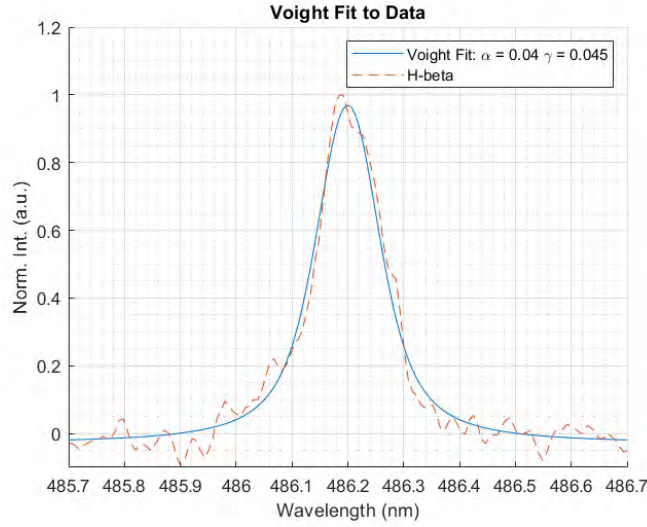
Figure 17. Voight fit to the H-Beta data.

The Voight fit in Fig. 17 determined that there is a 50/50 split in Gaussian and Lorentzian broadening mechanism. The total experimental broadening is determined by

$$\Delta\lambda_{\text{exp}} = \frac{1}{2}\Delta\lambda_L + \sqrt{\left(\frac{1}{2}\Delta\lambda_L\right)^2 + (\Delta\lambda_G)^2}. \tag{6}$$

Since the Voight fit showed that the broadening between Gaussian and Lorentzian is 50/50, we can presume that the Stark half-width $\lambda_{1/2}$, which has a Lorentzian profile, and the instrument broadening, which has a Gaussian profile, is 50/50 of the broadening of the H-beta line. Ignoring Doppler and Van Der Waals broadening, the total Stark broadening is given by

$$\sqrt{\Delta\lambda_{exp}^2 - (\Delta\lambda_G)^2} = 2\lambda_{1/2}. \tag{7}$$

Then using the quasi-static Stark equation, the electron density N_e is found to be $1.422 * 10^{15} \frac{1}{\text{cm}^3}$, which according to the McWhirter criterion, is not an LTE plasma.

These are just preliminary results and need to be investigated further in FY21.

3.   Findings and Conclusions

The significance of the results achieved to-date is as follows.

For the ultra-high-efficiency relativistic magnetron work, the most significant result achieved to date is that for the MDO and the relativistic magnetron with radial extraction, we have identified a new path forward involving the split-cathode that we have jointly developed with researchers at the Technion. This is a significant advancement and will be more fully developed in FY21.

Regarding the MILO, we enumerate:

1. The length of the pulse makes data acquisition a bit difficult as the plasmas are either relatively low density or are due to arcing in the system.
2. We do not believe the plasmas we observe are in LTE, so line ratio analysis is not possible.
3. We need to perform further measurements so we can attempt to study broadening of lines.
4. We plan on fielding this system once again after we get a handle on the data analysis.
5. It is our goal to also field this work with a streak camera for time-resolved measurements.
6. We would like to field polarization spectroscopy in FY21.
7. We plan on using a quartz window and solarization resistant fibers in future shots to capture high UV spectra (above ~250 nm).

These measurements will then need to be carried over to the MILO as the most important thing we need to solve is the radiation collapse plaguing crossed-field devices. We have recently had some success in reducing cathode neutral desorption in a MILO (in numerical space) and I believe that solving this is critical to yielding a high impact path forward for HPM sources. Finally, we need to find a paradigm shift for these devices and mitigate plasma evolution and beam neutralization so that we move past incremental progress. The ongoing development of new cathodes will be critical in this regard.

4. Plans and Upcoming Events

For the ultra-high-efficiency relativistic magnetron work, the plans in the upcoming year are to design a split-cathode for NSWC, for UNM's MDO on the PI-110, and for UNM's magnetron with radial extraction on the PI-110 and to implement them in experiments.

Major milestones would be successful testing of the MDO and magnetron with radial extraction using a split-cathode.
For the MILO, we hope to proceed forward with the build of the MILO driver. In addition, spectroscopic measurements, cathode testing, and LSP simulations will continue.

A major milestone will be the build of the MILO driver.

5. Transitions and Impacts
As part of its collaboration with NSWCDD, UNM is transitioning its MDO with TC, and it will transition its MDO with split-cathode. In addition, we are presently developing/designing a new MILO for use in irradiation of targets of interest to the Naval warfighter. This will include our novel frequency agile design. We will transfer any cathode developments for this design which will be fielded at Dahlgren Navy facilities.

6.   Collaborations

Agency/Org	Performer	Project Name	Purpose of Research/ Collaboration
NSWCDD	John Kreger, Jack Chen, and Jon Cameron Pouncey	HPM collaboration	We discussed proceeding with MDO and transparent cathode testing at NSWC
AFRL/RX	Steven Fairchild	HPM cathode collaboration	We are discussing collaborative research on HPM cathodes
AFRL/RD	Brad Hoff	HPM cathode and switch collaboration	We are discussing collaborative research on HPM cathodes and pulsed power switches
Technion, Haifa, Israel	Yakov Krasik and John Leopold	Comparison of magnetic mirror vs. cathode rod and reflector	Optimize suppression of magnetron leakage current via an electron beam in a squeezed state
Tech-X	Peter Stoltz	MILO PIC/Hybrid simulations	Effects of desorption from anode on MILO operation
Confluent Sciences	John Luginsland	MILO PIC/Hybrid simulations	Effects of desorption from anode on MILO operation; high impact outcomes
Weizmann Institute of Science	Yitzhak Maron	Diagnostics	Time-resolved spectroscopic diagnostics in high power, cross-field devices
Drexel University	Genevieve Dion	Cathodes	Large area cathode assembly
DexMat	Dmitri Tsentalovich	Cathodes	Providing base material for sewn cathodes
Verus Research	Sameer Hemmady	MILO	High impact outcomes

7.   Personnel

Principal investigator – Edl Schamiloglu (0.5 person month)
Co-investigator or Co-PI – Salvador Portillo (2.5 person months)
Business Contact – Melissa Dee Sanchez
Team Members – none
Subs – none

8.   Students
Artem Kuskov (Ph.D. student – 6 person months)

Braulio Martinez-Hernandez (M.S. student – 6 person months)

Stacie Hernandez (B.S. student, 6 person months)

Joe Chen (M.S. student – 3 person months)

Shaho Hamadamin (M.S. student – 3 person months)

Robert Beattie Rossberg (B.S. student – 4 person months)

Andrew Gilbert (B.S. student – 4 person months)

Rena Berdine (B.S. student – 2 person months), graduated and now working on national security applications for Northrop Grumman in Baltimore Office

Ian Chavez (B.S. student – 2 person months), graduated and now a graduate student working on conformal antennas with Dr. Christos Christodoulou at UNM

9.   Technology Transfer
N/A – except for ongoing collaboration with NSWC DD on MDO and MILO, and joint experiments.

10.   Products, Publications, Patents, License Agreements, etc.
Peer-reviewed publications acknowledging this grant:

> a.   Producing a Magnetized Lower Energy, High Electron Charge Density State Using a Split Cathode
> b.   Physics of Plasmas
> c.   J. Leopold, Y. Krasik, Y. Bliokh, and E. Schamiloglu
> d.   Keywords: high power microwaves; virtual cathode; magnetron with diffraction output; MDO; squeezed state
> e.   Distribution Statement: Unlimited release
> f.   Publication Status: published
> g.   Publication Identifier Type: DOI
> h.   Publication Identifier: https://doi-org.libproxy.unm.edu/10.1063/5.0022115
> i.   Publication Date: 20 September 2020
> j.   Volume: 27
> k.   Issue: 103102
> l.   First Page Number: 103102-1
> m.   Publication Location: College Park, MD
> n.   Acknowledgement of Federal Support? Yes
> o.   Peer Reviewed? Yes

Conference Papers

None

Conference Presentations

None (we had three ICOPS presentations that were originally supposed to be presented May 2020 but ICOPS was moved to December 2020 due to COVID so the presentations are not included in this reporting period).

Books

J.W. Luginsland, J.A. Marshall, A. Nachman, and E. Schamiloglu, *Advances in High Power Microwave Sources and Technologies using Metamaterials* (IEEE Press/Wiley, New York, NY, 2021) (in preparation).

Theses

None

Websites

MILO HPM laboratory: www.unm.edu/~sportil. MILO HPM laboratory web site showcasing some of the work being carried out on pulsed power and HPM source development.

Patents

None

Other Products:

None

11. Point of Contact in Navy

NSWCDD – John Kreger and Jack Chen – we have periodic (at least quarterly) telecons and several (at least twice yearly) in person visits.

12. Acknowledgement/Disclaimer

Material Assessment for High Power RF Systems

Grant No. N00014-19-1-2599

Annual Report for Fiscal Year 2020

Period of Performance: October 1, 2019 to September 30, 2020

Prepared by:

Dr. Somnath Sengupta, Principal Investigator
Powerhouse Consulting Group
3210 Boones Lane
Ellicott City, MD 21042-2138
Tel: (443) 820-7798
Email: somnath@powerhouseconsultinggroup.com

Grant or Contract Number: N00014-19-1-2599
Date Prepared: November 29, 2021
Project Title: Material Assessment for High Power RF Systems
Annual Summary Report: FY2020
Principle Investigator: Somnath Sengupta, 443 820 7798; somnath@powerhouseconsultinggroup.com;
Small Business

Section I: Project Summary

1. Overview of Project

The benefits of frequency agility and beam shaping utilizing electronically tunable materials have been demonstrated in communication systems and sensing systems. For communication systems such advances have led to the 5G implementation. For high power microwave (HPM) such advances could mean avoiding equipment fratricide and tunable radomes that could switch its transmittance, as needed, to protect sensitive equipment. Sidelobe emission reduction may also reduce the radar cross section (RCS) of naval antennas (**Figure 1**). Development of such a capability will assist in reducing Electromagnetic Interference/Electromagnetic Compatibility (EMI/EMC) issues and assist in the transition of HPM directed energy weapons (DEWs) to the warfighter. Although a material solution exists for implementing frequency agility and beam shaping; it has not been assessed for high power application.

Figure 28. Powerhouse's electronically controlled materials can provide novel applications like dynamically tuned radomes

The **goal** of this grant is to assess the material system for moderate RF incident power aimed for directed energy applications. The science question to answer was: what are the material parameters and geometry of the tunable dielectric materials to enable a configurable, high-average RF power transmit system with an intent to reduce side-lobes in the emission far-field? What is the characteristic behavior of these materials as a function of incident RF power, and what is the dependence on bandwidth? Once the project is completed, the high power radio frequency (HPRF)/HPM program will have an assessment of the functionality of a tunable material under high RF incident power. This will enable the HPRF/HPM programs to assess how this material can be applied for on-the-move HPRF/HPM systems with reduced sidelobe EMI/EMC concerns.

The **approach** included the fabrication and then collection of the material's response functions (ε', ε'', tunability, intermodulation products (IP3), and breakdown voltages). Tunability is defined as the % change in dielectric constant of the material with applied electric field.

The key **technology advancement/payoff** are to reduce the probability of EMI/EMC (fratricide) reduced; reduction of EMI/EMC enables Navy to pursue shipboard, high-power electromagnetic maneuver warfare while maintaining the ability to communicate.

2. Activities and Accomplishments

There were overall two iterative tasks for the program: fabrication of the material compositions and characterization of the materials. We fabricated molar combinations of Barium Strontium Titanate (BST)

in the paraelectric regime. The dielectric constant, dielectric loss, tunability, breakdown voltages, and RF power handling capability were measured for all these combinations. The best material combination was chosen for fabrication of the low loss oxide composites through the addition of refractory oxides. In total, we measured 24 different variations of compositions for 4 dielectric performance parameters- ε, $\tan\delta$, % tunability, and the third order intermodulation distortion product (IMD).

Material Background

Tunable dielectric materials offer design flexibility for frequency agile components. Barium Strontium Titanate has been researched for several years. The cornerstone of the research has been the lowering of the electronic loss factor combined with designable dielectric constants in a wide variety of form factors. The parameters of interest have been the dielectric constant ε, dielectric loss ($\tan\delta$), and % tunability. Tunability is defined as the % change in dielectric constant of the material with applied electric field. *However, no effort has been made to assess the properties of this class of material for high RF power applications.*

Barium Strontium Titanate, $Ba_xSr_{1-x}TiO_3$, is a member of ferroelectric materials, which has wide applications in electronic industries. Small variations of Sr substitutions in BST play a major role that can lead to different applications. Based on the ratio of Ba:Sr, the material can be at ferroelectric or paraelectric phase. Our work focuses on material compositions in the paraelectric phase: lesser loss, no hysteresis, etc.) (**Figure 2**). Furthermore, substitutional oxides in the Ba:Sr sites have shown to alter the dielectric constant, tunability, and loss of the material.
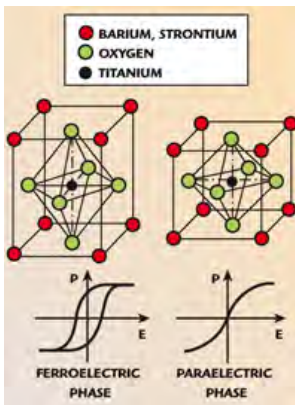
Figure 2. The paraelectric phase compositions of BST were used for all materials in the program.

Figure 3 shows the material fabrication steps of the ceramic formulations of BST. X-ray diffraction (XRD) is utilized to confirm the phase of the material (**Figure** 4).
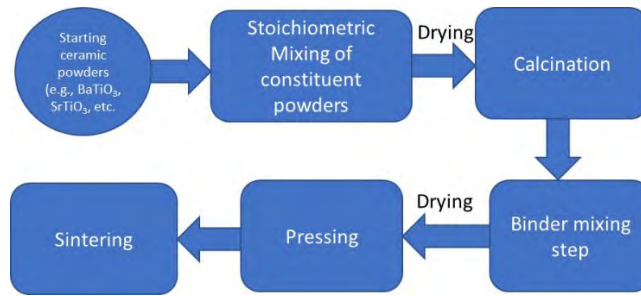
Figure 3. Ceramic fabrication steps for BST
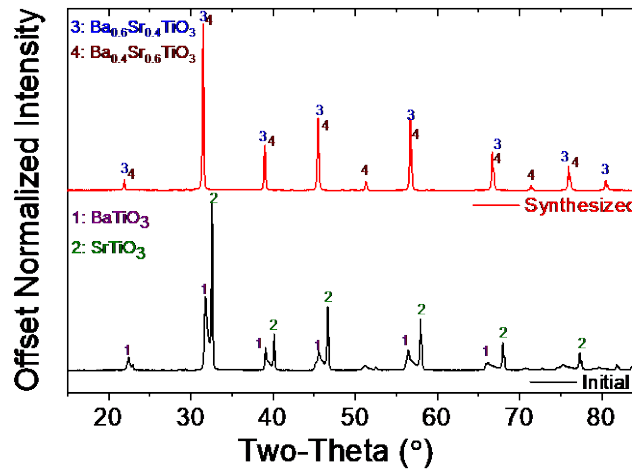
Figure 4. XRD confirmed that the jar milled powder mix converted to the perovskite phase during calcination

The calcined powder is then mixed with an organic binder and mixed in a jar mill with the recommended solvent for the binder. The binder-mixed powder is then dried and uniaxially pressed at about 7000 psi to form a pellet. The pressed pellet was sintered according to its sintering profile that depends on the composition. The as sintered pellets were measured for volumetric density and porosity (**Figure 5**). After this step, we have now confirmed the phase and near-theoretical density of the materials.

134
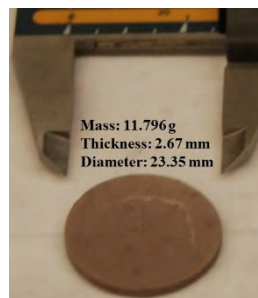
Figure 5. The sintered density of the ceramic pellets was more than 95% of the theoretical density of the material (5.41 gm/cm^3 for $Ba_{0.6}Sr_{0.4}TiO_3$)

Table 1 below shows the requirements for size and surface finish of the ceramic materials. ***For this program, we have focused up to 1 GHz measurements and IMD3 measurements.***

Parameters	Size	Surface Finish
Tunability	Not Applicable	Smooth for metallization
1 GHz (ε & $\tan\delta$)	15 mm (0.3mm-3 mm thickness)	Optical Finish
10 GHz (ε & $\tan\delta$)	22mm x22mm; 0.95 mm thickness	Optical Finish
15 GHz (ε & $\tan\delta$)	14mm x 14mm; 0.6 mm thickness	Optical Finish
90 GHz (ε & $\tan\delta$)	75mm; 0.5 mm to 1.5 mm thickness	Optical Finish
IMD3	2 mm x 2 mm x 1mm	Optical Finish

Table 1 shows that the material must withstand some stringent machining conditions to be applicable for a wide range of applications. The material was cut and polished to determine if it could withstand the mechanical preparation steps (**Figure 6**).
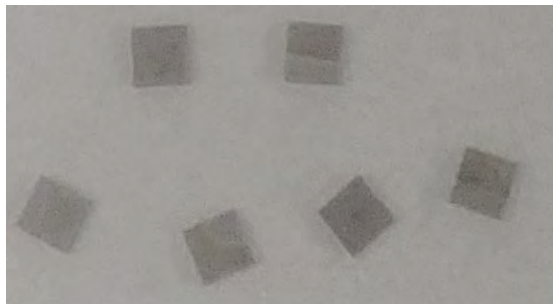
Figure 6. BST samples- *both side polished, 2 mmx2mm,1 mm thick samples* shown to withstand conventional dicing and polishing methods

We utilized cost-effective screen-printing methods to pattern electrodes on our ceramic samples for tunability measurements. The silver ink was purchased from Dupont and the screened patterns were cured as per the supplier's temperature/time schedule. The sheet resistance of all silver patterns was measured by a two-probe method and found to be fractional ohms (1 Ω) at a probe distance of 0.5 inch (**Figure 7**).
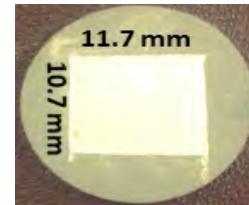
Figure 7. Typical screen-printed electrodes on both sides of the ceramic

Table 2 shows representative dielectric constant and tanδ values of $Ba_{0.6}Sr_{0.4}TiO_3$ mixed with 9 wt%, 16 wt%, and 60 wt% of Oxide III and one composition of $Ba_{0.6}Sr_{0.4}TiO_3$ mixed with 10wt% Oxide IV. A DE 5000 setup was used to collect values at 100 kHz. *The tanδ numbers are not quoted since they are not reliable in their error bar.* A 16453 A (**Figure 8**) setup was used to collect the data from 1 MHz to 1.8 GHz; however, the fringe effects at about 1.5 GHz may influence the reliability of the data at 1 GHz. The data shows that above 1 MHz, the epsilon values of the compositions are relatively similar*. **The question to answer is, how high in the frequency range will this epsilon value remain within the measurement error? Can it be 100 GHz?*** Powerhouse is investigating that question in our internal research and development program.

Table 2. Relative dielectric constant and insertion loss of BST/Oxide III compositions. The values are within +/-10%. The extreme data points (1 MHz and 1 GHz) have higher error bars.

Composition	@ 100kHz		@ 1 MHz		ε @ 10 MHz		ε @100 MHz		ε @ 1 GHz	
	ε	tanδ	ε	tanδ	ε	tanδ	ε	tanδ	ε	tanδ
$Ba_{0.6}Sr_{0.4}TiO_3$ with 9 wt% Oxide III	1650		675	0.02	610	0.01	610	0.015	<600	0.025
$Ba_{0.6}Sr_{0.4}TiO_3$ with 16 wt% Oxide III	460		245	0.01	245	0.007	245	0.007	<240	>0.02
$Ba_{0.6}Sr_{0.4}TiO_3$ with 60 wt% Oxide III	80		80	0.007	80	0.004	80	0.004	80	>0.02
$Ba_{0.6}Sr_{0.4}TiO_3$ with 10 wt% Oxide IV	680		240	>0.01	240	>0.015	240	>0.025	>240	>0.03
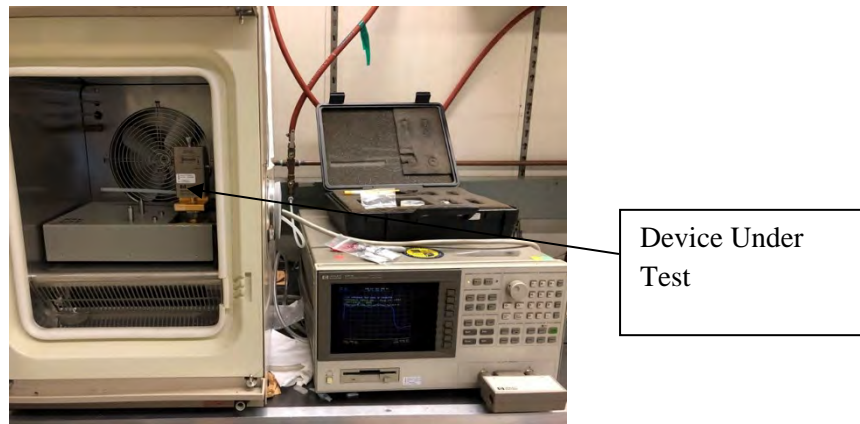
Figure 8. A HP16453A test fixture was used with a HP 4291A analyzer for the ε and tanδ measurements

<u>Tunability</u>

Tunability is defined as the % change in dielectric constant of the material with applied electric field. For the BST class of material, the tunability decreases (**Table 3**) with the addition of Oxide II material, while

the insertion loss decreases too; however, no matter the composition, the tunability can be recovered by applying a higher biasing field (**Table 4**).

Table 3. Addition of low loss oxides reduces the tunability of the composites.

Composition	% tunablity at 1 V/micron bias field
BST 60/40	50
BST (50/50)	15
BST 60/40/10 wt% Oxide III	30
BST 60/40/ 15 wt % Oxide III	20

Table 4. Higher biasing field produces higher tunability (BST/Oxide IV sample).

Applied Field (V/µm)	ε	% Tunability
0	680	30
0.5	460	45
0.8	370	50
1.6	230	67

Lastly, **Figure 9** shows the variability of capacitance as a function of temperature. It is important to note that the variability can be controlled by the application of an external DC bias field.
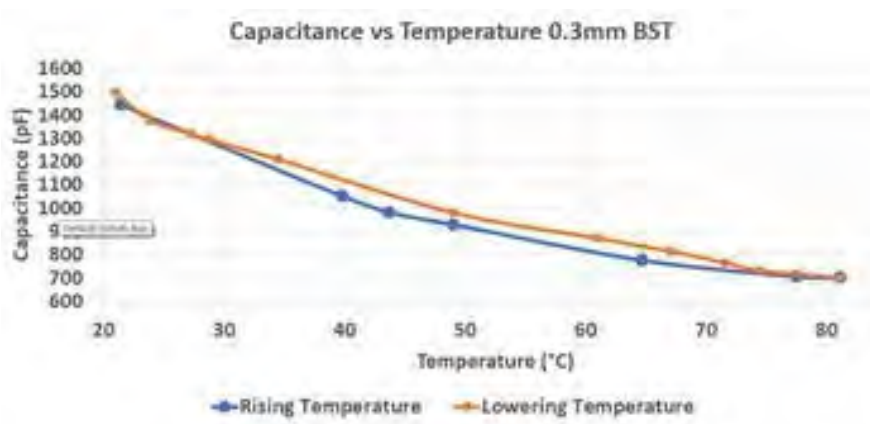
Figure 9. Variability of BST ceramics capacitance (and therefore ε) as a function of temperature

Intermodulation (IMD) Data

The intermodulation data was collected by utilizing the setup of an established radio manufacturer, Softronics, Ltd. All BST/Oxide III formulations were measured (**Table 5**). Since the lowest loss material composition was that of BST/60 wt% Oxide III, we compared the IMD values of that sample at two 24.9 dBm signals to that of two 36.9 dBm signal input at 1 GHz (**Table 6**).

Table 5. The IP3 values of the compositions shown in Table 5 are significant for their high-power RF applications.

Composition A (60/40 BST with ~9 wt% dopant)			
F1 (dBm)	F2 (dBm)	2f2-f1 (dBc)	2f2-f1 (dBc)
35	35	-33	-33
Composition B (60/40 BST with ~16 wt% dopant)			
26.4	26.4	-32	-32
Composition C (60/40 BST with ~60wt% dopant)			
24.9	24.9	-31.7	-31.8

Table 6. For 17 times increase in input power at 1 GHz, the BST material showed an IMD3 increase of less than 8 dB.

F1 (dBm)	F2 (dBm)	2F2-F1: F1 RATIO	2F1-F2: F2 RATIO
36.9	36.9	-23.6 dB	-23.6 dB
24.9	24.9	-31.7 dB	-31.7 dB

3.   Findings and Conclusions

The results showed that the material is rugged, inexpensive, and can be manufactured in various shapes and sizes. Furthermore, the composition of the materials can be altered to control the dielectric properties of the material: an additional dimension of material control along with processing parameters. The dielectric constant can range between several thousands to hundreds depending on the composition and the frequency. It was also found that the dielectric constant changed from DC to MHz; from MHz to GHz it was relatively constant. The insertion loss of the material, for some compositions, was in the 10^{-3} range. The tunability of the materials, with an applied bias field of 2 V/μm, ranged from 40% to 60% tunability. Tunability can be increased substantially (70% or greater) with higher bias field. The two-tone intermodulation data showed that the material has great prospect in handling high(er) RF power. For 17 times increase in input power at 1 GHz, the BST material showed an IMD3 increase of less than 8 dB. As an example, in a power amplifier or other active circuitry, the IMD3 typically has a slope of 2-3, meaning that for each dB increase in the incident power, the IMD3 rises by 2-3 dB. So, it suffices to say that devices designed from our material will not have any significant impact on the IMD3 performance of the entire system.

The **outcome** of the work has provided us with an understanding of the material compositions that provide low insertion loss while attaining tunability for agile systems. RF power handling characteristics are also

understood; they have much lower intermodulation products than active components at similar power levels. As for manufacturability, the robust nature of the material was proven through machining of a wide variety of shapes and sizes.

4.   Plans and Upcoming Events

For the ONR Grant #– N00014-19-1-2599, we have accomplished what we had set out to do. Our assessment for high power RF materials have shown the following.

1.   The compositional impact on the dielectric properties of this family of materials. This combined with optimized processing conditions will open vistas for use in the high power microwave arena that were hitherto unaddressed.

2.   The probability of high-power handling of these materials that can be controlled with compositional variation.

Essentially, we have demonstrated a class of material whose properties can be tailored for any RF/microwave application with an immense potential of handling high power. Collaboration has been a cornerstone of success of this work, as mentioned in the "Interaction with Others" section. The application of this material family for naval applications is clearer than what it was at the beginning of the program. Most importantly, this material has now been introduced to a variety of potential users and collaborators. Powerhouse has also conducted our own internal research and development in the 3D printing of these materials. Another topic of assessment was the demonstration of thick films. Preliminary data has shown that our compositions can produce tunable thick films; the loss and other parameters will be measured as part of the follow-on program.

Therefore, we believe that our progress justifies the consideration for Phase 2 continuation work on scaling up the material family for manufacturing assessment.

5.   Transitions and Impacts

Not Applicable

6.   Collaborations

One of the highlights of this work has been the productive interaction with many technical groups that included those in the government, academia, and industry. We believe that ONR will benefit immensely from these interactions. The following is a summary of the interactions:

1.   NRL High Power Microwave Section, Code 5745 (Andreadis/Addissie/Croman/ Drikas/Mendez). The Code 5745 HPM team has been the cornerstone of our work with regards to HPM applications, locating adequate measurement facilities within NRL, and discussing future applications to steer the work towards meaningful data collection. The collaboration continues. Powerhouse and the Code 5745 team are now establishing a capability within NRL for routine measurement of material properties from MHz to several GHz range. Discussions for designing and testing components based on these tunable materials are also underway.

2.   NRL Advanced Materials Section, Code 6127 (Laskoski). The Code 6127 team has been a great collaborator during the fledgling days of this program and throughout the COVID-19 ordeal. Under a CRADA, the team has provided help with sintering, XRD, and other analysis techniques. The data for the sintering steps, density measurements, and XRD were obtained in Dr. Laskoski's laboratory. We are currently exploring the opportunity of designing and fabricating extremely high epsilon materials for conformal antenna applications.

3. NSWCDD E13, HPM Technology Development Branch (Gehman). Dr. Gehman's insight and inquiries about the ceramic fabrication processes and the crystallographic phases were invaluable for the research.

7.   Personnel

Principal investigator: Somnath Sengupta
Business Contact: Somnath Sengupta
Team Members: Dr. Idan Mandelbaum

8.   Students

This program was utilized to train adults with autism on sustainable high technology laboratory skills. It is our hope that we will continue to develop cutting edge science and technology for the Navy while impacting employment for a severely underrepresented group.

9.   Technology Transfer
Not Applicable

10.   Products, Publications, Patents, License Agreements, etc.

Not Applicable

11.   Point of Contact in Navy

Dr. Tim Andreadis; Code 5745; Naval Research Laboratory. Last Contact: January, 2021.

12.   Acknowledgement/Disclaimer

High-Power Microwave Generation by Compact Linear Transformer Driver Technology

Grant No. N00014-18-1-2499

Annual Report for Fiscal Year 2020

a.   Period of Performance: October, 1, 2019 to September 30, 2020

Prepared by:

     Professor Ryan McBride, Principal Investigator
     University of Michigan
     Department of Nuclear Engineering and Radiological Sciences
     2355 Bonisteel Blvd
     1906 Cooley Building
     Ann Arbor, MI 48109-2104
     Tel: (734) 763-7504
     Email: mcbride@umich.edu

Grant or Contract Number: N00014-18-1-2499
Date Prepared: January 31, 2021
Project Title: High-Power Microwave Generation by Compact Linear Transformer Driver Technology
Annual Summary Report: FY2020
Principle Investigator: Ryan McBride, 734-763-7504, mcbrider@umich.edu
University of Michigan, Department of Nuclear Engineering and Radiological Sciences

Section I: Project Summary

1. Overview of Project

Abstract:　　　The efficient generation of high-power microwaves (HPM) from compact generating equipment is of critical importance to the United States Navy and Department of Defense (DoD). Applications include: radar, signal jamming, electronic warfare, counter IED (improvised explosive device), and vehicle stoppers. Example systems where HPM is critical include the Patriot Missile and the Aegis Combat/Weapon System. This project is exploring the use of compact linear transformer driver (LTD) technology to drive various gigawatt-class, narrow-band (~1 GHz), high-power microwave (HPM) sources, such as the magnetically insulated line oscillator (MILO). LTDs are low-voltage, low-impedance drivers. An LTD-driven HPM source could become one of the most compact, low-voltage, GW-class HPM sources available for ONR/DoD directed energy programs. To obtain this performance, a rich assortment of physics issues will be studied. For example, as we increase the driver power, electrode plasmas (particularly from contaminants adsorbed onto electrode surfaces) can become problematic. If plasmas form in the anode-cathode gap with densities >1e10 electrons/cc, then L-band microwaves (1 GHz) can become attenuated significantly. We will study these low-density plasmas by combining particle-in-cell simulations with experimental measurements from a vast array of diagnostics, including energetic particle detectors, Zeeman and Stark spectroscopy, self-emission imaging, and laser-based probing and imaging techniques. The use of LTD technology to drive an HPM source is advantageous for several reasons. First, the driver impedance and driver voltage is tunable, because LTD systems are modular. The PI's team is assembling a 4-cavity LTD facility called BLUE (Bestowed LTD from the Ursa-minor Experiment) at the University of Michigan (UM). The driver impedance of BLUE can be varied from 1 to 30 ohms. Second, the pulsed-power components in LTDs are completely encased in metal, thus minimizing stray high-voltage fields and electrical interference. Third, LTDs can be rep-rated up to (and possibly beyond) 0.1 Hz, thus increasing the average power. Additionally, rep-rating has the potential benefits of electrode conditioning and decontamination, therefore allowing us to emulate standard industry practices in the fabrication of commercial microwave tubes. The effects of various rep-rates will be tested directly. This document describes the progress to date on this project, which includes the status of the BLUE facility, the status of a MILO recently acquired for this project, and simulations of this MILO driven by an input power pulse similar to what BLUE will provide. This document also describes the research products produced by this effort, including publications and presentations.

Objective:　　　To explore the use of linear transformer driver technology for driving high-power microwave sources, including GW-class magnetically insulated line oscillators and potentially other crossed-field devices.

Introduction:　　This project will study GW-class, narrow-band HPM devices, operating at a frequency ~1 GHz. Such devices are driven by pulsed power technology. Pulsed power involves the use of high-voltage capacitors and fast switching techniques to store electrical energy over long time scales and discharge the energy over fast time scales; because power is the rate at which energy is delivered, the fast discharge time leads to power amplification. Often the peak powers obtainable in HPM can be quite large (~GW), but this usually comes at the expense of high average input powers. This project will explore the use of LTD technology (an exciting new compact and efficient pulsed power technology) to drive various HPM sources.

An important attribute of LTD technology is that it has the potential to be rep-rated up to (and possibly beyond) ~0.1 Hz.

In narrow-band HPM, the pulsed-power driver is used to apply a large, fast-rising voltage pulse across a vacuum-filled anode-cathode gap (A-K gap). This A-K gap then serves as the load for the pulsed-power driver, sometimes being referred to as a "diode" load. The large applied voltage (and its associated electric field) can cause electrons to be emitted from the cathode surface; this is especially true if the cathode is treated in a way that favors emission of electrons (e.g., velvet covered cathodes). If the voltage applied across the A-K gap is an appreciable fraction of the electron's rest mass energy (511 keV), then the predominantly vacuum-filled region within the A-K gap can become populated with relativistic electrons. Longer timescale electromagnetic fields [~DC fields relative to the faster radio frequency (RF) timescales of interest] can then be applied to direct these electrons into a well-formed electron beam. The electron beam can then be modulated to amplify and/or excite RF electromagnetic waves.

In crossed-field devices (CFDs) – such as relativistic magnetrons and crossed-field amplifiers – an approximately DC electric field **E** and an approximately DC magnetic field **B** are applied at right angles to one another, so that the well-known **E**×**B** drift velocity ($\mathbf{v} = \mathbf{E} \times \mathbf{B}/B^2$, where B is the scalar magnitude of the magnetic field) can be used to drive and steer the electron beam. To get the beam to interact with an RF field, the beam is driven in close proximity to a slow-wave structure (i.e., an anode structure with periodically spaced metal vanes). A synchronized, modulating interaction between the beam and the RF wave can then be obtained if the magnitude of the drift velocity $v=E/B$ is well matched to the phase velocity of the RF wave propagating in the slow-wave structure. A bunching instability, called the phase-focusing mechanism, causes the beam to become modulated, enhancing the RF output.

To drive the electron beams, this project will use a pulsed-power technology called linear transformer drivers. The LTD concept was pioneered in 1995-1997 at the High Current Electronics Institute (HCEI) in Tomsk, Russia, by Kovalchuk, Vizir, Kim, and colleagues. Since then, the LTD concept has been advanced further by HCEI as well as researchers at Sandia National Laboratories and many others worldwide. LTDs have been called the greatest advance in prime-power generation since the invention of the Marx generator in 1924.

In the late 2000's, a collaboration was developed between HCEI, Sandia National Laboratories, and the University of Michigan (UM) to bring LTD technology to the United States. In 2006--2007, five 3-m-diameter, 1-MA, 100-ns LTD cavities were tested at HCEI with resistive and electron-beam diode loads. In July of 2007, one of these HCEI cavities was shipped to UM, becoming the MAIZE facility and the first 1-MA, 100-ns LTD in the United States. In 2008, ten more 1-MA, 100-ns LTDs cavities were shipped to Sandia, becoming part of the Mykonos facility. Additionally, smaller (1.25 m in diameter), lower-current cavities were shipped to Sandia, becoming the Ursa Minor facility. The Ursa Minor facility stacked 21 of these 1.25-m-diameter cavities together to obtain a high-impedance driver for high-energy x-ray source development:
https://www.sandia.gov/Pulsed-Power/research_facilities/Ursa_Minor.html

Four of the Ursa Minor cavities were recently shipped to UM, where we are now assembling them into the BLUE facility (Bestowed LTD from the Ursa-minor Experiment) to drive HPM sources for this project.

Background: This project, using LTDs to drive HPM sources, is both basic and applied research, involving HPM design and optimization with particle-in-cell (PIC) simulations and experimental optimization of driver impedance using the 4-cavity BLUE LTD facility. BLUE will provide a variable drive voltage of 50–800 kV and a variable drive impedance of 1–30 Ω. Our approach will also involve the study of electrode plasmas (particularly from contaminants adsorbed onto electrode surfaces), which can become problematic. If plasmas form in the anode-cathode gap with densities $>10^{10}$ electrons/cc, then L-

144

band microwaves (1 GHz) can become attenuated significantly. We will study these low-density power flow plasmas by combining particle-in-cell simulations with experimental measurements from a vast array of diagnostics, including energetic particle detectors, Zeeman and Stark spectroscopy, self-emission imaging, and laser-based probing and imaging techniques.

2. Activities and Accomplishments

Substantial progress was made in this period assembling and testing BLUE and the MILO load. As reported previously, graduate student Brendan Sporer has made incredible progress assembling and improving the Ursa Minor LTD cavities donated by Sandia National Lab. Assembling a new pulsed power system is a challenging process that can require trial and error to navigate high voltage insulation issues, and BLUE was no exception. But with all electrical components installed, and a clear plastic lid in place, we conducted our first shots into a resistive load (Figure 1). A custom triggering system driven by a PT-55 pulser triggers the cavity, and switch performance can be monitored via a series of fiber optics and linear avalanche photodiodes (Figure 2). This particular innovation was spurred by referee comments in our paper published during this reporting period (A. P. Shah, P. C. Campbell, S. M. Miller, J. M. Woolstrum, B. J. Sporer, S. G. Patel, N. M. Jordan, R. M. Gilgenbach, and R. D. McBride, "Optimization of switch diagnostics on the MAIZE linear transformer driver", Rev. Sci. Instrum. **90**, 124707 (2019)). At present, we have not fully implemented it on BLUE, but it will become a necessity as more cavities (and switches) are brought online.

Figure 29. First shot on BLUE. The clear plastic lid allows the interior of the cavity to be observed during operation and for operation without ferromagnetic cores. The resistive load is mounted within the vacuum chamber on top of the cavity.
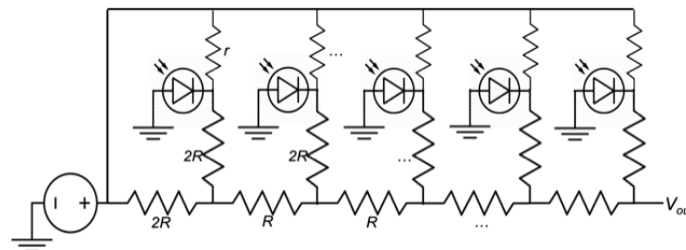
Figure 30. Schematic diagram of the switch monitoring circuit that was designed and partially implemented on BLUE. The system uses an avalanche photodiode array coupled to a resistive ladder network to monitor many switches simultaneously while only using a few oscilloscope channels to save resources.

During this period, we also completed construction of the vacuum system for BLUE and the MILO, including a turbo pump, cryo pump, electro-pneumatic gate valve, flexible bellows, scroll pump, and a 2-component, full-scale vacuum gauge. While the vacuum system was able to pull the chamber down to the low 10^{-5} torr range, the solenoid in the gate valve was destroyed by feedback from discharging BLUE. To resolve this, and other EMI issues, a ceramic break was installed to isolate all of the vacuum hardware and electronics from the BLUE cavity.

Subsequently, a current-viewing resistor (CVR) was installed in the resistive load, and the first calibrated current measurements were obtained (Figure 3). The initial resistive load shots provided an estimate of the current based on measured load resistance and the LTD charge voltage, but the CVR provided a very accurate measurement of BLUE's current pulse.

Figure 31. First 12 load-current calibration shots on BLUE (measured using CVR).

Our experience with the 1-MA MAIZE LTD showed that (for these L-3 switches) isolating switches during a pre-fire, and strong vacuum purges after each shot, are two key components of maintaining reliabil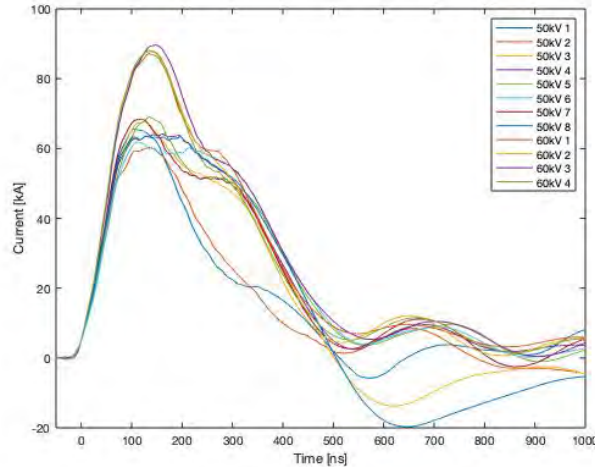ity. To this end, we replaced each of BLUE's ~1 kΩ copper sulfate resistors with a 5-resistor chain of 15 kΩ (75 kΩ total) solid state resistors from HVR. These resistors are a special composite that is designed for use with large, transient pulses, and we now use a similar configuration within MAIZE. The additional charging resistance increases the charging time of BLUE, but also isolates neighboring switches in the event of a pre-fire. Without this isolation, neighboring capacitors will discharge through the pre-firing switch, resulting in a charge-transfer for that switch that exceeds its rating, and long-term damage to the switch (and, thus, an increase in future pre-fires). Additionally, Brendan designed and implemented an electro-pneumatic switch purge system and integrated it into BLUE's existing Arduino microcontroller. This rapidly and thoroughly purges the switches after a shot, clearing them of debris and improving reliability.

We hired a new post-doc to work on this project, Roman Shapovalov, who has a lot of pulsed power experience from working with Rick Spielman at Idaho State University and Pierre Gourdain at University of Rochester. In early March, shortly after Roman joined the group, the lab was shut down due to COVID-19 orders from the state and university. This halted experimental progress, but allowed Roman to model BLUE using the SCREAMER, a pulsed-power circuit modeling code developed by Dr. Mark Kiefer at Sandia National Labs. While we had previously modeled BLUE in LTSpice, Roman was able to implement a Martin spark-gap switch model in SCREAMER, rather than assuming a constant resistance for the spark-gap switches. As shown in Figure 4, this results in differences in the pulse shapes near the pulse take-off point at 0 ns. With this Braginskii-Martin formalism, the switch resistance is inverse to the time-integral of the 2/3 power of the switch current (the current action integral). From 10 to 100 ns the switch resistance drops from 200-300 Ω down to 2-3 Ω. The final switch resistance varies from 20 mΩ to 540 mΩ, depending on the load.
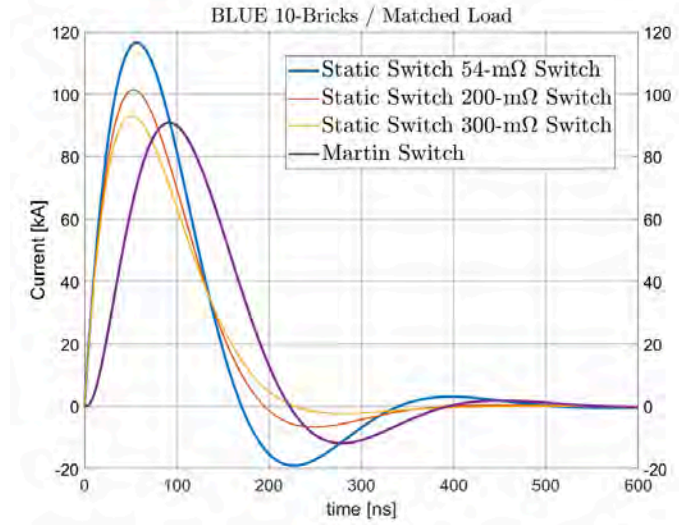
Figure 32. Improved modeling of BLUE by using the Martin spark-gap switch model in SCREAMER, rather than assuming a constant resistance for the spark-gap switches. A static switch over-predicts the peak current and under-predicts the risetime.

We also took advantage of this time to begin designing a pre-magnetizer system for BLUE. To this point, we had been operating BLUE in a horizontal orientation with a plastic lid, and were about to test the strength of the plastic lid in a vertical orientation (carrying the weight of the transformer oil and electrodes) when the COVID shutdown occurred. The insulating lid breaks the circuit around the oil section of the LTD, eliminating the need for ferromagnetic cores. The down side was significantly increased EMI and reduced strength. It was determined that both of these negatives would be unacceptable for the MILO, so a solid-state pre-magnetizer (Figure 5) was assembled and tested when lab operations resumed in June. The pre-magnetizer worked as expected (Figure 6), and the observed LTD current aligned with simulation and previous experience.

Figure 33. Photos of the new pre-mag system developed for BLUE by PhD student Brendan Sporer. The system premagnetizes the ferromagnetic cores inside the BLUE cavities. The system has been tested and is operational.

Figure 34. The first three shots of the cavity AFTER the initial pre-mag tests (with NO pre-magnetizing between shots). The pre-mag effects are as is expected based on LTspice modeling and similar res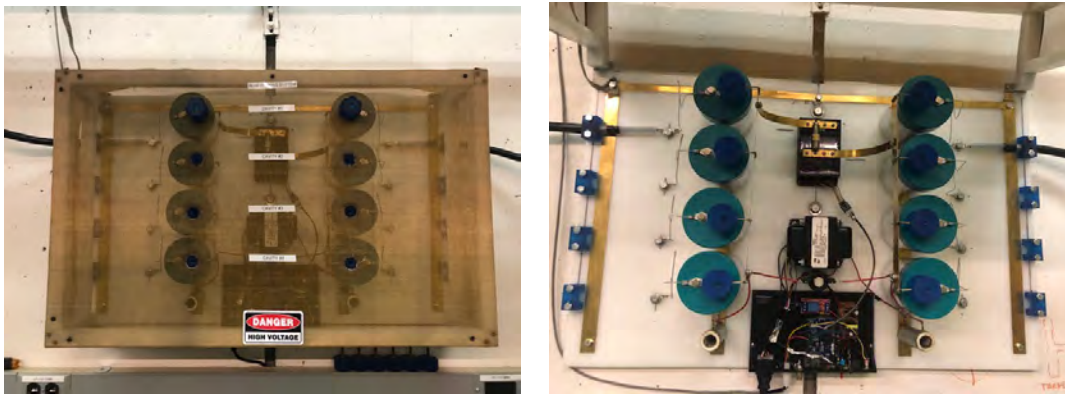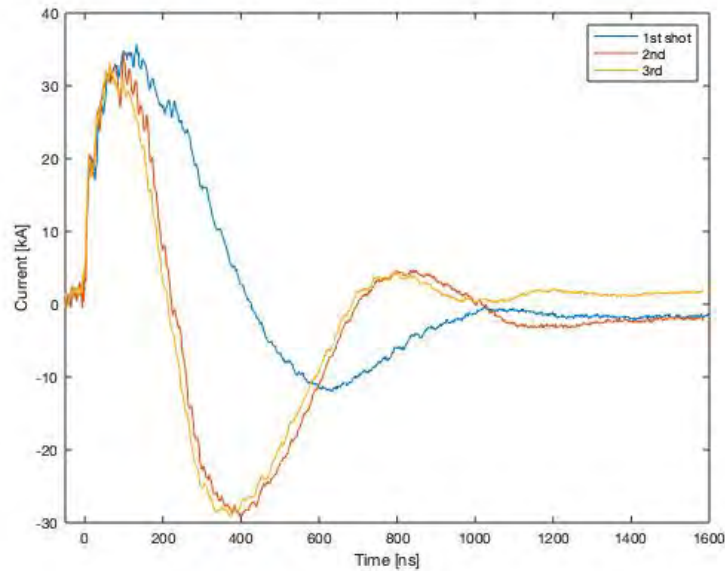earch from other LTD facilities (e.g., MAIZE). In particular, both the energy in the initial positive current pulse is increased and the energy in the reverse current pulse is decreased when pre-magnetization is used immediately prior to the shot being taken.

The triggering system for BLUE uses a PT-003 trigger module to step up a 5V signal to 300 V, which then triggers a PT-55 pulse generator to output a 50-kV trigger pulse to a custom trigger generator composed of a single 40-nF capacitor and a spark gap switch. During tests of the pre-magnetizer system the PT-003 trigger module failed. The PT-003 is no longer manufactured, and most modern alternatives are larger, more expensive, slower, and/or have higher jitter. The PT-55 itself is also no longer available, and cannot be manufactured anymore due to the lack of the radioactive krytron triggers it requires.

Consequently, Prof. Simon Bland at Imperial College London has been developing a solid-state PT-55 replacement, and shared some information about the front-end triggering system he employs. Using this information, PhD students Brendan Sporer and Akash Shah developed a P-channel metal–oxide–semiconductor (PMOS) circuit that steps up a 5-V signal to 300 V with sub-nanosecond jitter and a delay of ~12 ns. However, this delay decreases to almost zero when a >10 V trigger is used. The BNC555 pulse generator already used on the experiment for sub-ns timing is capable of providing this signal. With this development, testing on BLUE was able to continue.

To assemble the MILO, we fabricated a new cathode extension, adapter flange, and end window, then mounted the MILO to BLUE for initial vacuum tests, which were successful (Figure 7). Initial tests confirmed basic operation of the system with 50, 60, and 70 kV charge voltages. Diagnostics were limited and the cathode was just a bare stainless steel cylinder.

148
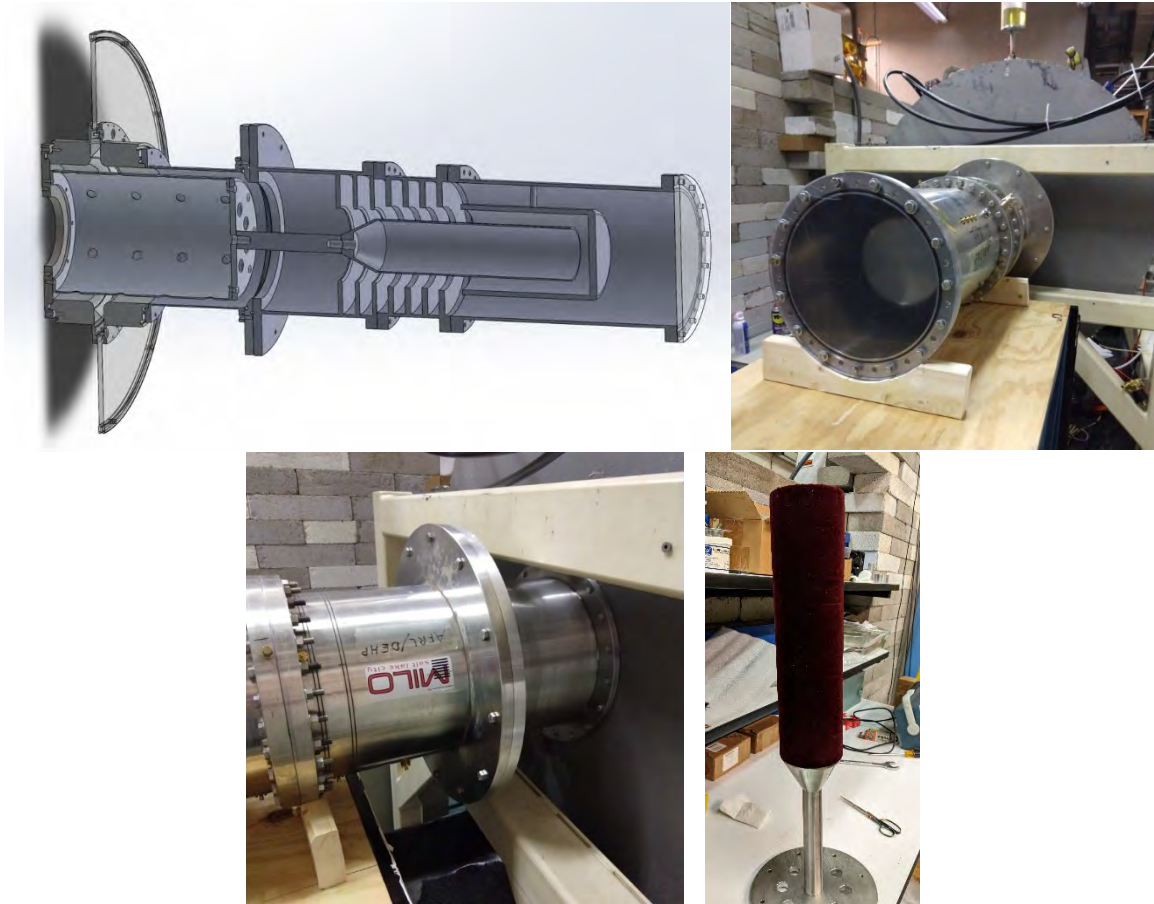
Figure 35. (top) CAD model of complete BLUE/MILO assembly (left/center) Photos of the AFRL MILO installed on BLUE for vacuum leak testing and initial tests. (right) Velvet covered cathode installed after initial tests to improve current delivery and uniformity.

After verifying a good vacuum and basic operation, the MILO was disassembled to upgrade the cathode, as shown in Figure 7. This velvet, supplied by Frank Hegeler at Naval Research Lab, is what NRL uses in many of their cathodes, and similar velvet was used on the cathode of this MILO when it was initially tested at AFRL. It will increase current emission and uniformity over the bare stainless steel. Additionally, a Rogowski current monitor was fabricated, calibrated, and installed in the MILO adapter flange.

The subsequent set of experiments were a major milestone for the project, successfully demonstrating microwave generation on a MILO driven by the BLUE LTD. In a sequence of shots at a ±70 kV charge voltage, BLUE was observed to generate up to 16 kA, and ~1.19 GHz microwave oscillations were observed in the final 3 cavities of the slow wave structure (Figure 8). The oscillations began ~35 ns into the pulse and lasted until 115 ns into the pulse (i.e., a total pulse length of ~80 ns). At present, the B-dots that record these signals are not calibrated, and can only provide frequency information. A method of calibrating them is currently under investigation. These oscillations were not observed on most shots, and the explanation for that behavior is a subject of active research.

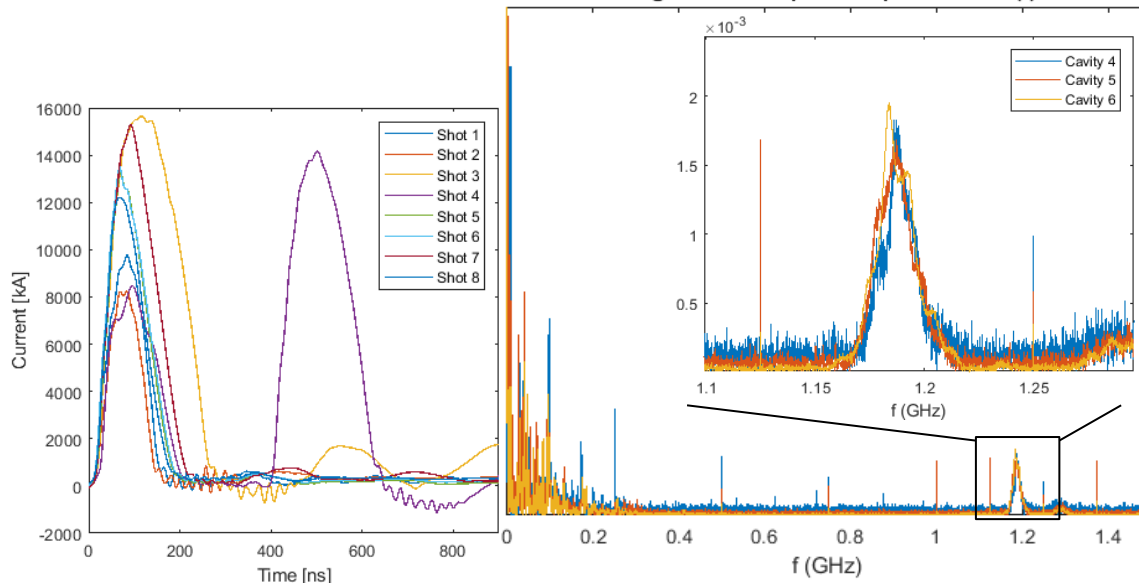Figure 36. (left) MILO current as measured by the integrated Rogowski current monitor. The double peak in shot #4 is the result of a pre-fire. (right) FFT of a B-dot within the last 3 cavities of the slow wave structure, indicating oscillations at ~1.19 GHz.

3. Findings and Conclusions

Within the past year we completed assembly of BLUE, including its vacuum, triggering, pre-magnetization, switch monitoring, and switch purging systems. Calibrated current measurements were made using a resistive load. The full MILO was assembled and mounted to BLUE. Initial experiments are complete and have demonstrated microwave oscillation at ~1.18 GHz for ~80 ns with a ±70 kV charge voltage and up to 16 kA. We also published our initial simulations of this system in D. A. Packard, A. Cooleybeck, N. M. Jordan, B. J. Sporer, A. E. Mazarakis, Y. Y. Lau, R. M. Gilgenbach, and R. D. McBride, "HFSS and CST Simulations of a GW-Class MILO," IEEE Trans. Plasma Sci. 48, 1894 (2020); https://doi.org/10.1109/TPS.2020.2990163.

4. Plans and Upcoming Events

In the remaining months of the project, we will continue to upgrade the diagnostic suite on BLUE and the MILO to expand our characterization of the device performance. While the MILO is already outfitted with many B-dot probes, the signal to noise ratio is still quite poor and new double-shielded cables have been purchased to improve this. Additional Rogowski current monitors will be employed to monitor current flow within the device, improving our understanding of electron dynamics. A capacitive voltage monitor is being designed as well. Simultaneously, we will be working to incorporate an additional BLUE cavity into a stacked LTD module.

5. Transitions and Impacts

This research project (and Prof. McBride's HPM program) just began in June of 2018, thus all of the transitions and impacts have been in the direction from Sandia and AFRL to the University of Michigan. Upon testing the donated equipment, we will begin to transition research outputs, technology products, and trained students/PhDs back to these labs.

Prof. McBride has developed and taught a brand new course on pulsed power this semester (UM-NERS 590) based on "primer" paper in IEEE TPS: https://doi.org/10.1109/TPS.2018.2870099. This course will be offered remotely to other universities in the fall of 2022, and every 2 years thereafter.

6.   Collaborations

As part of this program/project, we are collaborating with Dr. Brad Hoff of the AFRL, who is providing guidance on what is important to directed energy programs in the Navy and Air Force and who has also sent us a mini-LTD pulser for HPM device testing. Similarly, we are collaborating with Dr. Kyle Hendricks of the AFRL, who has sent us a working crossed-field HPM device (along with its CAD models) for testing on BLUE.

We have also been collaborating with Dr. Jon Douglass, Mr. Tommy Mulville, Mr. Matt Sceiford, Dr. Josh Leckbee, and (previously) Dr. Matt Wisher, all of Sandia National Laboratories, who have been working to help us with the transition of the four Ursa Minor cavities to the University of Michigan, where they are part of the BLUE LTD facility. It is of strategic importance to Sandia's pulsed-power development labs that students are being trained in new LTD technology.

Additionally, we have been working with Dr. Patrick Corcoran and Dr. David Phipps (both of L3Harris) to work through the issues with our L3 switches on both MAIZE and BLUE.

This program is also allowing us to collaborate with Prof. Allen Garner of Purdue University, who has his own ONR HPM funding to test out a non-linear transmission line (NLTL) HPM source on an LTD. We will be providing the LTD and Prof. Garner's group will be providing the NLTL source. Prof. McBride recently gave a guest lecture on pulsed power and LTDs at Purdue University as part of Prof. Allen Garner's NUCL 697 course on Pulsed Power and Vacuum Electronics.

Recently, we have collaborated with Prof. Simon Bland of Imperial College London on the development of fast, solid-state pulse generators for LTD triggers. They are a much-needed replacement for discontinued PT-55 and PT-003 trigger generators.

7.   Personnel

PI - Prof. Ryan McBride ~1.5 person months - National Academy Member: No
Co-PI - Dr. Nicholas Jordan ~3 person months - National Academy Member: No
PhD Student - Mr. Brendan Sporer ~9 person months - National Academy Member: No
PhD Student - Mr. Alexander Mazarakis ~4 person months - National Academy Member: No
Post-Doctoral Fellow - Dr. Roman Shapovalov ~9 person months - National Academy Member: No

8.   Students
2 graduate students, 1 undergraduate student:

Mr. Brendan Sporer: PhD student
Primarily supported by this ONR YIP MILO project (construction of BLUE)

Mr. Alexander Mazarakis: PhD student
Fully supported by this ONR YIP MILO project (experimental testing of MILO on BLUE) until his departure from UM in Feb 2020.

Mr. Drew Packard: PhD student
MILO simulation for this ONR YIP MILO project (supported by other ONR HPM projects: Multi-Frequency RPM and/or applied-B/planar MILO projects)

Ms. Anna Cooleybeck: Undergraduate student
MILO simulation for this ONR YIP MILO project

9. Technology Transfer

Regarding LTD work in general, we have been in communication with folks at the Naval Research Lab (Joe Schumer, Jacob Zier, and Tom Mehlhorn), Sandia National Labs (see above), and the AFRL (see above). In 2018, we published an invited tutorial on LTDs with Joe Schumer and Jacob Zier of the NRL and Jon Douglass and Josh Leckbee of Sandia National Laboratories (see Section 10 below). In 2019, we published a new fiber-optic-based technique for monitoring many spark-gap switches in an LTD cavity with a limited number of oscilloscope channels with Sonal Patel of Sandia.

We planned laboratory visits for Yeong-Jer "Jack" Chen, John Kreger and Matt McQuage from NSWC Dahlgren as well as Walter Sessions at Georgia Tech Research Institute (GTRI), but COVID travel restrictions have prevented those visits to date. We will work to accommodate a visit when possible.

10. Products, Publications, Patents, License Agreements, etc.

Publications resulting from this project:

Archival Publications

1. D. A. Packard, A. Cooleybeck, N. M. Jordan, B. J. Sporer, A. E. Mazarakis, Y. Y. Lau, R. M. Gilgenbach, and R. D. McBride, "HFSS and CST Simulations of a GW-Class MILO", IEEE Trans. Plasma Sci. **48**, 1894 (2020); https://doi.org/10.1109/TPS.2020.2990163.
2. R. V. Shapovalov, R. B. Spielman, P.-A. Gourdain, R. D. McBride, "Scaling Pulser Output Parameters for Standard and Dry Brick Configurations", Phys. Rev. Accel. Beams. **23**, 100401 (2020); https://doi.org/10.1103/PhysRevAccelBeams.23.100401.
3. A. P. Shah, P. C. Campbell, S. M. Miller, J. M. Woolstrum, B. J. Sporer, S. G. Patel, N. M. Jordan, R. M. Gilgenbach, and R. D. McBride, "Optimization of switch diagnostics on the MAIZE linear transformer driver", Rev. Sci. Instrum. **90**, 124707 (2019); https://doi.org/10.1063/1.5113866.

Conference Papers

1. R.V. Shapovalov, N.M. Jordan, B. Sporer, R.D. McBride, "BLUE MILO axial diode gap optimization using the pulsed-power circuit code Screamer", ICOPS 2020, Dec 2020. [accepted]
2. B. Sporer, N.M Jordan, R.D. McBride, "Testing of the Prototype BLUE Linear Transformer Driver (LTD) Cavity at University of Michigan", ICOPS 2020, Dec 2020. [accepted]
3. B. Sporer, N. Jordan, R. Shapovalov, D. Packard, R. Gilgenbach, R. McBride, "Testing of the First BLUE Linear Transformer Driver (LTD) Cavity at the University of Michigan", 62nd APS-DPP, Nov 2020. [accepted]
4. D.A. Packard, Y.Y. Lau, C. Swenson, N.M. Jordan, B. Sporer, R. Shapovalov, R.D. McBride, Y.Y. Lau, R.M. Gilgenbach, "Theory, Simulations, and Experiments on Magnetically Insulated Line Oscillator (MILO) at the University of Michigan", 62nd APS-DPP, Nov 2020. [accepted]
5. N.M. Jordan, D.A. Packard, S.C. Exelby, P.C. Campbell, B.J. Sporer, A.P. Shah, G.V. Dowhan, T.J. Smith, C.J. Swenson, Y.Y. Lau, R.D. McBride, R.M. Gilgenbach, "High Power Microwave and Pulsed Power Development at the University of Michigan", IPMHVC 2020, Knoxville, TN, May 2020. [Invited] [cancelled]
6. D.A. Packard, N.M. Jordan, Y.Y. Lau, R.M. Gilgenbach, B.W. Hoff, "Experimental Investigations of High Power Microwave Sources at the University of Michigan", DEPS Directed Energy Student Workshop, West Point, MD, Mar 2020.
7. B.J. Sporer, N.M. Jordan, R.D. McBride, "Status Update on the BLUE Linear Transformer Driver (LTD) System at the University of Michigan", 61st APS-DPP, Ft. Lauderdale, FL, Oct 2019.

Books: None

Book Chapter: None

Theses: None

Websites: None

Patents: None

Other Products: Identify any other significant products that were developed under this project. Describe the product and how it is being shared.

a. Description: Developed models and simulations of crossed-field devices for use on the BLUE LTD facility. Also developed a SolidWorks CAD model of the BLUE LTD facility.
b. Product Type: models

11.   Point of Contact in Navy

Dr. Joseph Schumer
Head, Pulsed Power Physics Branch
Plasma Physics Division
Naval Research Laboratory
(202) 841-2766
joe.schumer@nrl.navy.mil

Date we last discussed HPM research: June 25, 2019

12. Acknowledgement/Disclaimer

Multi-frequency High Power Microwave Generation and Amplification via Optically Gated Electron Beams

Grant No. N00014-20-1-2681

Annual Report for Fiscal Year 2020

Period of Performance: May 18, 2020 to September 30, 2020

Prepared by:

Prof. Peng Zhang, Principal Investigator
Department of Electrical and Computer Engineering
Michigan State University
428 S. Shaw Ln
East Lansing, MI 48824
Tel: 517-353-3654
Email: pz@egr.msu.edu

Department of Electrical and Computer Engineering, Michigan State University

Section I: Project Summary

1.   Overview of Project

Abstract: Electron beam based high power microwave (HPM) devices are critical to a variety of defense applications for Navy and more broadly the Department of Defense (DOD). This project explores the fundamental physics of density modulation of electron beam emission via combined mechanisms of thermionic/field/photo-emission and the interaction of such premodulated beams with circuits for HPM generation and amplification. This report provides an executive summary of our recent theoretical modeling efforts. We studied the modulation of photoelectron emission using two lasers of the same frequency. Our results demonstrates the capability of using interference modulation by single-frequency laser pairs, instead of two-color lasers, for modulating both the emission current and the photoelectron energy spectra. Using our quantum model for photoemission, we showed that optical field tunneling induced by ultrafast lasers can occur at an ultralow incident field strength of 0.03 V/nm, by adding an atomically thick dielectric coating on a metal nanoemitter, due to enhanced plasmonic resonance. Over a wide range of laser fields, the emission current density from the coated photoemitter is enhanced by at least 2 orders of magnitude as compared to the bare emitter. We also wrote an Invited Tutorial-Review article on recent theory of beam-circuit interactions for traveling wave tubes.

Objective: The objective of this project is to provide a foundational understanding of the underlying physics in optically gated electron emission and its interaction with microwave circuits. The goal is to provide a guideline for the design of compact HPM devices with the ultimate high power output and extremely flexible frequency tunability. The ultrafast electron emission due to pulsed laser, or optical gating, would potentially provide unrivaled precision in phase-control of electromagnetic signals from electron based HPM devices. The potential of selective gating of multiple beams would provide strong flexibility for multi-frequency HPM applications.

Introduction: Traveling wave devices utilize the collective interaction of an electron beam with a periodic structure to convert electron beam energy into electromagnetic radiation. They are key elements in telecommunication systems, satellite-based transmitters, military radar, communication data links, and electronic countermeasures. There continues to be strong interests in increasing the output power, frequency tunability, and bandwidth of traveling wave devices, for uses as radiation sources and power amplifiers, from GHz to THz and beyond. For the development of coherent radiation sources, it is desirable to minimize the threshold beam current for triggering oscillation. In contrast, for high power traveling wave tube (TWT) amplifiers, unwanted oscillations pose a major threat to their operation. For novel contemporary traveling wave devices, such as metamaterial-, photonic crystal- and advanced Smith-Purcell-based traveling wave devices, improving efficiency remains a major challenge.

In vacuum microwave tubes, the energy conversion from electron beams into electromagnetic radiation relies on beam modulation, by either density modulation or velocity modulation. Density modulation is achieved by controlling the electron emission from the cathode. Velocity modulation is achieved by passing the electrons through an RF electric field that modulates the velocities of the electrons. At present, TWTs

mainly reply on velocity modulation of the electron beam for power amplification. After the electron velocities are modulated, there is a substantial delay before velocity modulation becomes density modulation, until useful gain is produced. Significant improvements in TWT performance can be enabled by density modulation during emission. In particular, with density modulation, velocity dispersion in the beam can be minimized and the substantial portion of the interaction circuit for the purpose of converting velocity modulation into density modulation can be eliminated. This would result in compact devices with reductions in overall dimensions and weight, through the elimination of the premodulation circuit. Furthermore, density modulation during emission would eliminate the launching loss of the input RF signal, which is a serious intrinsic problem in TWTs based on velocity modulation.

In this project, we will explore density modulation in optically gated electron emission. This is motivated by the recent rapid development in ultrafast lasers and photonics, which has opened up unprecedented advances to control electron beam dynamics at ultrashort spatial-temporal scales. The research on implementing both high power and frequency tunability in HPM devices will provide a critical disruptive capability using high power microwaves. The theory will also be valuable to neighboring fields such as novel miniaturized electromagnetic radiation sources, nano-optoelectronics, ultrafast physics, material science, and accelerator technology.

Background: The idea of using direct current modulation of electron beams in microwave amplifiers has existed for decades. Historically, density modulation was accomplished with a grid that lays over the surface of a thermionic emitter to control the electron emission. Because of the finite transit time of the electrons across the cathode-grid space, this modulation technique is only effective up to 2 GHz for state-of-the-art devices. With the advancement of vacuum microelectronics and field emitter arrays (FEAs), the gate-to-emitter spacing has been reduced into submicron scale, which significantly decreases the electron transit time. Density modulation about 5 GHz by gate modulating of the FEA has been demonstrated; however, there are significant challenges for using FEAs in high power tubes, because the premature failure due to arcing often occurs at current levels much smaller than the design requirements. Breakdown is a major challenge for FEAs because of the high fields within the structure and the thin-film gate electrode. An electrical short between the gate and any individual emitter will burn out the entire FEA and render it unusable. While shields can be added to mitigate the damaging effects of the electrical shorts, high operating voltage is needed to field emitter arrays to draw sufficient current.

Photoemission provides an alternative method to generate premodulated electron beams, which relaxes the requirement of high operating voltage in field emission, thus eliminating possible arcing and circuit breakdown. More importantly, pulsed laser induced (or assisted) electron emission offers the possibility of manipulation and control of coherent electron motion in ultrashort spatiotemporal scales. These advantages would benefit the development of advanced compact HPM devices.

2.   Activities and Accomplishments

The main new activities and accomplishments during this performance period (18 May 2020 - 30 Sep 2020) include: 1) Interference modulation of photoemission from biased metal cathodes driven by two lasers of the same frequency; 2) plasmon-enhanced resonant photoemission using atomically thick dielectric coatings; and 3) a tutorial-review of recent theory of TWTs.

INTERFERENCE MODULATION OF PHOTOEMISSION DRIVEN BY TWO LASERS OF THE SAME FREQUENCY

We utilize two lasers of the same frequency to modulate the photoelectron emission by their phase delay. This work is in collaboration with Dr. John Luginsland of Confluent Sciences, LLC. Compared to the two-color laser configuration, single-frequency laser pairs can be more easily implemented in experiments since they relax the requirement of higher order harmonic generation, which becomes increasingly difficult in the high laser intensity regimes. The intensity ratio of the single-frequency laser pairs can be tuned over a

much wider range than the two-color laser system. Using a quantum mechanical model, we studied the time-resolved photoelectron energy spectra and emission current modulation under different laser and dc fields.

Under the action of two laser fields $F_1 \cos(\omega t)$ and $F_2 \cos(\omega t + \theta)$ and a dc electric field F_0, the time-dependent potential barrier near the surface of the cathode reads,

$$\Phi(x, t) = \begin{cases} 0, & x < 0 \\ E_F + W_{eff} - eF_0 x - eFx \cos(\omega t + \varphi), & x \geq 0, \end{cases} \tag{1}$$

where E_F is the Fermi energy of the metal cathode, $W_{eff} = W - 2\sqrt{e^3 F_0 / 16\pi\varepsilon_0}$ is the effective work function with Schottky effect, with W being the nominal work function, e is the elementary charge, ε_0 is the free space permittivity, x is the distance away from the cathode surface ($x = 0$), and F is the magnitude of the total laser field due to the two laser fields $F_1 \cos(\omega t)$ and $F_2 \cos(\omega t + \theta)$,

$$F = \sqrt{(F_1 + F_2 \cos\theta)^2 + (F_2 \sin\theta)^2}. \tag{2}$$

From Eq. (2), it is clear that the magnitude of the total laser field depends strongly on the phase delay of the two lasers θ, which is expected to provide similar current modulation as in the two-color laser setup. The resultant phase $\varphi = \arcsin(F_2 \sin\theta / F)$, the effect of which becomes important for photoemission only in very short laser pulses when carrier-envelope phase matters. For laser pulses longer than about 10 cycles, it can be well approximated by continuous-wave excitation for photoemission. Thus, in this study we ignore the effects of the absolute phase and set $\varphi = 0$ without loss of generality. Based on the exact quantum theory of photoemission, the time-averaged normalized emission current density, defined as the time-averaged ratio of the transmitted probability current density over the incident probability current density, $\langle w(\varepsilon, x, t) \rangle = \langle J_t / J_i \rangle$, can be obtained as,

$$\langle w(\varepsilon) \rangle = \sum_{n=-\infty}^{\infty} \langle w_n(\varepsilon) \rangle, \quad \langle w_n(\varepsilon) \rangle = \frac{(eF_0\hbar/\sqrt{2m})^{1/3}}{\pi\sqrt{\varepsilon}} |T_n|^2, \tag{3}$$

where $\langle w_n \rangle$ denotes the normalized emission current density through the nth channel with emitted electron energy $\varepsilon + n\hbar\omega$ due to the n-photon contribution, $\hbar$ is the reduced Plank constant, m is the electron mass and T_n represents the transmission coefficient of electron wave functions, which is calculated from,

$$2\sqrt{\varepsilon}\delta(l) = \sum_{n=-\infty}^{\infty} T_n \left[\sqrt{\varepsilon + l\hbar\omega} P_{n(n-l)} + \frac{\hbar}{\sqrt{2m}} Q_{n(n-l)} \right], \tag{4}$$

where $\delta(l)$ is the Dirac delta function, l and n are integers, P_{nl} and Q_{nl} are the Fourier coefficients, which are functions of laser field F, DC field F_0, and laser frequency ω. For the special case of zero dc field $F_0 = 0$, the time-averaged normalized emission current density becomes,

$$\langle w(\varepsilon) \rangle = \sum_{n=-\infty}^{\infty} \langle w_n(\varepsilon) \rangle, \quad \langle w_n(\varepsilon) \rangle = \text{Re}\left(|T_n|^2 \sqrt{E_n/\varepsilon} \right), \tag{5}$$

where T_n is still calculated from Eq. (4). These analytical results in Eqs. (3) - (5) are obtained by solving the time-dependent Schrödinger equation exactly with the potential energy given in Eq. (1). We would like to point out that although the calculation here is equivalent to photoemission using a single laser with varying intensity, our proposed method of using two lasers provides more degrees of freedom for experimental control, and also offers the capability of measuring the emitted electron spectra versus time after emission, i.e. time-resolved photoelectron energy spectra.
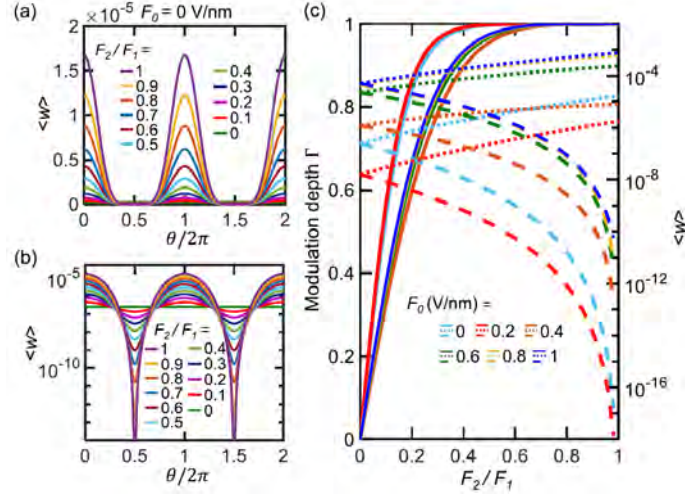
Fig. 1. Photoemission current modulation due to two lasers of the same frequency with electric fields F_2 and F_1 and a phase delay of θ. (a) Normalized total time-averaged emission current density $\langle w \rangle$ as a function of phase difference θ for different F_2/F_1, when the dc field $F_0 = 0$. (b) Semilog plot of $\langle w \rangle$ in (a). (c) Current modulation depth Γ (solid lines) as a function of the laser field ratio F_2/F_1 for different dc fields F_0. Dotted (dashed) lines in (c) are for the maximum (minimum) emission current density $\langle w \rangle$ at $\theta = 0$ ($\theta = \pi$). Here, F_1 is fixed as 1.8 V/nm.

We find that a strong current modulation ($> 90\%$) can be achieved with a moderate ratio of the laser fields (< 0.4) even under a strong DC bias (Fig. 1). The nonlinear effects of the DC field, cathode materials, and laser wavelength on both the emission current level and modulation depth are examined. The strong dependence of photoelectron energy spectra on the phase delay of the two lasers demonstrates promising potential for the application of time-resolved photoelectron spectroscopy using single-frequency laser pairs. Our study may inspire new routes toward many applications requiring both high photoemission current and strong current modulation, such as tabletop particle accelerators, photoelectron microscopy, and x-ray sources.

We also examine the photoemission current modulation depth Γ for cathode materials with different work functions and for various incident laser wavelengths (Fig. 2). We fix the dc field $F_0 = 0.8$ V/nm and laser fields $F_1 = 1.8$ V/nm and $F_2 = 0.3$ V/nm. Under the same illumination condition, the electron emission current depends strongly on the work function, however, the modulation depth Γ varies only slightly. This is because Γ is predominantly determined by the ratio of the laser field strengths. Figure 2 shows the effect of laser wavelength on both emission current and modulation depth for a tungsten cathode. The nonlinear dependence may also be attributed to the change of the ratio $W_{eff}/\hbar\omega$ near resonant n-photon processes.
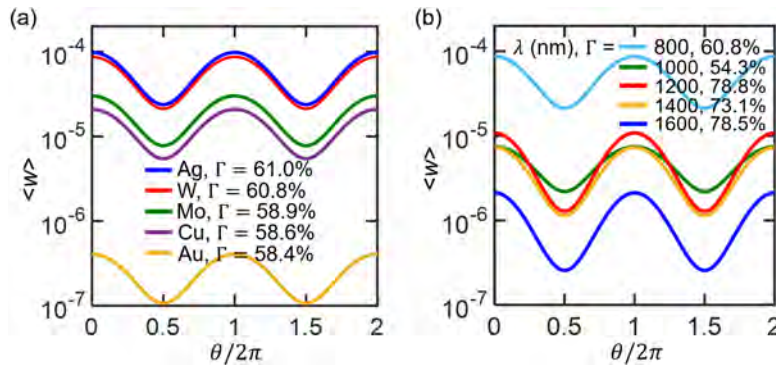
FIG. 2. Normalized total time-averaged emission current density $<w>$ as a function of the phase difference θ, for various (a) cathode materials and (b) incident wavelengths. In (a), the laser wavelength $\lambda = 800$ nm ($\hbar\omega = 1.55$ eV). The nominal work function of different materials is $W_{Ag} = 4.26$ eV, $W_w = 4.31$ eV, $W_{Mo} = 4.6$ eV, $W_{Cu} = 4.65$ eV, and $W_{Au} = 5.1$ eV. In (b), the metal is tungsten. Here, the dc field F_0 is 0.8 V/nm and the laser fields F_1 and F_2 are fixed at 1.8 and 0.3 V/nm respectively.

PLASMON-ENHANCED RESONANT PHOTOEMISSION USING ATOMICALLY THICK DIELECTRIC COATINGS

Photoelectron emission, or photoemission, from a nanotip driven by an ultrafast laser offers an attractive route to generate high brightness, low emittance, and spatiotemporally coherent electron bunches, which are central to high power electromagnetic sources, free-electron lasers, time resolved electron microscopy, carrier-envelope-phase detection, and novel nanoelectronic devices. Despite extensive research exploring efficient multiphoton absorption at low laser intensities or optical field tunneling at high laser intensities, the use of photoemission from nanotips is still limited by its low emission current and low quantum efficiency.

We studied the enhancement of photoemission by coating metal nanoemitters with an atomically thick dielectric. The thin coating is able to enhance the local optical field near the emitter tip through plasmonic resonance, where optical field tunneling can be accessed at a significantly reduced incident laser intensity. The physics behind this effect lies in the considerably enhanced plasmon resonant fields highly confined within the dielectric coating (in addition to the geometrical plasmon field enhancement) and the lowered tunneling barrier due to the electron affinity. We performed optical simulations and employed our quantum photoemission model to investigate the photoemission processes under the plasmon resonant conditions on both bare and coated Au-nanopyramid field emitters. The quantum photoemission model is constructed by solving the time-dependent Schrödinger equation exactly for an effective triangular barrier. It is found that, over a wide range of laser fields, the emission current density from the coated photoemitter is enhanced by at least 2 orders of magnitude as compared to the bare emitter (Fig. 3). The optical field emission regime can be reached at a much smaller field strength compared to bare emitter.
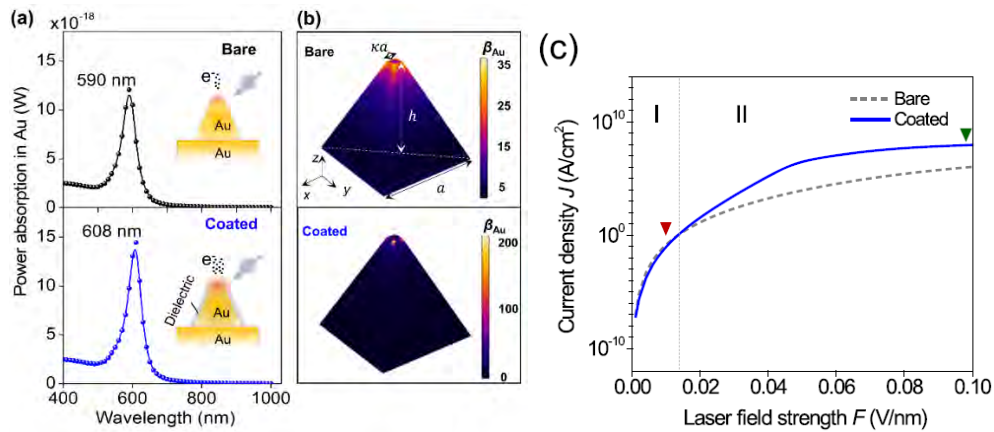

Fig. 3. Resonant photoemission. (a) Schematic of the resonant photoemission from either bare or coated Au-nanopyramid field emitters (insets) with their simulated plasmon resonances. (b) Corresponding simulated resonant field enhancements β_{Au} at the Au surface. In the simulation, the nanopyramid has fixed side length $a = 40$ nm, height $h = 40$ nm, and aspect ratio $\kappa = 0.1$. It is either bare or coated with a dielectric layer with thickness $d = 1$nm and refractive index $n = 1.5$. (c) The photoemission current density J as a function of the field strength of the incident laser F, for the bare or coated photoemitters.

The proposed mechanism is independent of the geometry of the metal nanoemitter, and practically the coating could protect the metal nanoemitters from corrosion or metalatom migration under intense optical fields. The ideas presented in this work may result in the fabrication of strong-field photoemitters with higher yields and longer lifetimes.

The work is published in ACS Nano. Using plasmonic resonant enhanced emitters, it is expected to be able to achieve strong photoemission even with low intensity lasers that are affordable and widely available.

RECENT THEORY OF TRAVELING-WAVE TUBES

We reviewed the recent theory of traveling-wave tubes (TWTs). This work is in collaboration with Dr. John Luginsland of Confluent Sciences, LLC. The traditional Pierce theory was first briefly reviewed. We provided several natural extensions to the Pierce theory to describe phenomena not previously considered in the small-signal regime. These include harmonic generation in TWTs, the effect of high beam current (or space charge effects) on both the beam mode and circuit mode of TWTs, and discrete cavity analysis of TWTs.

The classical Pierce theory was formulated for a single (fundamental) frequency, that of the input signal; however, in a TWT with an octave bandwidth or greater, in particular the widely used helix TWT, the second harmonic of the input signal may also be within the amplification band and thus may also be generated and amplified, with no input at this second harmonic frequency. It is shown that the second harmonic arises mostly from a newly discovered dynamic synchronous interaction instead of by the kinematic orbital crowding mechanism that is the most dominant harmonic generation mechanism in other microwave devices. The methodology provided here, which is a natural extension of Pierce's original theory, may be applicable not only to TWTs but to other high-power microwave sources.
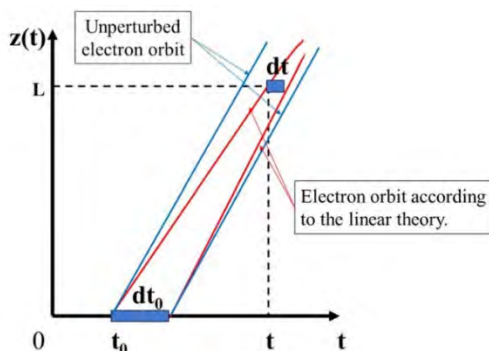

Fig. 4. An (exaggerated) illustration of harmonic generation due to orbital crowding.

In beam-circuit interactions, the space-charge effect of the beam is important at high beam currents. In Pierce's TWT theory, this space-charge effect is modelled by the parameter which he called Q in the beam mode. A reliable determination of Q remains elusive for a realistic TWT. It was discovered that the circuit mode in Pierce's theory must also be modified at high beam current, an aspect overlooked in Pierce's original analysis. This circuit mode modification is quantified by an entirely new parameter called q, introduced for the first time in TWT theory. For the example using a realistic tape helix TWT, we find that the effect of q is equivalent to a modification of the circuit phase velocity by as much as two percent, which is a very significant effect.

We have demonstrated that a coupled circuit model can reproduce the electromagnetic structure of a full TWT, and that this allows one to add spatial non-uniformity to the slow wave circuit. Additional work that we have done shows that as the number of cavities becomes large, the normal mode analysis naturally transitions to a wave description. This provides an explicit link between standard Pierce theory (wave) and

a means to incorporate finite length effects, internal reflections, manufacturing errors, and individual cavity differences into a Pierce style analysis.

This work was published as an Invited Tutorial paper in Plasma Research Express.

3.   Findings and Conclusions

We have demonstrated strong density modulation of photoemission current using two-lasers of the same frequency. We have explored a way of enhancing photoemission current using thin dielectric coating on an emitter by plasmon resonance. We have reviewed recent theory on the basic physics of beam-circuit interaction of TWTs for high power microwave generation and amplification.

The PI has been a Co-Guest Editor with Drs. Brad Hoff and Wilkin Tang of AFRL for the 2020 Special Issue of IEEE Transactions on Plasma Science on High-Power Microwave and Millimeter Wave Generation.

4.   Plans and Upcoming Events

We will develop new models to study electron emission due to pulsed laser excitation. This will be used to evaluate the time-dependent physics of electron emission, which is important to the generation of short electron bunches for HPM excitation. We will investigate the method of adding dielectric coating to increase field emission current under DC bias. These studies will pave the way to achieve efficient density modulation of the electron beam immediately after emission. We will further explore the space charge effects in Pierce theory and identify the small q quantity for a realistic TWT. We plan to develop new theory for beam-circuit interaction for density modulated beams using optical means. We also plan to run CST simulation to test the beam-circuit theory.

5.   Transitions and Impacts
Not Applicable.

6.   Collaborations
John Luginsland, Confluent Sciences.
Brad Hoff, Air Force Research Laboratory.
Wilkin Tang, Air Force Research Laboratory.
Steve Fairchild, Air Force Research Laboratory.
Ricky Ang, international collaborator, Singapore University of Technology and Design, Singapore.
Lin Wu, international collaborator, Institute of High Performance Computing, Singapore.
Y. Y. Lau, University of Michigan.
John Verboncoeur, Michigan State University.
Allen Garner, Purdue University.

7.   Personnel

Principal Investigator: Peng Zhang, 1 person-month, National Academy Member (N).
Teams Members:
Patrick Wong, Postdoc, 3 person-months, National Academy Member (N).
Yi Luo, graduate student, 3 person-months, National Academy Member (N).
Yang Zhou, graduate student, 5 person-months, National Academy Member (N).

Business Contact: Casie Medina
Subs: None

8.   Students
2 graduate students assisting during reporting period.

9.   Technology Transfer
Not Applicable at present. Future plan is discussed in Section 4 above.

10.   Products, Publications, Patents, License Agreements, etc.
Publications resulting from this project:
<u>Archival Publications</u>

1. Y. Luo, J. Luginsland, and Peng Zhang, "Interference modulation of photoemission from biased metal cathodes driven by two lasers of the same frequency", AIP Advances 10, 075301 (2020). Peer-reviewed, Distribution A, Federal Funding Acknowledged. https://doi.org/10.1063/5.0010792

2. B. Hoff, W. Tang, R. Seviour, and Peng Zhang, "Guest Editorial - The Eighteenth Special Issue on High-Power Microwave and Millimeter-Wave Generation", IEEE Trans. Plasma Sci., 48, 1858 (2020). Peer-reviewed, Distribution A, Federal Funding Not Acknowledged. https://doi.org/10.1109/TPS.2020.2998878

3. P. Wong, Peng Zhang, and J. Luginsland, "Recent theory of traveling-wave tubes: a tutorial-review", Plasma Res. Express 2, 023001 (2020). **[Invited Tutorial Paper]** Peer-reviewed, Distribution A, Federal Funding Acknowledged. https://doi.org/10.1088/2516-1067/ab9730

4. X. Xiong, Y. Zhou, Y. Luo, X. Li, M. Bosman, L. K. Ang, Peng Zhang, and L. Wu, "Plasmon-Enhanced Resonant Photoemission Using Atomically Thick Dielectric Coatings", ACS Nano, 14, 8806 − 8815 (2020). Peer-reviewed, Distribution A, Federal Funding Acknowledged. https://doi.org/10.1021/acsnano.0c03406

11.   Point of Contact in Navy

Kevin Jensen, NRL, 25JUN2020; Brad Hoff, AFRL, 10JUN2020; Wilkin Tang, AFRL, 10JUN2020; Don Shiffler, AFRL, 8SEP2020; Steve Fairchild, AFRL, 8SEP2020; Jason Marshall, NRL, 7SEP2020.

12. Acknowledgement/Disclaimer

Compact High-Power Microwave Oscillators

Prepared by:

Dr. Alan Phelps, Principal Investigator
Physics Department
University of Strathclyde
John Anderson Building
107 Rottenrow East
Glasgow, Scotland, UK G4 0NG
Tel: +44 141 548 3166
Email: a.d.r.phelps@strath.ac.uk
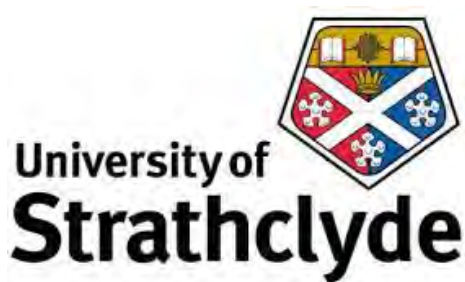
Grant or Contract Number: N62909-18-1-2122-GRANT12538355, N00014-18-S-B001
Date Prepared: January 31 2021
Project Title: Compact High-Power Microwave Oscillators
Annual Summary Report: ONR HPM 2020 Program – FY20 Annual Report
Principle Investigator: Alan Phelps, +44141 548 3166, a.d.r.phelps@strath.ac.uk
                 University of Strathclyde, Scotland, UK

Section I: Project Summary

1. Overview of Project

Abstract:
Researchers in the Atoms Beams and Plasmas (ABP) Group at the University of Strathclyde (UoS), Scotland, UK, are engaged in a basic research investigation of a novel X-band (8 – 12GHz) Cherenkov oscillator that operates without the requirement for an externally applied magnetic field. This is achieved via exploitation of the self-field generated forces of the electron beam as it propagates through the source interaction region, resulting in predicted output powers of ~300MW at ~9.4GHz when driven at ~500keV ~2kA. This corresponds to an electronic efficiency of ~30%. The operation of the source appears reasonably insensitive to variation in the beam parameters, maintaining resonance at ~9.4GHz, and >100MW output, over an extended range of electron energies (400 – 600keV, with beam currents scaled accordingly).
Objective:
Develop an X-band High Power Microwave (HPM) source that functions without the requirement for externally applied magnetic-insulation of the driving electron beam. Over the reporting period, the intention was to progress the investigation of the source from numerical prediction through to commencement of experimental measurements.
Introduction:
The current reporting period (Oct 1 2019 – Sept 30 2020) spans portions of Project Year (PY) 2 and 3 (PY2 running from June 14 2019 –June 15 2020). The intended work over this period involved the assembly of the prototype source (by early 2020) and the commencement of experimental testing (by end of PY2 through the whole of PY3). The emergence of Covid-19/Sars-Cov-2, at the end of 2019, has significantly affected this work schedule, with supply-chain disruption becoming apparent in early 2020 and severe workplace/travel restrictions coming into force from March 2020. Researchers regained limited access to the UoS campus in mid-July 2020, with both access and supply-chain disruption ongoing at the time of writing.

The following report covers the research undertaken over the reporting period and updates on the UoS' efforts to mitigate these issues, since last reporting at the end of PY2.

| ABP group	Atoms Beams and Plasma research group, based in the Physics Department of the University of Strathclyde.
GHz	Giga-Hertz: 1,000,000,000 Hertz or 1,000,000,000 full-wave oscillations of the field-pattern per second.
HPM	High Power Microwave: refers to microwave sources / amplifiers with output powers >100MW
keV / kA	Kilo-electron-Volt / kilo-ampere: 1000 Volts / 1000 Amperes
MW	Mega-Watt: 1,000,000 Watts
PiC	Particle in Cell: a numerical code that considers both the electromagnetic fields and discrete particles within the "cells" used to define the simulation volume.
UoS	University of Strathclyde.
X-band	A region of the EM spectrum between 8 – 12GHz
PY	Project Year: for the present project this refers to the period running from June 15 in one year till June 14 in the following year
BWO	Backward-Wave Oscillator
EM	Electro-Magnetic wave / field / spectrum
SIBWO	Self-Insulating Backward-Wave Oscillator
A-K gap	Anode – Cathode (German "Kathode") gap: refers to the spacing between the cathodic emitter and anode plane of the electron accelerating diode
VNA	Vector Network Analyzer
ns	Nano-second: 0.000,000,001 seconds

Table 3: List of abbreviations/terminology

Table 4: List of figures

Background:

The UoS has been carrying out basic research on a mildly-relativistic (500keV) self-insulating Cherenkov oscillator, that shares much in common with the conventional relativistic Backward-Wave Oscillator (BWO), while incorporating elements common to the klystron [1 – 4]. This produces a hybrid-source with higher potential efficiency than achievable without the "klystron" elements. The dominant characteristics remain BWO-like, leading to this new source being termed the Self-Insulating BWO (SIBWO). A schematic cross-section of the prototype geometry is shown in Figure 1.
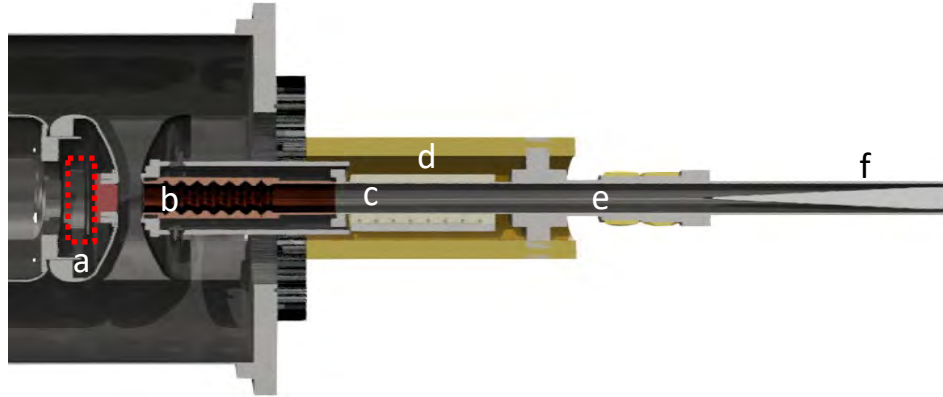
Figure 37: Schematic cross-section of SIBWO prototype assembly noting (a) A-K gap of accelerating diode (b) interaction region (c) beam dump (d) linear-stage location for A-K gap adjustment (e) field probe diagnostics and (f) attenuating load termination

The accelerating diode is formed by a grounded anode-grid, located some distance downstream of a negatively biased cathode emitter, forming an anode-cathode gap (A-K gap, Figure 1(a)) that determines the current drawn from the emitter for a given applied potential. The interaction region (Figure 1(b)) is located directly following the anode-grid, mounted within a movable support structure, allowing adjustment of the A-K gap via translation of a linear stage (Figure 1(d)). A set of discrete rare-earth magnets are used to form a beam-dump (Figure 1(c)), prior to sampling of the output, using a set of distributed D-dot field probes (Figure 1(e)), to determine operating mode and output power. The bulk of the output pulse is absorbed in a load termination (Figure 1(f)).

The numerical and experimental work, performed in investigation of this source over the reporting period, is presented in Section 2, divided into sub-sections describing the progress on the different aspects of the source construction.

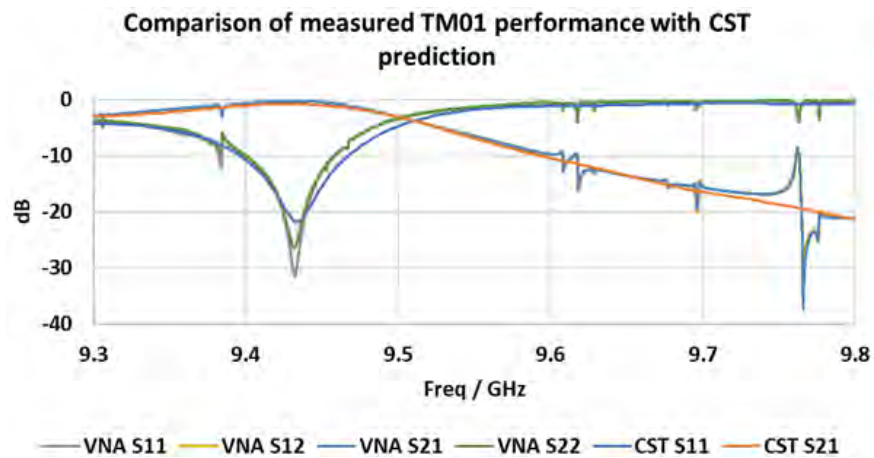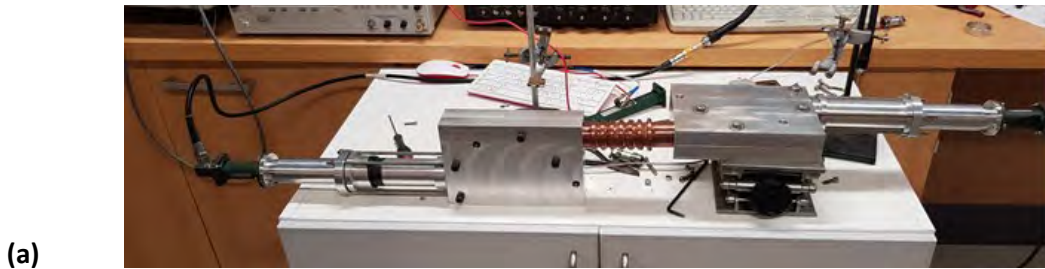## 2.   Activities and Accomplishments

Accelerating Diode:
Since last reporting [4] access to the UoS campus has resumed, albeit on a much reduced basis. This led to a redesign of the diode geometry to mitigate against loss of manufacture/assembly time. The design shown in Figure 1 makes use of readily available parts, such as standard ISO 316 stainless-steel pipe and torispherical end-caps, as a means of simplifying the construction without significantly affecting performance.

Modelling of the revised geometry showed the peak E-field stresses remained less than a factor of 2 above the DC breakdown limit (~20MV/m [5]) at ~30MV/m, which should be sufficiently low as to prevent breakdown during the applied voltage pulse-duration (~200ns). Manufacture of the cathode and the moving anode-face assemblies were carried out in-house, with the bounding anode-vessel placed for external manufacture due to its size. Should any issues arise with the externally placed component(s), due to the ongoing effects of the Covid-19 pandemic, the UoS has in place further mitigation strategies that will allow progression of the source to experimental testing with minimal additional delay.
Interaction Region:
Prior to the March - July 2020 lockdown, a second interaction region was manufactured, fully in-house at the UoS, to the same specifications as that reported in [4], but with thicker copper sidewalls, making it suitable for use in vacuum (i.e. in the hot experiment).

(a)

Comparison of measured TM01 performance with CST prediction

(b)

——VNA S11 ——VNA S12 ——VNA S21 ——VNA S22 ——CST S11 ——CST S21

Figure 38: (a) shows the experimental assembly for testing cold-performance of the prototype SIBWO interaction region (b) Comparison of predicted and measured transmission and reflection response(s) from the hot-test variant of the SIBWO interaction region.

Figure 2 shows the transmission and reflection responses of the hot-test interaction region, measured using an Anritsu MS4647A Vector Network Analyzer, showing very good agreement with the predicted performance from CST: Microwave Studio. This gives confidence that the interaction region should function as predicted in hot testing.

Beam Dump:
The prototype SIBWO incorporates a "beam dump" used to deposit the electron beam on the drift-tube wall. It should be stressed that the inclusion of this "external magnetic field" component is not intrinsic to the operation of the SIBWO, it is purely a consequence the prototype assembly, employed as a means of preventing incidence of high-energy electrons on the E-field pick-up probes. The dump is formed by a set of discrete Samarium Cobalt (grade Sm2Co17) rare-earth magnets, positioned such that the magnetic field does not negatively affect the propagation of the beam through the interaction region, but successfully decouples it from the co-propagating output microwave pulse prior to diagnostic sampling.
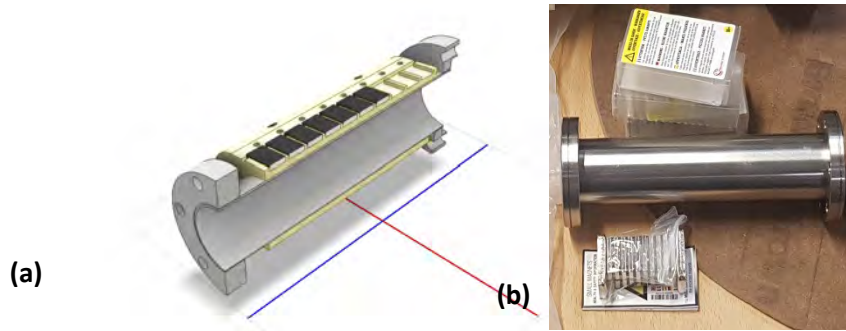
Figure 39: (a) shows a schematic of the beam-dump in cross-section (b) shows manufacture of components underway.

The necessary magnets are in-hand, with additional/alternate magnets available for tuning of magnetic field profile if required. The UoS will undertake such tuning, via Hall-probe measurement of the magnetic field profile, prior to incorporation within the experiment.

Field Probe Diagnostics:

As reported in [4], the UoS manufactured and experimentally verified the operation of a proof-of-concept variant of the diagnostic, proving it could discern between signals propagating in the TE_{11} and TM_{01}. Through the March – July 2020 lockdown period the UoS further developed the diagnostic, producing a more compact design that should provide additional means of modal discrimination in the sampled output signals. Figure 4 shows the design for the hot-test diagnostic.
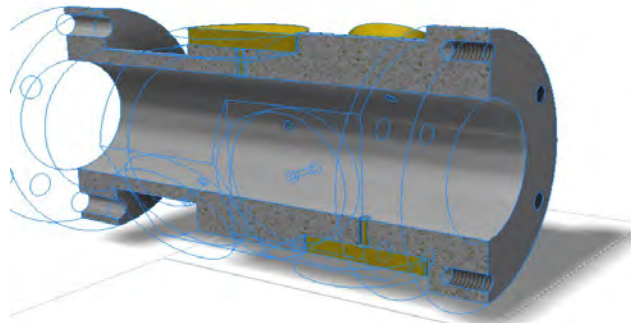
Figure 40: Shows the schematic cross-section of the field diagnostic, formed of 6 (2 sets of 3) D-dot probes, arranged to allow discrimination between different propagating modes in the SIBWO output pulse.

At the time of writing, the required field-probes are in-hand and the probe body is awaiting in-house manufacture.

Load Termination:

Since reporting in [4], the UoS has obtained the required load termination for hot testing of the SIBWO prototype, along with sufficient additional material to manufacture an alternate load if required. The load is shown in Figure 5. It is a high-power TC2000 cone-load manufactured by Thorndike Corp. MA, USA. The performance was measured in the same manner as the field-diagnostic, indicating at least -30dB of attenuation across the frequency range of interest.
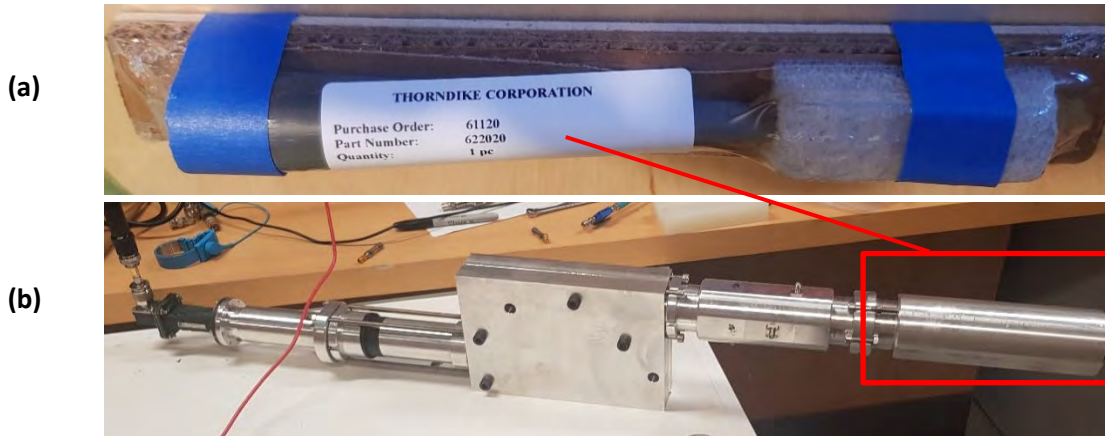
Figure 41: (a) the TC2000 cone load termination (b) the cold-test assembly for determining load performance, with load location indicated

The hot-test mount for the load forms part of the vacuum vessel and was under manufacture at time of writing.

References:
1. Phelps A.D.R., Compact High-Power Microwave Oscillators, ONR HPM Program – FY 2018 Report, December 2018.
2. Phelps A.D.R., Compact High-Power Microwave Oscillators, ONR HPM – RPPR Interim Progress Report - End of 1st Project Year Report [June 15, 2018 – June 14, 2019], July 2019.
3. Phelps A.D.R., Compact High-Power Microwave Oscillators, ONR HPM Program FY 2019 Report, November 2019.
4. Phelps A.D.R., Compact High-Power Microwave Oscillators, ONR HPM – RPPR Interim Progress Report - End of 2nd Project Year Report [June 15, 2019 – June 14, 2020], June 2020.
5. Gilmour A.S., Microwave Tubes, Artech House, 1986

3.   Findings and Conclusions

Cold testing of the interaction region, diagnostic design, and load termination is complete, with all components showing very good agreement with numerical predictions of performance. At time of writing, assembly of the prototype SIBWO was underway, with all key components approaching completion of manufacture. Experimental testing is now expected in early 2021, beginning with characterization of the accelerating diode.

The impact of Covid-19 on the intended work schedule for FY20 of the project has been significant, delaying the manufacture of key components and the commencement of experimental testing. Throughout, the UoS has worked to mitigate delays, where possible, through refinement of the prototype design and the procurement of additional in-house manufacturing capabilities.

4.   Plans and Upcoming Events

- December 2020: Presentation of the SIBWO via oral paper at ICOPS 2020 by Dr. P MacInnes
    - A second, poster paper, given on the accelerating diode by Mr. B. Crampsey
- April 2021: Presentation of the SIBWO via poster paper at the IoP Physics of Plasmas Conf. by Dr. P MacInnes.
- First quarter 2021: Completion of SIBWO assembly and characterization of accelerating diode
- Second quarter 2021 through to end of project: Experimental investigation of SIBWO prototype operation
- Throughout next Project Year (PY3): design of potential launch antenna design for future application(s).

5.   Transitions and Impacts
Not applicable at this stage

6.   Collaborations
Collaboration with Dr. Simon Cooke and Dr. Igor Chernyavskiy at NRL in modeling and design of the electron accelerator.

7.   Personnel

Principal investigator: Prof. Dr. Alan D. R. Phelps
Person months worked: 4
National Academy Member: Yes
Nationality: UK

Co-investigator and Co-PI: Prof. Dr. Kevin Ronald
Person months worked: 4
National Academy Member: Yes
Nationality: UK

Co-investigator: Dr. Philip MacInnes
Person months worked: 12
National Academy Member: No
Nationality: UK

Business Contact: Mrs. Alison McFarlane, RKES, University of Strathclyde

8.   Students

1 undergraduate student undertook a Summer Internship, working on a project of direct relevance, with funding provided by the EPSRC Summer Internship Scheme.

9.   Technology Transfer

We have undertaken collaborative discussions with Dr. Simon Cooke, NRL, in relation to modeling of the electron accelerator.

10.   Products, Publications, Patents, License Agreements, etc.

Publications resulting from this project in the current reporting period:
Conference Papers*
(1) A self-insulating, high-power, microwave source, P. MacInnes, K. Ronald, S.J. Cooke, I.A. Chernyavskiy, A.D.R. Phelps, 5th Microwaves in Plasmas and Beams Workshop, UK, 4-5 December 2019.
(2) Self-insulation of a high-power Cherenkov oscillator, operating in the X-band, P. MacInnes, S.J.Cooke, I.A., Chernyavskiy, K. Ronald, A.D.R. Phelps, 47th IEEE International Conference on Plasma Science (ICOPS-2020), Virtual Conference, 6-10 December 2020.
(3) Dynamics of highly energetic electrons in novel accelerating diodes, B. Crampsey, P. MacInnes, K. Ronald, A.D.R. Phelps, 47th IEEE International Conference on Plasma Science (ICOPS-2020), Virtual Conference, 6-10 December 2020.

*Paper (1) was presented during this reporting period. Papers (2) and (3) were written and submitted during this reporting period and scheduled for presentation in the FY21 reporting period.

11.   Point of Contact in Navy

Ryan Hoffman ONR, ryan.hoffman@navy.mil
Tim Andreadis NRL, tim.andreadis@nrl.navy.mil
Jesus GilGil NRL, jesus.gilgil@nrl.navy.mil
Alexander N. Vlasov NRL, alexander.vlasov@nrl.navy.mil
Simon J. Cooke NRL, simon.cooke@nrl.navy.mil
Igor A. Chernyavskiy NRL, igor.chernyavskiy@nrl.navy.mil
Matthew McQuage NSWC, matthew.mcquage@navy.mil
Predrag Milojkovic ONRG , predrag.milojkovic.civ@mail.mil
Charles R. Eddy, Jr. ONRG, charles.r.eddy12.civ@mail.mil

During FY20 meetings to discuss research progress were held, via the internet, on a monthly basis with SJC & IAC (NRL).

12.   Acknowledgement/Disclaimer

Geodesic Luneburg Lenses for High Power Applications

Prepared by:

Dr. Oscar Quevedo-Teruel, Principal Investigator
KTH Royal Institute of Technology
Brinellvägen 8, 114 28
Stockholm, Sweden
Tel: +46-72-844 41 64
Email: oscarqt@kth.se

Section I: Project Summary

1. Overview of Project

The main goal of this project is to investigate the possibilities of geodesic lenses for high-power antenna applications, which find application in radar systems.
More specifically, this project has the following main objectives:
- To identify the fundamental limitations of geodesic lenses.
- To determine the limitations of geodesic lenses at high power applications.
- To study the potential use of fully metallic geodesic lenses at X- and Ku-bands.

To accomplish these objectives, we are aimed to develop a code based on ray tracing that characterizes geodesic lens antennas. Our code will be able to produce a fast and accurate solution for the radiation pattern and radiation efficiency. This method will be able to state the limits that this technology offers.

When the code is ready, we will proceed to design some antenna demonstrators. These two antennas will be aimed to handle high power, as in commercial radar systems. The antennas will have integrated feeding networks, and a flare structure to produce a highly efficient radiation. The frequency of operation for these demonstrators will be between 10-20 GHz, in the X- and Ku-bands. These prototypes will be validated in the KTH facilities.

In addition to the naval relevance for radar systems, the results achieved in this project could be used for civil applications, such as commercial radars in cars and ground terminals for satellite communications. Other possible applications of this technology include 5G/6G communications and spectroscopy detectors.

2. Activities and Accomplishments

During the first 4 months of the project (June 2020 to September 2020), we have been working on the development of a ray tracing code that could accurately model the operation of geodesic lenses and describe their performance in terms of radiation patterns. Our first goal was to reproduce the results produced by a Luneburg lens with a geodesic lens.

A Luneburg lens is a graded-index lens that perfectly transforms a spherical/cylindrical wave into a plane wave at the opposite side of the excitation. Luneburg lenses are an attractive solution for communications and radar systems since they have low scan losses. However, their principal drawback for high-power applications is that they must be implemented with dielectric materials, which are lossy and limit the amount of handled power. Equivalents to Luneburg lenses can be achieved with geodesic lenses. These geodesic lenses are completely metallic and can manage high power.

The first version of our code calculates the direction of the rays in a geodesic shape based on the Fermat principle that states that the light takes the shortest path between two points. The shape that mimics a Luneburg lens including the calculated rays is illustrated in Fig. 1. These rays provide information on the amplitudes and phases at the aperture which are necessary to calculate the radiation patterns.

(a)   (b)
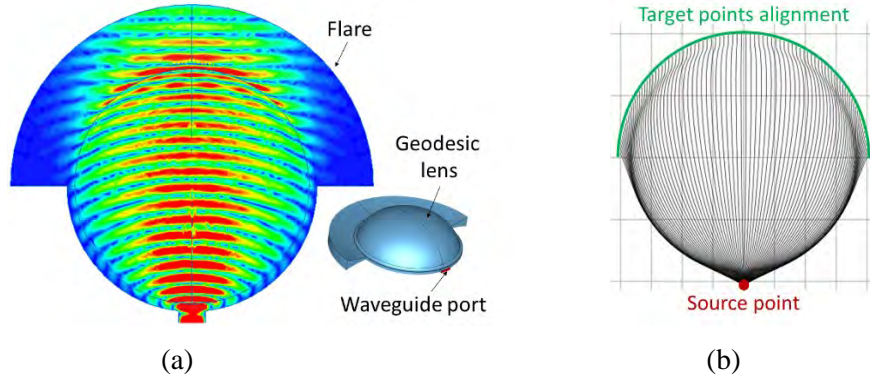
Fig 1: Geodesic shape that mimics a Luneburg lens
(a) Electric field representation (HFSS simulation) and (b) Ray tracing over the surface.

We have computed the radiation pattern for a geodesic lens that mimics a Luneburg lens. To validate our results, we have carried a comparison with HFSS and CST (commercial software) as illustrated in Fig. 2. These results show a good agreement between HFSS/CST software and our code. The main advantage of our code is that it computes the radiation pattern in few seconds, while commercial software takes hours. Furthermore, when the gain (and size of the antenna) increases, the computational time in commercial software significantly increases, while our code is not tremendously affected. Therefore, prior to our code, it was impossible to optimize geodesic lenses. The next step is to integrate our code with an optimization tool, so a desired radiation pattern can be achieved at-hand.
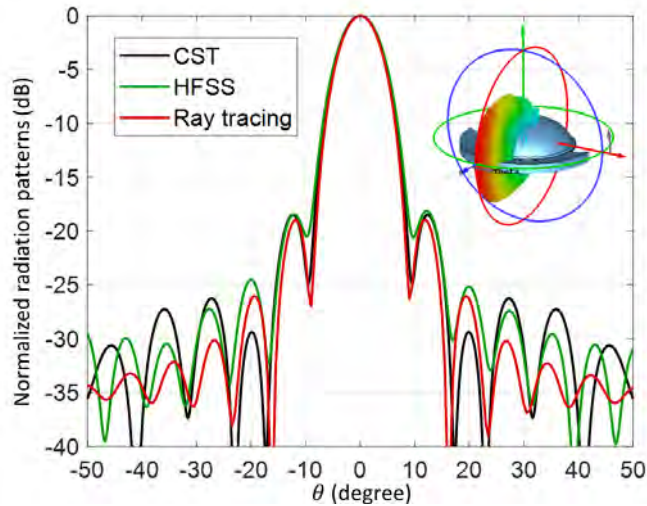
Fig. 2: Comparison of the radiation patterns obtained with the HFSS, CST and our ray tracing code.

3.   Findings and Conclusions

We conclude that our ray-tracing is able to accurately describe the operation of geodesic lenses that mimic the operation of Luneburg lenses. The procedure must be tested for more complex geodesic lenses in which the rays are not aligned at the other size of the lens to produce a plane wave.

The results are promising since the code is very fast. To be precise, our codes is several orders of magnitude faster than commercial software. Therefore, this code could be potentially used to optimize the operation of the lens, especially for large antennas (high gain). The main parameters that could be optimized are the

174

side lobe levels and the direction of the main beams in the radiation patterns. Furthermore, the code could be used to compress the size of the geodesic lenses with non-rotational shapes.

4. Plans and Upcoming Events

The next steps are to continue validating the code for other types of geodesic lens antennas with more complicated distributions of the rays. Once the code is validated for rotationally symmetric shapes, we will extend the code for non-symmetrical shapes. These shapes would give a new degree of freedom to tailor radiation pattern, including the possibility to minimize the side lobe levels. When the code is available, we will incorporate an optimization tool, which will permit the design ad-hoc of radiation patterns. Finally, we will demonstrate the potential use of geodesic lenses for high-power applications with the manufacturing and testing of two geodesic lens antennas in the X- and Ku-bands.

In terms of dissemination, we are planning to present part of our work in international conferences. However, now, the dissemination through conferences has been difficult due to the COVID-19. Our intention is to present this work for the first time at the IEEE APS/URSI 2021 symposium, which has been moved from summer 2021 to December 2021 due to the COVID-19. This is the largest conference in antennas and propagation, and it will have an appropriate audience to present our results. Our first journal paper is expected in 2021. In this paper, we are expected to demonstrate the operation of the ray tracing code.

In our plan for the first 4 months of this project, we did not plan to complete any major milestone or dissemination yet. Therefore, we are progressing according to the plan. The first major milestone is the competition of the ray tracing code, which should be done during 2021.
Recommendations for Future Work: N/A.

5. Transitions and Impacts

Since the produced results in this project are still at an early stage, there have been no transitions.

6. Collaborations

For the development of the ray tracing tool, two Spanish universities and the European Space Agency have shown their intentions to collaborate with O. Quevedo-Teruel at KTH. More specifically, the researchers who are interested in this topic are:
- Prof. Francisco Mesa from University of Seville, Spain.
- Prof. German Leon, from University of Oviedo, Spain.
- Dr. Nelson Fonseca from the European Space Agency.

From the implementation point of view, Dr. Astrid Algaba-Brazalez and other members of her team in Ericsson AB are interested to implement a similar concept for 5G/6G communications. Prof. Jean-Paul Guillet at University of Bordeaux wants to collaborate with KTH to develop this concept for radars at 120 GHz with the support of Ariane Space. Funding applications have been submitted in these cases in collaboration with the European Space Agency. They are under evaluation.

7.   Personnel

All the participants in this project are at KTH Royal Institute of Technology.

Principal investigator: O. Quevedo-Teruel (Associate Professor)
Team Members:
-   Dr. Sarah Clendinning (post-doc).
-   Qingbi Liao (PhD student).
-   Federico Giusti (MSc student).

8.   Students

Qingbi Liao (PhD student) and Federico Giusti (MSc student) contributed to the project. Both are students at KTH Royal Institute of Technology. They are expected to graduate in 2021.

9.   Technology Transfer
No transfer of technology has been conducted.

10.   Products, Publications, Patents, License Agreements, etc.

No publications have been produced during the first 4 months.

11.   Point of Contact in Navy

The two main contacts during the first 4 months were:
-   ONR Global: Predrag Milojkovic (predrag.milojkovic.civ@cvr.mil)
-   Navy: Ryan Hoffman (ryan.hoffman@navy.mil)

12.   Acknowledgement/Disclaimer

ONR Industry Contract Summaries

Contract Number: N00014-19-C-1008
Project Title: Active/Passive Limiters for High Power Radio Frequency (HPRF)
Contract Period of Performance: 23 Jan. 2019 – 22 Jan. 2023
Principle Investigator: Dr. Sameer Hemmady, sameer.hemmady@verusresearch.net, (805)-558-5604
Organization: Verus Research, Albuquerque, NM

Project Summary

In this body of research, Verus studied physical mechanisms for High Power Radio-Frequency induced nonlinear responses of front-end components typically found in RF receivers. Verus categorized the physical mechanisms from the small-signal linear regime of operation to the large signal nonlinear regime which comprises a continuum of states spanning non-persistent effects and persistent effects (which includes degradation and eventual damage). Similar responses were characterized for other RF front-end components, such as mixers and analog-to-digital convertors (ADCs). This body of research is anticipated to benefit the Navy's High Power Electronic Warfare (HPEW) applications and missions by way of developing prescriptions for more effective HPRF waveforms against RF receivers of interest.

Contract Number: N00014-20-C-1083
Project Title: Leveraging Predictive Effects for Devising Collaborative HPRF/Cyber Engagement Paradigms
Contract Period of Performance: 9 June 2020 – 8 June 2023
Principal Investigator: Dr. Sameer Hemmady, sameer.hemmady@verusresearch.net, (805)-558-5604
Organization: Verus Research, Albuquerque, NM

Project Summary

The focus of this research effort is to leverage recent advancements in predictive effects research for devising collaborative High Power Radio Frequency (HPRF)/Cyber engagement paradigms for complex electronic targets of interest. In the current base effort, Verus Research has focused on performing experiments that establish how software pre-conditioning of an electronic asset can demonstrably alter its HPRF susceptibility, as quantified through its empirically generated Probability of Effects (Pe) curves. In the current Option, Verus Research has utilized predictive effects to devise agile attack waveforms. This has direct implications to mission-level concept of operations (CONOPS) for HPRF platforms in terms of extending its range to effect or alternatively increase its ability to penetrate and affect electronic assets housed deeper inside targeted infrastructure facilities.

Reimbursable Task Summary

Grant or Contract Number: N0001419WX01455, N0001420WX00247
Project Title: HPM Key Target Effects on Electronics (UWB Effects)
Period of Performance: 1 Dec 2018 to 31 Dec 2020
Principle Investigator: Zach Drikas, (202) 767-6629, zachary.drikas@nrl.navy.mil,
Organization: U.S. Naval Research Laboratory, Washington DC

Project Summary
The U.S. Naval Research Laboratory (NRL) investigated the effects and phenomenology of high-power ultra-wideband (UWB) signals on sensitive electronics to begin to systematically develop an UWB effects database. Effects were induced by a range of novel, high-power, UWB sources developed by NRL. These sources have the ability to generate high peak-power signals that also have high pulse repetition frequencies (PRFs). In addition to observing and categorizing effects, NRL also conducted analysis on the phenomenology of UWB signal interaction with electronics including the contribution of PRF to effects.

SBIR/STTR Summaries

Grant or Contract Number: N00014-15-C-0160, SBIR Phase I
Project Title: Compact, Collapsible, or Conformal Antenna Design for Emerging High Power Radio Frequency (HPRF) Sources
Period of Performance: 14 Sep 2015 to 14 Sep 2020
Principle Investigator: Robert Koslover, 903-565-0389, rkoslover@sara.com
Organization: Scientific Applications & Research Associates, Inc., Colorado Springs, CO

Project Summary
The Phase II Option 2 part of this program represented a shift in emphases, per an agreement between ONR and SARA, for SARA to design and fabricate modular, arrayable, UWB-capable antenna elements to support Active Electronically-Scanned Arrays (AESAs) driven by the novel compact solid-state sources being developed/advanced in parallel under the ONR-supported UMKC OSPRES program. We identified several options, executed numerous analyses, and ultimately selected, optimized, and engineered a Balanced Antipodal Vivaldi Antenna (BAVA) as a modular array building-block. Custom BAVAs sufficient to construct a 5x5 array were fabricated, assembled at SARA, and shipped to the customer. We envision that a larger (e.g., 16x16) array of these or similar elements could serve well as part of an integrated OSPRES system.

Contract Number: N68335-16-C-0050, SBIR Phase II
Project Title: High Speed and High Voltage Capacitors for Naval HPRF Directed Energy Applications
Period of Performance: 20 Jan 2016 to 1 Jul 2020
Principle Investigator: Quentin Diduck, 585 451-5755, qdiduck@ballisticdevices.com
Organization: Ballistic Devices, Santa Clara, CA

Project Summary
The primary objective of this project was to demonstrate component reliability and suitability to HPRF applications. This included evaluating components under high stress conditions (high current, high voltage, resonance conditions) to determine suitability for purpose. It also included identifying component reliability issues, resolving weaknesses, and enhancing capacitor performance and reliability and if possible improve energy density. Resonant capacitor operation induces extreme mechanical stress and has introduced structural failures. Alternative materials used in the construction have to meet strict electrical and mechanical requirements. During this project efforts were primarily focused on trying to identify an epoxy or adhesive that supports C0G operation of the device and developing thinner dielectric layers for lower voltage operation while maintaining energy density. There are many difficulties in achieving this. In particular most materials that are suitable for C0G operation have a very low dielectric constant, which makes the energy density difficult to achieve. As well, most high-k dielectric adhesives tend not to list their dielectric constant in their specification, due to most electronic applications desiring a low-K material. Several adhesives and epoxies were tested as well as the fortifications of epoxy materials with ceramic powder all in an effort to reduce the change in capacitance with temperature. During this project one material system was identified as a possible candidate that enabled C0G operation, and experiments were conducted with different material systems in an attempt to identify a suitable process.

SBIR/STTR Summaries

Contract Number: N00014-16-C-1038
Project Title: Compact Megavolt Switch Utilizing Novel Switching Mediums
Period of Performance: 7 Apr 2016 to 10 May 2021
Principle Investigator: Michael Abdalla, 505-830-3000, mda@asrcorporation.com
Organization: ASR Corporation, Albuquerque. NM

Project Summary
The design of compact pulsed power systems is an emerging art. One of the key approaches is to engineer the system to eliminate auxiliary subsystems while increasing the performance of every element in the system. This is a vast departure in philosophy from conventional pulse power design. Of prime importance is the approach to high voltage insulation and the performance of switches. Conventional spark gap switches consist of two electrodes enclosed in a cylindrical dielectric vessel long enough to prevent surface flashover and held together with tie-rod. Such switches trade off ease of manufacture and (large) size for reliability. These commercially available switches typically use sulfur hexafluoride (SF6) gas and requires a continuous supply. The continuous supply requirement has SWaP implications for systems: a gas cylinder or reservoir must be included near the switch adding weight and volume. ASR has developed compact spark gap switches using the approach of tailoring the shape of the inner surface of the housing to inhibit the internal surface flashover, thus reducing the overall length of the switch. ASR favors hydrogen as a switching medium because of its switching properties. A design for a hermetically sealed switch concept has been completed.

SBIR/STTR Summaries

Grant or Contract Number: N68335-17-C-0041, STTR Phase II
Project Title: Advanced Silicon Diode Switch for HPRF Systems
Period of Performance: 15 Feb 2017 to 16 Jun 2021
Principle Investigator: Steven Bellinger, 785-532-7087, bellinger@radectech.com
Organization: Radiation Detection Technologies, Manhattan, KS

Project Summary
The Office of Naval Research has identified a need for new solid-state switch (diode) materials and demonstration thereof in standard form-factor mountings and use. ONR envisions these switches to be used in High Power Radio Frequency (HPRF) applications. The program goal is to jumpstart a commercial switch package design, focusing on fast rise-time, cooling considerations for continuous operation, and improving/optimizing the switches for operational use. Silicon photoconducting solid-state switches (Si-PCSS) are inexpensive semiconductor-based switches used in commercially available HPRF instrumentation. Silicon-based photoconductive switch technology, despite its widespread industrial use, has not reached its limit in repetition-rate nor voltage-holdoff or recovery-time. The research has aimed to find the limits of switch voltage breakdown, while the objective of the development effort was to build, test, demonstrate and compare a transition-capable Si-PCSS system, built on first-in-class 10-kV modules. Commercialization of the Si-PCSS developed for this project was driven by the needs of the Navy, wider-DoD & DOE communities, and commercial pulsed power users. Phase II included a significant packaging and integration effort of the Si-PCSS to address thermal, environmental, laser considerations, and safe operation. Main objectives were: (1) design, build and demonstrate a Si-PCSS module, transmission line, laser, and cooler assembly; (2) perform trade study of diode lifetime killers, hold-off voltage, and required laser light to achieve a 10-kV module with optimal support systems. The success of the phase II effort was building Si-based PCSS 10kV-modules and coupling those modules to microwave radiation technologies.

Grant or Contract Number: N68335-17-C-0112, SBIR Phase II
Project Title: Affordable Compact HPRF/HPM Attack Warning System
Period of Performance: 5 Apr 2017 to 28 Jun 2022
Principle Investigator: Todd Chauvin, 408-702-8066, t.chauvin@saphotonics.com
Organization: SA Photonics, Los Gatos, CA

Project Summary
SA Photonics' Wideband Agile Threat Sensor (WATS) addresses the Navy's need for an affordable and compact High-Power Radio Frequency / High-Power Microwave (HPRF/HPM) attack warning technology that detects, characterizes and precisely geo-locates HPRF threats while being fully immune to HPRFs. WATS consists of multiple completely passive HPM probes connected by fiber optic cables to an electronic processing system. In addition to characterizing key statistics of detected attacks, the WATS system when deployed with multiple sensors at well-known locations is able to localize the direction the attack originated from as well as estimate the range of the HPM attack source.

SBIR/STTR Summaries

Grant or Contract Number: N68335-18-C-0761, SBIR Phase I
Project Title: Drift Step Recovery Diode (DSRD) for Wideband (WB) and Ultra-Wideband (UWB) Pulse Generation
Period of Performance: 15 Oct 2018 to 30 Apr 2020
Principle Investigator: Jason Sanders, 615-424-1467, jason@transientplasmasystems.com
Organization: Transient Plasma Systems, Torrance, CA

Project Summary
The objective of this project is to develop drift step recovery diode components for high power microwave technology applications. The solicitation indicated that the Phase I effort should result in the development of a single DSRD with a level of performance that will enable further development of relatively compact solid-state sources that are useful for directed energy applications. The devices that were developed during Phase I were shown to be capable of generating the required pulses, though there was some part-to-part variation in performance. TPS was did not receive a Phase II award, but it was granted a Phase I Option, which allowed TPS to improve its process and demonstrate reliable parts capable of achieving all and exceeding some of the target specifications that are the goal of the Phase II effort. TPS has continued to work with ONR on the development of high power closing switch technology that is enabled in part by the DSRD opening switch technology developed during this effort. TPS has submitted a white paper indicating potential next steps for DSRD technology and would be happy to discuss further with any interested parties.

Grant or Contract Number: N68335-19-C-0071, SBIR Phase II
Project Title: Fast Rise-time High Power Radio Frequency (HPRF) Pulse Shaping
Period of Performance: 20 Nov 2018 to 31 Jul 2021
Principle Investigator: Michael Butcher, 505-338-2179, michael.butcher@verusresearch.net
Organization: XL Scientific/Verus Research, Albuquerque, NM

Project Summary
The technical objective of the Phase II SBIR is to develop an HPRF pulse shaping capability that will operate between 1-4 GHz and handle up to 8MW of power. The High-Power Pulse Shaping (HPPS) system provides the Navy an augmented capability that can be added to existing long pulse, slow rise HPRF sources such as high-power magnetrons or klystrons and be able to convert those output pulses to a shorter, square pulse output. The Navy can use this capability for various lethality and counter-electronics testing purposes. In Phase II, Verus Research developed a prototype High Power Microwave (HPM) pulse shaping capability in the form of a microwave waveguide switch. Use of this switch for high power pulse shaping expands the test capability for HPM weapon effects testing, to better assess the lethality of HPM weapons against operationally relevant threats. This enables development and delivery of more capable HPM weapons for non-kinetic counter electronics applications more rapidly. This capability also enables faster responsiveness to emerging threats reducing test and evaluation time.

SBIR/STTR Summaries

Grant or Contract Number: N68335-19-C-0255, SBIR Phase II
Project Title: Miniaturization of High Average Power, High Peak Power, Wide Bandwidth Antennas and DSRDs
Period of Performance: 3 Jul 2019 to 22 Jun 2023
Principle Investigator: Michael Abdalla, 505-830-3000, mda@asrcorporation.com
Organization: ASR Corporation, Albuquerque, NM

Project Summary
The overall problem addressed here is one of dopant and heterostructure optimization of tried-and-true silicon drift step recovery diodes (DSRDs), with decreased rise time and increased reverse current density ratings from structures that enable higher current and lower internal impedance operation. Silicon is the material of choice as it provides a sustainable commercial path and can perform in excess of the stated metrics set forth by this proposal. The primary area of research focus in Phase I was to investigate strategies to incorporate focusing into the antennas to reduce overall volume. True electrically small antennas (ESA) have been considered. Due to bandwidth limitations for true ESA designs, alternate compact antennas have been considered.

Grant or Contract Number: N68335-19-C-0445, SBIR Phase II
Project Title: Navy-Electronic Battle Damage Indicator (eBDI) Tool for Non-Kinetic High-Power Radio-Frequency (RF) Engagements
Period of Performance: 29 Aug 2019 to 31 May 2022
Principle Investigator: Donald Voss, 505-255-4201, donv@vosssci.com
Organization: Voss Scientific, Albuquerque, NM

Project Summary
A critical need exists for a compact and reliable electronic Battle Damage Indicator (eBDI) tool for use in a directed energy (DE) battlefield in which High Power Radio Frequency (HPRF) devices are employed. In the Phase I effort, Voss Scientific demonstrated the feasibility of building an Autonomous Damage Assessment Module (ADAM) capable of meeting the Navy electronic Battle Damage Indicator (eBDI) requirements by utilizing a man- or UAV-portable electronics package with multiple methods of emplacement, both covert and overt. In addition to broad-spectrum data collection, ADAM will use an extremely-narrowband data collection methodology in the brass-board eBDI device. The resulting ADAM eBDI system will be denoted as ADAM Gen-I. The performance of ADAM Gen-I will be demonstrated in both laboratory and in one or more field tests, with the goal of reaching TRL 5.

SBIR/STTR Summaries

Grant or Contract Number: N68335-20-C-0486, SBIR Phase I
Project Title: Diamond Based Semiconductor Pulse Shaper
Period of Performance: 8 Jun 2020 to 8 Dec 2020
Principle Investigator: Paul Quayle, 919-593-8595, quayle@glcrystal.com
Organization: Great Lakes Crystal Technologies, East Lansing, MI

Project Summary
Great Lakes Crystal Technologies (GLCT) and Michigan State University (MSU) have teamed to develop high power, diamond-based semiconductor pulse shaper technology for sharpening high voltage 3-5 ns driving pulses to a rise time of less than 100 ps and a dV/dt of greater than 200 V/ps to enhance the performance parameters of high power microwave (HPM) pulse generators. The pulse shaper under development is based on an integrated diamond-based drift step recovery (DSRD) diode and diode avalanche shaper (DAS). A diode device produced during the project showed a good ideality factor of 1.3. Simulations support the concept of a diamond-based pulse shaper that meets the target performance levels.

Grant or Contract Number: N68335-20-C-0487, SBIR Phase I
Project Title: Solid-state, Sub-nanosecond Pulse Sharpener for Generating High Power Impulses
Period of Performance: 8 Jun 2020 to 20 Sep 2021
Principle Investigator: Jason Sanders, 615-424-1467, jason@transientplasmasystems.com
Organization: Transient Plasma Systems, Torrance, CA

Project Summary
The Office of Naval Research issued this SBIR topic to fund the development of a solid-state closing switch capable of producing high power UWB electrical pulses. This proposed effort will investigate Silicon Avalanche Shaping/Sharpening (SAS) device structures for both Si and SiC, with Si being viewed as the conservative approach for achieving the threshold specifications of this topic. Less work has been done to investigate the capabilities of SiC for SAS devices, but its superior material properties suggest it is likely well suited for impact-ionization avalanche switching, which does not rely on long minority carrier lifetime for practical implementation in the same way Drift Step Recovery Diodes (DSRDs) do. The significantly shorter intrinsic region that can be achieved with a SiC SAS-type device is expected to result in higher dV/dt capability compared to Si due to shorter transit distance through the device and reduced effective resistance. Devices have been designed and simulated during Phase I, and a Phase II effort has been awarded. In Phase II solid-state devices capable of switching kW-MW power pulses with risetimes faster than 300 ps at high pulse repetition rate will be fabricated and tested. These devices will add to the United States' high power UWB technology portfolio and will advance system capabilities for directed energy applications.

SBIR/STTR Summaries

Grant or Contract Number: N68335-21-C-0062, SBIR Phase II
Project Title: Drift Step Recovery Diode (DSRD) for Wideband (WB) and Ultra-Wideband (UWB) Pulse Generation
**Period of Performance:** 8 Oct 2020 to 31 Oct 2022
Principal Investigator: Ranbir Singh, 703-996-8200, ranbir.singh@genesicsemi.com
Organization: GeneSiC Semiconductor Inc., Sterling, VA

Project Summary
Drift step recovery diodes (DSRDs) are the fastest semiconductor opening switches reported to-date and are a critical enabling technology for realizing ultra-wide band (UWB) high-power microwave sources which are of great interest for US Navy applications. The main goal of this two-Phase SBIR project is to develop silicon carbide drift step recovery diodes as a reliable and qualified product for insertion into the next-generation ultra-wide band, high-power microwave sources. Capitalizing on the superior intrinsic advantages of the semiconductor material silicon carbide (SiC) over silicon, this project will develop ultra-high speed SiC based DSRDs with single-chip ratings of > 2 kV and ≥ 100 A, with significantly faster switching capability. This will reduce the number of series-connected devices necessary to realize ultra-high voltage 20-50 kV pulse generators with sub-nanosecond switching capability.
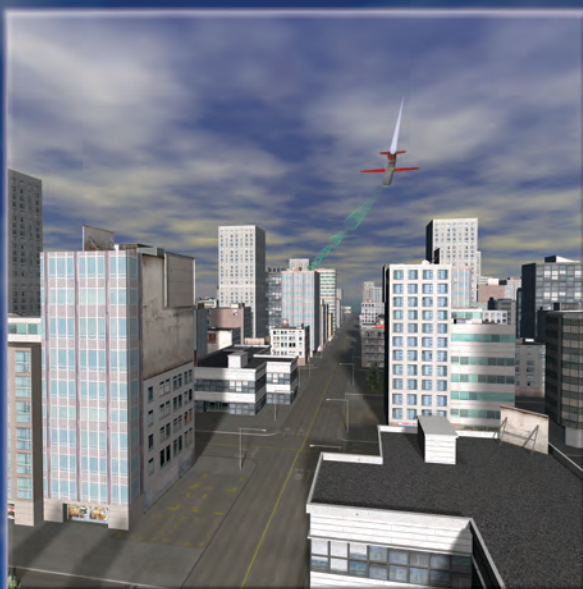
Office of Naval Research
875 N. Randolph Street
Arlington, VA 22203-1995
www.onr.navy.mil